Thesis submitted for the degree of Doctor of Philosophy at the Unive
Leicester

by

James Henry Sambrook Blight M.Geol. (Leicester)
Department of Geology
University of Leicester

December 2006

ProQuest LLC
789 East Eisenhower Parkway
P.O. Box 1346
Ann Arbor, MI 48106-1346

Abstract

To date, relatively little is known about the geological and tectonic evolution of Southern Mongolia, despite its emerging importance as a mineral exploration frontier province. The distribution of porphyry Au, Cu and Mo mineralization in the region is strongly controlled by the tectonic regime governing the northern margin of the Palaeo-Asian Ocean. The Saykhandulaan basement inlier in southern Mongolia constitutes a critical window into the Palaeozoic development of this margin, and consequently, understanding the tectonic evolution of this area is important in both an academic and economic context.

By broadly characterising the geological and tectonic evolution of the southeast Gobi region, this project elucidates the geological evolution of a relatively unstudied accretionary margin. It provides both a robust spatial and temporal framework within which to interpret the mineralization identified to date, and new insights for focusing mineral exploration efforts in potentially fertile areas.

Through fieldwork, five litho-tectonic domains are defined; (1) the Northern Slate Belt, comprising Devonian greenschist grade pelites and psammites with deep-marine to coastal siliciclastic protoliths; (2) the Saykhandulaan Valley Lineament Zone (SVLZ), a tectonised zone of faulted and lithologically altered volcanic rocks; (3) the High Strain Belt, consisting of tightly folded and flattened metamorphosed clastic sedimentary rocks; (4) the Molasse Succession, consisting of relatively undeformed coarse conglomerates and sandstones and; (5) the Oyut Ulaan Volcanic Group, a nearly 5 km-thick folded Carboniferous volcanic succession that hosts the mid-Carboniferous Oyut Ulaan mineralised intrusive complex. The structural architecture of the inlier records several ductile and brittle deformations, including folding of all lithologies to differing degrees, folding of cleavage in the Northern Slate Belt, thrusting along the SVLZ and exhumation of the tightly folded High Strain Belt. Field relations, geochemical signatures and the absolute age of the Oyut Ulaan intrusive complex show that, with the Oyut Ulaan Volcanic Group, it forms a co-magmatic volcano-plutonic complex. Volcanic and intrusive lithologies have subduction zone-related signatures. The Oyut Ulaan Volcanic Group is comprised of four formations with volcanic lithologies and thick intercalated siliciclastic and volcaniclastic sediments.

Chemostratigraphy of the Oyut Ulaan Volcanic Group illustrates an evolving magma chamber with periodic replenishment by new magma batches. One other intrusion within the Saykhandulaan inlier and six other intrusions within the neighbouring Mandakh inlier were geochemically analysed and U-Pb zircon dated, showing, broadly, that a 180 km long belt of monzonitic intrusions were emplaced in the mid-Carboniferous (between 338.93 and 323.12 Ma) and post-collisional granites and A-type syenites were emplaced in the Early Permian (292.34 Ma).

The combined results of this study indicate that whilst economic mineralisation identified in the region to date is associated with early intrusions in an emerging continental-arc setting, the later stages of arc magmatism resulted in a significant EW belt of intrusions and volcanic deposits, which are also host to prospect mineralization. The youngest parts of this belt track the transition from a continental-arc to a post-collisional magmatic environment.

Acknowledgements

First and foremost, I thank my parents, Laurence and Jane Blight, for ceaseless encouragement, timely and generous financial and logistical support, constant concern for whether I am eating well, and for supplying genes that are apparently conducive to getting the job done. I'd also like to thank my sister Amy, for being a source of enthusiasm, encouragement and style.

The supervision I have received during my project has been second to none; efficient, helpful and constructive. I often find myself chortling at the antics of other people's supervisors (though none from Leicester of course), and feeling very lucky to have had oversight from the most excellent team of Dr W. Dickson Cunningham and Dr Michael G. Petterson, and in later years, Dr Quentin G. Crowley.

Dickson started this all off by directing me to the original project advertisement whilst I was in the 4th year of my Mgeol, in 2002. He then spent 4 years; using his extensive contacts and knowledge of Mongolia to make my field seasons run smoothly; tirelessly reviewing my scribblings; and putting up with my occasionally over-enthusiastic knocking on his door. I also thank him for introducing me to the concept of English grammar, of which I was hitherto unaware.

Mike Petterson is a legend. A kind of pint-sized singing geological troubadour, he has accompanied and encouraged me on many exploits, including my main fieldwork, an excellent trip to the lake district (in which I hobbled up and down hill and dale with a knackered leg), numerous conferences, and many lunches and drinking sessions in the pub. His financial and logistical support made my second field season possible, and his academic supervision made it successful. His friendship and support during difficult times went beyond the call of duty.

Jon Naden of the BGS also provided excellent in-field supervision, encouraging me to better plan my work, and set objectives, without which the quality of my fieldwork would have suffered considerably. Jon also suggested I present both a talk and a poster at my first academic conference. For this, I am particularly indebted to him, as it resulted in one of the best days of my life, and an ensuing night out in Belfast of epic proportions.

This project would not have been possible without the logistical and scientific support of Ivanhoe Mines Ltd. Specifically I would like to thank Doug Kirwin, Chris Wilson, Paul Carter and Tim Corbett for generous and well organised logistical support. Tom Sant,

Andrew Stewart and Rohan Wolfe provided in-field scientific data, discussions, tours of mineral occurrences, and welcome company at the end of long field seasons.

I thank the Society of Economic Geologists for providing financial assistance for the fieldwork component of this project through a Hugh E. McKinstry Student Research Grant.

Quentin Crowley supervised my work at the National Isotope Research Laboratory (NIGL) with great patience, and was very forthcoming with help, both with the practical aspects at the lab, and subsequently with quick and detailed responses to my queries during write-up. I also want to thank other staff at NIGL including Randall Parrish, Steve Noble, Jane Evans, Béatrice Bullock-von Moos and Adrian Wood.

Helen Crowther, whom I first met a long time ago, has been a wonder over the last 14 months. Her support, love and advice have been essential to my happiness and sanity. Helen has also been instrumental in my passing my driving test, by sitting in the passenger seat of my car, and making it possible for me to get thousands of miles of practice (quite a big deal for me after 5 un-successful attempts!).

I have been lucky, living in Leicester to be surrounded by old school friends from Barry. David 'Billy' Anthony and Pamela Bowyer have been fantastic over the last four years, and I salute them for having helped me move house on numerous occasions, and of course for the many nights drinking round at theirs, crashing in their spare room, and eating breakfast cooked by Bill, who is becoming a culinary genius (and thanks also to Belina, Buffy and Beatrix for all the eggs).

After his degree in geology at Cardiff, Simon Crockford broke north to Nottingham for a degree in architecture, just in time to be talked into accompanying me to Mongolia in 2004, (a decision he may still be rueing). I thank him for his excellent field support, for keeping me supplied with; abstract conversation and a golfing partner on the steppe (until I lost all our balls in one game); for being an expert wielder of a GPS unit, for spotting some of the only fossils in the area, and for generally fixing things up and sorting stuff out. Simon made the second field season one hundred percent more awesome than the first. Thank you buddy.

Amanda Jeffery put up with me for many years, and I thank her for that, for all the great times too, and for coping well with me calling her from the Gobi on the satellite phone to tell her both my drivers had disappeared and I was stranded.

Thanks to my housemates (a finer cohort you will rarely meet) who welcomed me into their house after my second field season; Alex 'Jeff Beck' Parker (for being in house IT

support, and all the lifts to places), Steve 'Cappy' Rippingon (for discussions of Mongolia, and all the beers) and Tom 'Tomster' Salter (for IT help, good advice, being the most together guy in the house by far, and all the incredible puns), I'd like to thank Bungie for keeping the four of us entertained.

Thanks to my G40 office-mates; the inimitable Dr Graham Andrews (for encouragement, suggestions, and setting a fine example of how to write up) and Ben Ellis (for cups of tea, more cups of tea, cake, and then a nice cup of tea)

Thanks to my colleagues; Dave Cornwell (for all the snowboarding and lifts to places), Peter Fitch (for being an excellent chap, and for putting up with my constant presence at is house when Helen was living there), Simon Jowitt (for scientific chats, papers, and just for being THE JOW), Marc Reichow (for lifts to NIGL and science help & advice), Dan Smith (all the music, science, whisky and DoW).

Thanks to members of staff in the geology department for discussions, help and guidance; Gawen Jenkin (also thanks for all the shouts of encouragement at home-time), Charlie Moon, Mike Norry, Mike Branney, Sarah Davies, Jan Zalasiewicz, Nick Marsh, Rob Kelly, Tim Brewer, Steve Temperly, Richard England, Andy Saunders, Andrew Myers, Colin Cunningham.

And to the remaining staff and postgrads who I've not mentioned: you've enhanced my time here by making the department a fun and friendly place to be, I thank you all.

I've been at Leicester a long old time, and when I first arrived here in 1998, I couldn't have imagined that almost a decade later I'd still be here, not getting much sleep, sitting in an office, surrounded by monitors, thinking about Mongolia and geology. Over that time many people have come and gone, some legendary times have been had, and I've met a lot of people that I feel honoured to be able to call friends. These people are too numerous to mention directly, but to you all I say 'cheers' and hope to see you out there sometime.

James Blight

December 22nd, 2006

Table of Contents

Index of Figures

Chapter 1

Chapter 2

Introduction 1

This thesis concerns the Palaeozoic crustal evolution of the Saykhandulaan inlier, a large area of basement exposure within the Southeast Gobi Desert region of Mongolia (Fig. 1.1). The Saykhandulaan inlier contains one of the largest areas of basement rock exposure in southeast Mongolia and thus provides an important window into the Palaeozoic crustal evolution of the region. The inlier contains a wide range of Palaeozoic lithologies, including diverse volcanic rocks, siliciclastic and volcaniclastic sedimentary rocks and a major monzonitic intrusion (the Oyut Ulaan intrusive complex) which has potential economic copper-gold mineralisation. The Saykhandulaan inlier is within the Southeast Gobi Mineral Belt, which has developed into a major industrial exploration frontier province during the last fifteen years (Fig 1.1). In this thesis, the tectonic setting and geological history of the Saykhandulaan inlier are interpreted, and mineralised intrusions from the inlier and the surrounding region are put into spatial, temporal and lithological context (Fig 1.1).

The specific objectives of this project were: (1) to document the basement rocks of the inlier including their protoliths and environments of deposition; (2) to establish the structural architecture and extent and nature of metamorphism; (3) to describe the volcanic stratigraphy and establish its volcanic environment; (4) to document the magmatic evolution of the Oyut Ulaan intrusive complex, and its relationship to surrounding volcanic sequences within an evolving tectonic setting; (5) identify age and geochemical character of the Oyut Ulaan intrusive complex and other mineralised intrusions from the region, in order to investigate the timing and distribution of silicic magmatism and associated mineralisation within the Southeast Gobi Mineral Belt and; (6) to test existing terrane models for Palaeozoic arc magmatism and accretion in southeast Mongolia.

Fieldwork was carried out over twenty weeks in the summers of 2003 and 2004, mainly within the Saykhandulaan inlier (Fig 1.1). A range of geological techniques was employed, including completion of structural transects, lithological mapping and sedimentological analysis of key sections, and sampling for petrological, geochemical and geochronological analysis. Six granitoids were also sampled for geochemical and geochronological analysis from the neighbouring Mandakh inlier (Fig 1.2).

Laboratory work was carried out at the University of Leicester, the British Geological Survey, and the NERC Isotopes Geosciences Laboratories, and included X-ray fluorescence, to measure major and trace element abundances for a suite of volcanic and intrusive

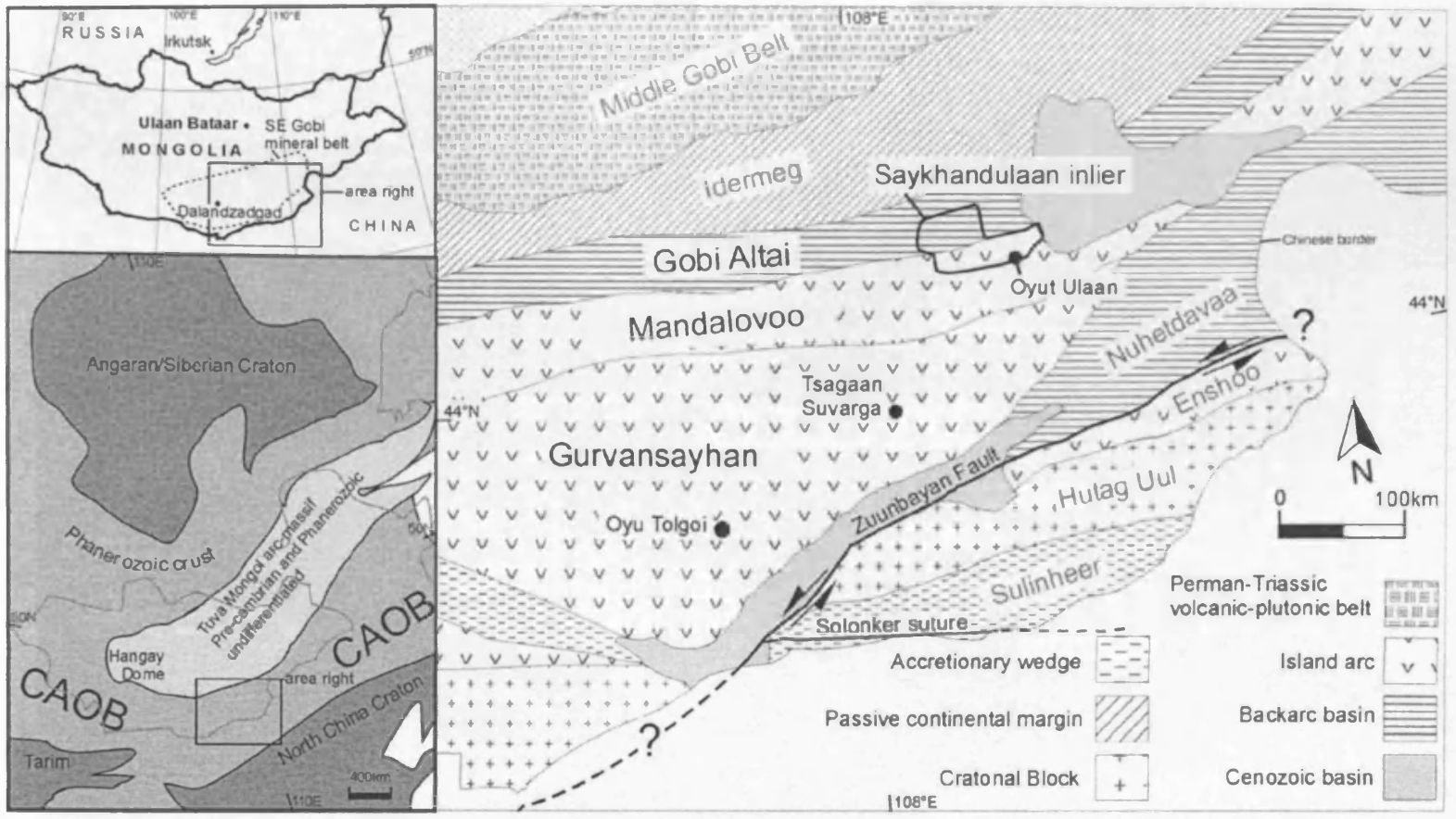

Fig 1.1 Tectonostratigraphic terrane map of South East Mongolia, after Badarch et al. (2002). Location and offset sense of Zuunbayan Fault after Lamb et al. (1999). Location of Solonker Suture after Xaio et al. (2003) Location of terrane boundaries in China not shown because of uncertain correlations there. Inset maps show regional political boundaries (top) and locations of Precambrian cratons and terrane collage comprising Central Asian Orogenic Belt (CAOB) after Şengör and Natal'in (1996) and Helo et al. (2006); bottom).

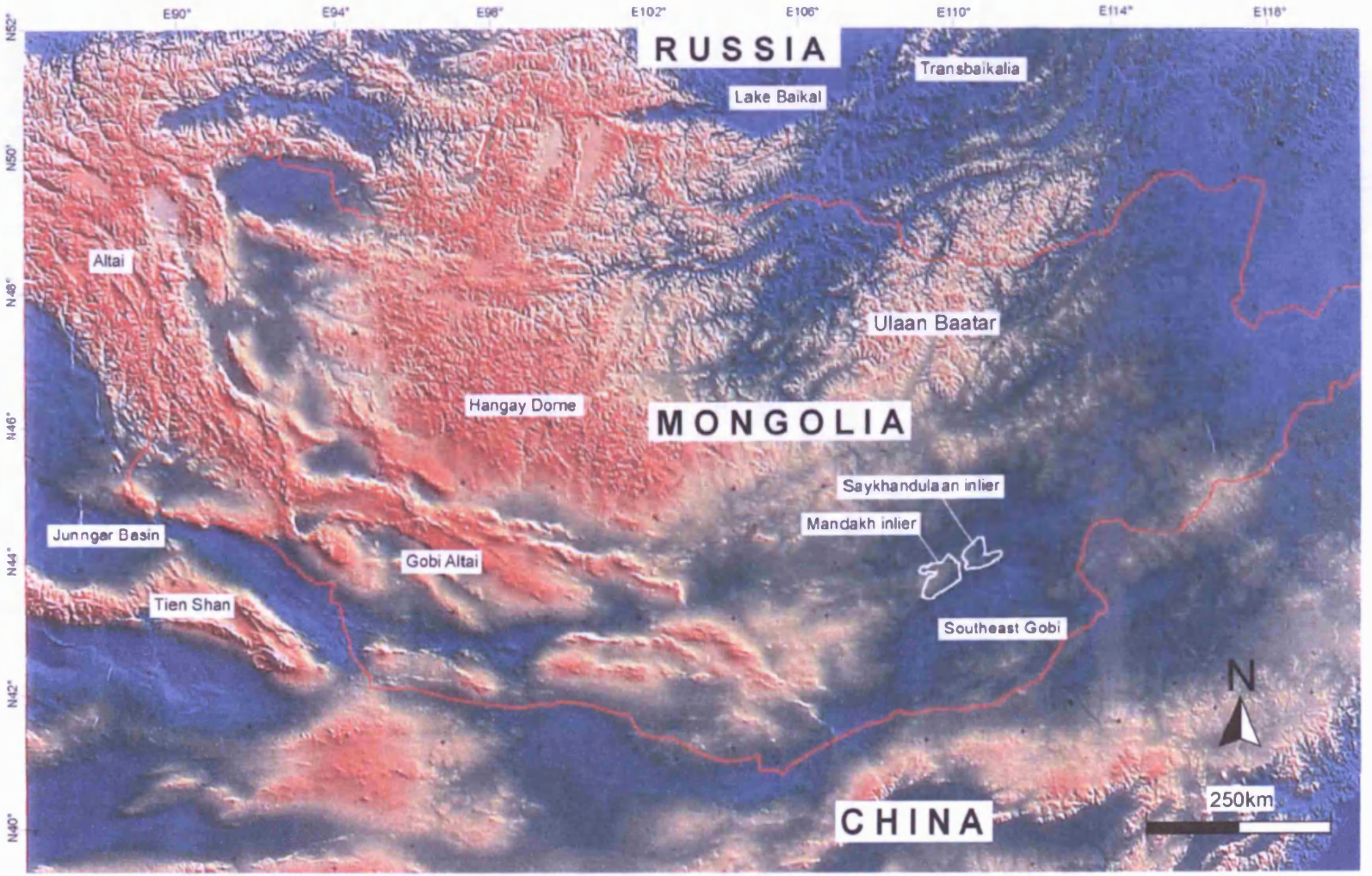

Fig 1.2 Digital elevation model of Mongolia showing locations of various mountain ranges.

samples; and U-Pb isotope geochronology, to develop a detailed time-sequence for the emplacement of mineralised intrusions and volcanism within the region. Petrography was carried out to document lithologies and textures, establish sedimentary provenance, and measure mineral modal abundances. Satellite image interpretation was undertaken, at several scales, to identify structures and geomorphological features.

1.2 Wider Context of Project

This project connects with longstanding geological research activities in Mongolia, carried out by members of the Crustal Processes Group at the University of Leicester. The project builds on previous work, concerning the structure and basin architecture of the Altai and Gobi Altai (Cunningham, 1998; Buchan et al., 2002; Windley et al., 2002; Cunningham, 2005; and references therein) however, it also represents a new direction because it concerns the basement evolution, crustal growth and metallogeny of southeast Mongolia. The project was funded by the National Environmental Research Council (NERC). The British Geological Survey (BGS) supported and co-supervised this work, and it forms part of ongoing involvement by the BGS into economic minerals research and international development. Ivanhoe Mines Ltd is carrying out a wide-ranging mineral exploration programme across southern Mongolia following on from their development of the giant Oyu Tolgoi (Fig 1.1, 1.3) gold-rich copper porphyry within the region. Ivanhoe Mines Ltd provided scientific and logistical support to this project.

1.3 Chapter Synopsis

This thesis contains three chapters that have each been prepared as pre-publication manuscripts.

In Chapter 2 the lithology and structure of the Saykhandulaan inlier are described. The inlier is comprised of Devonian-Permian lithologies, and has a dominant E-W structural grain. Results from cross-strike transects within the Saykhandulaan inlier reveal that it can be subdivided into five parallel E-W striking litho-tectonic domains; 1) the Northern Slate Belt, comprising Devonian greenschist grade pelites and psammites with deep-marine to coastal siliciclastic protoliths; 2) the Saykhandulaan Valley Lineament Zone (SVLZ), a tectonised zone of faulted and lithologically altered volcanic rocks; 3) the High Strain Belt, consisting of tightly folded and flattened metamorphosed clastic sedimentary rocks; 4) the Molasse Succession, consisting of relatively undeformed coarse conglomerates and

sandstones and, 5) the Oyut Ulaan Volcanic Group, a nearly 5 km-thick folded Carboniferous volcanic succession that hosts the mid-Carboniferous Oyut Ulaan mineralised intrusive complex. The Northern Slate Belt metasedimentary rocks record a northerly cratonic provenance, whereas all rocks to the south of the SVLZ have arc affinities. The SVLZ is interpreted to be a major terrane boundary between the Gobi Altai and Mandalovoo terranes. Two major deformation events are interpreted in the region; 1) back-arc basin closure and inversion involving regional scale folding and greenschist grade metamorphism in the Northern Slate and High Strain Belts; 2) contraction associated with Mandalovoo terrane accretion and final closure of the Palaeo-Asian Ocean to the south. Following terrane accretion and cessation of subduction, crustal extension and strike-slip faulting further modified the crustal architecture of the inlier. Chapter 2 has been submitted for publication in a special issue of the *Journal of Asian Earth Sciences* on the geodynamics and metallogeny of the Altaid Orogeny. It was favourably reviewed and is now awaiting final acceptance.

Chapter 3 focuses on the stratigraphy and magmatic evolution of the Oyut Ulaan Volcanic Group (OUVG). The OUVG is a sequence of volcanic and sedimentary rocks, which provides important evidence for the nature of arc activity in the southeast Mongolia sector of the Central Asian Orogenic Belt during the Carboniferous. The OUVG forms the southern part of the Saykhandulaan inlier, and is comprised of four distinct formations. The Yasun Eliy-e Formation is composed of basalts, basaltic andesites, conglomerates and immature volcanic sandstones and is intruded by the mineralised Oyut Ulaan Granite; the Gurvan Morin Höndiy Formation is comprised of interbedded coarse conglomerates, sandstones and thick andesites and basalts; the Shargyn Moghai formation is entirely composed of volcanic lithologies with a range of compositions from basalts to dacites; finally, the Tsagaan Nuruu formation is composed of thick ash-fall deposits punctuated by lava-like ignimbrites. Physical volcanological and sedimentological interpretations characterise three clear eruptive styles; periodic andesite volcanism in an actively eroding arc-setting, containing large rivers and swamps; highly effusive andesite-field volcanism; and explosive rhyolitic volcanism. Geochemical analyses of volcanic lithologies suggest the group represents subduction-related, mature, continental-arc volcanism. Interpretations of geochemical results relate surface processes of the volcano-sedimentary model to an evolving magma chamber. Magma pulses and replenishments are identified from variations in the chemostratigraphy. Zircon U/Pb isotope ages from a felsic volcanic horizon and a granitoid cobble from an intercalated conglomerate constrain the timing of extrusion of the

OUVG to the mid-Carboniferous, and show that the OUVG contains clasts derived from older arc-related plutons, emplaced, uplifted, eroded and deposited within around 10 M.y. Chapter 3 will be condensed and submitted for publication to *Earth and Planetary Science Letters* in 2007.

Chapter 4 has two parts. The first part documents the field relations, geochemical evolution and absolute age of the Oyut Ulaan intrusive complex, which cuts the Oyut Ulaan Volcanic Group. The Oyut Ulaan intrusive complex was selected for study because, at the onset of the project, it was a focus for exploration activity. Now, three years later, exploration interests have shifted elsewhere, but the complex remains of academic interest. Oyut Ulaan is a quartz-monzonite pluton, elongate in the EW direction, which is apparently fault bound on most sides. The main intrusion is cut by several sets of dykes of varying lithologies, and a tourmaline breccia pipe cluster that post-dates the dykes. The magmatic evolution and dyke paragenesis are discussed, and new absolute age data are presented for the quartz-monzonite and for a major andesite dyke swarm that cuts the intrusion.

The second part of chapter 4 concerns geochemical and geochronological data from one other intrusion within the Saykhandulaan inlier and six other intrusions within the Mandakh inlier (Figs. 1.2 & 1.3). The Mandakh inlier has a much larger proportion of its outcrop area taken up by granitoid lithologies. New absolute age data are presented for four of the intrusions, and comparisons are made between these bodies and the Oyut Ulaan intrusive complex, and also other mineralised and non-mineralised intrusions from the wider region. It is planned that chapter 4 will be condensed and submitted for publication to the Journal of the Geological Society in 2007.

Chapter 5 is a conclusion section in which results and interpretations from each of the preceding three chapters are synthesised, and integrated, to develop a new model for crustal growth and terrane accretion in southeast Mongolia.

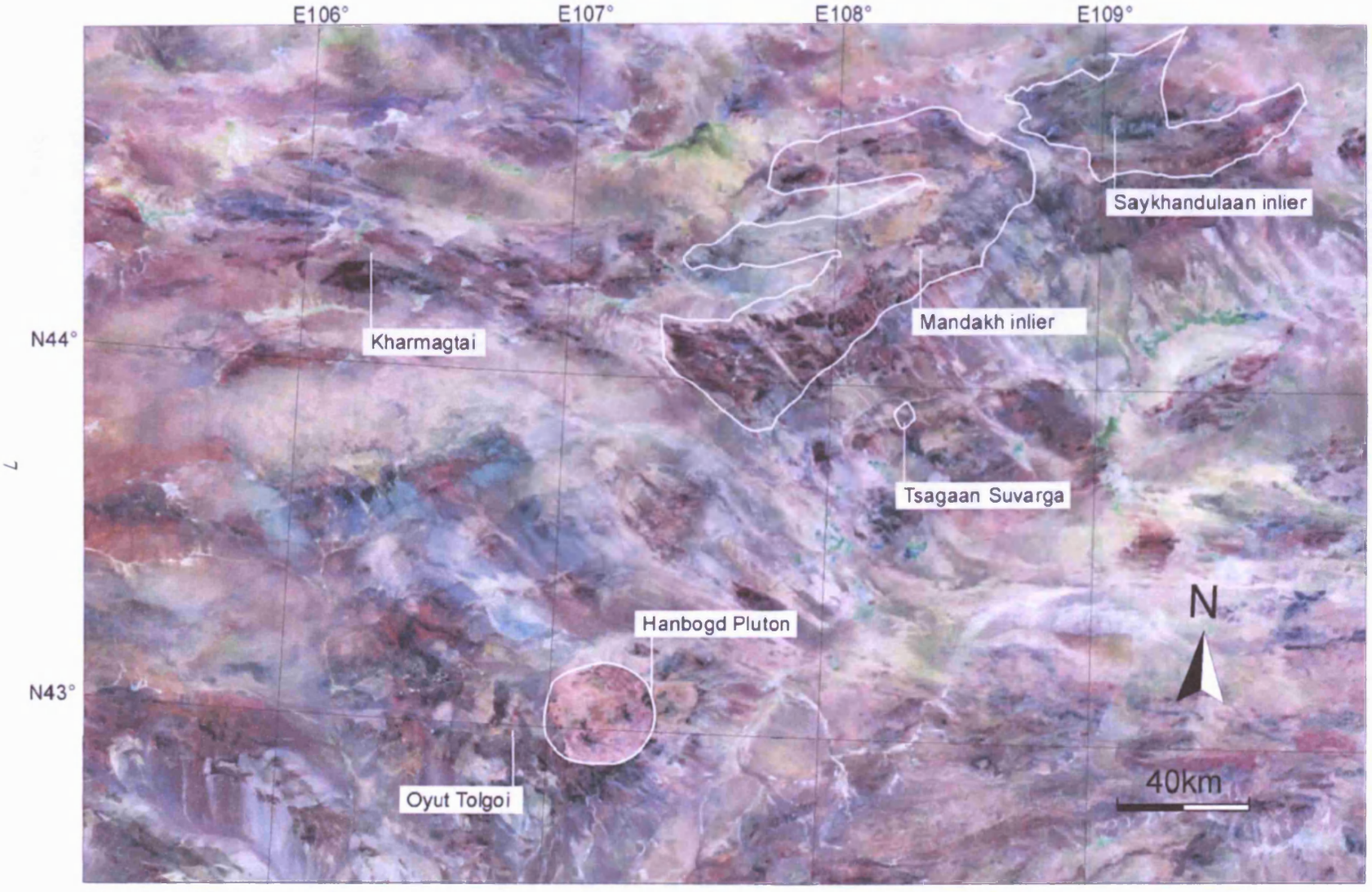

Fig. 1.3 Satellite image showing locations of inliers investigated in this study and mineral deposits from the SE Gobi region.

Crustal evolution of the Saykhandulaan Inlier, Mongolia: Implications for Palaeozoic arc magmatism, polyphase deformation and terrane accretion in the Southeast Gobi Mineral Belt

2

2.1 Introduction

The Gobi region of southeastern Mongolia lies within the Central Asian Orogenic Belt (CAOB), the Earth's largest area of Phanerozoic continental growth, and is a natural laboratory for documenting processes of terrane accretion and amalgamation (Şengör et al., 1993; Şengör and Natal'in, 1996; Badarch et al., 2002). Important mineral deposits have been discovered in the SE Gobi region during the last decade and consequently the region is now a major mineral exploration province. Nevertheless, few studies exist documenting the basement evolution and lithotectonic context of the SE Gobi mineral belt (Lamb and Badarch, 2001; Badarch et al., 2002; Xiao et al., 2003). This is partly because the area is remote, has low relief, and in general, displays poor outcrop exposure. However, the Saykhandulaan Inlier (Fig. 1.1), which crops-out 400 km to the south of Ulaan Baatar is unusual because it contains a large area of basement exposure and provides a good opportunity for unravelling the major tectonic, metamorphic and intrusive events that have affected the SE Gobi mineral belt. In addition, it hosts the Oyut Ulaan Cu-Au porphyry prospect and is along strike from other major exploration targets in the region. Therefore, a detailed multidisciplinary study incorporating field investigations and structural and geochemical analysis was carried out during 2004-2006 to document the crustal evolution of the Saykhandulaan Inlier and the terrane context of SE Gobi mineralisation.

2.1.1 Regional geology

The CAOB records terrane accretion and crustal growth between the Angaran craton (also known as the Siberian Craton) and the North China Craton from the Late Precambrian to Permian (Fig. 1.1). The CAOB reaches from Kazakhstan to Eastern Siberia and averages around 300 km wide (Xiao et al., 2003; 2004). Terranes in Southern Mongolia lie within the CAOB, to the north of the main Permian Solonker suture, which marks the final closure of the Palaeo-Asian Ocean in the Permian (Wang and Liu, 1986; Xiao et al., 2003; Li, 2006). The basement geology of South Mongolia consists of island-arc, backarc/forearc basin and accretionary prism terranes that accreted around a Precambrian cratonic block that lies under the Hangay Dome in central Mongolia (Fig. 1.1; Şengör and Natal'in, 1996; Badarch et al.

2002). These terranes record the tectonic evolution of the northern margin of the Palaeo-Asian Ocean during the Palaeozoic, generally interpreted to have taken place above a northward dipping subduction zone.

Two hypotheses exist for the formation of the Mongolian CAOB crust during the Palaeozoic. Şengör and Natal'in (1996), postulated one long-lived island-arc, with a complex history of magmatic front migration, strike-slip motion and oroclinal bending along its length prior to terminal accretion (Fig. 2.1a). An alternative model by Mossakovsky and Dergunov (1985), and developed by Ruzhentsev and Pospelov, (1992), Zorin et al., (1993) Mossakovsky et al. (1994), and Badarch et al. (2002), proposed the existence of multiple island arcs drifting across the Palaeo-Asian Ocean and accreting various arc-marginal basin terranes and ophiolite slivers before terminal collision against the southern margin of Siberia/Hangay (Fig. 2.1b).

Badarch et al. (2002) suggest that southeastern Mongolia is dominated by two Ordovician-Carboniferous island-arc terranes (Fig. 1.1), the Gurvansaykhan and Mandalovoo terranes, which are surrounded by the Ordovician-Carboniferous Gobi Altai back-arc/fore-arc terrane to the north and the Nuhetdavaa back-arc/fore-arc terrane to the

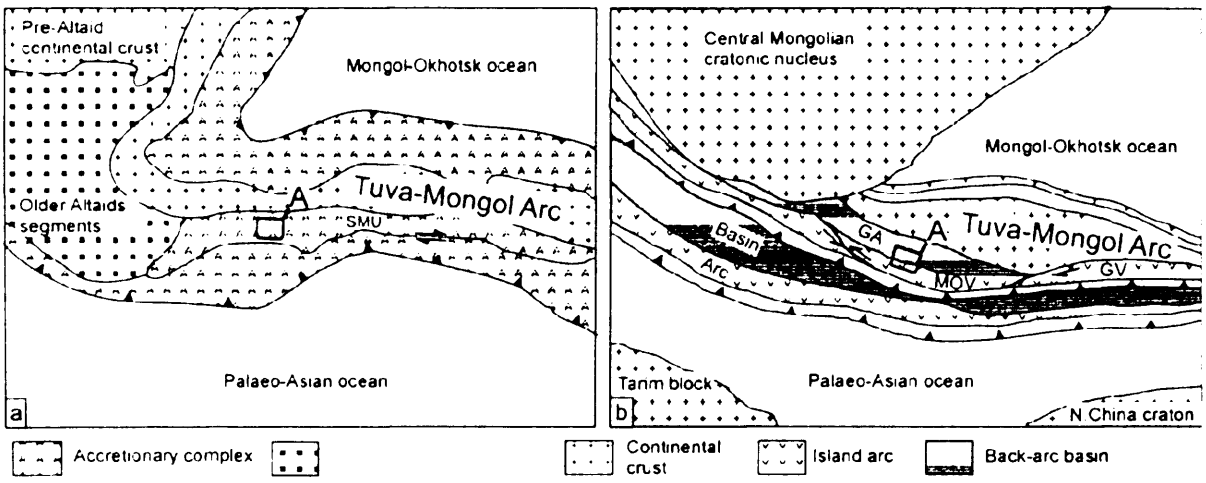

Fig. 2.1 Two interpretations of the tectonic setting in southeast Mongolia during Devonian-Carboniferous time. a) Early Carboniferous palaeotectonic reconstruction of the Tuva-Mongol arc (after Şengör and Natal'in, 1996). Growth of the arc takes place via accretion above northward dipping subduction zone, and strike-slip faulting along the arc front. The South Mongolian Unit (marked SMU) is a subduction-accretion complex, which represents the majority of the Palaeozoic crustal growth in southeast Mongolia. Box A shows approximate position of the study area. b) Simplified reconstruction of Devonian-Carboniferous terrane positions in South Mongolia, after Badarch et al. (2002). The diagram shows two northward dipping subduction zones beneath parallel E-W island arcs. The Mandalovoo (MOV) and Gurvansayhan (GV) terranes represent laterally contiguous sections of the same arc. The Gobi Altai terrane (GA) is a back arc basin to the north of the arc. Back-arc/ fore-arc basins to the south (marked 'Basin') include, from west to east, segments identified by Badarch et al. (2002) as the Baaran, Atasbogd and Nuhetdavaa terranes (un-differentiated on diagram). The arc to the south (marked 'Arc') includes, from west to east, segments identified by Badarch et al. (2002) as the Baytag, Hashaat and Enshoo terranes (un-differentiated on diagram), box A shows approximate position of the field area (Fig 2.2).

south. The Gurvansaykhan and Mandalovoo terranes are interpreted to have originally been along-strike equivalents of a contiguous island arc, but dextral strike-slip faults shunted the Gurvansaykhan terrane southwest to its current location. South of these two terranes, near the Sino-Mongolian border, a series of parallel island-arc, accretionary wedge and cratonal terranes record a separate subduction-accretion history (Figs. 1.1, 2.1; Badarch et al., 2002).

Subsequent to Palaeo-Asian suturing at the end of the Permian, Mongolia underwent several periods of intracontinental deformation. Left-lateral strike-slip faults were active in southeast Mongolia from the Triassic to late Cretaceous (Lamb et al., 1999) and between 185-235 km of left-lateral offset occurred along the Zuunbayan Fault, which forms the southeast margin of the Gurvansaykhan terrane (Fig. 1.1). Further west, a Jurassic contractional phase of deformation is expressed by E-W trending thrust faults along the Mongolian-Chinese border (Zheng et al., 1996). Southeast Mongolia and adjacent regions of China experienced a major phase of NW-SE crustal extension during the Jurassic-Cretaceous (Meng et al., 2003). Jurassic-Cretaceous clastic and volcanic stratigraphy fill low-relief basins throughout the region including areas adjacent to the Saykhandulaan Inlier. The rifting is interpreted to be a distal effect of Pacific-rim back-arc extension (Graham et al., 2001). Cretaceous-Tertiary thermal uplift and volcanism are widely distributed in central, southern and southeastern Mongolia and are possibly related to a steady state thermal anomaly in the mantle beneath Mongolia and Eastern China (Barry and Kent, 1998). Sinistral transpressional deformation driven by the Indo-Eurasia collision, has reactivated the Gobi Altai region in south and west Mongolia during the late Cenozoic (Cunningham, 1998). However, there is only limited evidence for renewed tectonism in southeast Mongolia (Webb and Johnson, 2006)

Major porphyry copper discoveries in the region include the Oyu Tolgoi gold-rich deposit, which occurs within the Gurvansaykhan arc terrane, 260 km to the southwest of the Saykhandulaan Inlier (Fig. 1.1; Badarch et al., 2002). Mineralisation at Oyu Tolgoi is associated with arc related Siluro-Devonian porphyry magmatism intruded into lavas and clastic sedimentary rocks (Perello et al., 2001). Another important deposit is Tsagaan Suvarga, a copper-molybdenum porphyry hosted in a Devonian calc-alkaline granite complex, 120 km southwest of the Saykhandulaan Inlier (Fig. 1.1; Watanabe and Stein, 2000). To the north, the Mandalovoo terrane also contains several porphyry-style prospects in an east-west trending belt. Part of the Mandalovoo terrane lies within the Saykhandulaan Inlier and contains the Oyut Ulaan copper-gold prospect (Fig. 1.1).

2.2 Litho-tectonic domains

The Saykhandulaan Inlier spans the boundary between the Gobi Altai terrane to the north, and the Mandalovoo terrane to the south (Fig. 1.1). The Saykhandulaan Valley Lineament Zone (SVLZ) trends approximately east-west and marks the terrane boundary through the inlier (Fig. 2.2). Five lithological and structural domains are identified within the inlier (Fig. 2.2). North of the SVLZ is the Northern Slate Belt (NSB) which contains folded siliciclastic meta-sediments. The NSB is overlapped in the east and north by several basalt fields (undated, but probably correlative with Jurassic-Cretaceous lavas elsewhere in the region). The SVLZ is 1 - 1.5 km wide and contains a range of lithologies, including volcanic rocks of the Saykhandulaan Valley Formation (SVF) which mainly consist of altered intermediate and felsic lavas. To the south of the SVLZ are several parallel litho-tectonic domains. The High Strain Belt (HSB) contains greenschist grade meta-sandstones and conglomerates deformed into tight-to-isoclinal folds. It is exposed across the full east-west width of the inlier. The Molasse Succession (MS) contains relatively undeformed conglomerates, sandstones and mudstones, and crops out to the south of the HSB. The Oyut Ulaan Volcanic Group (OUVG) contains a wide range of volcanic and sedimentary

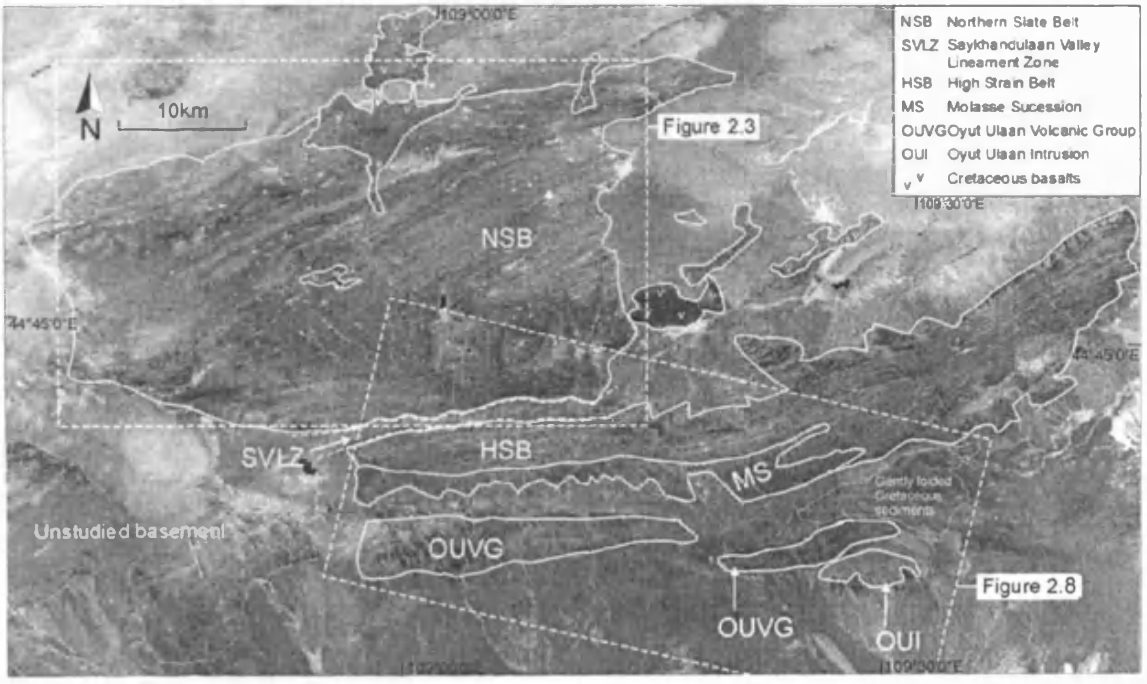

Fig. 2.2 Landsat image of Saykhandulaan Inlier, location shown in Fig. 1.1. Litho-tectonic domains marked: NSB - Northern Slate Belt; SVLZ - Saykhandulaan Valley Lineament Zone; HSB - High Strain Belt; MS - Molasse Succession; OUVG - Oyut Ulaan Volcanic Group; OUI - Oyut Ulaan Intrusion. Areas outside of marked litho-tectonic domains contain Mesozoic-Cenozoic sedimentary cover sequences and lavas.

lithologies and defines the southern margin of the inlier. The Oyut Ulaan Intrusion (OUI) cuts rocks of the OUVG in the southeast corner of the inlier (Fig. 2.2). The inlier is surrounded by basins containing Upper Jurassic to Cretaceous and Quaternary sediments (Figs. 2.2, and 2.3; Graham et al., 2001). The inlier contains subdued topography with a maximum relief of 50 m, outcrop quality is variable and in many areas contacts and faults are not exposed.

Lithological characteristics of each of the domains defined above are described in detail from north to south.

2.2.1 Northern Slate belt

The Northern Slate Belt is a folded meta-sedimentary sequence (Figs. 2.2 and 2.3). Its metamorphic grade reaches lower greenschist grade in some areas. In the north, this sequence is dominated by pelites with well-developed cleavage; the protolith coarsens to the south where fine- to medium-grained psammites locally dominate. An outstanding feature of this unit is the presence of abundant and volumetrically significant quartz veins.

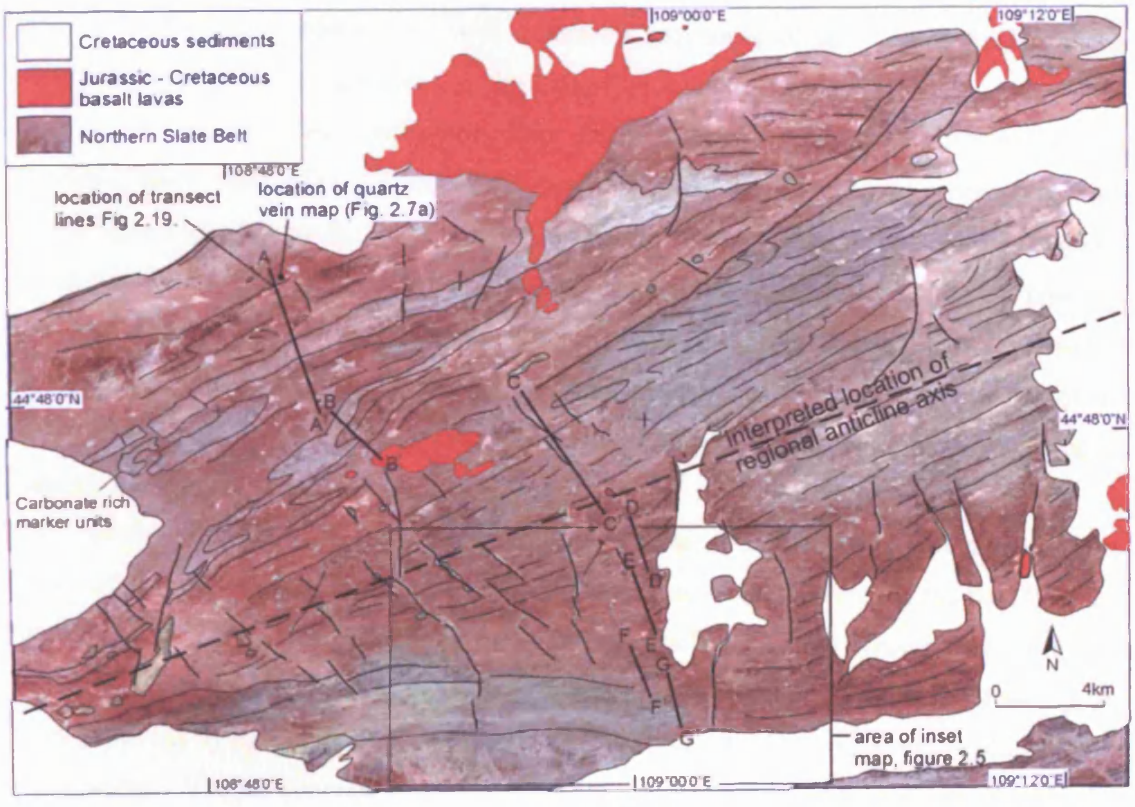

Fig. 2.3 Interpreted Landsat image of the Northern Slate Belt. Dominant NE-SW structural grain emphasised with fine lines. Locations of transect segments shown.

The main rock type of the NSB is grey pelite, which crops-out in beds 0.5 to 2 m thick throughout the belt. Few original sedimentary features were observed, but rare graded bedding occurs and in some localities units exhibit clay drapes and fine-sand lag-bases. The sequence also features sparsely distributed 20 to 50 cm thick beds of fine- to medium-grained meta-psammite which appear brown on weathered surfaces, and locally exhibit planar cross stratification (Fig 2.4 a).

In the west of the NSB where shallower stratigraphic levels are exposed, psammitic lithologies are dominant, featuring up to 1 m thick medium-grained units interbedded with relatively thin (20 to 30 cm) pelitic material. In one section, flame and lobe structures, rip-up clasts and swaley cross stratification (Fig 2.4 b) occur in the psammite beds and provide younging criteria, however, original sedimentary features were rarely observed outside of psammite dominated areas.

Lithologies from the southwest corner of the NSB are generally less-deformed, are of a lower metamorphic grade than the rest of the belt, and are sandstone dominated. Lithological logs from the south of the NSB show tabular sandstone bodies of between 10 and 50cm thickness, interbedded with mudstone sequences of up to 1 m thick. Flame structures, lag bases, rip-up clasts and climbing ripples are present (Fig. 2.5).

In thin-section, the sand-grade units show different degrees of deformation and metamorphism, from relatively uncleaved greywacke (Fig 2.6, a and b), to greenschist-grade psammites (Fig 2.6, c to f). The metamorphic fabric consists of recrystallised quartz grains and a micaceous slatey cleavage. Several samples display a penetrative crenulation cleavage and some have isolated kink bands. Locally, siderite forms a cement and secondary replacement phase. The rocks are generally more calcareous in the northern sector of the NSB; sparse outcrops of a bio-micritic limestone with small broken crinoid fragments occur near its northern boundary.

Throughout the NSB, quartz veins cut the succession, the largest of which can be seen from tens of kilometres away and form the highest topographic features in the belt (Fig. 2.7 The veins trend ENE, deviating from the orientation of the regional cleavage by 10 to 20°. Three generations of veins occur, the oldest are metre-wide veins (Fig. 2.7 b) which are commonly cut by main mega-vein bodies (Fig. 2.7 a), which are, in turn, cut by thin quartz-stockworks. Visible mineralisation is rare, although manganite (MnO·OH) was observed within zones densely penetrated by 30-70cm wide veins. The giant veins and vein zones are found in discrete corridors, with other areas exhibiting little to no veining. Several of the

Fig 2.4 a) Planar cross stratification in meta psammite of Northern Slate Belt; **b)** Swaley cross stratification in meta-psammite of Northern Slate Belt

Fig. 2.5 a-f) Lithological logs from southern zone of Northern Slate Belt. Coarser lithologies documented in these logs, occur in south of belt where psammitic bands are thicker and more widespread. Elsewhere, to the north, the belt is dominated by pelites with slatey cleavage. g) fine grained psammite and pelite interbeds similar to log c. h) flame structure preserved in relatively un-metamorphosed sandstone and mudstone from log f, beds young to top right.

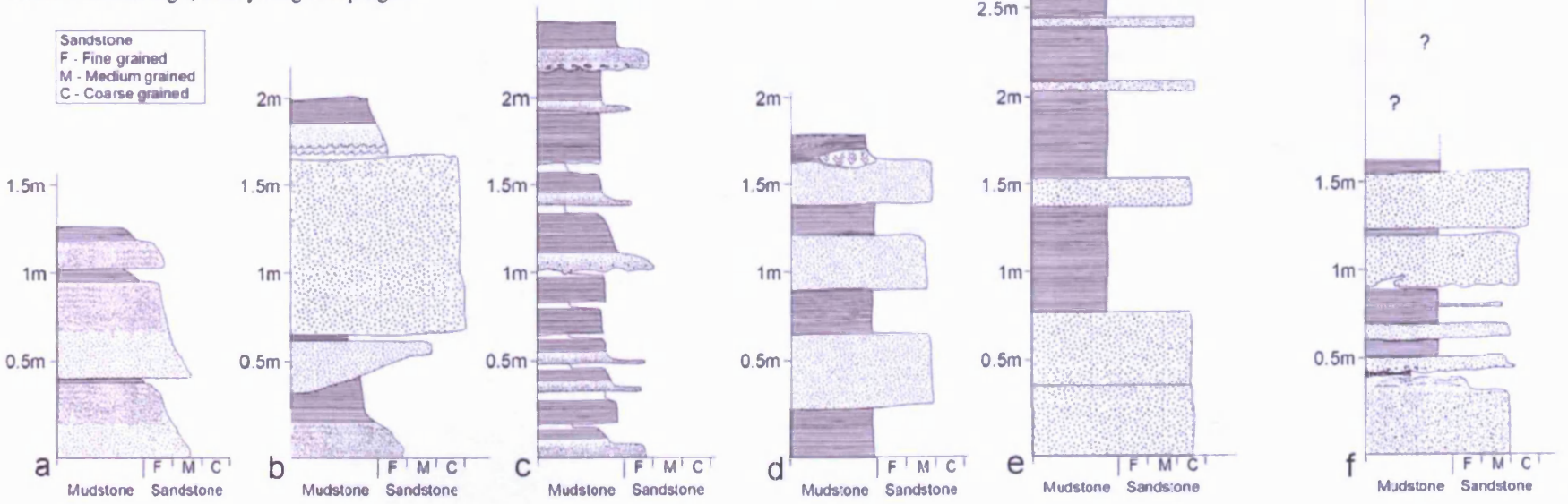

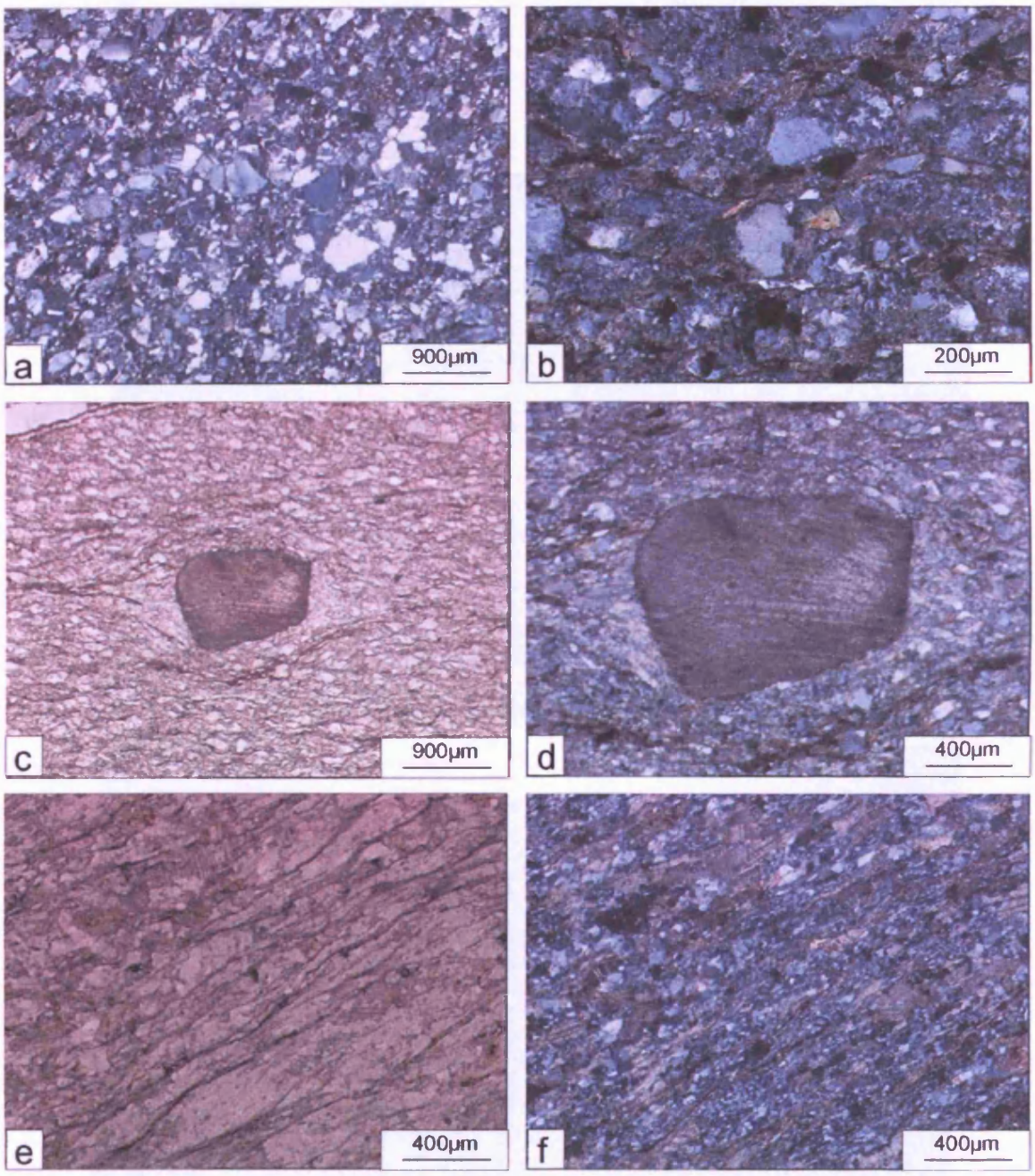

Fig 2.6 a), b) Greywacke from NSB in XPL,; **c) & d)** deformation around lithic clast in fine greywacke from NSB PPL, XPL respectively. **e) & f)** greenschist grade metapsammite with clear cleavage.

Fig. 2.7 a) Map of large en-echelon quartz vein array (location noted on Fig. 2.3) with arrows to show interpreted dextral shear sense. b) View NE of major quartz vein outcrop. c) View SE from top of vein outcrop, more large veins visible in distance. d) View NE of composite vein array.

larger tabular veins cut regional fold hinges and some smaller veins have saddle reef morphologies. Sets of veins have both right stepping (Fig. 2.7 a) and left stepping en-echelon morphology. The veins are largest in the southeast of the NSB, where the deepest stratigraphic levels are exposed. The veins are spatially related to coarser lithologies, and at several locations, psammitic beds feature stockworks of quartz veins. The geological map of Mongolia (Tomurtogoo, 1999) shows the NSB to be Devonian in age. However, no absolute radiometric ages are available for this assemblage.

2.2.2 Saykhandulaan Valley Lineament Zone

The SVLZ runs approximately east-west (085N) across the inlier, forming a 1 to 1.5 km wide corridor of small isolated hills with little outcrop, between the NSB to the north and HSB to the south (Figs. 2.2 and 2.8).

Volcanic strata of the Saykhandulaan Valley Formation are best exposed in a ridge that trends 070, in its western reaches of the SVLZ (see box marking location of outcrop on Fig. 2.8). An approximately 200m thick sequence of extrusive rocks (Fig. 2.9) crops out in this ridge. An amygdaloidal trachydacite (>20m) is at the base of the succession. This is overlain by a white rhyolite (~90m), which contains sub-planar flow-bands and local zones of intense flow-folding. A variably-brecciated trachyte (70 m) lies above this, and another trachyte (>25m), featuring dense euhedral feldspar phenocrysts, lies at the top of the sequence. Rhyolites and trachytes crop out at numerous other localities throughout the zone, commonly in prominent ridges with similar 070 trends.

Along the southern edge of the SVLZ, at the foot of some of the steepest and highest topography in the inlier, basic dykes crop-out, both parallel and perpendicular to the lineament. Brecciated and fractured lithologies are common near the ends of the prominent ridges in the zone. Cataclastic microtextures are seen in thin-section from several samples in these areas. Quartz in some of the felsic lithologies has been extensively recrystallised.

The geological map of Mongolia (Tomurtogoo, 1999) shows the area of the SVLZ to be Carboniferous and Permian in age. However, no absolute radiometric ages are available for lithologies from within the SLVZ.

2.2.3 High-Strain Belt

The HSB is the zone of highest deformation in the inlier (Fig. 2.8). Its northern margin is the abrupt southern edge of the SVLZ. Directly south of the SVLZ, altered, green, cobble- to boulder-conglomerates, containing clasts of mafic extrusive lithologies, form

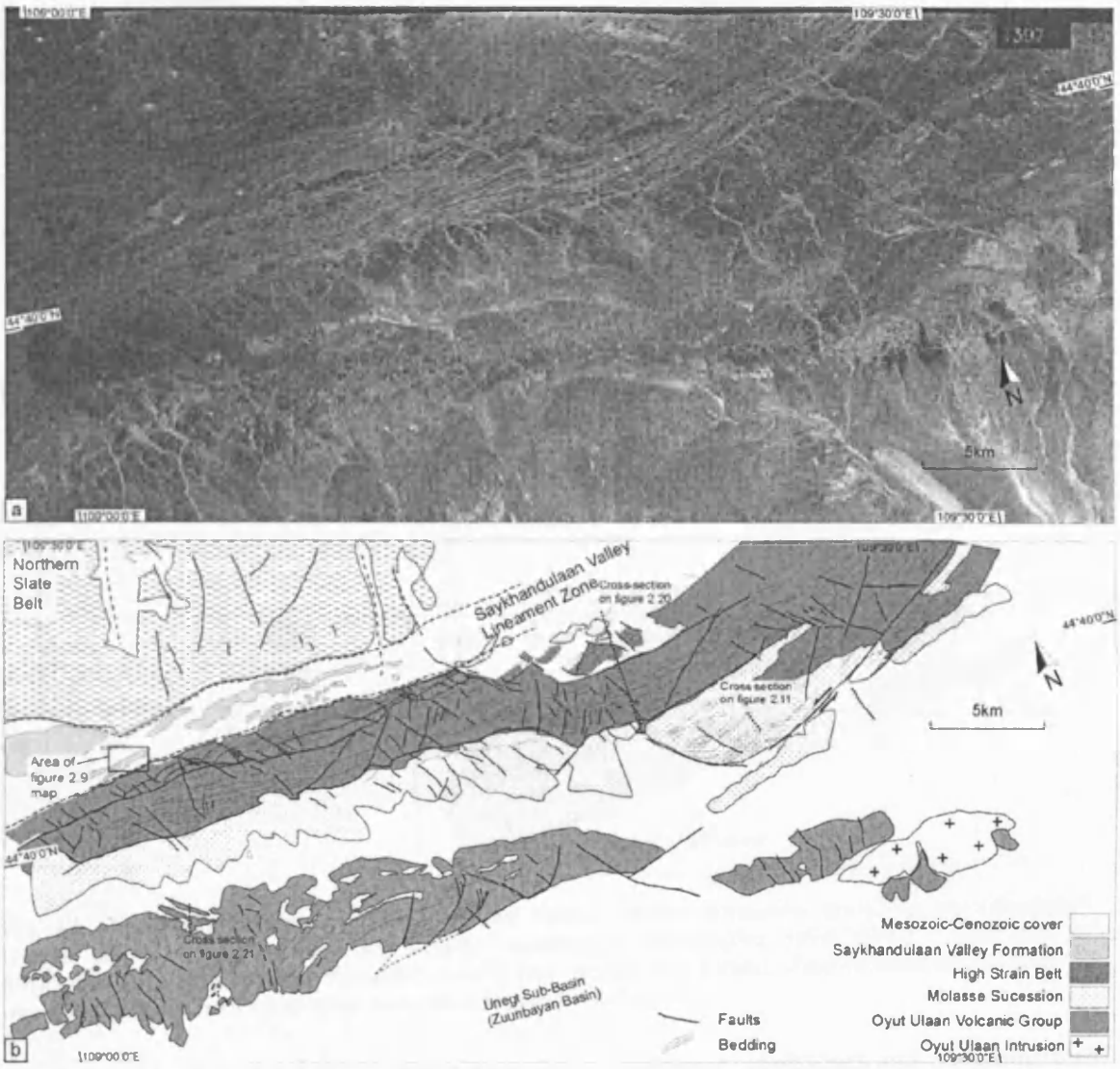

Fig. 2.8 - a) Aerial photograph of the southern part of the field area. Location of Fig. shown in Fig. 2.2. Notice dominant ENE-WSW structural grain. b) Interpretation of Fig. 2.8 a showing litho-tectonic units: High Strain Belt, Molasse Succession; Oyut Ulaan Volcanic Group; Oyut Ulaan Intrusion. Dominant structural grain marked with fine lines. Faults, observed and interpreted, marked with thicker lines. Locations of transect lines shown.

ENE trending ridges comprising the highest topography of the inlier (Fig 2.10). The metamorphic grade appears locally elevated; some metabasite clasts are entirely altered to amphibolite. Two parallel bands of these higher-grade rocks occur in the north of the HSB, with a narrow band of greenschist-grade meta-clastic rocks between them. The relationship between the areas of lithologies with different metamorphic grades is not clear, as the contact between them is not exposed.

South of the meta-conglomerates, the HSB is comprised of meta-clastic rocks featuring a range of protolith grain sizes from mud to gravel-conglomerate. This part of the belt is similar to the NSB; cleavage is generally dominant, and the rocks are of greenschist grade,

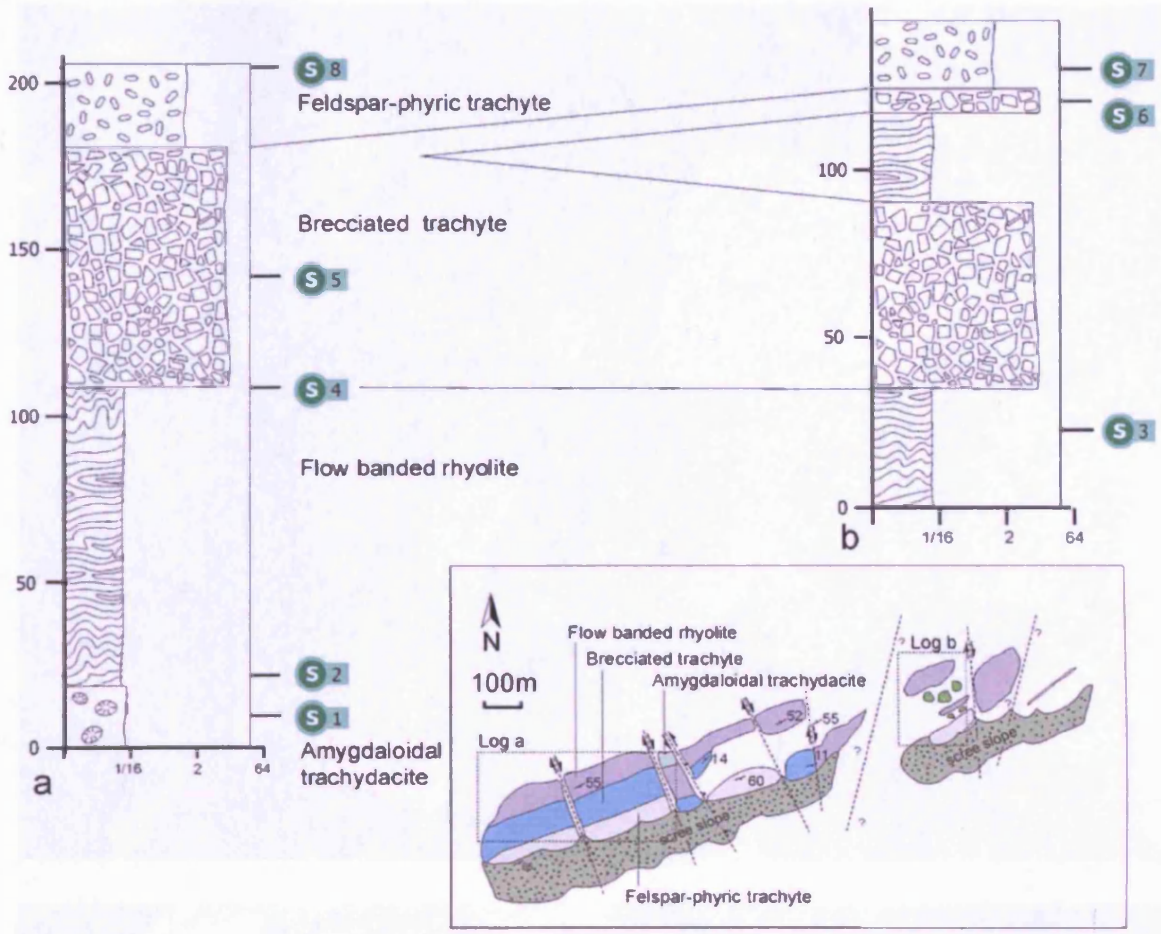

Fig. 2.9 Stratigraphic columns for Saykhandulaan Valley Volcanic Formation, grain size and lithological features shown. Samples taken for analysis numbered in stratigraphic order; S1-S8. Inset map of Saykhandulaan Valley Volcanic Formation outcrop (see Fig. 2.8 for location). Fault orientations and sense of movement inferred from topographic features and contact offsets.

comparable to that of the NSB meta-clastic rocks. However, sandstones and conglomerates are the main protolith here, compared with mudstones in the NSB. Coarse sandstones are widespread, are generally 0.5 to 2m thick and display cross-stratification, graded and lenticular bedding, and laminated mudstone tops featuring ripple structures.

The geological map of Mongolia (Tomurtogoo, 1999) shows the HSB to be early Carboniferous in age. However, no absolute radiometric ages are available for this assemblage.

2.2.4 Molasse Succession

The Molasse Succession (Fig. 2.11) is characterised in the west by un-metamorphosed coarse conglomerates, and in the east by interbedded fine sandstones and mudstones.

Thick channel-based conglomerates mixed with coarse sands (Fig. 2.11, log a) dominate the molasse succession. The conglomerate beds are poorly sorted, heterolithic,

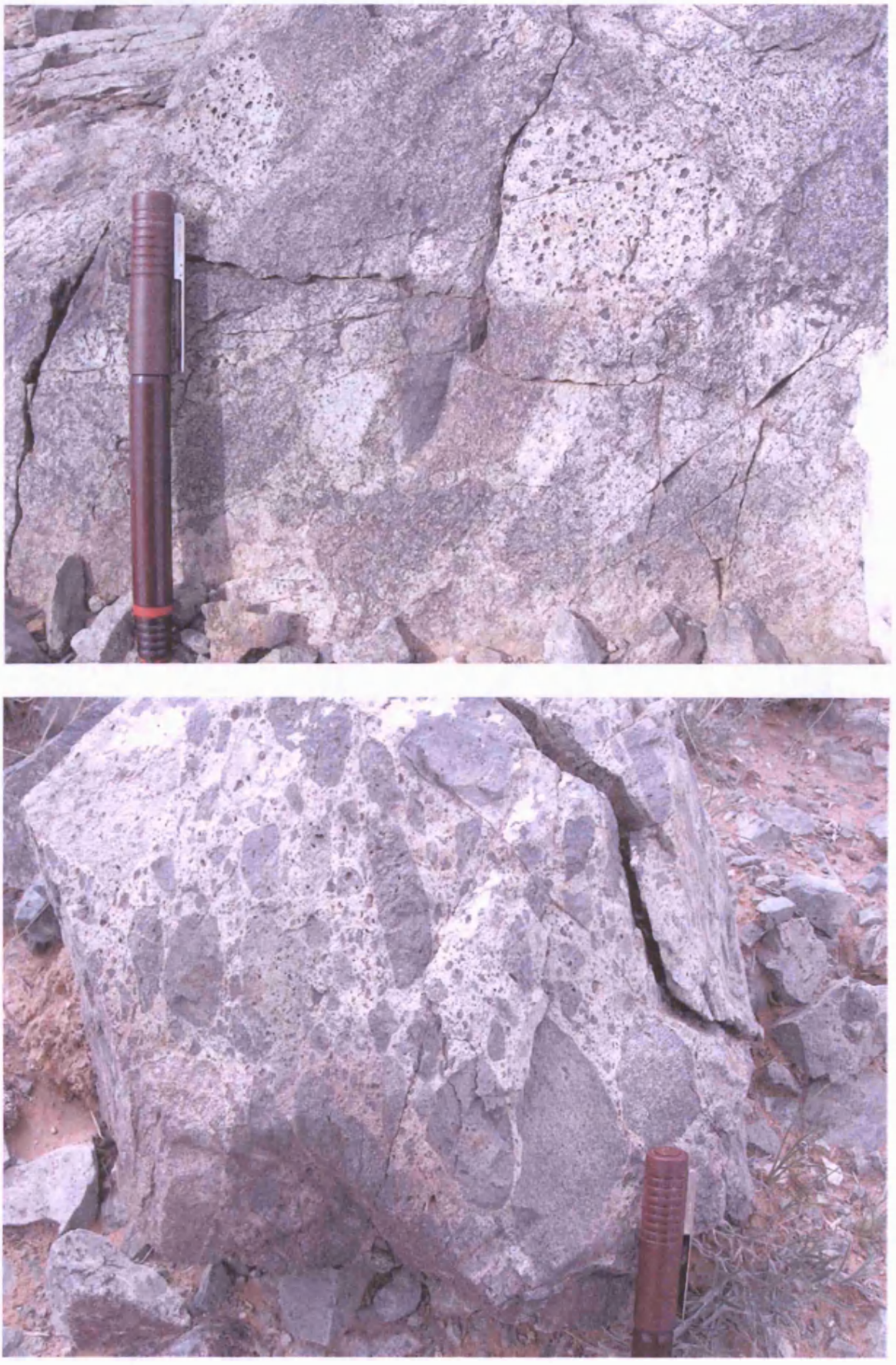

Fig 2.10 Conglomerates from the northern margin of the High Strain Belt.

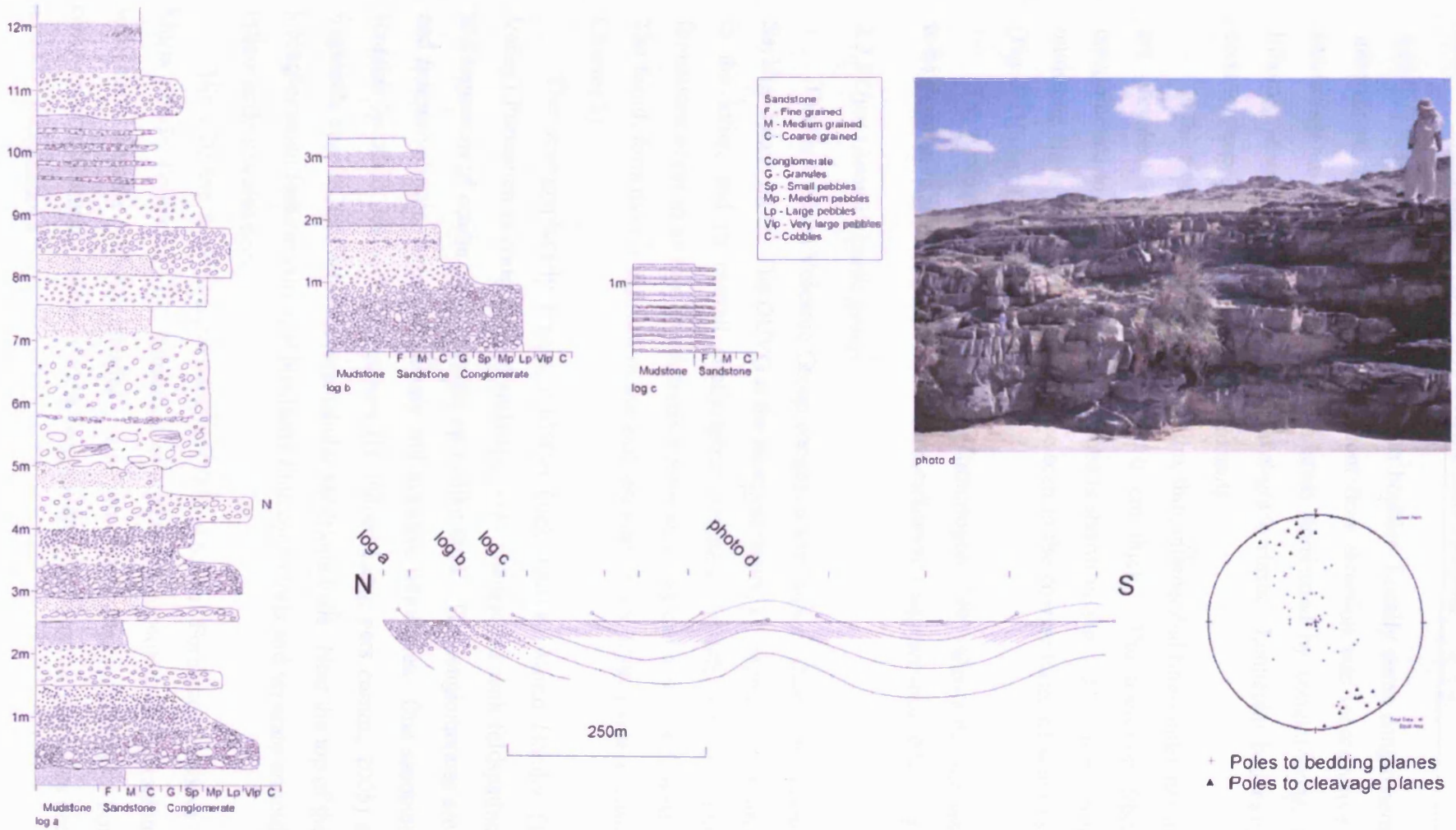

Fig. 2.11 Lithological logs and photographs from Molasse Sucession (MS) showing fining upward tendency from conglomerates to intercalated fine-sand and mudstones. Photograph of horizontal sandstone and mudstone beds Logs and photograph located on inset transect line (location of transect shown on Fig. 2.8). Lower hemisphere, equal area stereoplot of MS structural data

with grain sizes ranging from granule to boulder. Locally some conglomerate units show imbrication, but evidence for a prevalent flow direction was inconclusive. The coarse sandstones comprise both a matrix in areas dominated by conglomerate, and the main lithology elsewhere, with scattered gravel-grade clasts. Lenticular bed morphologies are common, especially in the conglomeratic units.

In the east of the Molasse Succession, thin, interbedded fine-sandstones and mudstones are prevalent in pairs approximately 10 cm thick. The transition from dominantly conglomerate to sandstones and mudstones is shown in Fig. 2.11, log b. Intra-formational mudstone clasts and ripple structures are seen in the coarser bases of some sandstone units (Fig. 2.11, log c).

The geological map of Mongolia (Tomurtogoo, 1999) shows the Molasse Succession to be Permian in age. However, no absolute radiometric ages are available for this lithology.

2.2.5 Oyut Ulaan Volcanic group

The Oyut Ulaan Volcanic Group comprises four distinct formations in the south of the Saykhandulaan Inlier. The OUVG is the most volumetrically significant volcanic succession in the inlier, and its overall stratigraphic thickness exceeds 4000m. Three of these formations occur in an area of relatively continuous outcrop in the south west of the inlier. The fourth formation is exposed in the east, adjacent to the Oyut Ulaan intrusion (Fig. 2.8; Chapter 3).

The stratigraphically lowest, c.1500m thick, Gurvan Morin Höndiy (Three Horse Valley) Formation is comprised of andesitic lavas interbedded with feldspathic sandstones and sequences of coarse conglomerates up to 30m thick. The conglomerates are heterolithic and feature volcanic, meta-sedimentary and intrusive lithologies. One sandstone sequence contains lycopsid tree-bark impressions (H. Falcon-Lang, pers comm., 2005) and lithified fragments near its base below several tabular sandstone beds. Near the top of the formation, a conglomerate features crinoidal bioclastic limestone clasts and separate crinoid fragments. Pillow andesites also occur.

The c.2000m thick Shargyn Moghai (Yellow Snake) Formation is above the Gurvan Morin Höndiy Formation. It is comprised of a relatively monotonous succession of basaltic andesites, basaltic trachyandesites and trachyandesites. Locally, boulder-grade conglomerates featuring volcanic, meta-sedimentary and intrusive lithologies occur, but are laterally discontinuous.

The c.1000m thick Tsagaan Nuruu (White Ridge) Formation is comprised of a number of distinctive 5 to 10 m thick felsic lavas, which are blocky and crystalline, and form positive topography, interbedded with ca.60 m thick mudstone and siltstones, which are sparsely exposed. Near its top, between felsic lavas, the formation contains 2 to 3m thick basalt lavas and thinner intervals (25 to 35m) of sandstone units and black, organic mudstones with plant fragments.

The Yasun Eliy-e (Dead Vulture) Formation is isolated from the rest of the group stratigraphy in the east; its vertical thickness is unconstrained but is at least 1500m. It forms the host rocks to the Oyut Ulaan intrusion (Fig. 2.8) and is lithologically similar to the Ghurban Morin Höndiy Formation, but does not display thick conglomerate sequences. Volcanic sandstones and andesitic lithologies are dominant, with some basic lavas in the upper parts of the formation.

The Yasun Eliy-e Formation is the only part of the OUVG to be cut by minor intrusions. In the north, a 1 m wide olivine-phyric basalt dyke trends 130; south of this, in the centre of the area a small dioritic intrusion with a roughly circular surface expression, only 20m in diameter, cuts the volcanic-sedimentary succession.

The rocks of the OUVG are un-metamorphosed and relatively unaltered, compared to the rest of the inlier. Epidotisation locally occurs proximal to faults, fractures and carbonate veins.

The geological map of Mongolia (Tomurtogoo, 1999) shows the OUVG to be Carboniferous in age. Recently obtained zircon U-Pb ages, detailed later in this thesis (Chapter 3; Appendix B) indicate a mid-Carboniferous age for the OUVG volcanic succession. These ages constitute part of a larger regional data set that is being prepared for a separate publication.

2.2.6 Oyut Ulaan Intrusion

The Oyut Ulaan intrusion crops out in the southeast corner of the Saykhandulaan Inlier (Fig. 2.2). Together with the OUVG it forms the Oyut Ulaan volcano-plutonic complex. It is elongate, around 10 km east to west, and 3 km north to south. To the south, it is bordered by part of the Cretaceous rocks of the Zuunbayan basin, on other sides it is in intrusive contact with basement rocks of the Saykhandulaan Inlier. The contact zone is rarely exposed; it is covered by drift in most areas, but the margins of the intrusion are evident on satellite imagery (Fig. 2.8; Chapter 4; Fig. 4.2).

The main intrusion is cut by several dyke swarms, which have a range of compositions and orientations. A series of 1 to 100cm wide pink fine-grained felsic dykes run east-west parallel with the intrusion's long axis. Five- to ten-metre thick dark-green andesite dykes cut the felsic dykes. These are primarily observed in the central area of the intrusion. Their general trend is northwesterly, but they form a sector of an apparently radial set striking between 285 and 310.

The Oyut Ulaan intrusion and the surrounding country rocks host several mineralised features. To the northeast of the main intrusion there is an E-W elongate series of sulphide bearing quartz vein-stockworks within the volcanic country rock. The stockworks are hosted in potassically-altered andesite, and are adjacent to an east-west trending dyke. A second mineralised feature occurs along the SE margin of the intrusion within a zone of margin-parallel quartz veins and wall rock screens. This prospect consists of hard, silicified pods, surrounded by altered wall-rock that has a visibly obvious malachite presence. A tourmaline breccia-pipe cluster forms a series of rounded black hills within the intrusion. These hills are a topographic high point and appear in stark contrast to the pink-white granite landscape surrounding them. The tourmaline breccia pipes are spatially associated with minor pegmatite bodies.

The geological map of Mongolia (Tomurtogoo, 1999) shows the Oyut Ulaan intrusion to be Carboniferous in age. No published absolute radiometric ages are currently available for this lithology, however unpublished zircon U-Pb ages, recently obtained for this project, (Chapter 4; Appendix B) indicate a mid-Carboniferous age for the Oyut Ulaan Intrusion.

2.2.7 Mesozoic and Cenozoic cover sequences

Basaltic lavas, interpreted to correlate in age with Jurassic-Cretaceous lavas elsewhere in the region, lie unconformably on the Northern Slate Belt. The largest areas of lava are on the northern margin of the NSB, and to the east near the junction between the NSB, the eastern basin and the Saykhandulaan Valley Lineament Zone (Figs. 2.2 and 2.3). The lavas dip gently to the south and have layers between 5 and 10m thick, forming an extensive trap-topography. Several smaller basalt remnants sit on the NSB in various locations in the west.

In several localities near the inlier, partially lithified Cretaceous sediments are deformed and exposed. The best example of this is on the southern margin of the basin which lies to the east of the NSB. Throughout the inlier, interpreted faults that bound various lithological domains are generally hidden beneath recent alluvial cover sequences.

2.3 Provenance data

Thirteen samples from the Northern Slate Belt, High Strain Belt and Molasse Succession were point-counted for sandstone provenance. Several samples that were of an appropriate grain size for provenance work were discarded from this survey due to metamorphic grade and alteration. Five hundred points were counted for each thin section. The results are plotted on a quartz-feldspar-lithics ternary diagram (Fig. 2.12) and indicate that sediments of the NSB were derived from a cratonic source (average values; 88% quartz, 10% total feldspar, 2% lithic fragments). Clasts are generally angular to sub-angular.

Sediments in the HSB and MS were derived from volcanic arc domains at different stages of evolution (average values HSB; 9% quartz, 49% total feldspar, 41% lithic fragments; average values MS; 10% quartz, 2% total feldspars, 88% lithic fragments). The lithic fragments seen in the HSB are predominantly basalt or andesite with aphyric or trachytic texture, although small proportions of fine sandstone fragments and multicrystalline quartz grains also occur. A wide range of lithologies occur as fragments in

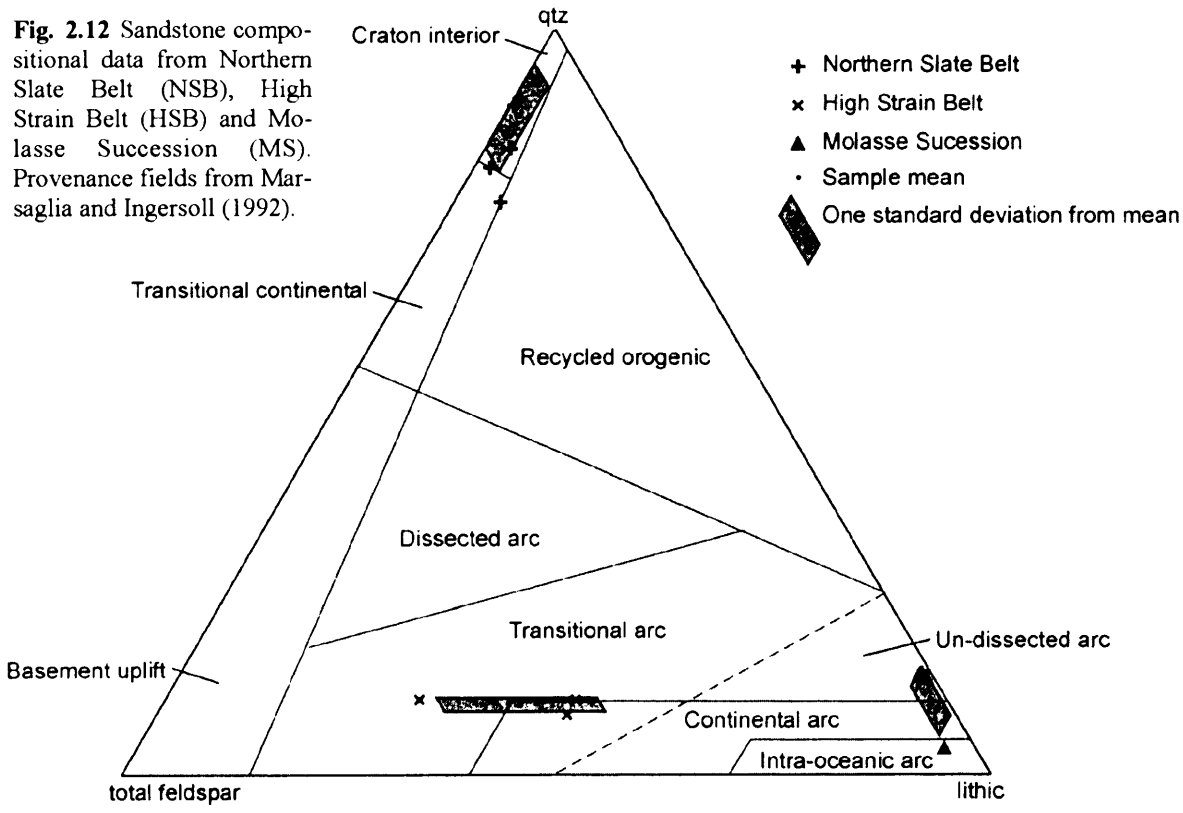

Fig. 2.12 Sandstone compositional data from Northern Slate Belt (NSB), High Strain Belt (HSB) and Molasse Succession (MS). Provenance fields from Marsaglia and Ingersoll (1992).

the MS, including various volcanics, granitoids, and sediments including sandstones and mudstones. In both the HSB and MS, grains are rounded to sub-rounded. The clear separation between the three populations in ternary space suggests different eroding source terrains.

2.4 Geochemical data

Seventeen volcanic samples from the Saykhandulaan Valley Formation were analysed using standard spectrometry techniques at the University of Leicester (Appendix A). The formation contains a sequence of dominantly high-K, calc-alkaline lavas with compositions that range from trachydacites and trachytes to rhyolites (Fig. 2.13). The bulk of samples are rhyolites. Harker variation diagrams (Fig. 2.14) illustrate some key geochemical characteristics and trends of the Saykhandulaan Valley Formation. MgO and CaO both fall with increasing SiO_2 and have distinctive changes in their geochemical gradient, Al_2O_3 and Fe_2O_3 decrease linearly with increasing SiO_2, these features suggest early mafic and feldspar

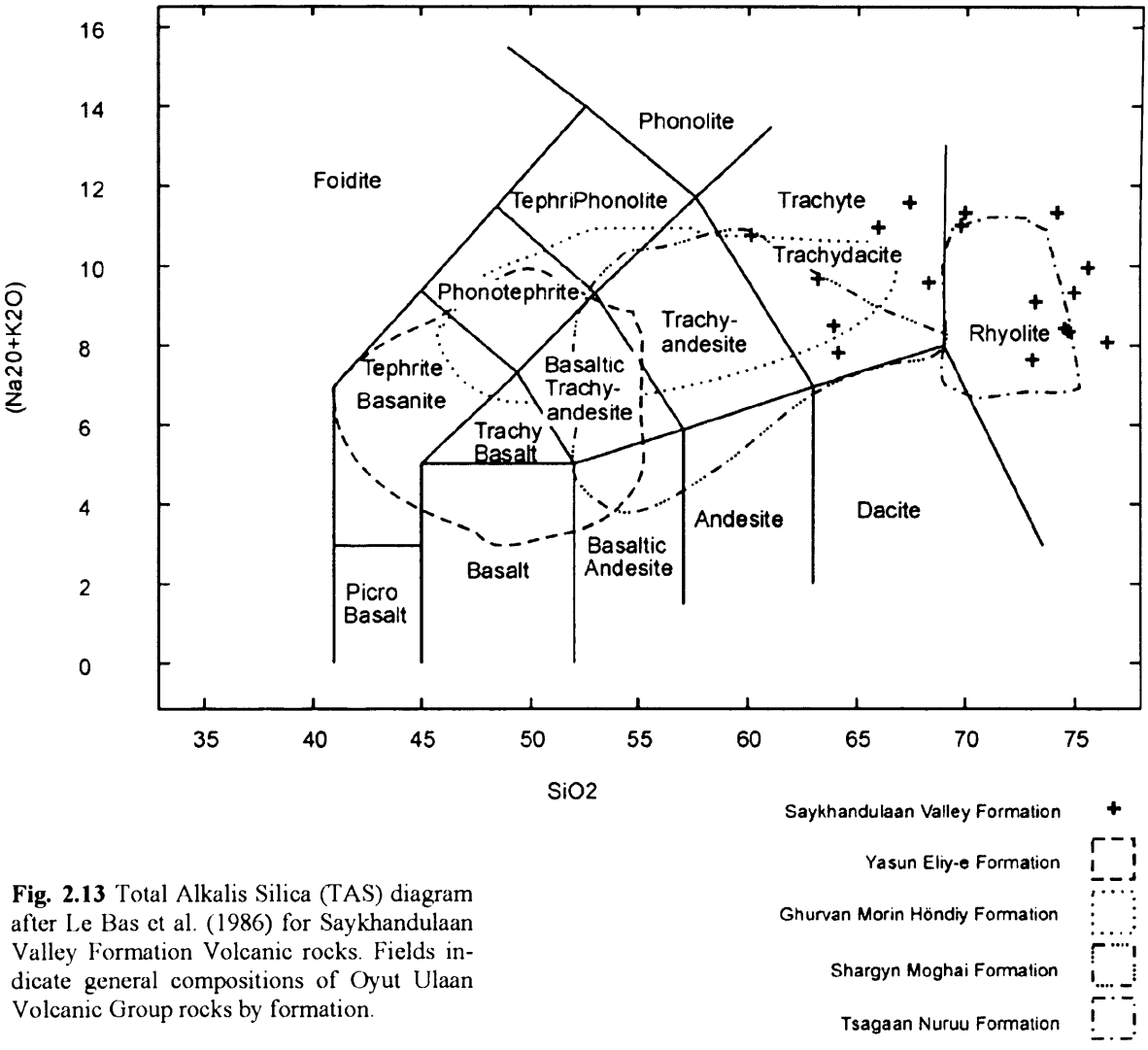

Fig. 2.13 Total Alkalis Silica (TAS) diagram after Le Bas et al. (1986) for Saykhandulaan Valley Formation Volcanic rocks. Fields indicate general compositions of Oyut Ulaan Volcanic Group rocks by formation.

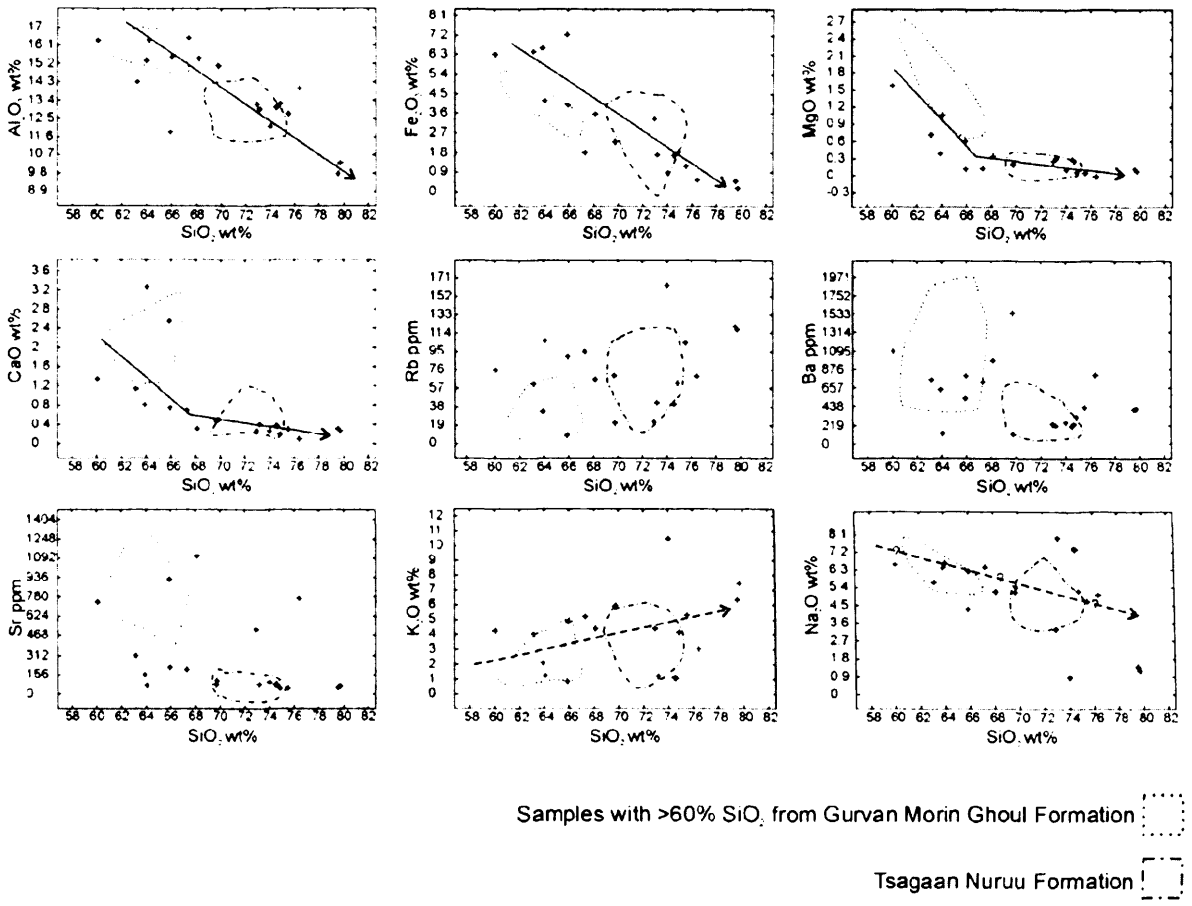

Fig. 2.14 Harker variation diagrams of Al_2O_3, Fe_2O_3, MgO, CaO, Rb, Ba, Sr, K_2O, Na_2O versus SiO_2. Fields indicate general composition of Gurvan Morin Höndiy Formation (with SiO2 values >60%) and Tsagaan Nuruu Formation. Arrows indicate fractionation trends.

controlled fractionation. Rb, Ba and Sr are scattered due to their post-emplacement mobility. K_2O and NaO_2 values show more scatter than other results, however, trends are discernible; increasing K_2O and decreasing NaO_2 with SiO_2 is suggestive of albite fractionation. Ba and Sr values suggest that the Saykhandulaan Valley Formation may have evolved by fractional crystallisation of feldspars and biotite. The liquid line of descent originates from a source chemically similar to the Oyut Ulaan granite (Fig. 2.15).

Eight analyses from known stratigraphic positions (Fig. 2.9) show evidence for systematic variations in composition. Plots of major and trace elements vs relative stratigraphic position show that there are consistent variations for several elements over time (Fig. 2.16). K_2O, Sr and Rb act compatibly, whereas the sequence becomes more enriched in Y. Other elements do not show discernible trends.

Multi-element normalised diagrams for the Saykahndulaan Valley Formation (Fig. 2.17) show strong negative anomalies for Nb, Rb, Sr, P and Cr and positive anomalies for

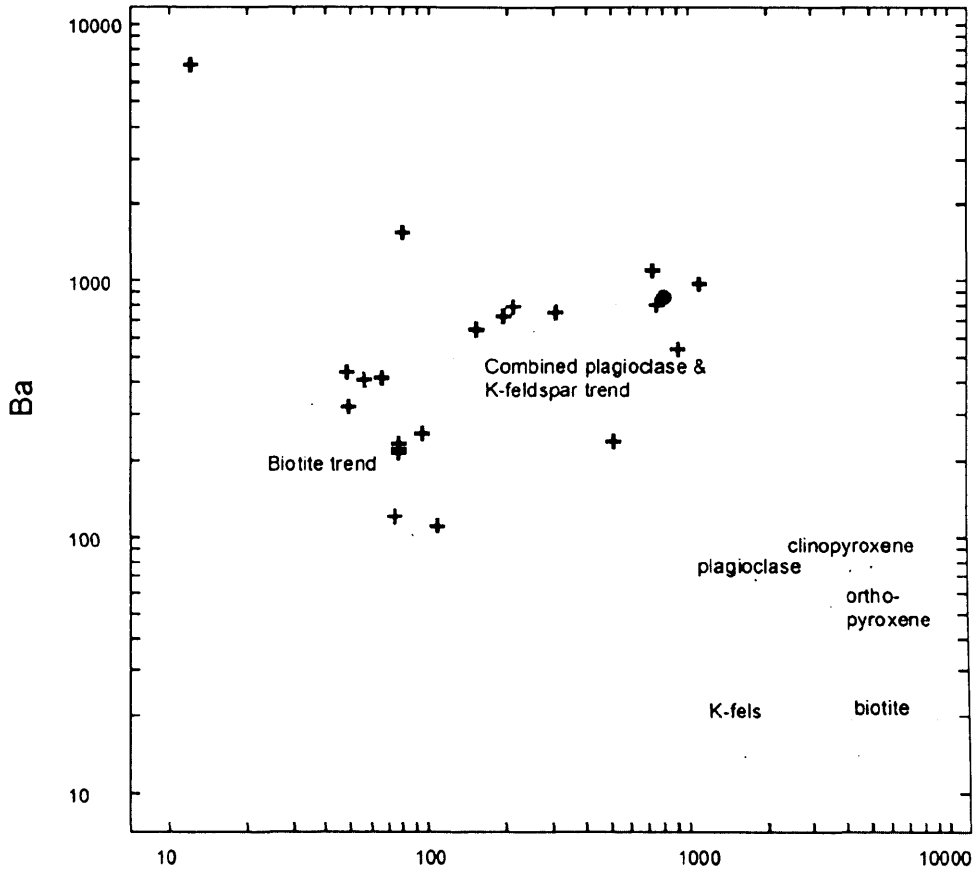

Fig. 2.15 Log Ba versus log Sr diagram for Saykhandulaan Valley Formation Volcanic rocks. Fractional crystallisation vectors for plagioclase, K-feldspar, biotite, orthopyroxene, clinopyroxene calculated from average values for Ba and Sr from Oyut Ulaan Granite, using partition coefficients for rhyolitic liquids from Rollinson (1993).

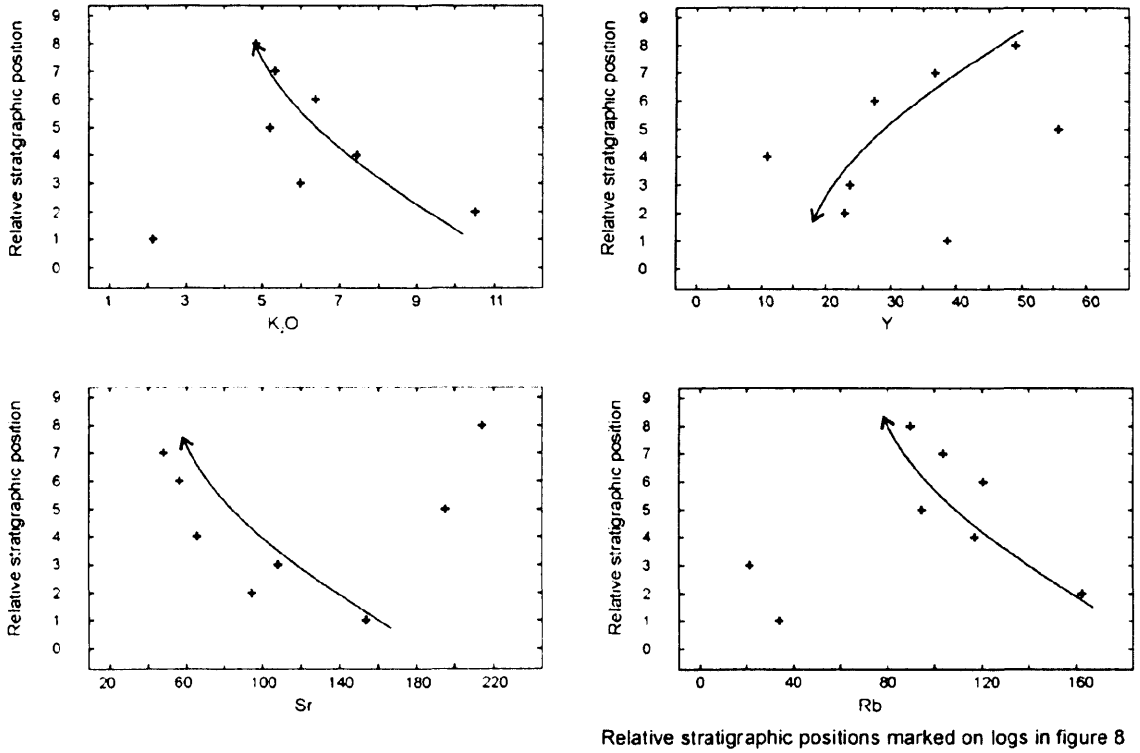

Fig. 2.16 Relative stratigraphic position versus Na_2O+K_2O, Y, Sr, Rb for Saykhandulaan Valley Formation volcanic rocks.

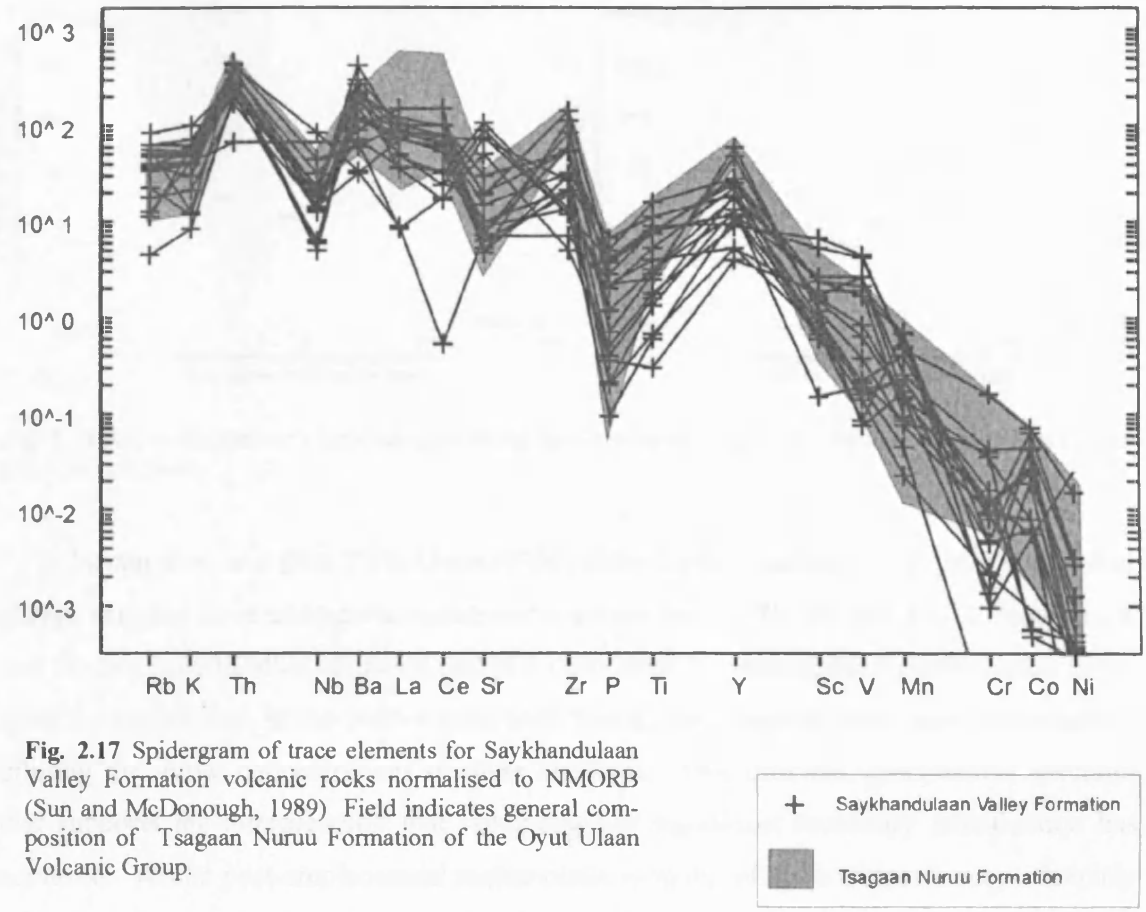

Fig. 2.17 Spidergram of trace elements for Saykhandulaan Valley Formation volcanic rocks normalised to NMORB (Sun and McDonough, 1989) Field indicates general composition of Tsagaan Nuruu Formation of the Oyut Ulaan Volcanic Group.

Th, Ba and Zr. The negative Nb anomaly and high ratio of low-field-strength-elements (LFSE) to high-field-strength-elements (HFSE) are both features typical of subduction related volcanism (Fig. 2.17; Saunders et al., 1980; Wilson, 1989). The negative Sr and Rb anomalies may be linked to feldspar and biotite fractionation. The Ba, Zr and Th positive anomalies may be linked to cumulus potassic feldspar and zircon.

Field observations and petrographic analysis indicate widespread silicification in the lavas of the Saykhandulaan Valley. Geochemical results support this observation; silica values between 76 and 80% are recorded for three samples (Fig. 2.13).

Graphical comparison of the trace element composition of an altered rock with its least-altered-equivalent allows the quantification of metasomatic processes that affected the altered sample (Grant, 1986). It is assumed that the sample identified as least-altered-equivalent has not undergone metasomatic alteration, and that, in the altered sample, Zr, Y, and Nb have remained relatively immobile. Trace element results for the two samples are plotted against each other, and a line of best fit, the isocon, is drawn through Zr, Y and Nb points.

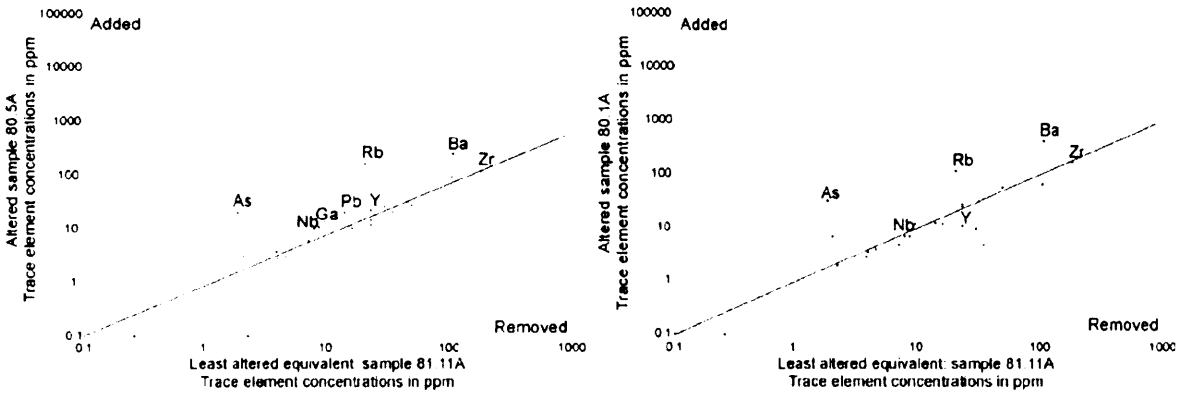

Fig. 2.18 Isocon diagrams of altered samples versus least-altered-equivalents for Saykhandulaan Valley Formation Volcanic rocks.

Isocon diagrams (Fig. 2.18; Grant, 1986) of the Saykhandulaan Valley rocks show that altered samples have undergone metasomatic enrichment of Rb, As and Ba. Zirconium, Y and Nb (along with other elements that plot on or near the isocon) have lower values in the altered samples than in the least-altered-equivalents; this suggests mass gain has occurred, diluting the initial concentrations of these elements. This provides geochemical evidence that supports the interpretation that volumetrically significant secondary silicification has occurred. Whilst post-emplacement metasomatic mobility of trace elements may adversely affect petrogenetic analysis (e.g. Fig. 2.13), silicification may have modified the position of samples on the TAS petrological discrimination diagram, causing compositions to plot in more evolved fields (Fig. 2.13).

The Saykhandulaan Valley Formation is chemically similar to the Tsagaan Nuruu Formation of the OUVG (Figs. 2.13 and 2.17). It also overlaps with the more silicic parts (>60%) of the Gurvan Morin Höndiy Formation (Fig. 2.14). Further discussion of the detailed geochemistry of the OUVG is found in Chapter 3.

2.5 Structural data

The strike of the dominant structural grain in the Saykhandulaan Inlier varies from 090 in the southwest, to 050 in the southeast and in the NSB. Folding occurs throughout the inlier and each litho-tectonic domain has a characteristic fold style. Cleavage is variably developed; the HSB and NSB display a widespread penetrative cleavage, whilst the MS, OUVG and rocks of the SVLZ are uncleaved or only affected by spaced cleavage.

At first-order, the NSB consists of regional-scale west-plunging folds, the limbs of which form a 'Z' across the belt (Fig. 2.4). Second-order folds occur on a scale of 10-100

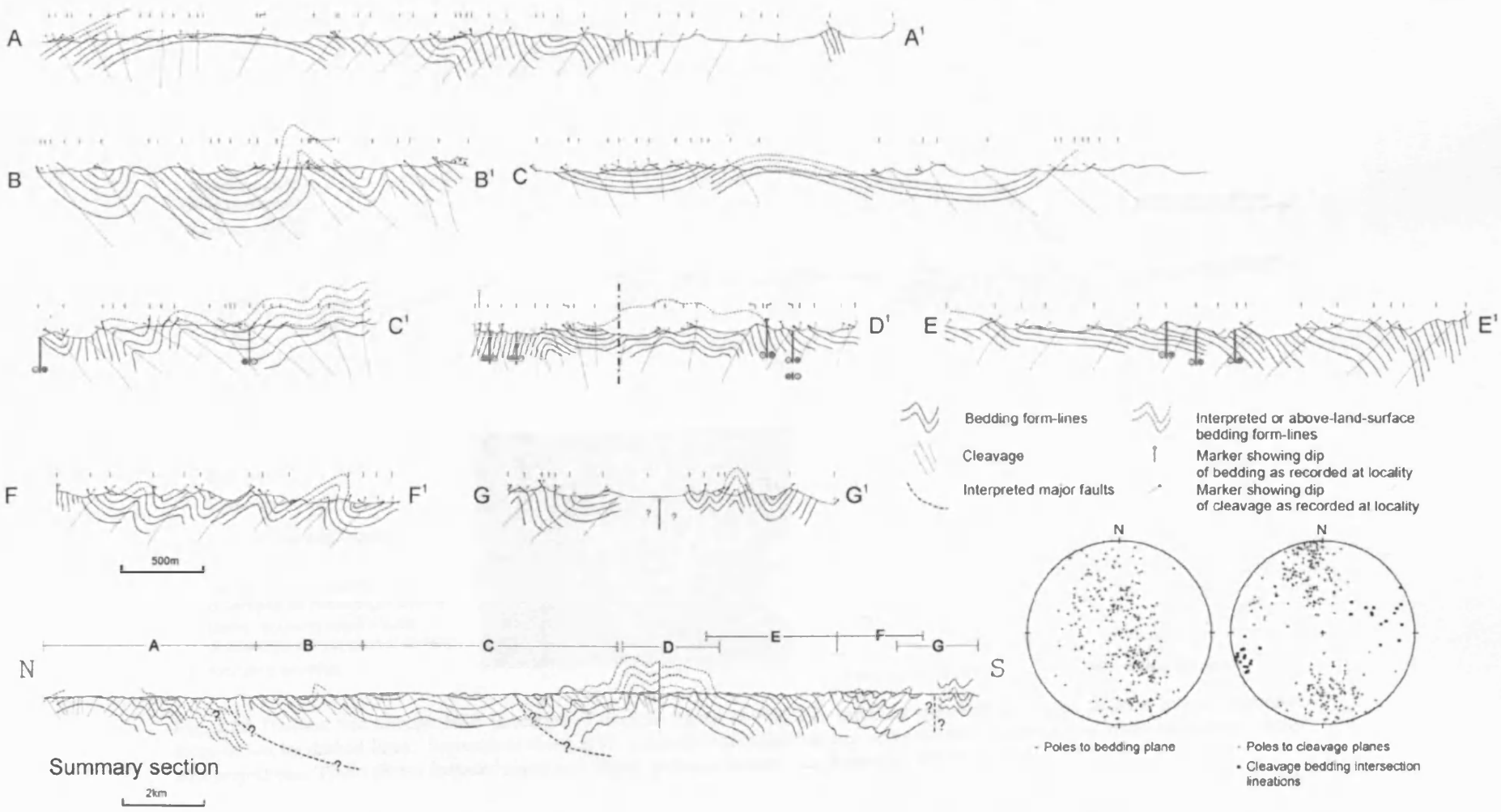

Fig. 2.19 Individual structural transects through Northern Slate Belt and combined summary section incorporating all lines. Bedding traced by form lines showing folds. Location of transect line segments shown in Fig. 2.3. Stereoplot 1. - NSB poles-to-bedding-planes on lower hemisphere equal-area stereoplot. Stereoplot 2 - NSB poles-to-cleavage-planes on lower hemisphere equal-area stereoplot. Summary section demonstrates kilometre scale first order folding within NSB.

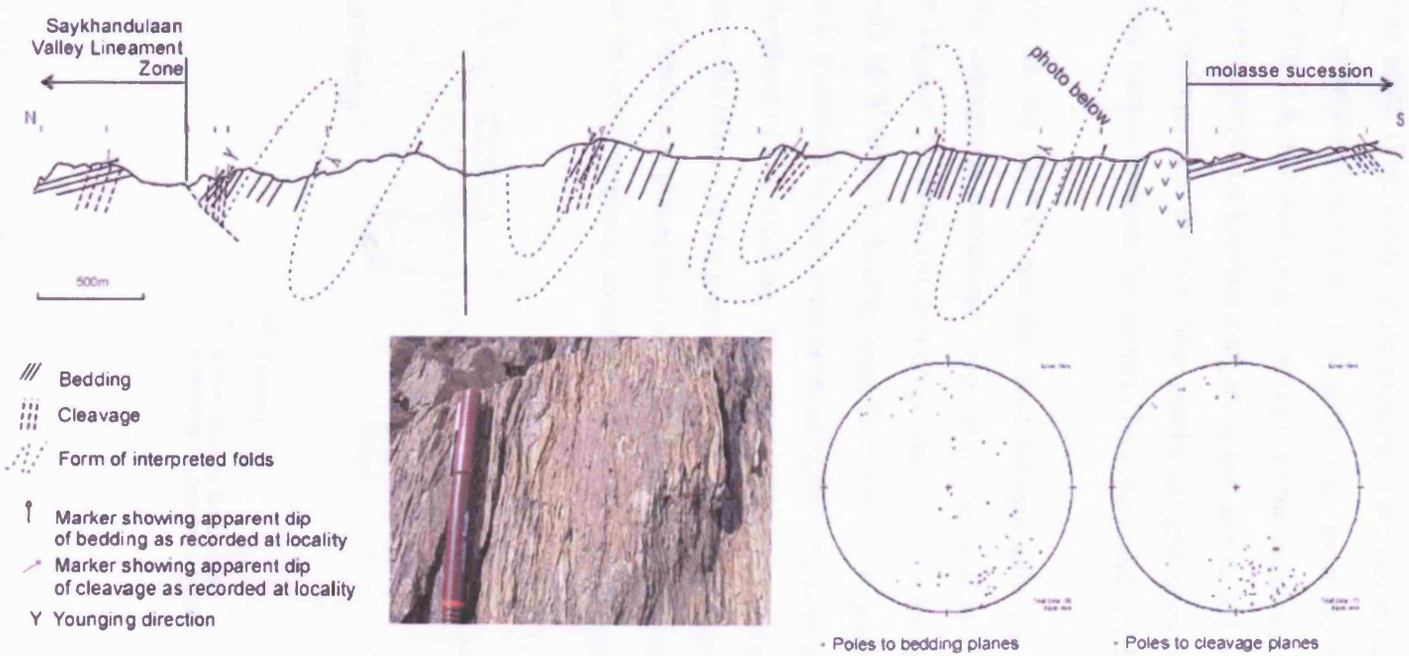

Fig. 2.20 Transect line through HSB (Location of transect shown on Fig. 2.8). Bedding and cleavage traced by form lines. Interpreted folds shown by dashed lines. Stereoplots show; HSB poles-to-bedding-planes and poles-to-cleavage-planes on lower hemisphere equal-area projections. Photo shows flattened clasts and spaced cleavage in meta-conglomerate, pen for scale.

m (Fig. 2.19). These folds plunge to both the east and west. Vergence varies through the zone, appearing to fan around first-order folds, which are upright.

The HSB features tight-to-isoclinal steeply-inclined folds which plunge to the east and west and verge south (Fig. 2.20). Fold closures were not directly observed in the field, however some apparent closures and low angle truncation can be identified on the aerial photograph in Fig. 2.8, and younging criteria prove the existence of fold hinges (Fig. 2.20). Other folds were observed on Landsat imagery at the eastern end of the HSB.

Bedding readings from the MS show gentle, upright, open folds (Fig. 2.11). Bedding becomes slightly steeper towards the northern boundary with the HSB (see cross section on Fig. 2.11).

The folds in the OUVG are the most recognisable on the ground. The three stratigraphically contiguous formations crop-out in the west in a first-order west-plunging syncline. The Tsagaan Nuruu Formation crops-out in the centre of this syncline (Fig. 2.21) and similar-style M-W folds in rhyolite lavas form positive topography. The northern limb of the syncline is truncated by east-west oriented faults. Poles to bedding planes (Fig. 2.21) trace the profile-plane of this syncline. Folds in OUVG have a slightly different trend from folds elsewhere in the inlier - striking around 090 (E-W) and plunging west.

Well developed axial planar cleavage characterises pelitic lithologies in both the NSB and HSB. The different vergence directions of the NSB is reflected in the wide range of

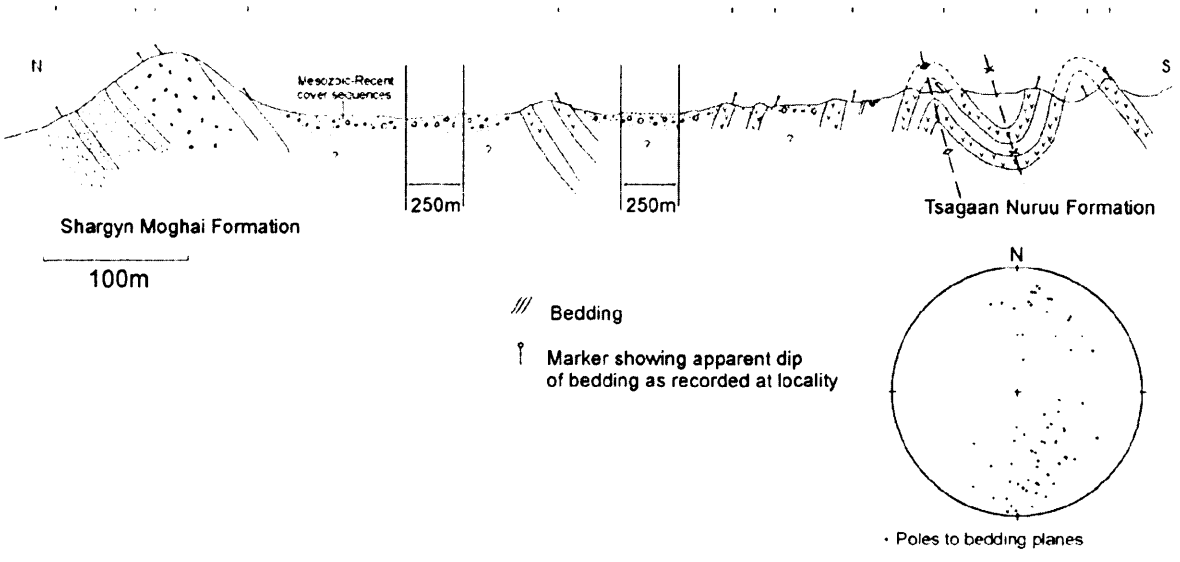

Fig. 2.21 Transect line through Oyut Ulaan Volcanic Group. Upper parts of Shargyn Moghai Formation (to left) comprise north limb of regional syncline that dips to south under Tsagaan Nuruu Formation which is deformed into m-w folds in core of syncline (to right). Location of transect shown on Fig. 2.8. Stereoplot: OUVG poles-to-bedding-planes on lower hemisphere equal-area projection.

cleavage orientations shown in Fig. 2.19. Cleavage-bedding intersection lineations which are a proxy for fold hinges, plunge both to the east and west (Fig. 2.19). Cleavage is dominant in the south-east corner of the NSB, and is deformed into tight, upright F_2 folds. Cleavage in the HSB is sub-parallel to bedding, and is steep and dominantly north dipping (Fig. 2.20). The coarse and relatively fresh lithologies of the MS do not contain a well developed cleavage, but where spaced cleavage was observed, it is near vertical and shows little variation compared to other domains (Fig. 2.11).

Remote sensing imagery reveals many faults that cut the Saykhandulaan Inlier, however, because of the near peneplain relief of the entire inlier, comparatively few faults have exposed surfaces with visible kinematic indicators. One of the best-exposed faults is a brittle thrust that defines the northern edge of the HSB in the east, which has partially consolidated upturned Mesozoic sediments in the footwall (Fig. 2.22c). Oblique-slip faults are exposed near the southern margins of the molasse succession. Both of these examples relate to post-Cretaceous fault movements at the boundary between Palaeozoic strata and

Fig. 2.22 a) Top to south backthrust zone in Saykhandulaan Valley Formation silicified rhyolite. View to west, width of photo - 5m. b) Detail of thrust surface showing down-dip slickenlines c) View to west of High Strain Belt greenschist-grade meta-conglomerates (left) thrust over partially consolidated near-vertical dipping Cretaceous sediments (right).

Cretaceous basin sequences; although the faults themselves could have formed earlier, and been subsequently reactivated. Within the Saykhandulaan Valley Lineament, north-dipping thrust faults crop-out in the silicified rhyolitic units of the Saykhandulaan Valley Formation (Fig. 2.22a). Striations indicating dip-slip movement are locally observed (Figs 2.22b, 2.23a). Three dimensional data was recorded from some strike slip faults (Fig 2.23b), but most strike-slip faults are not exposed at the surface and so are inferred to be vertical, because they from linear depressions and offset contacts and lithologies (Figs. 2.23 c and d).

Inferred normal faults define the eastern and western edges of the inlier. In the northeast, a normal fault-bound Cretaceous basin lies along strike from the NSB. The Cretaceous basin is bordered to the south, by the HSB. Where the Saykhandulaan Valley Lineament Zone joins the basin, there are a number of fault-bound troughs partially covered by onlapping Cretaceous sediments. The basement to these small depocentres appears to be faulted blocks of the HSB (Fig. 2.8).

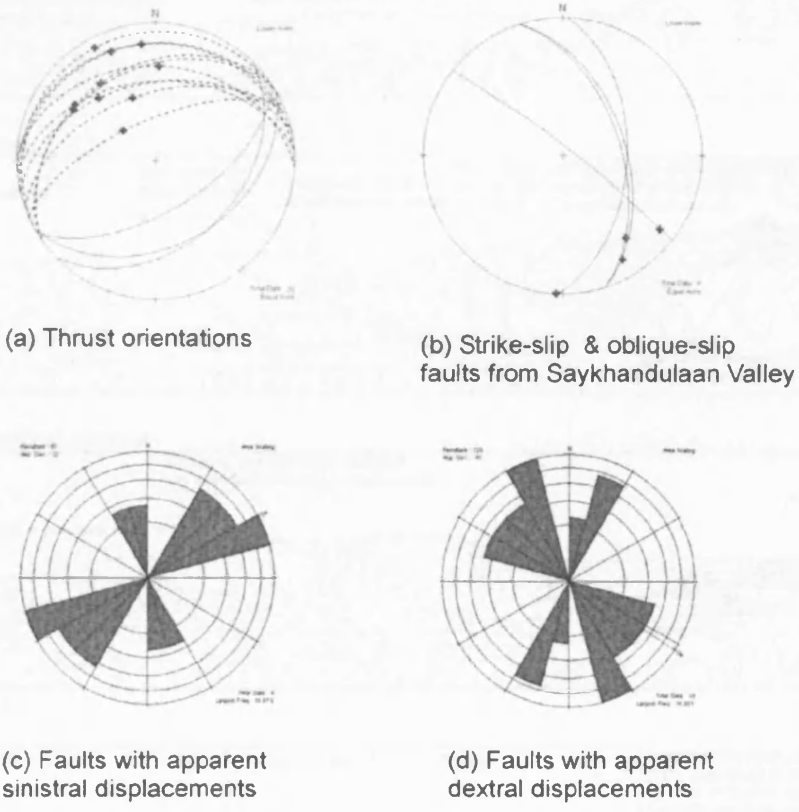

Fig. 2.23 a) Orientations of thrust faults - (unbroken line) and minor back-thrusts - (dashed line) from the Saykhandulaan Valley Lineament Zone. Striations on fault surfaces (crosses) indicate dominant dip-slip motion. b) Oblique-slip and strike-slip faults from back-thrusted zone in Saykhandulaan Valley. Striations on fault surfaces indicate dominant strike-slip motion. c) Orientations of brittle faults with apparent sinistral offsets from the whole inlier. d) Orientations of brittle faults with apparent dextral offsets from the whole inlier.

2.6 Discussion

The Palaeozoic geological evolution of the Saykhandulaan Inlier is dominated by siliciclastic sedimentation in a wide variety of environments, with erupted sequences of volcanic rocks, arc-related plutonism and contractional deformation (Fig. 2.24). Although major questions remain about the overall geological evolution of Southeast Mongolia, the

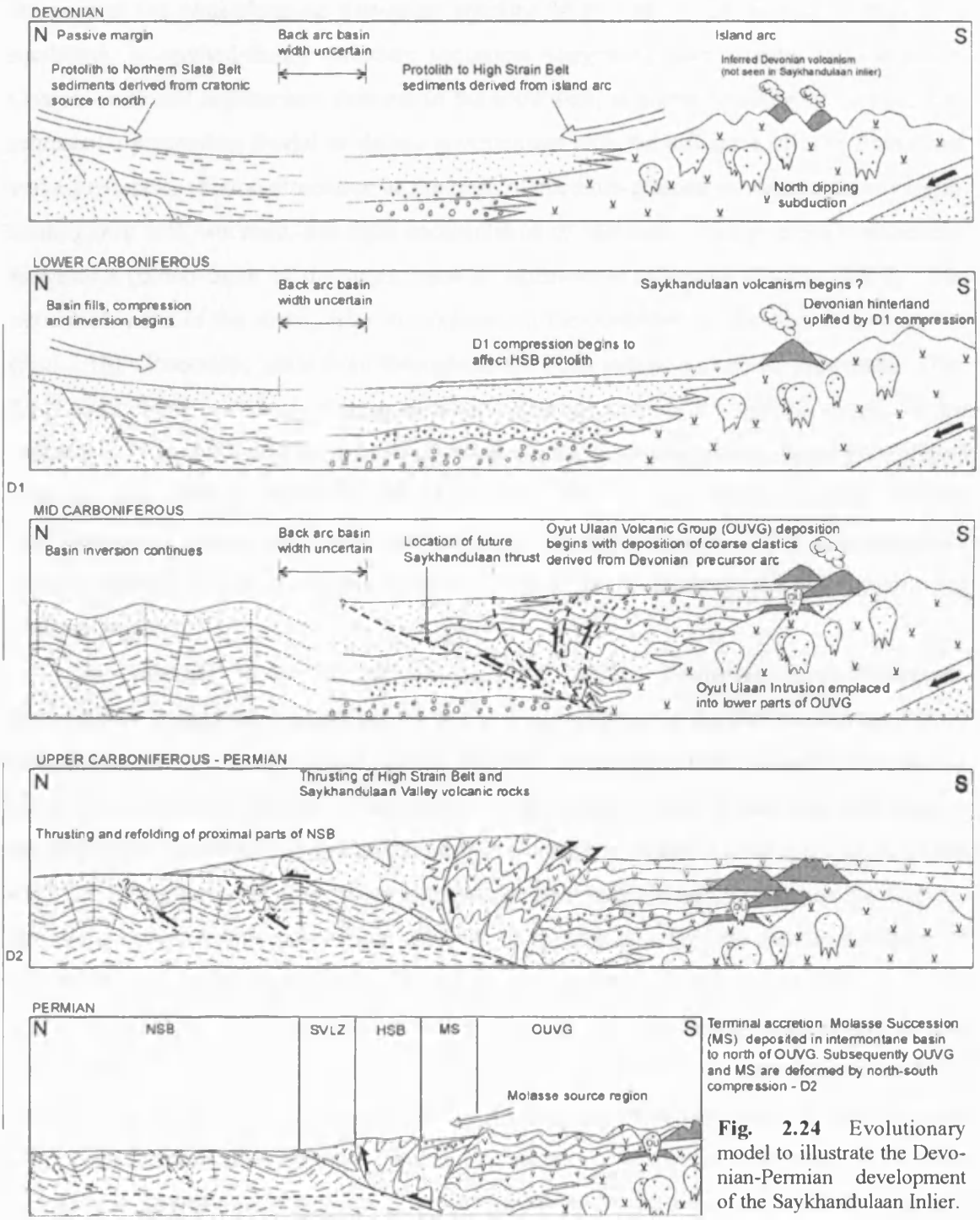

Fig. 2.24 Evolutionary model to illustrate the Devonian-Permian development of the Saykhandulaan Inlier.

lithological and structural data presented here provide the basis for the first detailed interpretation of Palaeozoic rocks of the region, and their terrane context.

The original depositional environment of the Northern Slate Belt pelitic and psammitic rocks is interpreted to represent a shelf-to-tidal shallowing-environment. The stratigraphically lowest parts of the NSB are interpreted to be exposed in the southeast, in the core of the west-plunging first-order anticline (Fig. 2.19). The dominant protolith is mudstone, in upward-fining turbiditic sequences suggesting deep marine sedimentation. Coarser units and sedimentary features in the southwest, at higher stratigraphic levels, may represent a prograding fluvial or deltaic environment with the influence of both fluvial and wave processes. Flame structures at the base of medium-grained sandstone units suggest loading onto soft, wet mud, and rapid accumulation of sediment. Swaley cross stratification suggests a palaeo-depth of the upper zone of storm-wave influence (Tucker, 1991). The uppermost parts of the stratigraphy are exposed in the northwest, in the first order syncline (Fig. 2.19). Psammitic units from throughout the NSB record a cratonic provenance (Fig. 2.12), and there is a high degree of provenance separation, in ternary space, of the sandstones in the NSB and those from elsewhere in the inlier, suggesting disparate sediment sources. The NSB is considered part of the Gobi Altai terrane, which is bordered to the north by passive margin and cratonic terranes (Fig. 1.1; Badarch et al., 2002). It is thus likely that the cratonic source of the sediments that formed the protoliths to the NSB was in this northern region.

The volcanic rocks of the Sakhandulaan Valley Formation have undergone considerable metasomatic alteration, related to fluids moving in the Saykhandulaan Valley Lineament Zone. The alteration makes accurate interpretation of primary geochemical signatures problematic though not impossible. Multi-element plots of trace-elements suggest the succession is volcanic-arc related, and it is chemically similar to the upper parts of the OUVG. It has, however, been more extensively deformed and tectonised than the OUVG, and the thickness of the succession suggests it represents a far less extensive history of volcanism.

The HSB is proximal to the NSB, is of a similar siliciclastic protolith and is also largely of greenschist metamorphic grade. However, the sediments that formed the HSB protolith have a dissected continental arc provenance and thus are probably south-derived (Fig. 2.12). Deformation obscures original sedimentary structures in most areas, but locally younging evidence was observed. The coarse-conglomerate parts of the HSB, near the

Saykhandulaan Valley, are interpreted to represent lower sections of the stratigraphy than the more voluminous sand- and granule-grade meta-clastic rocks to the south. The grain size range, cross-stratification and lenticular bedding suggest a sand-dominated braided river system as the depositional environment for the bulk of the HSB. Whilst the observed cross-stratification provided evidence of both younging direction, and the environment of deposition, the number of recorded instances was too few to unequivocally indicate a palaeo-flow direction.

The Yasun Eliy-e Formation, though not in direct contact with the rest of the OUVG, is interpreted to be the oldest volcanic formation as it is the least evolved. It has lithological similarities to and geochemical overlap with the Gurvan Morin Höndiy Formation, which is at the base of the contiguous volcanic stratigraphy in the west (Fig. 2.8).

In the Ghurvan Morin Höndiy Formation, various granite clasts in fan-glomerate successions that are intercalated with the volcanics suggest older, exhumed arc-crust was eroded during the early stages of OUVG volcanicity. It seems likely that this partially dissected arc could be the same source as that for the sediments that were the protolith to the HSB. The difference in grain size may suggest that the depositional environment of the HSB protolith was further from the eroding source than was the OUVG. Pillow andesites and lycopsid tree bark in sandstone suggests a shallow marine to coastal terrestrial palaeo-environment during early stages of the Oyut Ulaan volcanism.

The Shargyn Moghai Formation is almost entirely dominated by thick trachy-andesitic sheets with little intervening material; this suggests high volcanic-effusion rates.

In the Tsagaan Nuruu Formation, the succession is mainly composed of fine- to medium-grained volcaniclastic deposits. The precise nature of these units is unclear. They appear to have had a very large areal extent for felsic lavas, and were either particularly hot and of low viscosity on extrusion; formed by welding of rapidly emplaced pyroclastic flow; or were injected into the sediments laterally as sills. Sediments in the upper parts of the succession also suggest a marine marginal environment.

The poorly-sorted conglomerates of the MS represent a coarse-grained braided-river system which drained the OUVG. Fine sand and mudstone sequences may represent flood-related overbank sequences, or cyclic lake-sedimentation. The MS occurs unconformably on rocks of the HSB. Provenance data suggest the MS sediments were derived from an undissected arc of continental to intra-oceanic affinity (Fig. 2.12). It is interpreted to be the

youngest lithology of the inlier because it is un-metamorphosed and less deformed than the HSB, on which it lies unconformably.

At least four deformation events are recorded in the Saykhandulaan inlier. D1 is expressed in the NSB as a regional folding and cleavage forming event under lower greenschist grade metamorphic conditions. D1 folds generally trend ENE. Few Palaeozoic thrust surfaces were directly observed, however a few thrusts are tentatively interpreted from metamorphic breaks and fold asymmetry. The upright first-order folds of the NSB feature several zones of abrupt vergence changes, these are interpreted to be the effects of either blind-thrusts or thrusts that break the surface, but are obscured by drift (summary section; Fig. 2.19). South of the NSB unambiguous evidence for D1 was not observed.

D2 is a second contractional event, which has affected the entire inlier. Evidence for D2 consists of F2 folds of S1 cleavage, local crenulation cleavage and kink banding in the NSB. Quartz veins in the NSB postdate the formation of the S1 cleavage, and may have been emplaced parallel to cleavage planes during D2. The veins are spatially related to psammite units, which may have deformed in a more brittle manner compared to surrounding pelites, providing conduits for hot SiO_2-rich solutions. Intense folding and greenschist grade metamorphism within the HSB may have occurred during D1 and/or D2; no F2 folds of cleavage were identified.

South of the NSB, the Saykhandulaan Valley Lineament Zone is an important topographic and structural boundary, separating arc related rocks to the south, from basin sediments in the north. The zone itself is a 2 km-wide corridor of distributed cataclastic deformation, discrete faulting and abundant silicification. It is interpreted that the SVLZ may represent a south-dipping thrust zone, which brought the highest-grade rocks of the area (the HSB) to the surface during D1 and/or D2, entraining slivers of the Saykhandulaan Valley Formation in its base. Some minor north-dipping thrust surfaces are seen in the SVLZ, these are interpreted to be backthrusts.

The Molasse Succession and Oyut Ulaan Volcanic Formation have undergone the least deformation. The Molasse Succession has fold orientations that match those of the underlying HSB, but the folding is far less intense. Orientations of folds in the OUVG suggest it may have been affected by N-S shortening in contrast to the NNW-SSE directed compression seen in the rest of the inlier (Figs. 2.11, 2.21). Folding in the OUVG is interpreted to have occurred during D2 because the sequence lacks cleavage and evidence for metamorphism which are typical of D1 deformation to the north. Gentle folding in the

MS is interpreted to be a late-stage expression of D2. The D2 deformation of the OUVG must post-date the deposition of this group, and therefore has a mid-Carboniferous maximum age.

The Oyut Ulaan intrusion, which is emplaced in the lowermost and least-evolved parts of the OUVG, is elongate in a direction parallel to the axial trace of folds in the OUVG. Uranium-Lead zircon dates (Chapters 3 and 4) indicate that the Oyut Ulaan volcano-plutonic complex has a mid-Carboniferous age. This is consistent with regional evidence for Carboniferous arc-magmatism throughout southern Mongolia (Lamb and Badarch, 2001).

D3 represents Jurassic-Cretaceous crustal extension widespread in the region (Graham et al. 2001). Normal faults that cut the inlier and bound Cretaceous basins around the inlier are likely to have formed during D3.

Some strike slip faults that cut the inlier including the SVLZ cut all older structures and are therefore suspected of being the youngest faults in the region, and represent a fourth deformation event, D4 . Recorded sinistral minor faults, and major faults interpreted to have sinistral offsets trend 030-070, interpreted dextral antithetic shears trend around 160 (Fig. 2.25). Orientations of faults recorded in the field, and interpreted on satellite imagery (Fig. 2.25) suggest a sinistral Riedel-shear deformation regime during the Late Cretaceous or Tertiary. These fault displacements may have been co-genetic with brittle sinistral

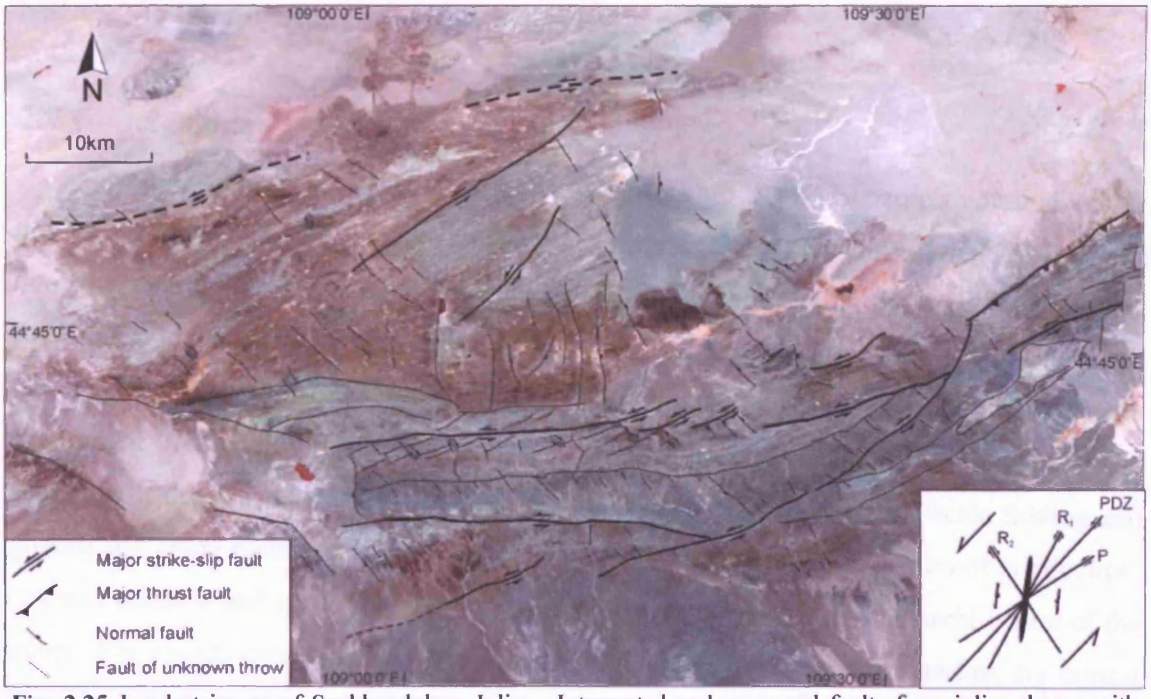

Fig. 2.25 Landsat image of Saykhandulaan Inlier. Interpreted and measured faults from inlier shown with movement sense. Inset sinistral Riedel-shear model shows predicted orientations of major and antithetic shears and normal faults. The orientation of Mezozoic regional sinistral movements compares well with array of strike- and oblique-slip faults identified in this study (Fig. 2.20).

movements on the nearby Zuunbayan Fault (Fig. 1.1; Lamb et al., 1999) during the Late Cretaceous or Tertiary.

The recognition that the Saykhandulaan inlier contains a southern volcanic arc complex and a northern deformed and metamorphosed marine basin assemblage, sheds light on the regional-scale tectonic events that were responsible for crustal growth in southeast Mongolia. The shortening and metamorphism within the NSB indicates closure and inversion of the basin between an arc to the south and a continental block to the north. No evidence was found for subduction, ophiolite obduction or accretionary prism development during closure of the NSB basin. Therefore, it is unlikely that the NSB basin was ever floored by oceanic crust and instead is interpreted to have been ensialic. The polarity of subduction beneath the arc-complex in the southern inlier was therefore probably north directed, consistent with other regional interpretations within the CAOB of Palaeo-Asian Ocean closure (Fig.2.1; Şengör and Natal'in, 1996; Badarch et al., 2002). Apart from local en echelon-vein arrays in the NSB, little evidence was observed for the Palaeozoic large-scale dextral movements postulated in the models of both Şengör and Natal'in (1996) and Badarch et al. (2002). Any major strike-slip displacements within the inlier were probably focused along the SVLZ and adjacent HSB, which represent the composite terrane boundary between the Gobi Altai and Mandalovoo terranes.

2.7 Conclusions

The Saykhandulaan inlier provides a window into the Palaeozoic evolution of the northern margin of the Palaeo-Asian Ocean in southeast Mongolia. Five major lithotectonic domains are distinguished that help elucidate the crustal evolution in the region. More than four thousand metres of volcanic rocks with arc geochemical signatures are documented, and the intrusion of the mineralised Oyut Ulaan granite suggest subduction-related magmatism. Two major deformation events are recorded related to back-arc basin closure, inversion and accretion of the Mandalovoo arc-terrane. Basin closure involved regional scale folding and greenschist grade metamorphism. Following terrane accretion and cessation of subduction, crustal extension and strike-slip faulting have further modified the crustal architecture of the inlier. The results presented here provide a useful framework for understanding the crustal evolution of adjacent regions within the southeast Gobi mineral belt.

The Oyut Ulaan Volcanic Group: Stratigraphy, magmatic evolution and timing

3

3.1 Introduction

A large area of southeast Mongolia is composed of volcanic arc terranes (Fig. 1.1) and the accretion of arc segments is a crucial component of crustal growth in the Central Asian Orogenic Belt. Economic mineralisation is associated with the volcanic-arc environment, including the copper-porphyry deposits for which southeast Mongolia is known. The stratigraphy of volcanic successions must be recorded and interpreted if the Palaeozoic evolution of southeast Mongolia is to be understood.

This chapter focuses on a succession of volcanic rocks within the Saykhandulaan Inlier - The Oyut Ulaan Volcanic Group. The volcanological processes that led to its formation have been characterised by the interpretation of new, detailed field observations. Models of the origin and evolution of key arc terranes are developed, with new geochemical and U-Pb zircon age constraints.

3.1.1 Regional geology

The two hypotheses that exist for the formation of the Mongolian CAOB crust during the Palaeozoic were discussed in Section 2.1. There have been many large scale models postulated for the development of volcanic arcs and terrane amalgamation in the region (Mossakovsky and Dergunov, 1985; Ruzhentsev and Pospelov, 1992; Zorin et al., 1993; Mossakovsky et al., 1994; Şengör and Natal'in, 1996; Badarch et al. 2002). Part of the problem in constructing a working palinspastic model lies in a lack of basic field data. Lamb and Badarch (1997; 2001) partially address this by documenting Palaeozoic stratigraphic sucessions and their geochemical characteristics from a range of localities throughout southern Mongolia.

Lamb and Badarch (2001) propose that an island arc existed between Edren in the west and Tsagaan Suvarga in the east during the Devonian (Fig. 3.1a). North of the Devonian island arc is a back-arc or trapped oceanic basin. In the Carboniferous, arc activity is split into two separate fronts, both built on the preceding Devonian arc material (Fig. 3.1b). Carboniferous arc activity in southeast Mongolia is linked with the Bogda-Northern Tien Shan arc in eastern Xinjiang province, China (Fig. 3.1b; Lamb and Badarch, 2001). Carroll et al. (1990) interpret the Bogda arc as intra-oceanic in the west, becoming more terrestrial

and continental in the east where it crosses the Sino-Mongolian border. A separate, parallel Carboniferous arc formed in the west at the same time, above the subducting northern margin of the Junggar Ocean (Lamb and Badarch, 2001). The mechanism that produces this duplication of arc fronts in the Carboniferous is not discussed, though several other palinspastic models for the region show dextral strike-slip duplication of arc sections during the Devonian and Carboniferous (Şengör and Natal'in, 1996; Badarch et al., 2002). All arcs are interpreted to have developed above northward-dipping subduction zones (Şengör and Natal'in, 1996; Lamb and Badarch, 1997, 2001; Badarch et al., 2002). Lamb and Badarch's (1997; 2001) tectonic model benefits both from being based on new, original field observations, and from being focused on a relatively small area, compared to some of the grand syntheses available elsewhere.

Geochemical and Nd isotope data from the Gurvansayhan Range indicate a juvenile oceanic arc was active in the region in the late Silurian to early Devonian (Helo et al., 2006). The authors state that this does not support the within-plate basalt affinity suggested by Lamb and Badarch (2001) for rocks from Gurvansayhan. However, this affinity is detected in rocks of Carboniferous age, and the work of Helo et al (2006) in the Gurvansayhan Range is focused on rocks for which they have established a Siluro-Devonian age. It appears that there is, in fact, no contradiction between the two models. Together they document an incipient, juvenile island arc which originated in the Silurian, became more evolved and alkaline during the Devonian, before the effects of back-arc rifting spread south into the area in the Carboniferous.

Whilst other parts of Mongolia have been a focus for detailed work in the last decade (Zorin et al., 1993; Lamb and Badarch, 1997; Cunningham, 1998; Lamb et al., 1999; Zorin, 1999; Buchan et al., 2001; Cunningham et al., 2001; Lamb and Badarch, 2001; Perello et al., 2001; Cunningham, 2005; Helo et al., 2006), the easterly reaches of the Mongolian Gobi have remained relatively unstudied. The field area for this study was selected, therefore, to establish the terrane context of the South Gobi Mineral Belt, and test existing terrane models for South Mongolia.

The Saykhandulaan inlier is situated around 150km to the northeast of Tsagaan Suvarga, and is comprised of a series of E-W trending lithotectonic domains. The inlier records the Devonian-Carboniferous history of the boundary between island arc dominated lithologies in the south and rocks formed from craton-derived basin sediments in the north.

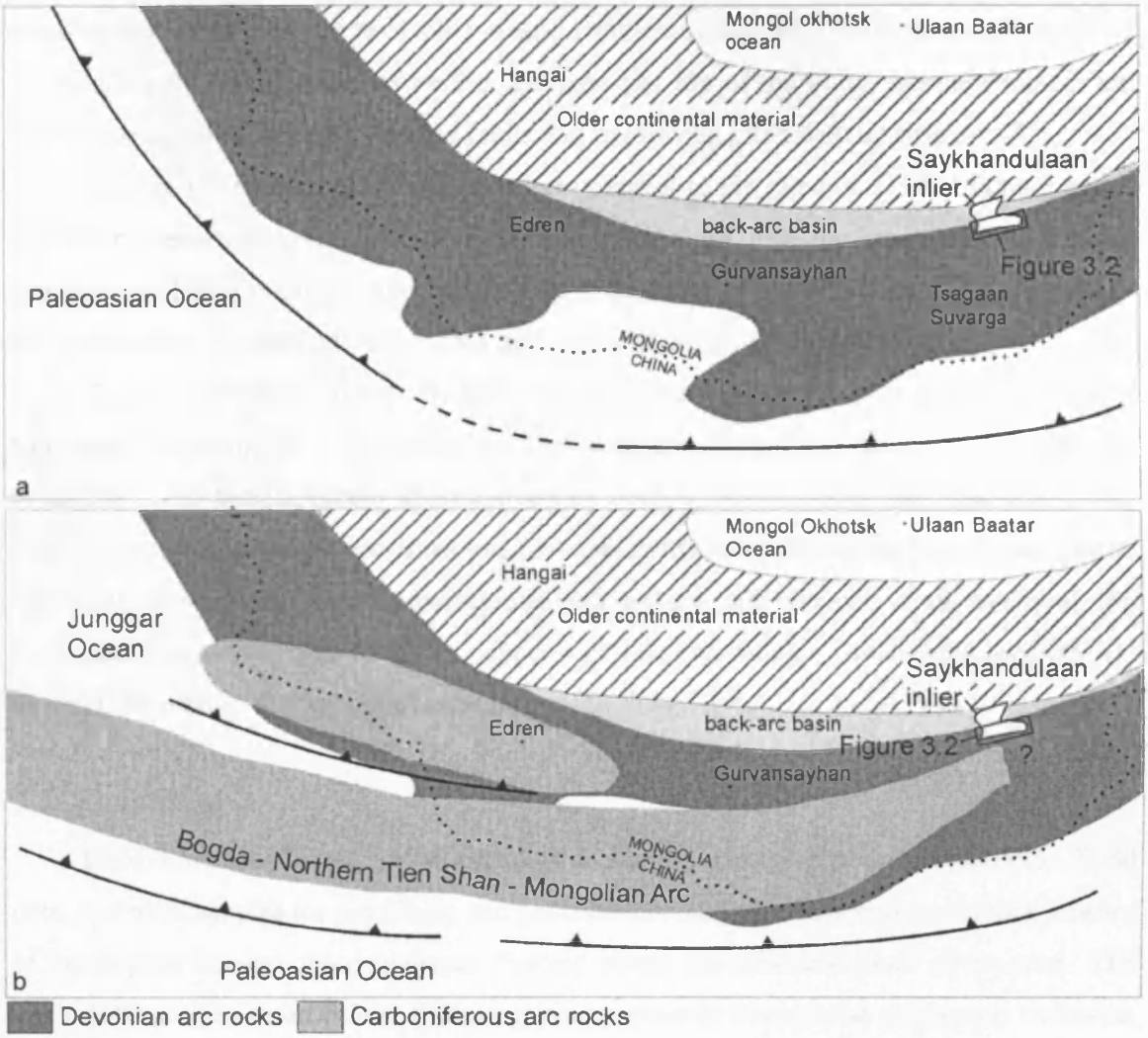

Fig. 3.1 Paleogeographic interpretations of south Mongolia redrawn from Lamb and Badarch (2001) a) Devonian b) Carboniferous. Location of Gurvansayhan and Edren localities from Lamb and Badarch (2001) shown. The Saykhandulaan inlier is the field area for this study.

The southernmost domain is a folded succession of Carboniferous volcanic and sedimentary rocks called the Oyut Ulaan Volcanic Group (Chapter 2), which is the subject of this chapter.

3.1.2 Oyut Ulaan Volcanic Group

The Oyut Ulaan Volcanic Group (OUVG) crops-out along the southern margin of the Saykhandulaan inlier in a 45 km long E-W trending belt (Fig. 3.2). The main outcrops are in the west of this belt in a 25 km E-W range of hills. The eastern outcrops form the country rocks to the Oyut Ulaan Intrusion and are separated from the western outcrops by an area of drift. The contiguous succession is around 4.6 km thick and is comprised of a variety of extrusive lithologies from basalt to rhyolite lavas and volcaniclastic sediments locally

interbedded with a wide range of silici-clastic sediments. The total stratigraphic thickness of 4.6 km is a minimum value, as neither the base nor top of the group are constrained, the outcrop being surrounded by inferred faults and unexposed ground on all sides.

The OUVG is tightly folded with hinges parallel to the regional E-W structural grain. The main western outcrops occur within the north-dipping limb and hinge zone of a major syncline. Folds are upright, have an inter-limb angle of 70°, and are plunging on average 30° to the west. Cleavage is rarely seen and the rocks are un-metamorphosed.

The OUVG has not previously been described in any literature. The geological map of Mongolia (Tomurtogoo, 1999) shows the area as an undifferentiated block of Carboniferous volcanics. The geographically-closest relevant work is that of Lamb and Badarch (1997; 2001) whose eastern-most localities are 150 km to the west of the Saykhandulaan Inlier. Lamb and Cox (1998) note Carboniferous sedimentary and volcanic strata overlying the Devonian Tsagaan Suvarga porphyry copper-molybdenum deposit, which is situated 100 km to the south west of the Saykhandulaan inlier (Fig. 1.1).

3.2 Field data

Field work was conducted to establish a detailed stratigraphy for the OUVG. Field data, and rock samples for petrologic and geochemical analysis, were collected along a series of lithological and structural traverses directed across the structural grain of the area. The key results are presented below, first progressing upwards through the contiguous sucession from east to west, then describing the separate area in the east. The locations of the traverses are shown on Fig. 3.2.

3.2.1 Gurvan Morin Höndiy Formation

The stratigraphically lowest, c.1500m thick, Gurvan Morin Höndiy (Three Horse Valley) Formation crops out in the east of the contiguous succession. The formation was principally observed in a dry river valley (line of transect shown in Fig. 3.2) that cuts across the dominant E-W trending structural grain (Fig. 3.2). It is comprised of 10 to 150m thick intermediate lavas and coarse conglomerates interbedded with >15m thick feldspathic sandstone sequences (Fig. 3.3). The lavas and conglomerates are cliff forming units, between which are zones of little to no outcrop. Lavas and conglomerates are mainly within the southern limb of a 1st order syncline and dip steeply to the north. Further north, the upper parts of the succession are deformed into a number of 2nd order folds indicative of

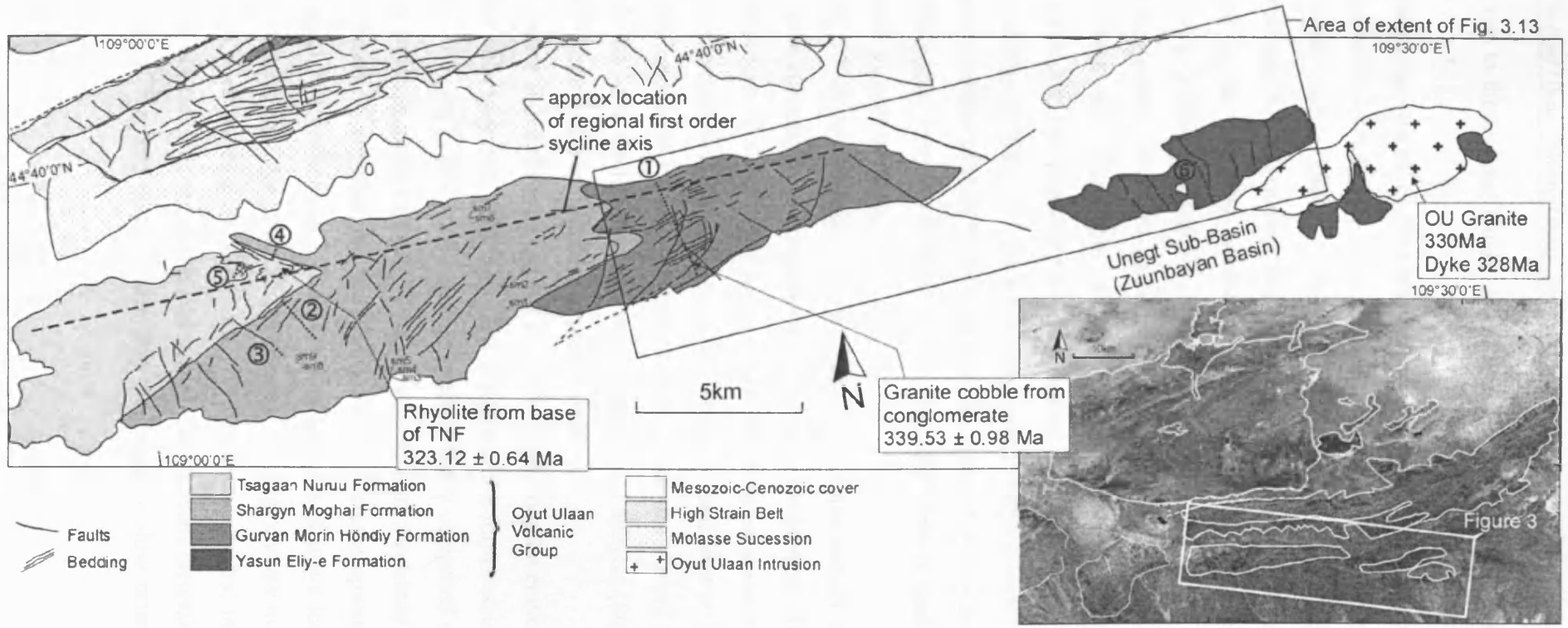

Fig. 3.2 Map of OUVG outcrop areas, showing the vertically contiguous Gurvan Morin Höndiy, Shargin Moghai and Tsagaan Nuruu Formations in the west and the Yasun Eliy-e Formation in the east, in contact with the Oyut Ulaan intrusion. Inset - satellite image of the Saykhandulaan inlier showing location of Fig. 3.2.
Dotted lines on map - locations of transects/stratigraphic sections study areas from various formations; ① GMHF; ②,③,④ SMF; ⑤ TNF; ⑥ YEF. Points sm1-9 indicate locations of SMF samples not marked on stratigraphy in **Fig. 3.8**

their proximity to the regional hinge. In the south, the formation is fault bound; its base is not seen.

The formation was subdivided into three units, designated A, B and C (Fig. 3.3). Unit A, at the base of the formation, is 500m thick and is composed of basic to intermediate lavas. These lavas occur in five 'stacks' in which individual flow units are indistinguishable; three of these stacks are 70 to 90 m thick and form major topographic features. The typical rock type in Unit A has blue-grey weathered surfaces. Subhedral to euhedral plagioclase phenocrysts are dominant, comprising between 30 and 70% of the rock (Fig. 3.4 a). Phenocryst size ranges from 1 to 10 mm, but both minimum and maximum size decrease within this range with stratigraphic height. Hornblende is a minor phenocryst phase, commonly subhedral, and generally 1 to 3 mm in size.

Local variations from this typical lithology include varying levels of vesiculation, and the occasional presence of flow foliation defined by oriented plagioclase laths. One unit is sparsely populated by long thin feldspar phenocrysts, often seen in agglomerations. Granite xenoliths occur in some sections.

Unit B, which conformably overlies Unit A, contains similar extrusive lithologies along with thick successions of conglomerates and some sandstones. The base of Unit B is defined by exposures of sedimentary rocks, which do not occur lower in the formation (Fig. 3.5 a). This sequence includes conglomerates, siltstones and several 1 to 3 m thick lavas separated from each other by thin sediment screens. In contrast to the extrusive lithologies from Unit A, the lavas in this sequence are dark grey and aphyric (Fig. 3.4 b), or contain only sparse (<1 mm diameter) hornblende phenocrysts.

Fifty metres above the base of Unit B, a 40m thick conglomeratic succession is overlain by a 60m thick lava stack (Fig. 3.6). The conglomerates form a series of beds of 2 to 20 m thickness. They are poorly sorted and are predominantly composed of pebble to boulder (max 70 cm) andesitic clasts supported by a coarse immature sandstone matrix. Some beds have erosive bases. Conglomerate clast sizes generally decrease upwards in this sequence, as do individual bed thicknesses. The overlying andesite displays loading and sediment injection structures at its base, with 50 cm 'flames' of conglomerate matrix 'intruding' the lava. A 50 m thick trachyandesite contains 10% 1-2 mm euhedral to subhedral feldspar phenocrysts at its base. The proportion and size of these crystals increases to 30% and 2 to 5 mm at the top of the lava stack, where they are strongly flow orientated, displaying a

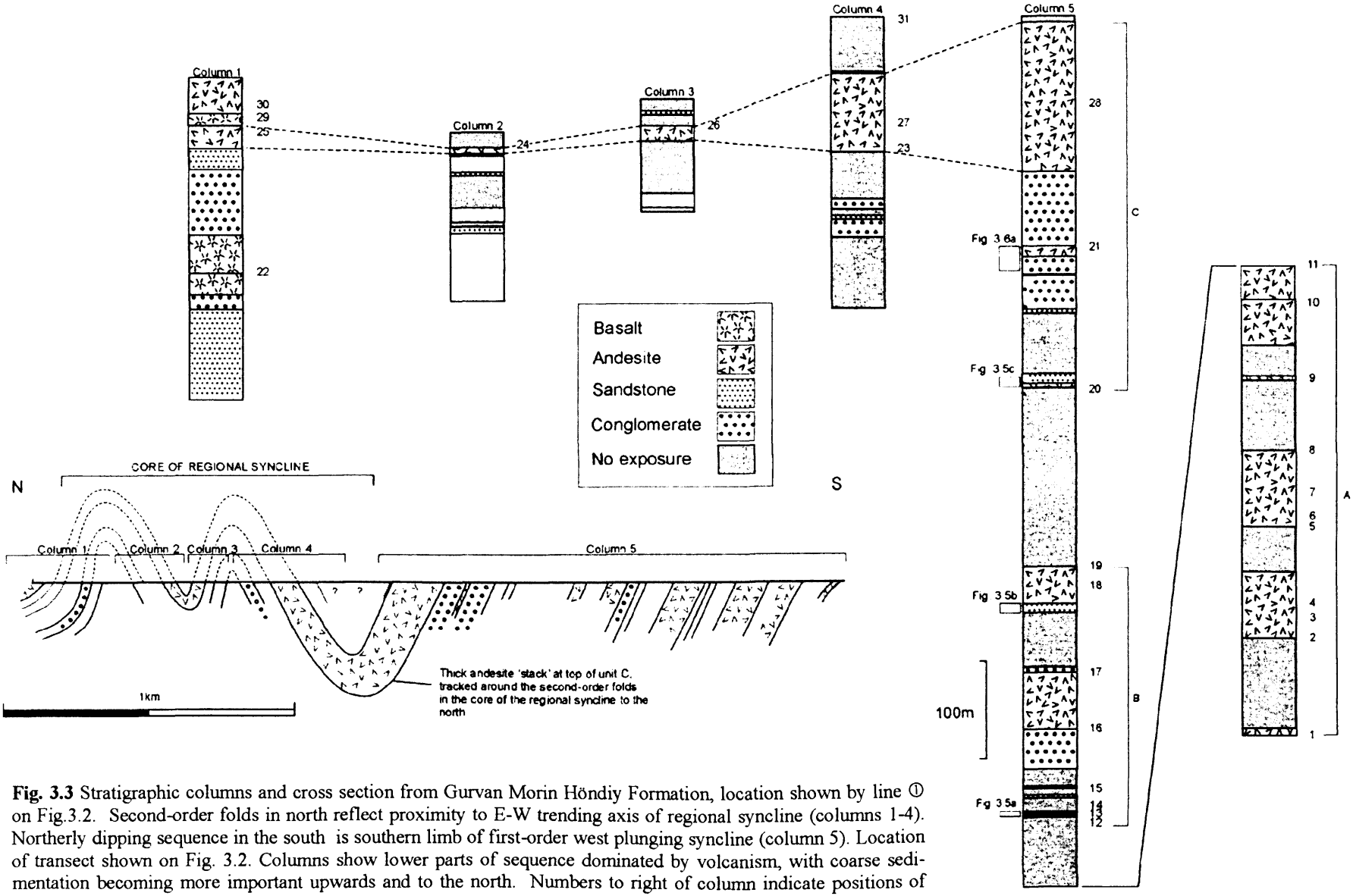

Fig. 3.3 Stratigraphic columns and cross section from Gurvan Morin Höndiy Formation, location shown by line ① on Fig.3.2. Second-order folds in north reflect proximity to E-W trending axis of regional syncline (columns 1-4). Northerly dipping sequence in the south is southern limb of first-order west plunging syncline (column 5). Location of transect shown on Fig. 3.2. Columns show lower parts of sequence dominated by volcanism, with coarse sedimentation becoming more important upwards and to the north. Numbers to right of column indicate positions of geochemical analyses.

trachytic fabric. Hornblende phenocrysts form 5 to 10 % of the rock in central parts of this section. Another conglomeratic bed lies above the andesite, similar to those below.

Sixty metres above the conglomerate lithologies, 60 to 200 cm thick sandstones and conglomerates with some thin shale-bands occur (Fig. 3.5 b). This sequence includes a 60 cm thick carbon-rich black-shale horizon. A further 40 m thickness of densely feldspar-

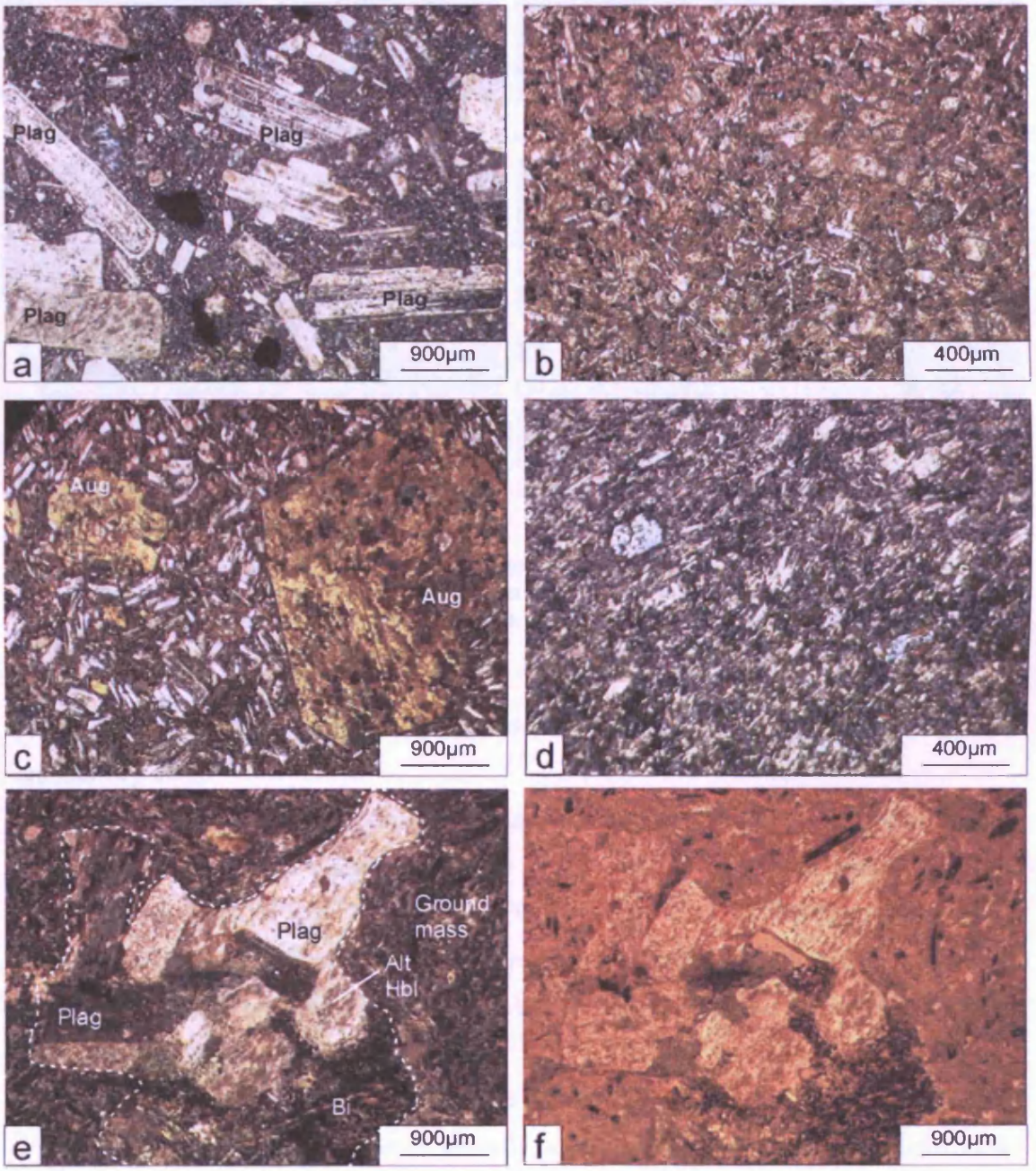

Fig. 3.4 Photomicrographs illustrating volcanic lithologies in OUVG. a) Basalt from GMHF with weakly flow-aligned euhedral plagioclase (labradorite) phenocrysts, b) Aphyric basalt from GMHF, c) Basalt from SMF with large augite phenocrysts and plagioclase lath microphenocrysts, d) Fine grained amygdaloidal basalt from SMF, e) Multi-mineralic granite microxenolith in SMF formation aphyric basaltic andesite. Xenolith contains biotite (Bi), plagioclase (Plag), altered hornblende (alt hbl), f) same feature as 'e' in plane polarised light, g-j overleaf.

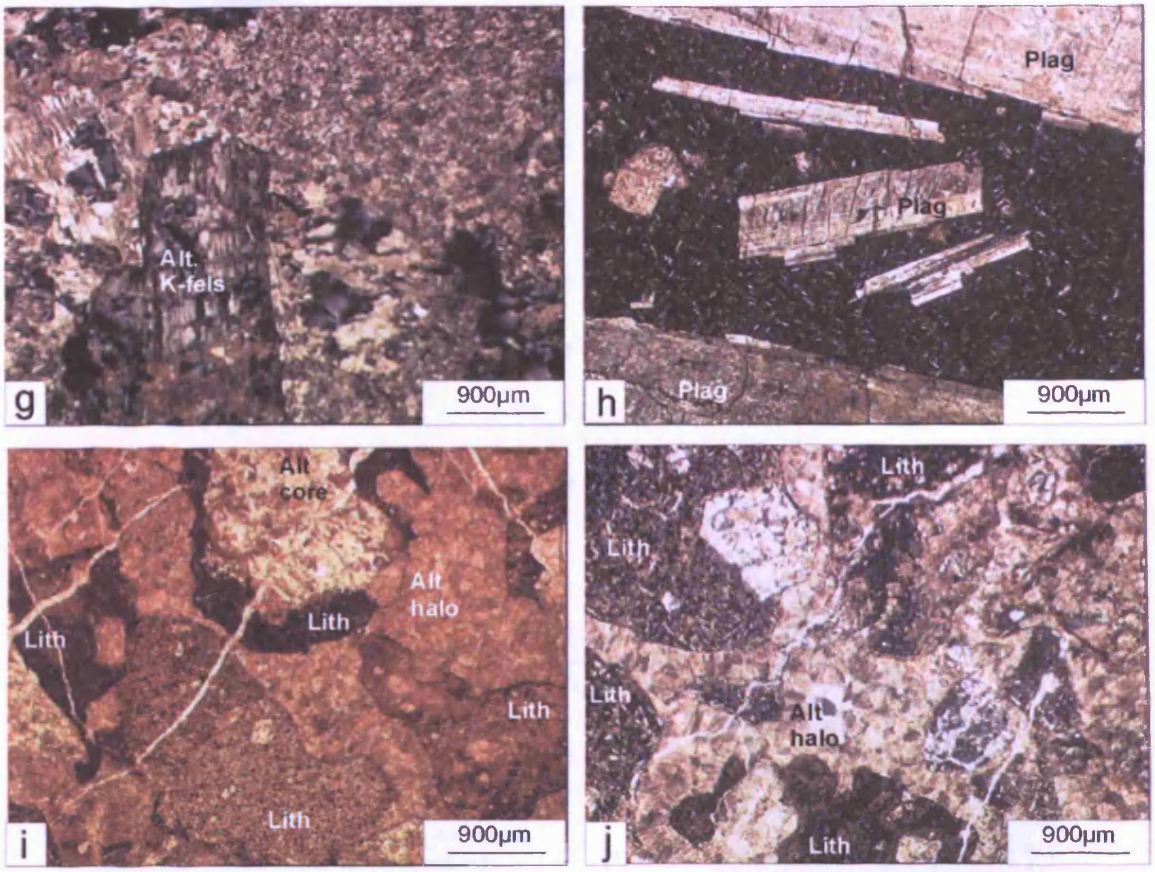

Fig. 3.4 (continued from previous page) g) Rhyolitic lithology from TNF, note altered feldspar crystal, apparently devitrified ground mass h) Basalt from upper part of TNF, very large euhedral plagioclase phenocrysts i) highly altered volcani-clastic lithic breccia, clasts of various basaltic lithologies with alteration haloes, in plane polarised light j) same as 'i' in cross polarised light

phyric andesite with 1 to 5 mm-long euhedral phenocrysts is exposed above these sedimentary units.

The uppermost part of Unit B is another relatively thinly bedded sedimentary sequence, featuring graded sandstones with cross stratified bases and bioturbation, and siltstones with lycopsid bark impressions (Fig. 3.5, c to e; H. Falcon-Lang pers. comm. 2005). One segment of lycopsid trunk occurs in apparent life-position (Fig. 3.5 d), whilst others are parallel to bedding (Fig. 3.5 e). Thin 1 to 3 cm thick seams of coal with Fe-oxide halos occur in these units.

Unit C is lithologically similar to Unit B containing thick conglomerates and andesites. The lithologies of Unit C were traced laterally around a series of second-order folds in the northern part of the GMHF outcrop area (Fig. 3.3), documenting lateral transitions in the sucession. In the south, the base of the unit is defined by <1 to 2m thick small- to medium-pebble conglomerate beds with an intercalated sandstone and shale unit, above which is a

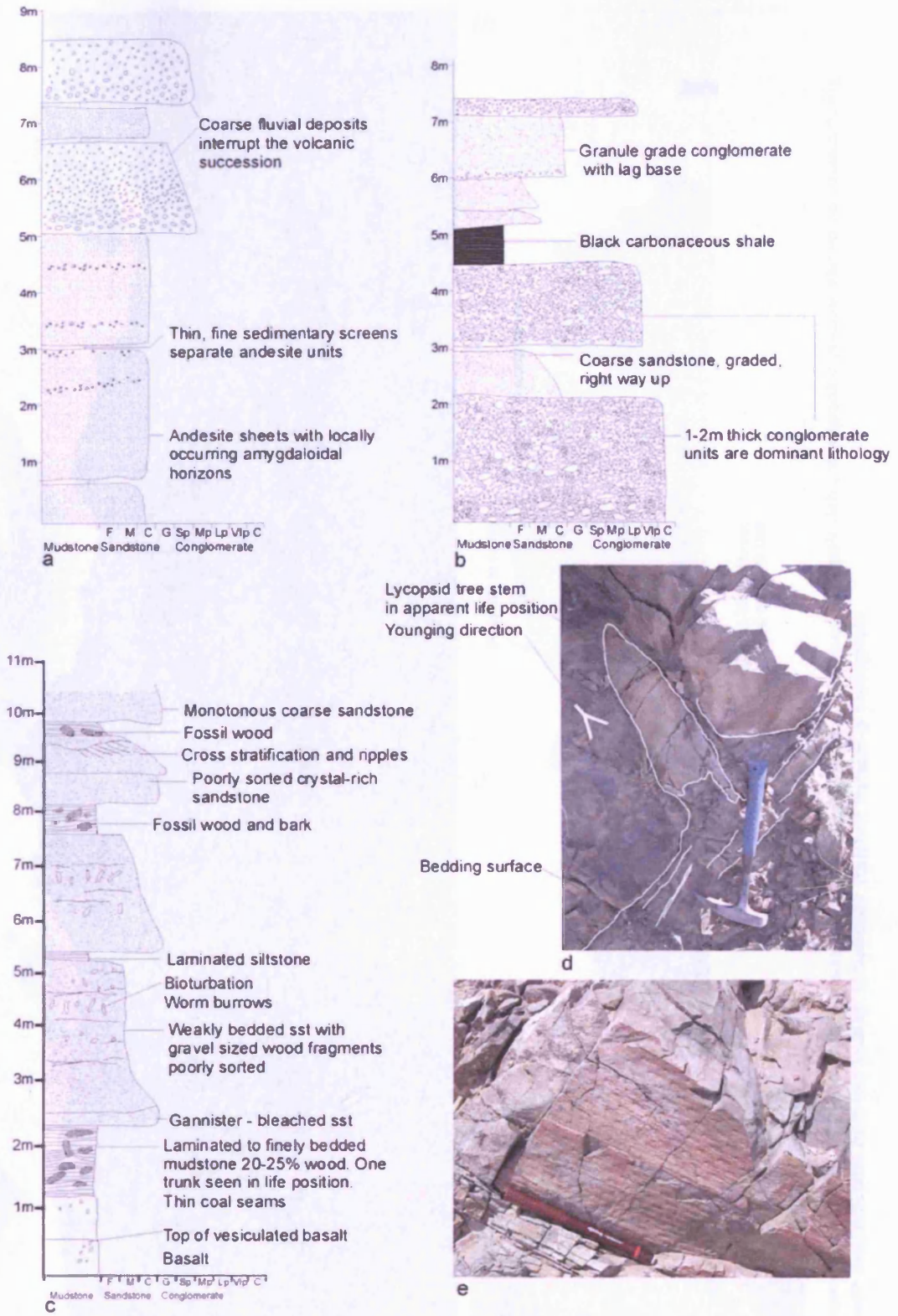

Fig. 3.5 a) Lithological log from locality 55.1 (stratigraphic position shown on Fig. 3.3) showing stratigraphically lowest sedimentary units in Gurvan Morin Höndiy formation. Sediment screens within lava sequence delimitate lava flow-units. b) Lithological log from locality 54.16 (stratigraphic position shown on column 4, Fig. 3.3) showing detail of sandstone and conglomerate beds in GMHF, features a carbon-rich black shale unit. c) Lithological log from locality 54.11 (stratigraphic position shown on column 4, Fig. 3.3) showing detail of sandstone shale beds in GMHF, features lycopsid bark impressions in mudstones and fine sandstones d) Photograph showing tree trunk apparently in life position standing perpendicular to the bedding surface e) Photograph showing lycopsid tree-bark impressions in situ.

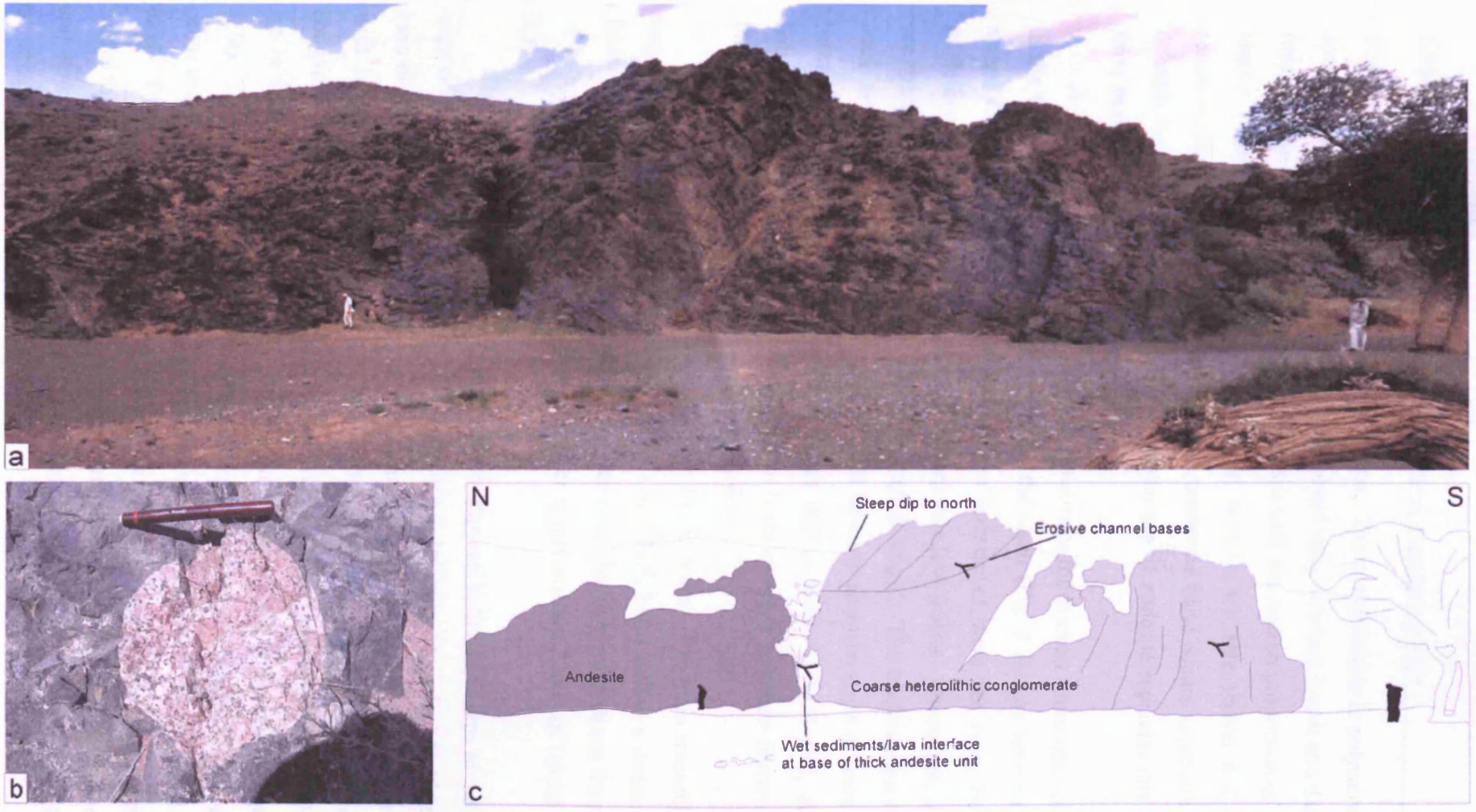

Fig. 3.6 a) Panoramic photograph showing 40m thick conglomeratic succession (right) beneath trachyandesite stack (left), stratigraphic position shown on column 5, Fig. 3.3, b) granite clast in coarse conglomerates from this locality, c) summary sketch of features in photograph.

50m thick sequence of massive conglomerate. The conglomerate is polymictic and poorly sorted, containing clasts of granite, andesite, sandstone, siltstone, basalt and dacite with sizes ranging from 10 to 100 cm. Granites comprise both the highest proportion of clasts and the largest clasts. Individual beds or bedding surfaces are rare within this conglomerate sequence; however, one 30 cm thick coarse-sandstone band occurs approximately midway through the unit. A 10 m thick densely feldspar-phyric andesite separates this conglomerate from another 80 m of similar lithology above.

A 140 m thick andesite stack, which constitutes the thickest continuous outcrop of lava in the GMHF, defines the top of Unit C in the south (Fig. 3.3). As with similar massive andesite stacks lower in the formation, lava boundaries were not seen, but the stack's thickness suggests it must represent several separate lava bodies. Phenocryst size and shape are the only factors which vary with stratigraphic height. The trachyandesites within this stack are generally more densely packed with feldspar phenocrysts than units lower in the formation. Phenocrysts are subhedral, range in size from <1 to 4 mm, and constitute between 50 and 80% of the rock. Trachytic textures are a common feature of the lava. Phenocryst size decreases upwards through the stack.

The lithologies of Unit C generally thin to the north. The main traceable unit is the large andesite stack at the top of the succession, which helps define a series of 2nd order folds. From structural reconstructions, it is estimated that this unit reduces from a thickness of 140m in the south to 20m in the north, over approximately 2.5km of lateral extent (Fig. 3.3).

The most complete section of stratigraphy exposed in the north dips to the north at the edge of the GMHF outcrop area. This sequence is laterally equivalent to Unit C. At the base of the sequence is a 50m composite sequence of 10 to 50cm thick coarse sandstones with intercalated mudstones, overlain by 40m of coarse sandstones, local channelised conglomerates and thin, cross-stratified mudstones. Several scoriaceous basalt horizons 50 cm in thickness were identified within this otherwise entirely sedimentary sequence (Fig. 3.7a). The relatively thinly bedded sediments contain many small-scale folds, which do not occur in other parts of the succession; these minor folds verge to the north and plunge to the west. They are a rare example of folding that occurs at an outcrop scale in the OUVG. Above this, the sequence continues to coarsen into a 6m thick pebble to cobble conglomerate unit containing mainly andesite clasts. Some large cobbles of bioclastic crinoidal limestone occur in this bed.

Seventy metres of aphyric basalt are intercalated with the conglomerate, as a 25 m thick lower unit and a 35 m thick upper unit. A 5 to 10 cm sandstone band divides the two lavas and the upper basalt unit has an undulating sediment-mixed base. Above the upper basalt is another 80 m of coarse, poorly-sorted heterolithic conglomerate with clasts up to 60 cm in size, of jasper, basalt, massive quartz and mudstone. In the top ten metres of the conglomerate, clast sizes decrease to granule-grade, indicating the section is right way up. The conglomerate is overlain by a 1 m thick mudstone, and 5 to 10 cm sandstone-mudstone graded units with coarse erosive bases, again indicating the section is right way up. Eighteen metres of poorly-bedded volcanic sandstone constitutes the highest sedimentary unit beneath the lava at the top of the formation.

The 20 m thick northern equivalent of the major andesite stack in Unit C lies near the top of the exposed lithologies in the north (Fig. 3.3). The top of this 5m-thick unit locally contains lenses of lava with scoriaceous texture. It is overlain by a 1 to 2 m thick basalt, the base of which holds entrained clasts of the trachyandesite. The basalt is overlain by the uppermost unit of the GMHF stratigraphy, an andesite sheet of 3 m minimum thickness, which features 1 to 2 m thick pillow lavas (Fig. 3.7 b), which confirm the northerly younging direction (Fig. 3.3).

The formation is most altered at its northern and southern margins and at the margins of thick lava sequences, where carbonate veins have epidotised haloes (Fig. 3.7 c).

3.2.2 Shargyn Moghai Formation

The c.2000 m thick Shargyn Moghai (Yellow Snake) Formation (SMF) is situated stratigraphically and conformably above the Gurvan Morin Höndiy Formation (Fig. 3.2). It is comprised of a relatively monotonous succession of basaltic andesites and andesites (Fig. 3.8). Around six hundred metres of stratigraphy from the upper half of this formation were recorded along one continuous transect and a succession from a parallel shorter transect along strike to the west was also documented. The transects cut across structural grain in the southern limb of the regional syncline (Fig. 3.2). The uppermost parts of the formation were recorded on the northern limb, below the overlying Tsagaan Nuruu formation. Reconnaissance fieldwork across the remainder of the SMF outcrop area indicated that the formation deviates little from the lithologies seen along the transects.

Bed thicknesses range from 2 to 10 m and are mainly identified through scarp and dip slopes. There is rarely more than 1 to 2 cm of rubbly volcanic detritus between lava sheets; most contacts are lava on lava, suggesting high effusion rates. Individual flows exhibit

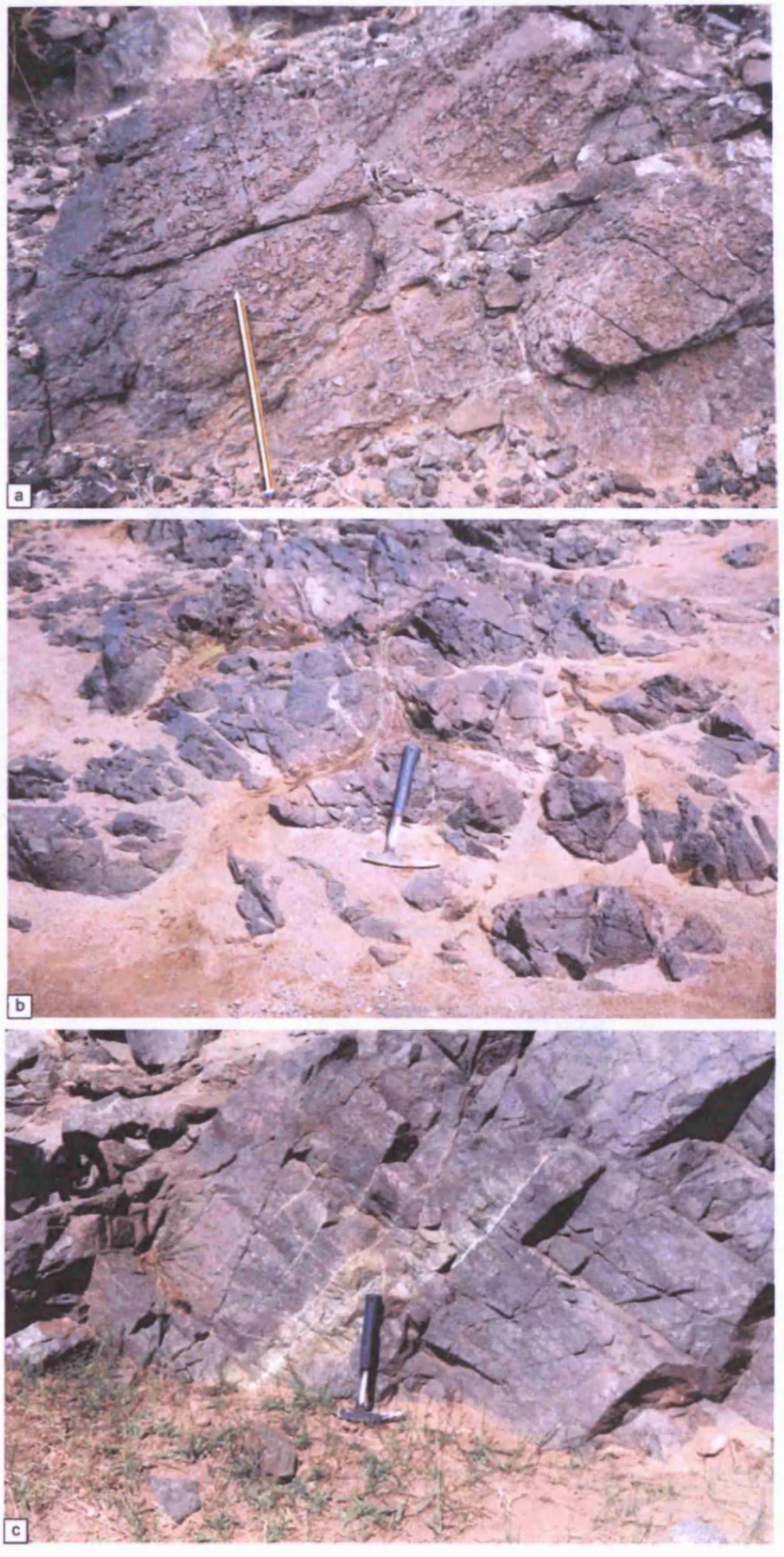

Fig. 3.7 a) Photograph showing scoriaceous texture from upper parts of GMHF stratigraphy, b) photograph showing andesite pillow-lavas from near the top of the GMHF stratigraph/y, c) 20cm wide epidotised alteration halo around carbonate vein in trachy-andesite.

Fig. 3.8 Stratigraphic columns from Shargyn Moghai Formation, transect study area shown on Fig.3.2, a) northerly dipping sequence in the southern limb of first-order west plunging syncline (line ② on Fig. 3.2), b) section of stratigraphy from 1200m along strike to west of column 'a' (line ③ on Fig. 3.2), c) top part of SMF formation in north beneath lowermost outcrops of TNF (line ④ on Fig. 3.2). Despite gaps in exposure, columns are dominated by lava and few intercalated sedimentary rocks are exposed.

variations in phenocryst phase and size, vesicularity, flow banding and brecciation - most sheets have relatively massive interiors and brecciated flow margins. Both aphyric and porphyritic textures occur, dominantly featuring euhedral plagioclase phenocrysts (Fig. 3.4, c & d). Groundmasses primarily consist of plagioclase micro-laths. Small, partially resorbed, granitoid particles occur in one section and are interpreted to represent wall-rock xenoliths, introduced during ascent (Fig. 3.4, e & f). Exposures in the uppermost 150 m of the formation contain siltstone-grade laminated volcaniclastic sediments that crop-out between c.10 m thick basalt lavas.

3.2.3 Tsagaan Nuruu Formation

The c.1000 m thick Tsagaan Nuruu (White Ridge) Formation (TNF) is comprised of a number of distinctive 5 to 10 m thick felsic units, which are blocky and crystalline, and form positive topography, interbedded with ca. 60 m thick fine-grained volcaniclastic sediments, which are sparsely exposed (Fig. 3.9). Near its top, between felsic units, the formation contains 2 to 3 m thick basalt lavas, 25 to 35 m sections of sandstone and 10 to 15 cm black organic-mudstones with plant fragments.

The Tsagaan Nuruu Formation crops out in the northwestern part of the contiguous stratigraphy, within the core of a first-order regional syncline. The high competency contrast between the relatively thin felsic units and the thick intercalated tuff sequences results in highly visible second order folds traced by the felsic units as ridges snaking across the landscape.

The lowest units of the TNF are two 5 m thick rhyolites sandwiching a 16 m thick granule-grade conglomerate with subangular to subrounded clasts of basaltic and andesitic lithologies exhibiting trachytic textures. The middle parts of the formation contain another five rhyolite beds, ranging between 5 and 18 m thick separated by 20 to 60 m swaths of almost no outcrop. Limited local exposures contain finely laminated and highly silicic fine-grained units, which appear to be volcaniclastic in origin. These are preferentially exposed near the bases of the blocky rhyolites.

In thin section, the rhyolites are predominantly composed of a fine-grained groundmass featuring spherulites of intergrown quartz and plagioclase, with euhedral phenocrysts of orthoclase constituting 5-10% of the rock mass (Fig. 3.4 g). It is suggested that these blocky rhyolitic units constitute lava-like ignimbrites or rhyolitic lavas of

abnormally low viscosity, which would explain the high aspect ratio, and wide areal extent of these units.

In the upper part of the TNF, intervals between blocky crystalline units are thinner and sequences are better exposed. In a 5 m thick bed of black shale beneath the eighth rhyolitic unit (Fig. 3.9), cordaites leaf impressions occur on bedding-parallel surfaces (Fig. 3.10 a). Interbedded 1 m thick massive sandstones and carbon-rich black shales occur below the ninth rhyolitic unit (Fig. 3.10 b). These black shaley tops of graded sandstones exhibit wood and leaf fragments and are overlain by a 5 to 30 cm thick bed of laminated siltstone. The bases of the massive sandstone beds have rip-up clasts of the underlying siltstone (Fig. 3.10 c). Where sandstone lies beneath a black shale horizon, it appears to form a gannister-style layer. Underlying these sediments is a 5 m thick, coarsely feldspar-phyric basaltic lava (Fig. 3.4 h).

The top of the TNF stratigraphy recorded here comprises around 60 m of almost continuous exposure near the core of the regional syncline. At the base of this sequence is exposures of a 1.5 m thick coarse immature sandstone bed, overlain by a 2 m thick feldspar-phyric, trachytic textured basalt, which in turn is overlain by a 2 m thick rhyolitic unit, similar to others from lower in the formation. Between this rhyolite and the next (and uppermost) unit is 10.5 m of mudstone interbedded at 1.5 to 4 m intervals with three coarse immature tabular sandstone beds of 20 to 40 cm thickness. The last rhyolite bed is 3.5 m thick and is overlain by 18 m of interbedded mudstones and coarse sandstones of 30 to 50 cm thickness. The uppermost unit recorded in the TNF is a poorly sorted matrix-supported

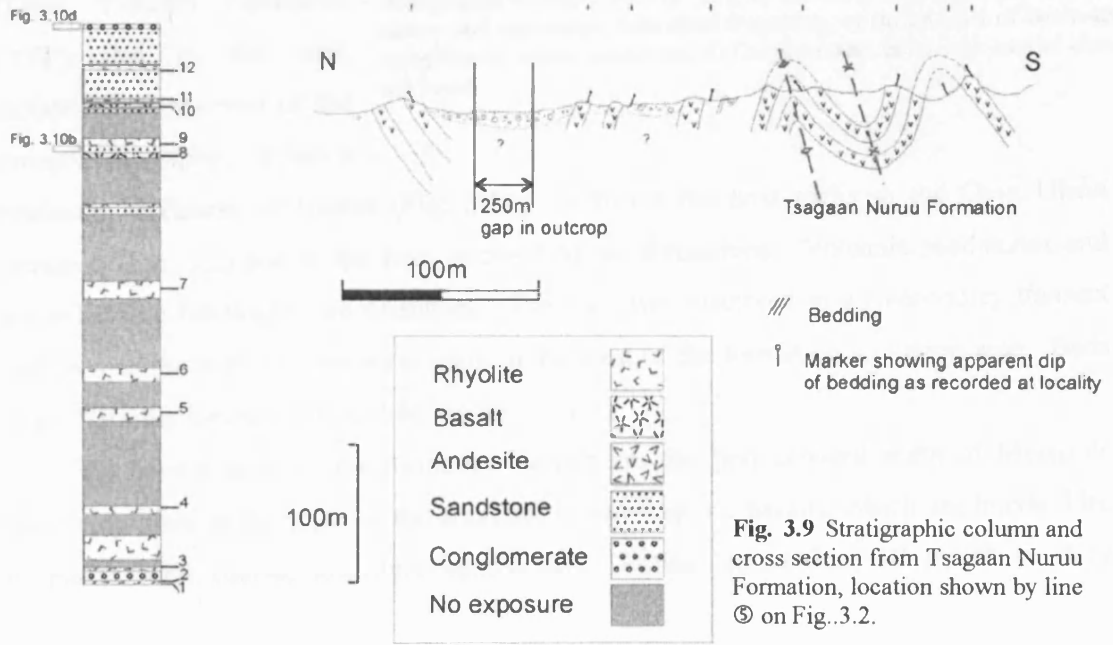

Fig. 3.9 Stratigraphic column and cross section from Tsagaan Nuruu Formation, location shown by line ⑤ on Fig..3.2.

conglomerate with pale, vesiculated felsic clasts of 1 to 10 cm diameter, in a dark matrix (Fig. 3.10 d).

The TNF may be considerably thicker than recorded here, as the syncline plunges to the west, where there is more outcrop. However, the stratigraphic relationship between the rocks further to the west and the TNF stratigraphy as described here is ambiguous, as the two are divided by large outcrop gaps interpreted to represent major structural breaks.

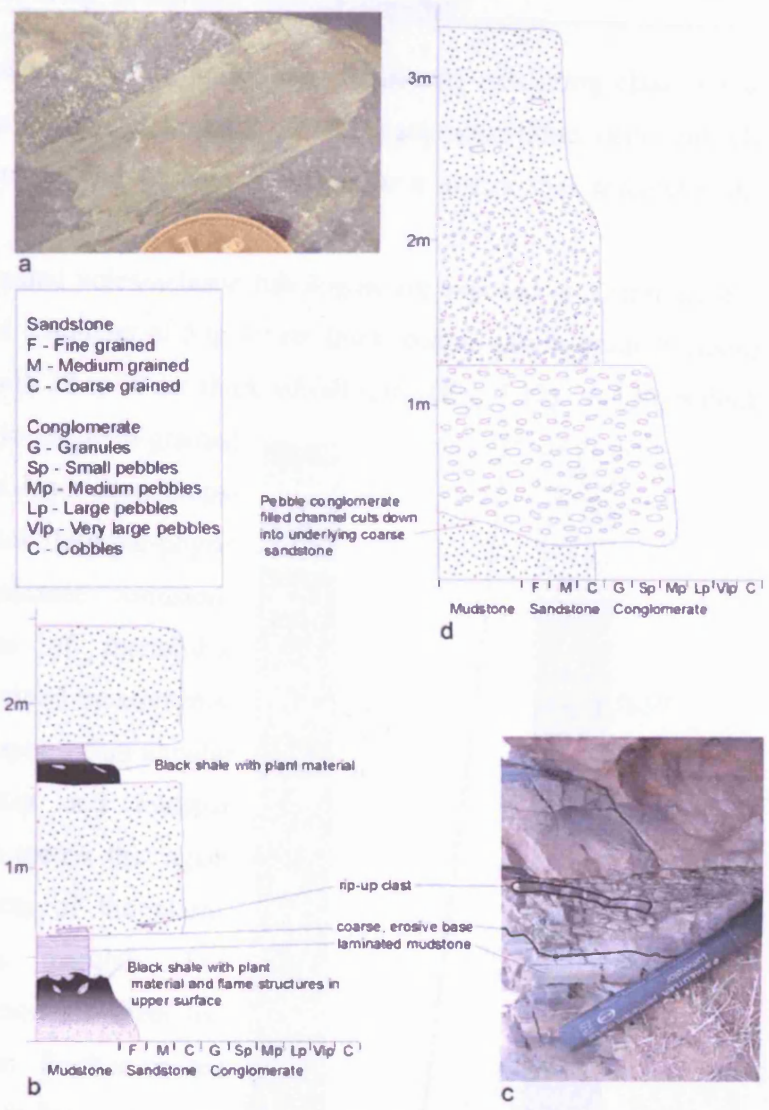

Fig. 3.10 Lithological logs and photographs from upper part of TNF (for stratigraphic position see Fig. 3.9), a) Cordiates leaf fragment, b) Sandstones and mudstones with plant fragments, c) rip up clast of laminated mudstone in coarse sandstone, d) Conglomerate units with curved channel bases.

3.2.4 Yasun Eliy-e Formation

The Yasun Eliy-e (Dead Vulture) Formation (YEF) lies in the east, isolated from the rest of the group stratigraphy. It has a minimum thickness of 1500m (Fig. 3.11). It forms the host rocks to the Oyut Ulaan intrusion (Fig. 3.2) and is the least evolved of the formations. Volcanic sandstones and trachybasaltic lithologies are dominant. The YEF was observed in a river-valley transect that crosses the regional structural grain in the west of the formation's outcrop area. Beds in the YEF dip between 25° and 60° to the north.

The lowest units of the formation (which are the first exposed north of Mesozoic basin sequences to the south of the area) are feldspar-phyric basalts, which are interbedded in places with coarse, immature sandstones. Further up-section, 10 to 20 m thick

trachybasalts are interbedded with poorly sorted conglomerates, exhibiting clasts up to boulder grade. Unlike the conglomerates from GMHF these are mono-lithic, being entirely comprised of blue-grey andesites and basaltic andesites in a matrix that resembles the volcanic ground mass.

A series of finely laminated volcaniclastic lithologies are exposed at a stratigraphic height of 475 m, consisting of a number of 5 to 10 cm thick, coarse, lapilli-grade horizons (Fig. 3.4, i & j) interbedded with 20 to 30 cm thick ashfall tuffs (Fig. 3.12). A 110 m thick sequence of volcanic fine- to medium-grained sandstones with local parallel-lamination crops-out between 5 to 10 m thick feldspar-phyric basalts. Overlying the volcanic sandstone sequence, further sequences of monolithic conglomerates feature well defined escarpments, and drift covered lee slopes. Sub-angular andesitic clasts with vesicles and feldspar phenocrysts occur in a coarse matrix that again resembles the fine groundmass of the clasts. Some clasts have diffuse margins. The stratigraphically lowest conglomerate sheet has an exposed thickness of 10 m. Further up the stratigraphy, 30 m of similar lithology crops out, beneath two 8 to 10 m thick basaltic andesite units. Between these lavas is a 30 cm thick brecciated red-jasper horizon, overlain by 20 m of feldspar phyric basaltic trachyandesite.

Upper parts of the stratigraphy are exposed in 5 to 10 m escarpments formed by trachybasalt and basaltic trachyandesites in second order west-plunging folds. Gaps in exposure are formed by the gently dipping lee slopes of these units and buried intercalated sequences. In thin section, these lavas are porphyritic and densely

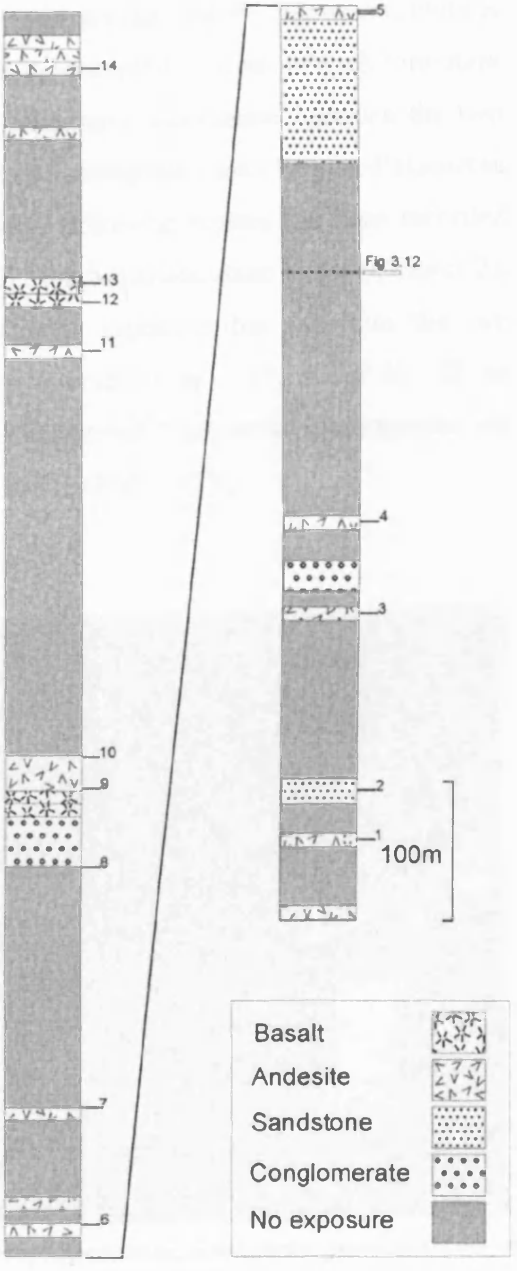

Fig. 3.11 Stratigraphic column from Yasun Eliy-e Formation, location shown by line ⑥ on Fig. 3.2.

packed with 0.1 to 1.0 mm euhedral plagioclases (An_{35}) and sparsely distributed but larger (2 to 3mm) hornblendes.

The YEF is the only part of the OUVG to be cut by minor intrusions. In the north, a 1 m wide olivine-phyric basalt dyke trends 130; south of this, in the centre of the area, a small dioritic intrusion with a roughly circular surface expression 20 m in diameter, cuts the volcanic-sedimentary succession.

The stratigraphic relation between the Yasun Eliy-e formation and the rest of the group is ambiguous. It lies in the east, and the group younging direction is with the plunge of the major syncline to the west, suggesting that the YEF predates the GMHF. However, there is 16 km of linear separation of poor exposure between the recorded sections of each formation (Fig. 3.13), and the possibility that there is some alternative association between the two cannot be ruled out. One explanation for the gap in the stratigraphy may be post-Palaeozoic brittle deformation. Evidence for a Mesozoic sinistral strike-slip regime has been recorded from both the greater region (Lamb et al., 1999) and the Saykhandulaan Inlier (Chapter 2). On satellite imagery, it appears that the area of poor exposure that separates the two formations is also where several major lineaments intersect (Fig. 3.13, a and b). If the sinistral and dextral (antithetic) fault movements interpreted from aerial photographs are reversed, the YEF moves closer to the base of the GMHF (Fig. 3.13 c).

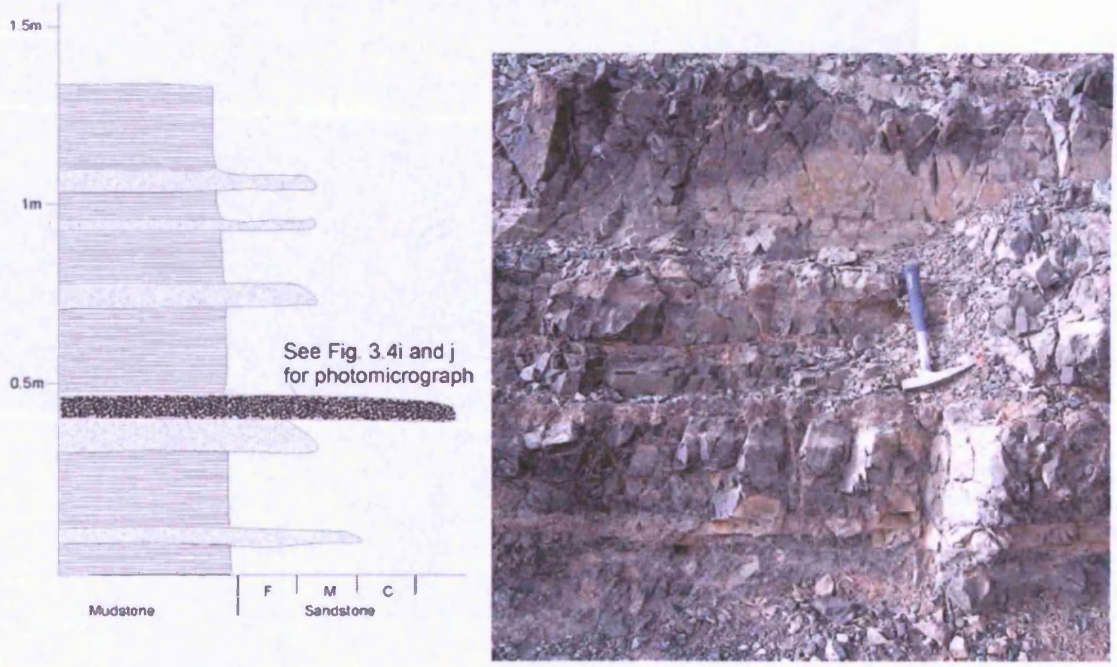

Fig. 3.12 a) Lithological log from YEF showing thin volcaniclastic units, stratigraphic position shown on Fig.3.11, b) photograph of logged sequence.

3.3 U-Pb dating of the Oyut Ulaan Volcanic Group

Two samples were analysed by Isotope Dilution Thermal Ionization Mass Spectrometry (ID-TIMS) at the NERC Isotope Geosciences Laboratory (NIGL), using analytical procedures as described by Noble et al. (1993). One dated sample was a welded ignimbrite from the lower parts of the TNF stratigraphy, the other was a granite clast from the coarse conglomerates in lower parts of the GMHF (Results - Appendix B).

Zircon crystals were separated from <355μm grained bulk-rock powder using standard vibrating-table, specific gravity and magnetic techniques. Crystal fractions for analysis were picked by hand under a binocular microscope; all analysed fractions consisted of single grains. Some zircon crystals were subjected to air abrasion (Krogh, 1982), whist others used a modified chemical abrasion technique (Mattinson, 2005). The zircon crystals were ultrasonically washed in 4N HNO_3, rinsed in ultra-pure water, then further washed in warm 4N HNO_3 prior to rinsing with distilled water, all of which aimed to remove surface

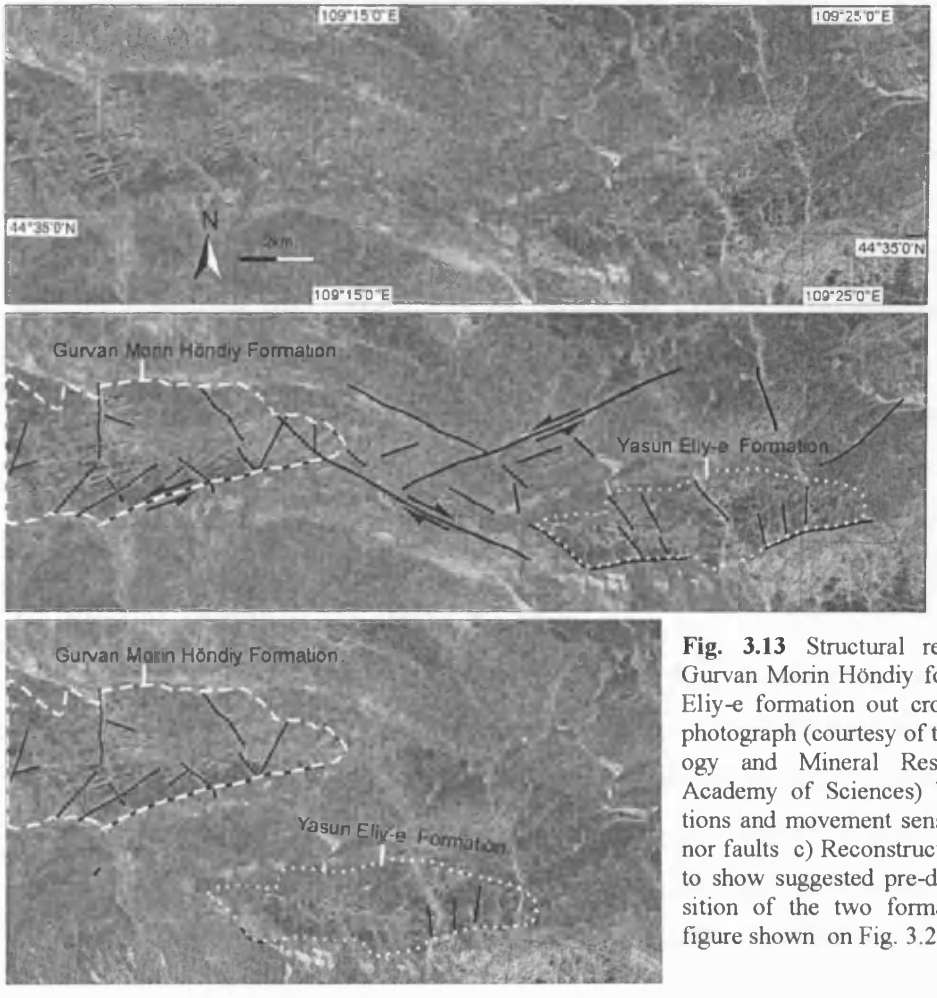

Fig. 3.13 Structural relationship between Gurvan Morin Höndiy formation and Yasun Eliy-e formation out crop areas. a) Aerial photograph (courtesy of the Institute of Geology and Mineral Resources, Mongolian Academy of Sciences) b) interpreted locations and movement sense of major and minor faults c) Reconstructions of major faults to show suggested pre-deformation juxtaposition of the two formations. Location of figure shown on Fig. 3.2.

contamination. A mixed ^{205}Pb - ^{235}U tracer was used to spike all fractions. Dissolved, spike equilibrated samples were not subjected to ion-exchange procedures but were converted to chloride and loaded onto degassed rhenium filaments in silica gel following a procedure modified after Mundil et al (2004). Isotope data were collected using a Thermo Electron Triton with SEM for ion counting, and Faraday cups for voltage measurement when ion counts exceeded 800,000 per second. Errors were calculated using numerical error propagation (Ludwig, 1980). Isotope ratios were plotted using Isoplot version 3 (Ludwig, 1993, 2003), and error ellipses reflect 2σ (95% confidence level) uncertainty. Mean Squared Weighted Deviates (MSWD) are calculated by dividing the sum of the squares of the mis-fits to the regression line by the number of data points minus two, and are a measure of the scatter of points. If scatter is limited to that caused by analytical errors, MSWD should = 1, too much scatter results in MSWD > 1 and too little (less than expected from analytical errors) results in MSWD <1. MSWD values near 1 give a high level of confidence that a true isochron is indicated by the data (McIntyre et al., 1966).

Lead blanks recorded during three separate batches of analysis ranged from 1.2 pg to 0.2 pg. Samples were blank corrected using the blank ^{204}Pb:^{206}Pb:^{207}Pb ratio. Correction for common lead in all samples was carried out using the Stacey-Kramers common lead evolutionary model (Stacey and Kramers, 1975), however the amount of common lead in the analysed zircons was negligible, as the correction was dominated by the Pb blank.

The rhyolite from the TNF yielded two single-grain zircon analyses, one concordant and one discordant (Fig. 3.14). The concordia age calculated for the concordant point is 323.12 ±0.64 Ma. This is the age of the base of the youngest formation of the OUVG. If both points are considered, the upper intercept is 322.9 ± 3.5. The extremely low MSWD (0.0026) is meaningless as it refers to only one point and so cannot measure scatter. When MSWD is calculated for the two points, the result is zero, as two points will always define a straight line, and there will be no scatter of those two points from the line they define.. Further data points from this unit are desirable.

The granite cobble from the GMHF yielded three overlapping, concordant, single-grain zircon analyses (Fig. 3.14). The concordia age calculated from these three points is 338.93 ±0.85 Ma. One further analysis was slightly discordant, but within error of the calculated concordia age, producing an average age of 339.53 $\pm$ 0.98 (supported by 4 analyses). Another result had a greater degree of discordance, and was excluded from the age calculation. The discordance encountered can arguably be attributed to lead loss.

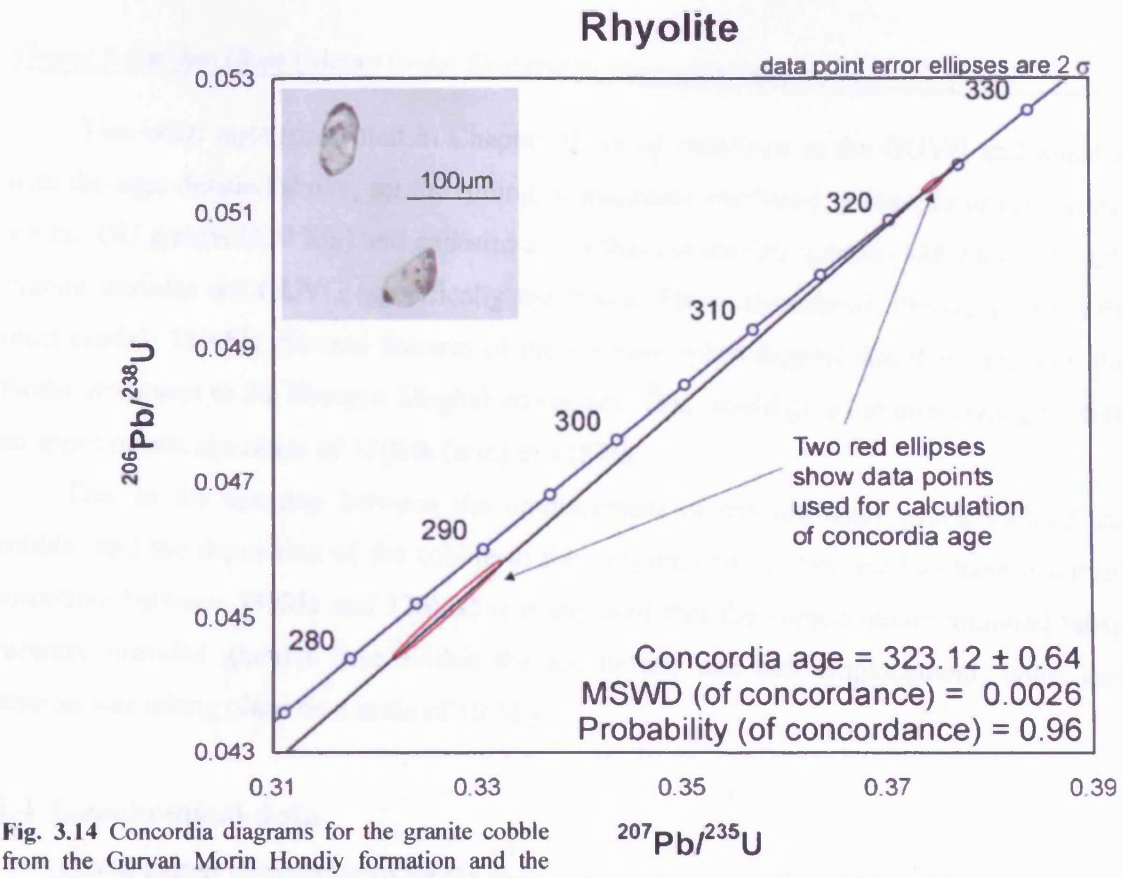

Fig. 3.14 Concordia diagrams for the granite cobble from the Gurvan Morin Hondiy formation and the rhyolitic unit from the lower parts of the Tsagaan Nuruu Formation. Thin ellipses show the data points, and corresponding errors. Grey-filled ellipse shows the calculated concordia age. Refer to text for an explanation of MSWD.

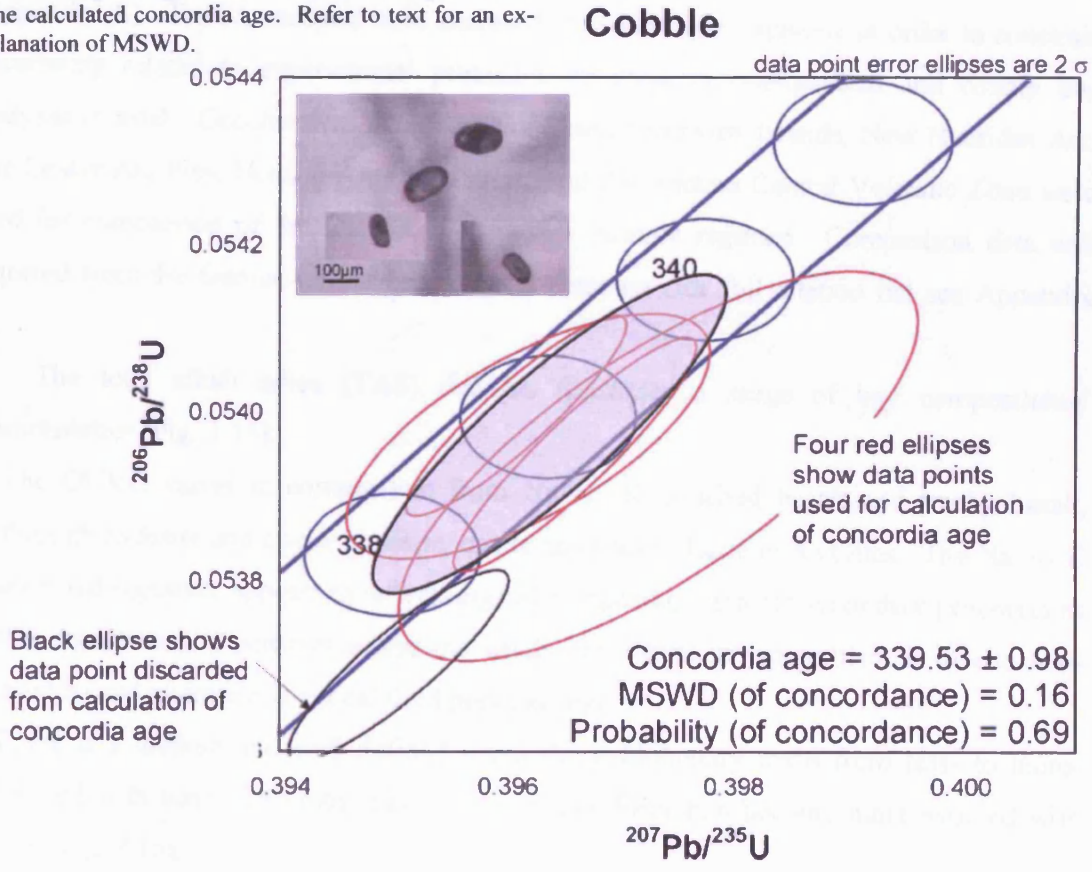

Two other ages (presented in Chapter 4) are of relevance to the OUVG and together with the ages detailed above, set the timing of magmatic evolution within the group. These are the OU granite (330 Ma) and andesite dykes that cut the OU granite (328 Ma). The OU granite intrudes the OUVG (specifically the Yasun Eliy-e formation); therefore, the YEF must predate 330 Ma. Several features of the andesite dykes suggest that they represent the feeder structures to the Shargyn Moghai volcanism. This would give the intervening GMHF an approximate age range of 330Ma (min) to 328Ma.

Due to the age gap between the emplacement of the intrusion which yielded the cobble, and the deposition of the cobble in the conglomerate (interpreted to have occurred sometime between 330Ma and 328Ma) it is apparent that the conglomerate included fairly recently intruded granites from within the arc terrane and that emplacement, uplift and erosion was taking place on a scale of 10 M.y.

3.4 Geochemical data

One-hundred representative whole rock samples from the Oyut Ulaan Volcanic Group were analysed using standard XRF spectrometry techniques at the University of Leicester (Appendix A). Twelve samples were analysed in duplicate or triplicate in order to constrain uncertainty related to experimental precision, resulting in one-hundred and twenty one analyses in total. Geochemical data from the South Sandwich Islands, New Hebrides Arc, The Lesser Antillies, Honshu Arc, Sunda Arc, and the Andean Central Volcanic Zone were used for comparison of the OUVG with known tectonic regimes. Comparison data was acquired from the Georoc online geochemical database (for full citation list see Appendix C).

The total alkali silica (TAS) diagram illustrates a range of key compositional characteristics (Fig. 3.15):

1) The OUVG varies in composition from Na +/- K enriched basalt and trachy basalt, through andesite and trachy andesite, dacite and trachy dacite to rhyolites. The Na +/- K enriched signature appears to reflect original composition and not secondary processes as this signature is a constant across the whole arc, whilst metamorphism is low to non-existent and alteration is a local field phenomenon.
2) There is a distinct and well defined magmatic evolutionary trend from less- to more-evolved with time. The most basic parts of each formation become more evolved with time (Fig. 3.15).

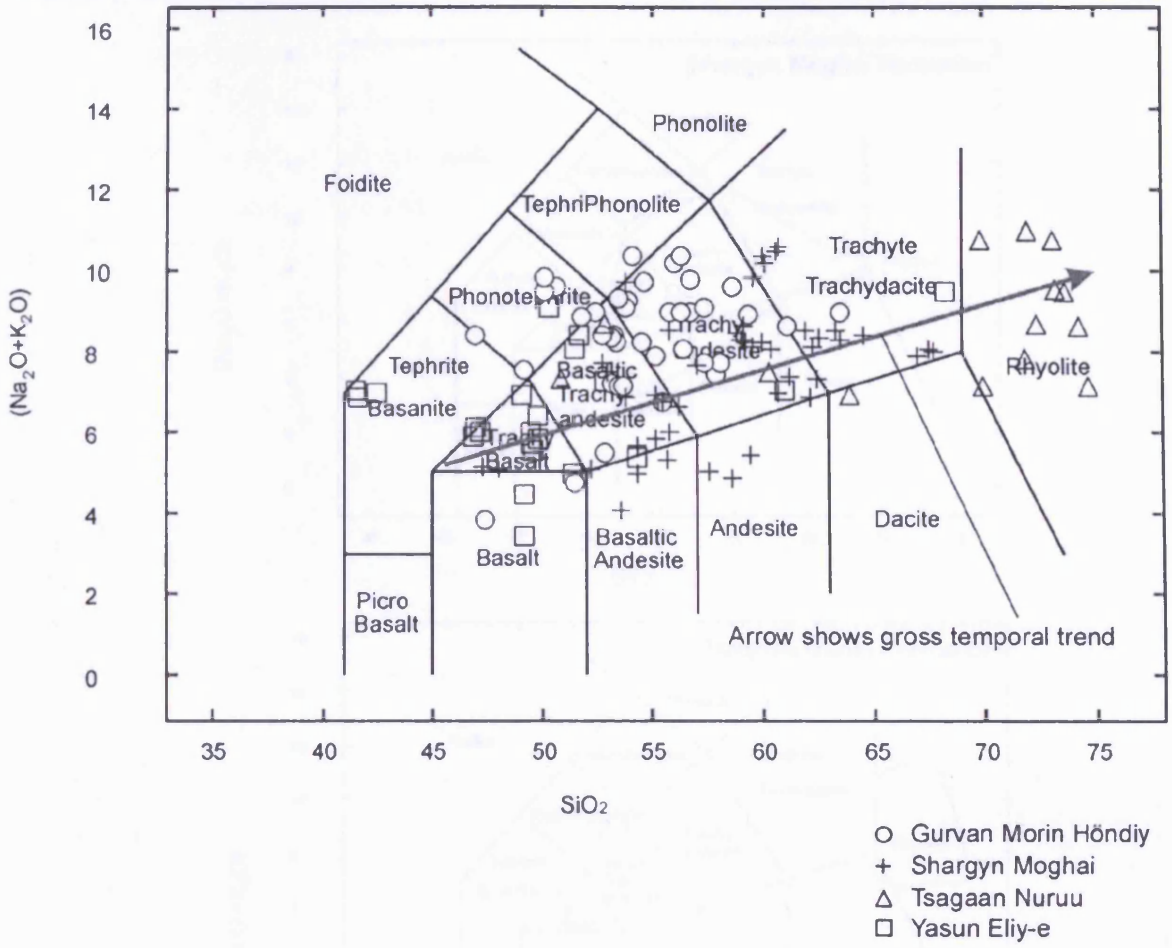

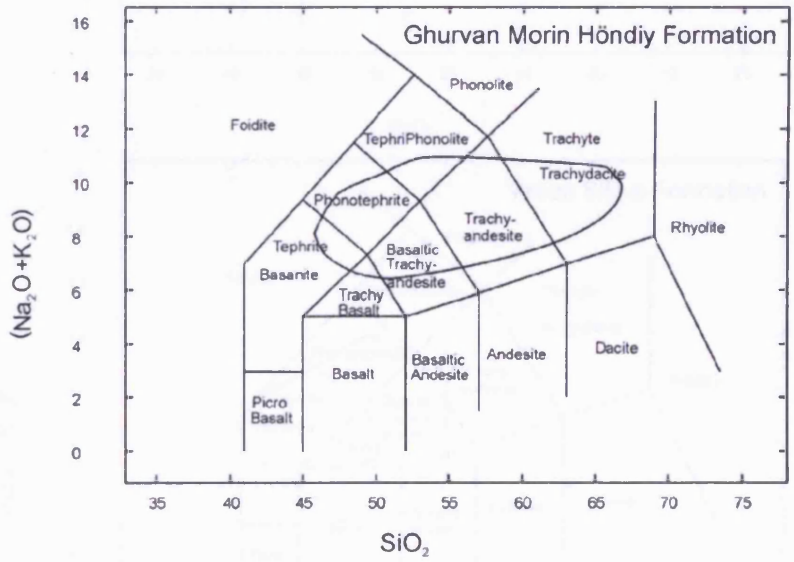

Fig. 3.15 Top; Total Alkalis Silica (TAS) diagram after Le Bas et al. (1986) for Oyut Ulaan Volcanic Group rocks showing wide range of compositions for both silica and alkalis. Bottom and overleaf; Thumbnail graphs showing field of analyses of each formation. Note that the most basic end of formation composition becomes more evolved with time.

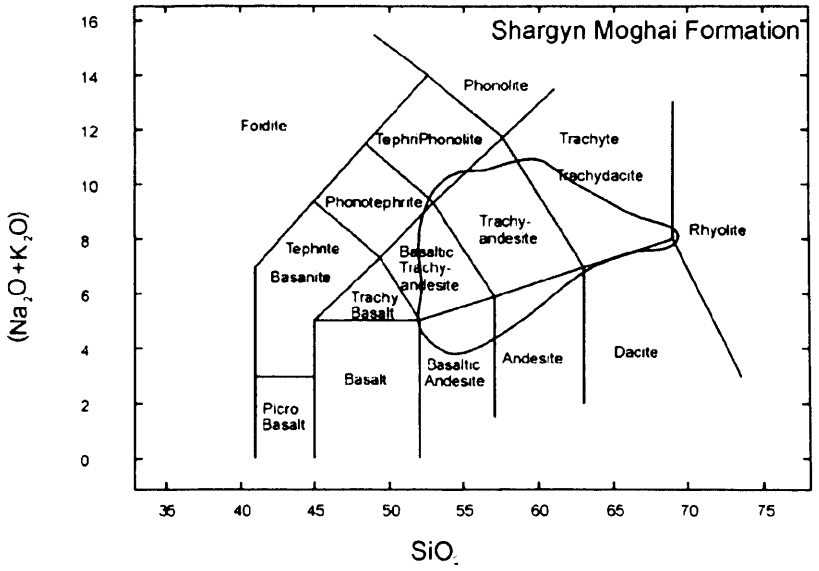
Shargyn Moghai Formation
Foidite
Phonolite
TephriPhonolite
Trachyte
Trachydacite
Phonotephrite
Trachy-
andesite
Rhyolite
Tephrite
Basanite
Basaltic
Trachy-
andesite
Trachy
Basalt
Basalt
Basaltic
Andesite
Andesite
Dacite
Picro
Basalt
(Na2O+K2O)
SiO2

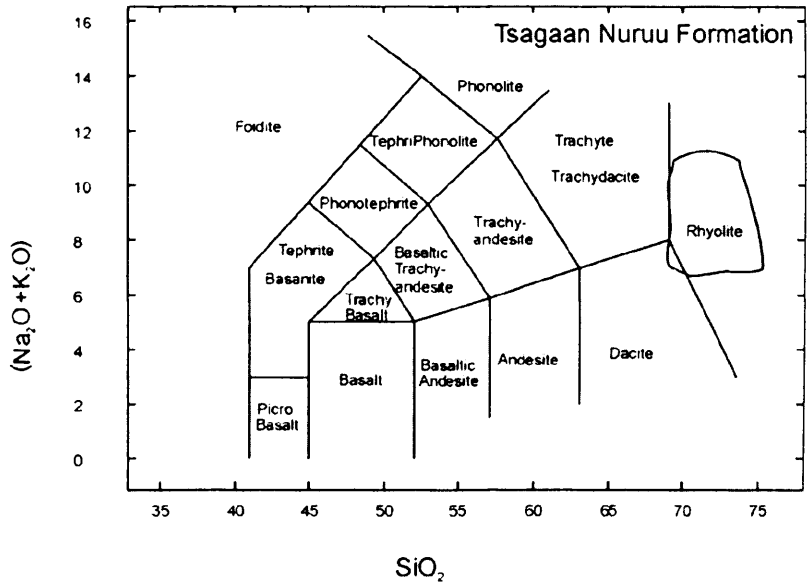
Tsagaan Nuruu Formation
Foidite
Phonolite
TephriPhonolite
Trachyte
Trachydacite
Phonotephrite
Trachy-
andesite
Rhyolite
Tephrite
Basanite
Basaltic
Trachy-
andesite
Trachy
Basalt
Basalt
Basaltic
Andesite
Andesite
Dacite
Picro
Basalt
(Na2O+K2O)
SiO2

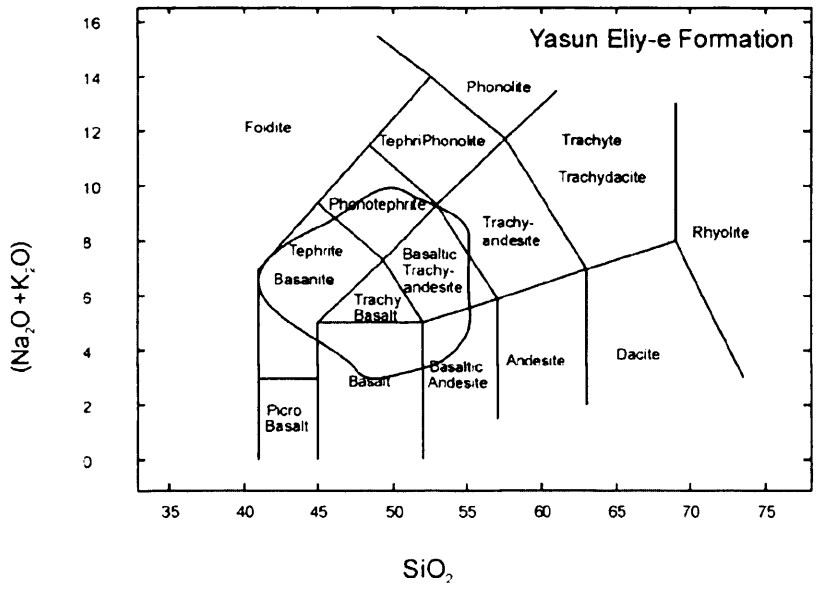
Yasun Eliy-e Formation
Foidite
Phonolite
TephriPhonolite
Trachyte
Trachydacite
Phonotephrite
Trachy-
andesite
Rhyolite
Tephrite
Basanite
Basaltic
Trachy-
andesite
Trachy
Basalt
Basalt
Basaltic
Andesite
Andesite
Dacite
Picro
Basalt
(Na2O+K2O)
SiO2

3) There is a sharp rise in silica values in the TNF formation compared to the other formations.

Trace element spidergrams illustrate the key characteristics of subduction-zone derived magmas; e.g. high ratios of low field strength/high field strength elements (LFSE:HFSE) and a negative Nb anomaly (Saunders et al., 1980; Wilson, 1989). Furthermore, the trace element signature of the OUVG most closely resembles patterns from mature oceanic/ continental arcs. Multi-element variograms (Fig. 3.16) show the closest compositional analogues are arcs and cordillera such as Sunda, Honshu, and the Andes, with elevated, convex upwards Sr-Th patterns and negative to gently concave upwards Ce-Y patterns. Ratio-ratio plots involving Zr, Ti, Nb, Ce, and Y (e.g. Nb/Y vs Zr/Y; Fig. 3.17) confirm that when the data are plotted in tightly constrained fields, the OUVG exhibit very similar compositions to highly evolved arcs such as Sunda, Honshu and the Central Andes.

Geochemical results generally show an evolutionary trend within the OUVG, from basalts at its base

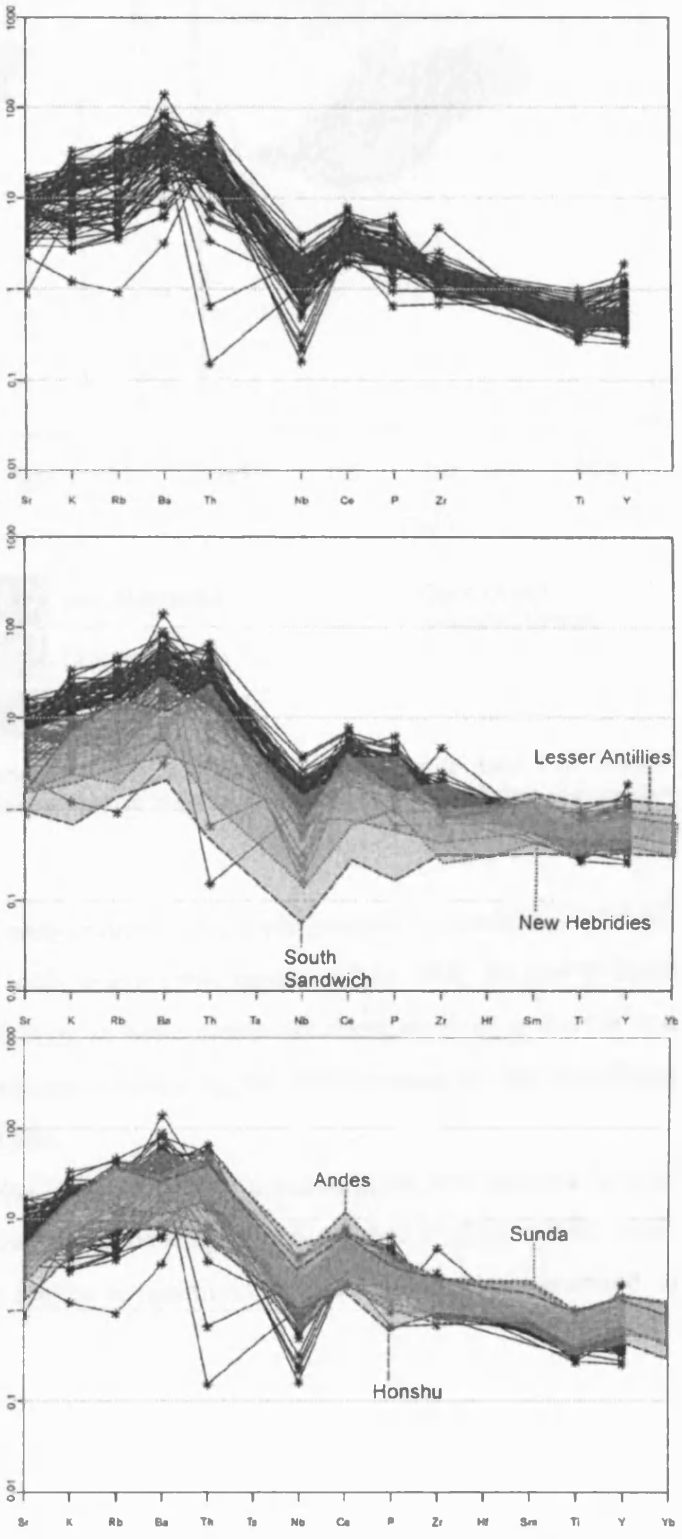

Fig. 3.16 Spidergrams for trace elements from YEF, GMHF and SMF. Fields show area of plots of comparative data from various published sources (see Appendix C). All data normalised to MORB values of Pearce (1983)

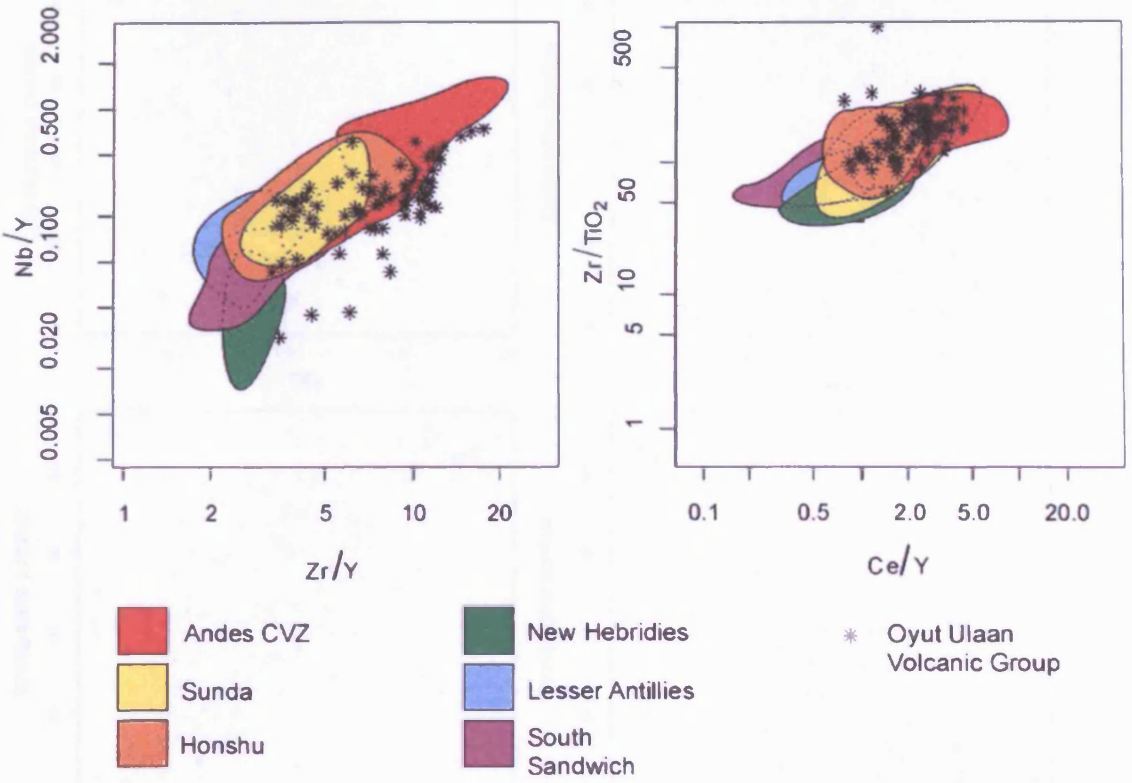

Fig. 3.17 Ce/Y versus Zr/TiO2 and Zr/Y versus Nb/Y diagrams for basalts and andesites from YEF, GMHF and SMF. Fields show summary data from known tectonic regimes. Data from various published sources (see Appendix C).

to volcaniclastic deposits of rhyolitic composition in its upper reaches. Abundances of CaO, TiO_2, Al_2O_3 and Fe_2O_3 generally fall with stratigraphic height, whilst SiO_2, Ba and Sr show general increases. Stratigraphic variations in some elemental abundances (e.g. Zr, Nb and Y) show variations that are more intricate, illustrating the development of the underlying magma chamber through time (Fig. 3.18).

The rhyolites of the TNF are weakly peralkaline to metaluminous, and have an A_2-type signature when plotted on granite discrimination diagrams developed by Eby (1990, 1992; Fig. 3.19). The A_2-type signature relates to granitoid magma chemistries generated in extensional environments.

3.5 Discussion

3.6.1 Physical volcanic model

The three contiguous formations in the west contain 4.6 km of stratigraphy from an evolving volcanic-sedimentary system, and record three distinct stages of volcanism: 1) commencement of volcanic activity within an energetic fluvial sedimentary environment, 2)

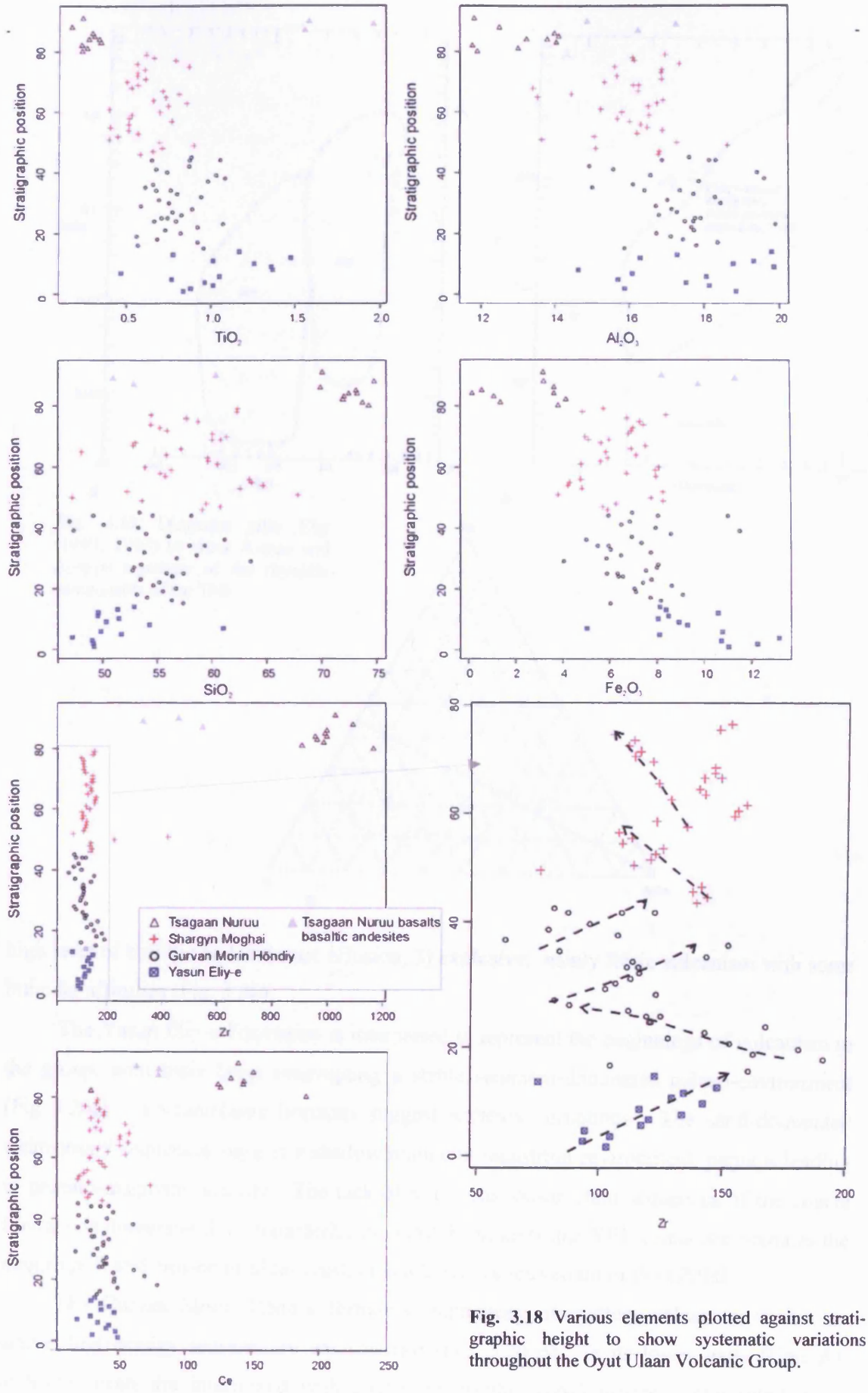

Fig. 3.18 Various elements plotted against stratigraphic height to show systematic variations throughout the Oyut Ulaan Volcanic Group.

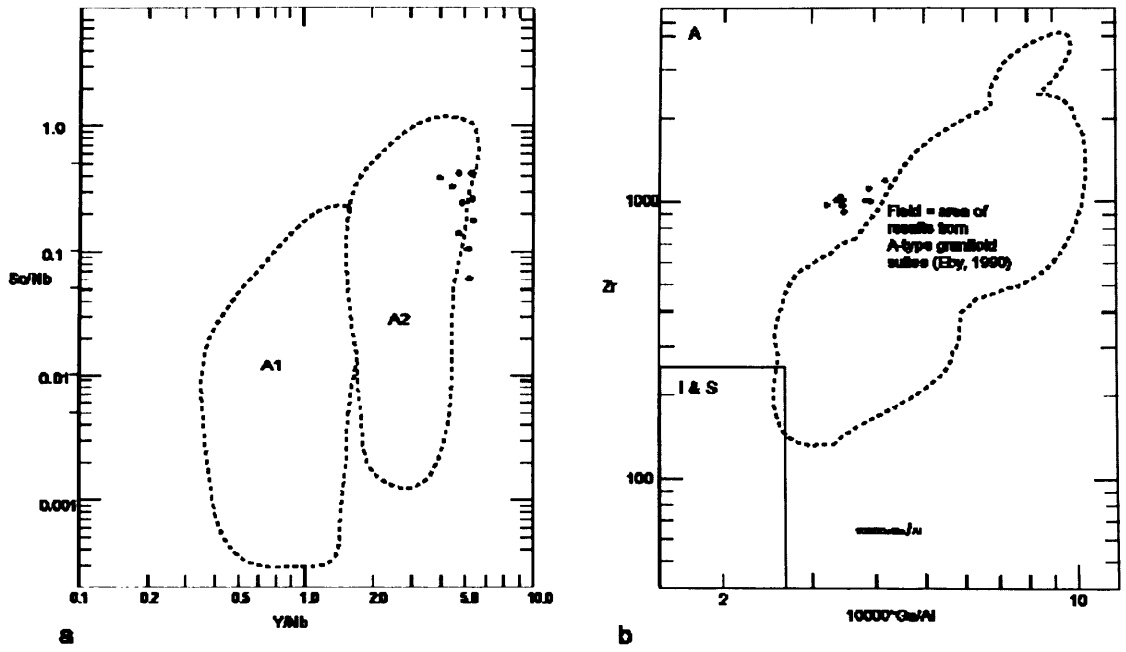

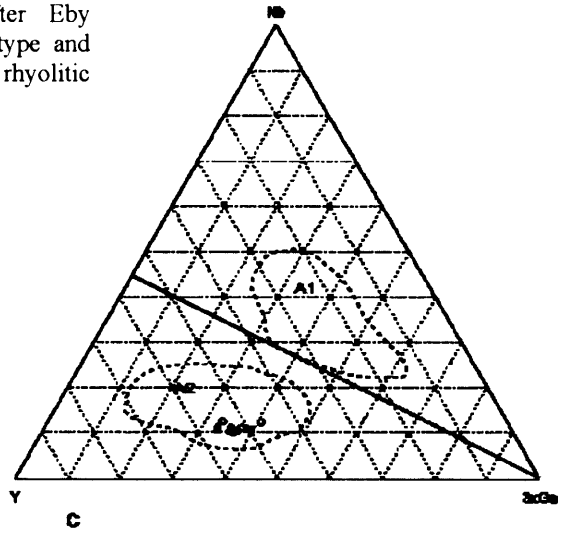

Fig. 3.19 Diagrams after Eby (1990; 1992) to show A-type and A_2-type signature of the rhyolitic components of the TNF

high rates of basaltic and andesitic effusion, 3) explosive, mainly felsic volcanism with some bimodal affinities (Fig. 3.20).

The Yasun Eliy-e Formation is interpreted to represent the beginnings of volcanism in the group, with basic lavas interrupting a stable sediment-dominated palaeo-environment (Fig 3.20a). Volcaniclastic horizons suggest explosive eruptions. The sand-dominated sedimentary sequences suggest a shallow marine or lacustrine environment, perhaps leading to phreato-magmatic activity. The lack of thick, erosion-resistant sequences of the coarse fluvial conglomerates that characterise the GMHF suggests that YEF volcanism predates the major uplift and erosion of older crust, or is a lateral facies variant of the GMHF.

The Gurvan Morin Höndiy formation represents intermittent volcanism within an active, high-energy sedimentary environment (Fig. 3.20 b). In its lower parts (Unit A), andesite sheets are intermixed with coarse heterolithic conglomerates, interpreted to be

deposited by large river systems eroding the uplands and depositing alluvial-fan sequences in the lower parts of the arc. Whilst their heterolithic nature points to a widespread provenance, the high proportion of large granite clasts suggests that the provenance-zone included uplifted sequences of earlier arc-magmatism. This suggests that at the base of OUVG volcanism, the area was not a simple immature island arc but had more in common with either an evolved island arc or a continental margin. The polymict nature of the succession's voluminous conglomerates shows that a varied geological hinterland was undergoing erosion contemporaneously with the Oyut Ulaan Volcanism.

Higher in the succession conglomerates have smaller clast-sizes, are more thinly bedded, and finer siliciclastic sediments become more common. Sandstones are commonly graded and have mudstone/siltstone caps, suggesting sub-aqueous turbidite-style deposition at some localities. Evidence of mature vegetation suggests a stable, terrestrial landscape and long inter-eruptive periods, leading to growth of plant life within a swamp-like environment. This is consistent with a palaeo-environment of braided rivers flowing into lakes and swamps in a warm, humid climate. The northwards thinning observed in lava sheets, suggests that volcanic vents were located to the south, and that lavas have wedge-like thickness patterns. Lava-sediment mixing at the base of some sheets suggests lava was emplaced onto wet sediment, resulting in loading structures. Pillow andesites at the top of the formation suggest some lava was being extruded within a sub-aqueous environment, though in light of the other evidence it is suggested that this was lacustrine or swamp-like rather than marine. The presence of bio-clastic limestone cobbles in conglomerates in the upper parts of the formation suggests proximal erosion of marine sequences, highlighting the growth of the arc from earlier marine settings.

In conclusion, it is hypothesised that stage one volcanism exhibits periodic andesitic effusion with long periods of volcanic acquiescence within a wet-humid semi-tropical environment. Initially, volcanism occurred within the rifted lowlands of a mature arc close to geologically diverse uplands. This environment likely contained large, intermittantly powerful rivers that had the capacity to transport and deposit large volumes of coarse material from the precursor arc-hinterland material to the volcanically active arc-graben. As time progressed the rate of effusion increased, as did the extent of low-swamp lands with standing lacustrine bodies and braided sand and silt bearing river systems.

The Shargyn Moghai Formation represents an abrupt change in volcanic style. It is composed almost entirely of basaltic andesite and andesite lava sheets and no non-volcanic

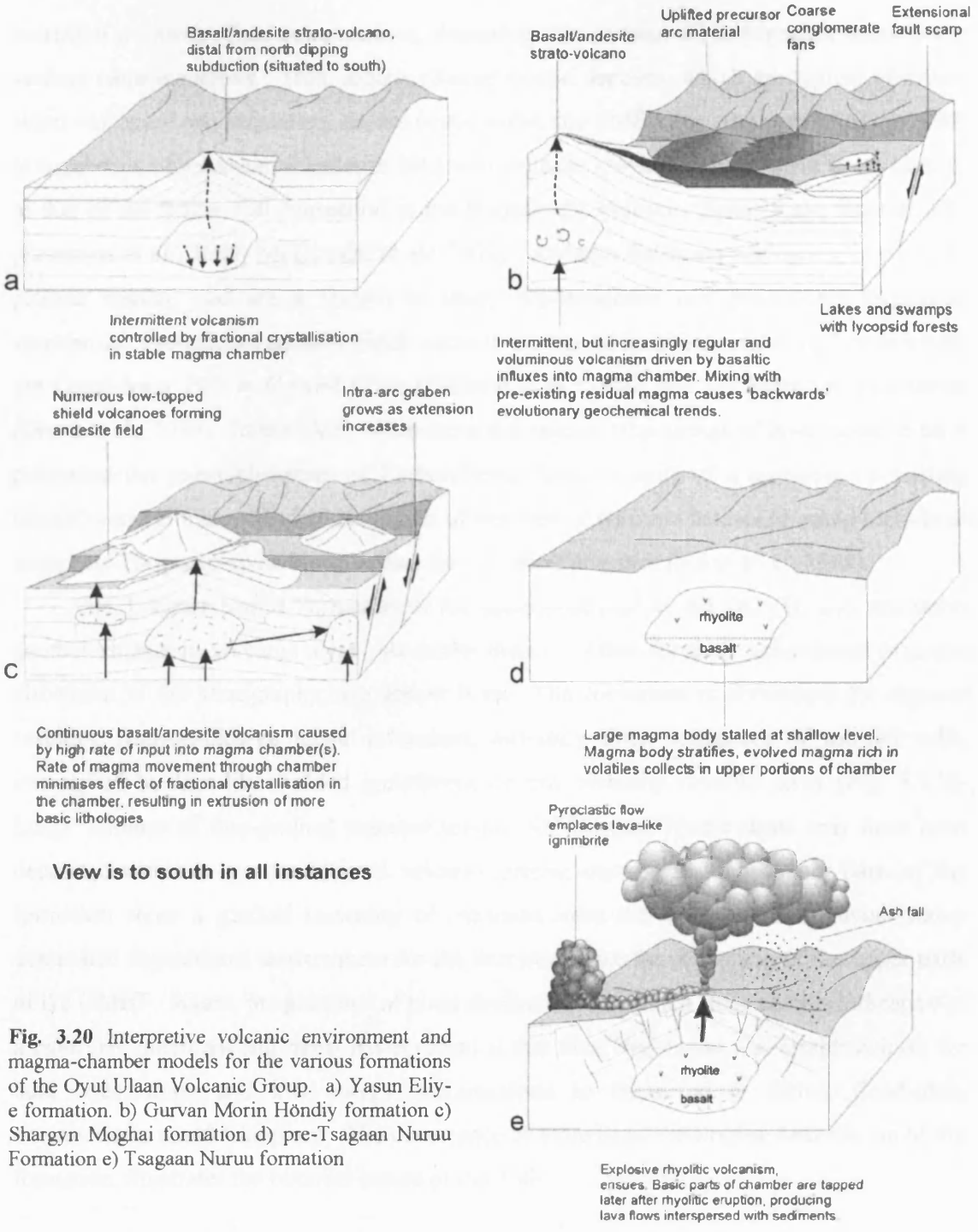

Fig. 3.20 Interpretive volcanic environment and magma-chamber models for the various formations of the Oyut Ulaan Volcanic Group. a) Yasun Eliy-e formation. b) Gurvan Morin Höndiy formation c) Shargyn Moghai formation d) pre-Tsagaan Nuruu Formation e) Tsagaan Nuruu formation

sedimentation occurs in this formation, suggesting an increase in effusion rates. Many sheet-on-sheet contacts are evident, expressed as trap topography (Fig. 3.20 c). Pillow-lavas do not occur, implying that the great bulk of volcanism took place sub-aerially. Voluminous volcanic deposition rapidly buried the aqueous environment present in the upper and northern parts of the GMHF. No pyroclastic activity is recorded, implying that even during

extrusion of intermediate compositions, degassing was widespread and magma paths to the surface were numerous. Thin, lobate, channel-bound deposits, which are typical of steep-sided volcanic-cone sequences, do not occur within the SMF. The stratigraphy of the SMF is suggestive of a sub-aerial andesite field with multiple low-angle shield-style vents, similar to that of the Birker Fell Formation in the Borrowdale Volcanic Group, Lake District, UK (Petterson et al., 1992; McConnell et al., 2002). Andesite fields are analogous, in form, to plateau basalts, and are a feature of many pre-stratocone and pre-caldera sequences worldwide. Pre-caldera andesite fields occur in a range of locations, including beneath both the Loma Seca Tuff in Central Chile (Hildreth et al., 1984) and the Santorini ignimbrites (Druitt et al., 1989). In the SMF, voluminous and regular outpourings of lava appear to have prevented the re-establishment of Carboniferous flora, in spite of a probably co-existing humid, warm climate. Modern analogues of this type of volcanic landscape could include an energetic, Tongariro-style, North-Island New Zealand province (Nairn et al., 1998).

The Tsagaan Nuruu Formation is the uppermost part of the OUVG, and represents another change in volcanic style. Andesite sheets, notable for their voluminous presence elsewhere in the stratigraphy, are absent here. The formation is dominated by deposits resulting from explosive felsic volcanism, including thick sequences of ash-fall tuffs, interrupted by lava-like welded ignimbrites or low viscosity rhyolite lavas (Fig. 3.2 e). Large volumes of fine-grained material suggest the Tsagaan Nuruu strata may have been deposited within a syn-depositional volcano-tectonic depression. The upper parts of the formation show a gradual lessening of extrusion rates and a return to a fluvial/swamp dominated depositional environment for the first time since the deposition of the upper parts of the GMHF. Again, the presence of plant detritus in carbon-rich shale units is indicative of a relatively quiescent and moist environment at this time; vegetation was established on the land once more, and low energy sedimentation in lacustrine or deltaic flood-plain environments could take place. The occurrence of more basic lithologies, near the top of the formation, illustrates the bimodal nature of the TNF.

3.6.2 Geochemical implications for the physical volcanic model

The least evolved formation is the YEF, which field and remote-sensing evidence suggests represents the deepest stratigraphy. The formation's vertical geochemical variation corroborates this interpretation, fitting in at the base of the group and becoming slightly more silicic with height (Fig. 3.18). The YEF varies from the rest of the group's Na-transitional signature; it is predominantly K-series alkaline. Zirconium abundances rise in

the YEF, showing a simple evolving trend of fractional crystallisation, with the residual magma becoming gradually more evolved. These data are consistent with a simple andesitic fractionation trend, with intermittent eruptions that tapped this gradually evolving source (Fig. 3.18 and Fig 3.20 a).

Unit A, at the base of the GMHF, has distinctive decreasing abundances of Zr and La with stratigraphic height (Fig. 3.18); this counter-evolutionary trend may result from a new influx of basaltic parent magma. The fact that this is expressed as a smooth trend rather than a sudden step suggests that the remaining residual magma from the YEF was mixed with a new, more primitive magma influx, whilst concurrent eruptions tapped the chamber (Fig. 3.20 b). The thick andesite sheets of the GMHF provide further evidence for periods of heightened magma chamber through-put. Upper parts of the GMHF show minor systematic fluctuations in Zr; both Unit B and Unit A show similar slight increasing trends with height (Fig. 3.18), which is interpreted as having been caused by new influxes of magma that were introduced to the underlying chamber, and which progressed through fractional-crystallisation controlled evolutionary trends in a similar manner to the YEF. It is interpreted that this pulsing magma replenishment produced long inter-eruption time gaps leading to the establishment of the relatively stable swamp-environments in the upper parts of the GMHF.

The SMF exhibits two consecutive sequences of decreasing Zr trends with height (Fig. 3.18). Other incompatible HFSEs also fall, but trends are less distinct. The highest abundances of Cr and Ni from the whole group are seen in the upper parts of the SMF, as are enriched TiO_2, Al_2O_3 and Fe_2O_3, indicating fresh and voluminous inputs of more primitive magma at this point. These trends imply that magma input rate into the underlying chamber was exceeding the rate of extrusion at the time of the SMF, causing the eruption of less evolved lava sequences (Fig. 3.20 c). This scenario supports the interpretation of high effusion rates in the SMF.

The TNF is predominantly composed of highly evolved silicic volcanic clastic deposits, geochemical results reflect this; most elemental abundances show a significant compositional gap from preceding evolutionary trends (Fig. 3.18). Intermediate and basaltic units at the top of the TNF show a return to a similar effusive eruptive style that occurred in earlier formations.

The general interpretations of the variation of OUVG geochemical data with stratigraphic height (Fig. 3.18) are:

1) An overall trend towards more SiO_2-rich magmas with time.

2) Saw-tooth patterns of elemental abundances with stratigraphic height are suggestive of a dynamic magma environment with pulses of primitive magma being introduced into the magma chamber(s) episodically.
3) Indications of magmatic evolutionary trends that differ from the predominant trend.
4) A clear compositional gap between the TNF rhyolites and the older parts of the OUVG.

3.6.3 Magmatic-tectonic model

OUVG is interpreted to record a series of tectonic events affecting a mature continental-style arc (Figs. 3.20 and 3.21). The OUVG constitutes a more north easterly expression of volcanic activity than has previously been recorded for the southern Mongolia Carboniferous arc (cf. Lamb and Badarch, 2001).

Magmatism began in the YEF within a relatively stable environment, its K-alkaline to signature may signify that volcanism here is indicative of an arc front somewhat removed from the subducting trench, if a simple K-h style trend was operational (Gill, 1981; Wilson, 1989).

Extension is interpreted as the trigger for volcanism in the OUVG, and particularly the increasing effusion rates of the Shargyn Moghai and Tsagaan Nuruu formations. The extension may have been produced by roll-back of the subducting slab, or transtension along the arc. This extension would have provided rejuvenated mountain fronts and river systems, and increased the number of potential magma conduits. The coarse conglomerates and thick andesite sequences of the GMHF suggest intra-arc extensional graben, with footwall uplift providing a hinterland of older arc material. Similar, ancient arc-graben depressions occur in the southwest cordillerian United States, and a modern analogue occurs in Central America (Fisher and Schmincke, 1994). Increasing extension, during the SMF times, led to the development of many magma conduits and vents resulting in high effusion rates. Some SMF lavas contain xenoliths of granite which are lithologically similar to the nearby Oyut Ulaan intrusion. Andesitic dykes cut the intrusion and are geochemically similar to the SMF. These dykes may represent the feeder structures to the SMF (Chapter 5).

Two possible hypotheses for the high silica sequences of the TNF are suggested: Firstly, the TNF followed a period of volcanic quiescence, the trapping of substantial magma volumes at shallow levels allowed for a protracted period of fractionation and lead to the development of a stratified magma chamber, with a concentration of volatile-rich rhyolitic fluids in its upper parts. This scenario could lead to explosive felsic eruptions, and the rapid

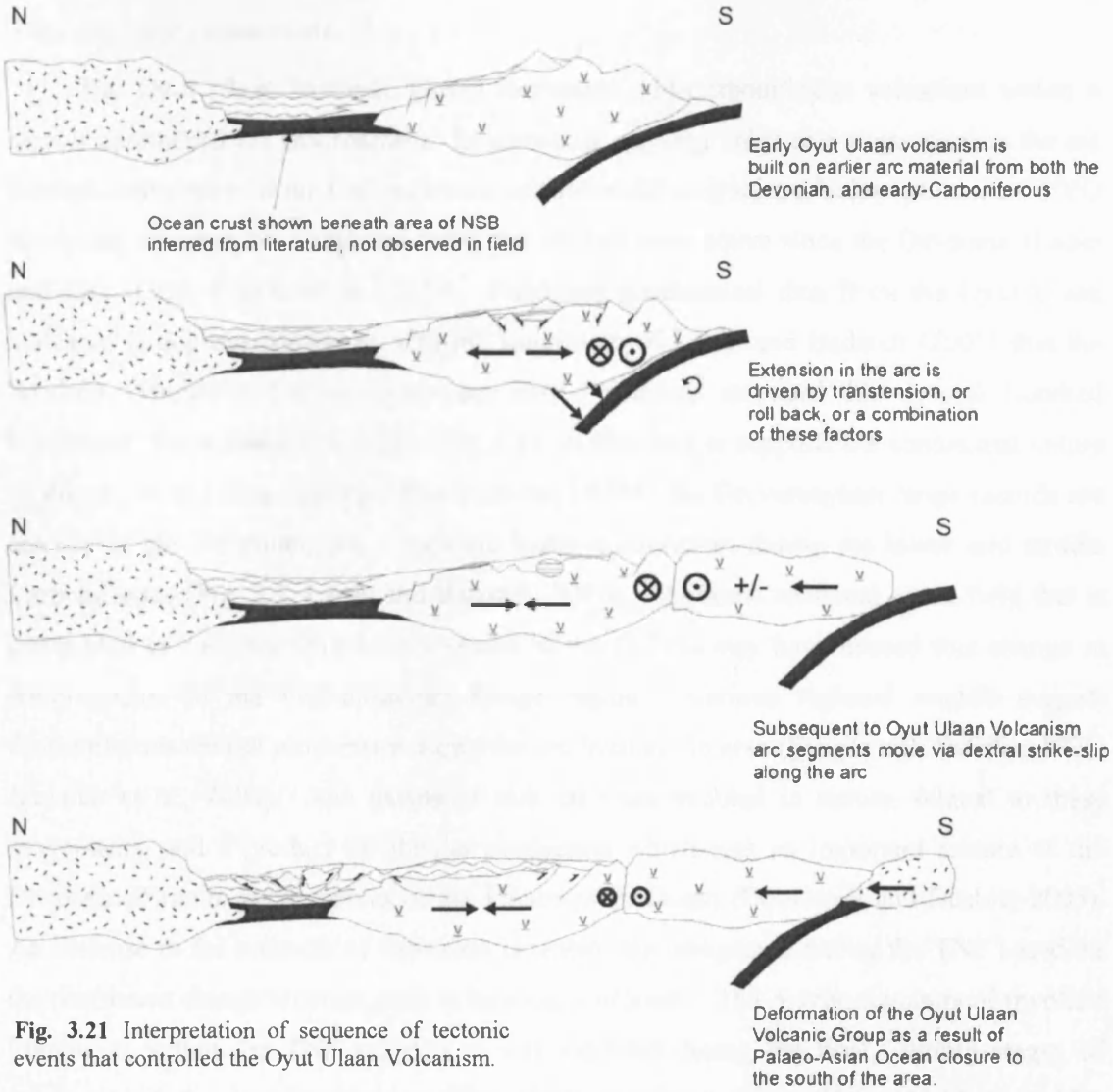

Fig. 3.21 Interpretation of sequence of tectonic events that controlled the Oyut Ulaan Volcanism.

emptying of the stratified chamber. Once the main chamber had been largely emptied, basic magma from its deeper parts was tapped and emplaced into a relatively quiescent environment, suggested by the black shales and organic matter in the upper parts of the TNF. However, it is not clear what process would have caused the pause in volcanism during which the magma chamber stratification could take place. A second hypothesis, that the TNF represents the beginnings of extension-related bimodal volcanism in the OUVG, is supported by the A-type chemistry of the rhyolites (Fig. 3.19), although only one of the non-rhyolitic lavas has a silica value below 52 wt% (Fig. 3.15). This second hypothesis appears more likely, as other characteristics of the OUVG indicate increasing extension; and a sudden pause in volcanism, after the high effusive rates of the SMF, appears counter-intuitive to this interpreted trend.

3.6.4 Regional Implications

The Oyut Ulaan Volcanic Group represents mid-Carboniferous volcanism within a mature continental arc environment. Evidence for ongoing uplift and magmatism in the arc through earlier parts of the Carboniferous occurs locally as granite cobbles within the OUVG sucession, whereas, on a regional scale, the arc had been active since the Devonian (Lamb and Cox, 1998; Perello et al., 2001). Field and geochemical data from the Oyut Ulaan Volcanic Group are consistent with the suggestion of Lamb and Badarch (2001) that the Southern Mongolia Carboniferous arc may "continue eastward for several hundred kilometres" from Tsagaan Suvarga (Fig. 3.1). It also further supports the continental nature of the arc in this area. Along strike from the OUVG the Gurvansayhan range records arc activity in the Devonian, but a back-arc basin environment during the lower and middle Carboniferous (Fig. 3.1; Lamb and Badarch, 2001). The same tensional stress field that is interpreted to have facilitated the eruption of the OUVG may have caused this change in environments in the Gurvansayhan Range region. Various regional models suggest Carboniferous dextral movements along the arc front in the area (Şengör and Natal'in, 1996; Badarch et al., 2002). The extension may be transtensional in nature, related to these movements, and a product of oblique subduction which was an important feature of the Devonian-Permian geodynamics of the Palaeo-asian Ocean (Dobretsov and Buslov, 2005). An increase in the intensity of extension is tentatively interpreted during the TNF based on the distinctive change eruption style to bimodal volcanism. The A-type signature of rhyolitic lithologies within the TNF suggests it was extruded during the final, waning stages of subduction-zone related magmatism (Eby, 1992), and the age of the TNF (323.12 ±0.64 Ma) therefore tentatively provides a maximum age for the cessation of subduction in this area. A modern analogue for the transition from calc-alkaline magmatism in an arc-environment to extension related A-type magmatism is America's Basin and Range province, where an early stage of extension, occurring as a result of intra-arc strike slip movements, can be distinguished from a later transition to continental post-accretion extensional tectonism (Zoback et al, 1981).

Some time after the emplacement of the TNF the OUVG was deformed into E-W trending folds. The deformation of the OUVG has three potential causes: Firstly, Badarch et al. (2002) show that to the south of the Devonian/Carboniferous arc are further arc sections and cratonic fragments (Enshoo, Hutag Uul; Fig 1.1). The docking of any of these terranes at the subduction zone may have caused the folding in the OUVG. Secondly, the dextral

strike-slip duplication and westwards migration of previously laterally contiguous arc-segments due to oblique subduction may have driven the compression. Thirdly, the folding in the OUVG may be considered to be related to closure of the Palaeo-asian ocean in the Permian (Xiao et al., 2003). Major brittle structures which define the outcrop pattern of the Saykhandulaan inlier were also formed at this time (Chapter 2).

3.7 Conclusions

The Oyut Ulaan Volcanic Group provides crucial information about the terrane evolution in southern Mongolia during the Carboniferous. It constitutes some of the youngest arc-material yet dated from Southern Mongolia and it represents one of the last phases of arc-volcanism prior to the final closure of the Palaeo-Asian Ocean in the Permian.

Lithological and geochemical data from the OUVG illustrate both the palaeo-geography and the volcano-tectonic regime at the time of emplacement. From incipient basic volcanism in a marine environment, through increasing extrusion rates amidst uplifted sections of precursor arc, to an evolved explosive upper-sequence, the OUVG documents a period of dominantly sub-aerial volcanism in a mature island arc or continental arc setting and extends eastwards the along-strike continuation of Carboniferous arc activity in south Mongolia and northwest China. The OUVG may span the transition from calc-alkaline arc magmatism, to bimodal, A-type post-orogenic magmatism; an important feature of the late Carboniferous and Permian growth of the CAOB.

Granites of the southern Mongolia Carboniferous arc: New age and geochemical constraints

4

4.1 Introduction

Over the past fifteen years, southern Mongolia has become a key region for both mineral exploration and research into processes of volcanic-arc development and terrane accretion. The discovery of important intrusion-related mineral deposits, such as the world-class Oyu Tolgoi gold-rich copper porphyry (Fig. 1.1), has encouraged efforts to understand arc magmatism and continental growth in the region. Whilst few studies exist detailing the basement evolution and lithological context within this SE Gobi Mineral Belt, fewer still present original absolute age data for any of the numerous granite intrusions which crop-out across the region.

This chapter addresses the paucity of age data by presenting new U/Pb zircon dates for five intrusions from a 200 km long belt 150 km to the northeast of Oyu Tolgoi (Fig. 4.1). One of these intrusions has previously been dated with Rb/Sr whole rock techniques (Batkhishig and Iizumi, 2001), whereas the other four have not previously been dated.

Following a summary of the regional geology and methods employed, the results section of this chapter is divided into two parts. The first concerns the Oyut Ulaan intrusion, a mineralised granite that crops out within the Saykhandulaan Inlier 400 km to the south of Ulaan Baatar (Figs. 1.1, 4.1 and 4.2). The field relations, geochemistry and age of this intrusion are documented in detail. Features that cross-cut the intrusion including dykes and hydrothermally mineralised sheeted vein complexes and stockworks, are described.

The second part of this paper constitutes a reconnaissance study of granites in the broader region, encompassing intrusions from a belt 200 km to the west of Oyut Ulaan along the regional structural grain, including those of the Mandakh inlier, situated to the WSW of the Saykhandulaan inlier (Fig. 4.1). In addition to new age data, some geochemical results are presented for each intrusion.

4.1.1 Regional geology

The Central Asian Orogenic Belt (CAOB) represents 1.3 Ga of tectonic activity that took place between initial rifting of Siberia and North China in the Palaeo-Meso Proterozoic (1516-1662 Ma; Wang and Liu, 1986), to final closure of the Palaeo-Asian Ocean along the Solonker suture in the Permian (Fig 1.1; Xiao et al., 2003). The geology of southern Mongolia, and specifically, the southeast Gobi, records the Ordovician to Permian evolution of

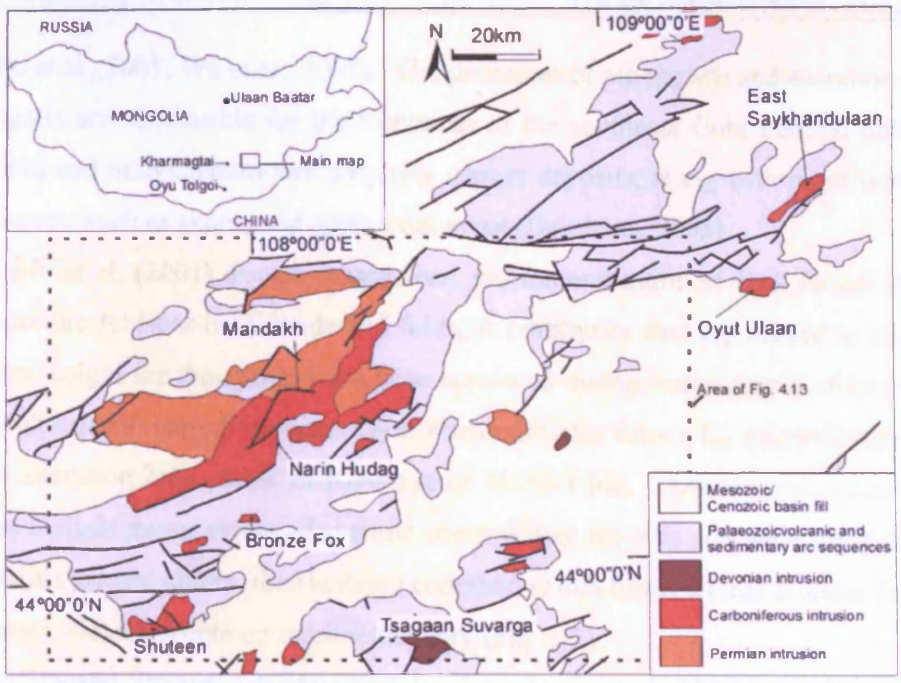

Fig. 4.1 Regional geological map showing distribution of granite bodies, Palaeozoic inliers, and Mesozoic and Cenozoic basins and faults, after Tomurtogoo (1999).

the northern margin of the Palaeo-Asian Ocean, with multiple phases of island-arc growth, back-arc rifting, and terrane accretion (Zorin et al., 1993; Şengör and Natal'in, 1996; Lamb and Badarch, 1997, 2001; Badarch et al., 2002).

Lamb and Badarch (2001) propose a Devonian arc that spanned from Edren in the west to Tsagaan Suvarga in the east (Fig. 3.1). They interpret Carboniferous arc-activity in south-east Mongolia as having been built upon pre-existing Devonian arc-crust, and consider it to be linked to the west, with Carboniferous arc rocks in Bogda Shan in the northern Tian Shan. This arc has oceanic affinities to the west (in eastern Xinjiang Province) but becomes more continental towards the Mongolian border and in regions further east (Carroll et al., 1990; Zorin et al., 1993). In chapter 3, evidence of Carboniferous continental-arc activity was confirmed in the Saykhandulaan inlier, extending eastwards the model of Lamb and Badarch (2001).

The emplacement of voluminous intrusive bodies is an important feature of continental growth within accreting terrane belts. This process affects all enviroments, from juvenile island arcs and continental cordilleras, to post-orogenic plateau regions (Harris et al., 1986; Wilson, 1989). After the final suturing of the Palaeoasian Ocean in the Late Permian (Xiao et al., 2003), and continuing into the Jurassic, voluminous, juvenile granitoids were emplaced into the Central Asian Orogenic Belt. These post orogenic intrusions are thought to indicate a major transfer of mantle material to the crust as a result of slab drop-off (Wu et al.,

2000; Zhu et al., 2001; Wu et al., 2002). The processes of arc growth and accretion in southern Mongolia are responsible for the formation of the southeast Gobi mineral belts, which feature gold and molybdenum-rich porphyry copper deposits, along with other intrusion related prospects such as skarns and epithermal veins (Dejidmaa, 2005).

Perello et al. (2001) discuss magmatism and mineralisation at Oyu Tolgoi (Fig. 1.1). The monzonitic feldspar-hornblende and feldspar porphyries that are related to mineralisation at Oyu Tolgoi are thought to have been emplaced during initial stages of arc-evolution in the late Silurian to early Devonian. Hydrothermal biotite from a Cu mineralisation-related K-silicate alteration halo yields an K/Ar age of 411+/-3 Ma. Post-mineralisation intrusive lithologies include minor stocks of syenitic composition, rhyolite and andesite dykes, and a major alkaline granite pluton, the Hanbogd complex, which forms a large circular feature (32 km diameter), clearly visible on satellite imagery (Fig. 1.3).

The Tsagaan Suvarga Cu-Mo porphyry deposit crops out 150 km to the NE of Oyu Tolgoi, and 45 km to the SE of the Saykhandulaan inlier (Fig. 4.1). Mineralisation is associated with small intrusions and dykes of a range of lithologies including diorite, granodiorite and syenite (Lamb and Cox, 1998). Lamb and Cox (1998) provide an Ar/Ar date of 364.9+/- 3.5 Ma for sericitic alteration associated with mineralisation at Tsagaan Suvarga. Watanabe and Stein (2000) provide an average Re/Os date of 370.4 +/-0.8 Ma from molybdenite. Post-mineralisation monzonite dykes have an Ar/Ar age of 313 +/- 2.9 Ma (Lamb and Cox, 1998). It should be noted that K/Ar and Ar/Ar dates for mineralisation have been shown to be affected by post-mineralisation events, whereas Re/Os molybdenite ages are considered more reliable (Rundle, 1981; Stein et al., 2000; Selby et al., 2002).

The Kharmagtai gold-copper porphyry district lies approximately 100 km to the north of Oyu Tolgoi, and 100 km to the west of the belt of intrusions investigated in this study (Fig. 1.3). Devonian marine sediments and volcaniclastics form the host rock to monzodiorite and diorite porphyry stocks which host porphyry mineralisation, along with mineralised breccia pipes and quartz vein stockworks (Kirwin et al., 2005). There are no published age data available for the Kharmagtai complex.

4.1.3 Methods

Fieldwork included mapping and sampling for petrographic, geochemical and geochronological analysis at numerous localities across the Oyut Ulaan Granite outcrop area, with particular focus on the granite margins, roof pendants, dykes and breccia pipes. Reconnais-

sance sampling of the other intrusions from the region was carried out along a road transect to the west of the Saykhandulaan Inlier.

Fifty-five samples were analysed using standard X-ray fluorescence (XRF) techniques at the University of Leicester. Six samples (one each from the following intrusions; Oyut Ulaan granite, Oyut Ulaan andesite dykes, Mandakh, Narin Hudag, Bronze Fox and Shuteen) were analysed by Isotope Dilution Thermal Ionization Mass Spectrometry (ID-TIMS) for isotopic abundances of U and Pb in zircon grains, at the NERC Isotope Geosciences Laboratory (NIGL), using analytical procedures as described by Noble et al (1993).

Zircon crystals were separated from <355 μm grained bulk-rock powder using standard vibrating-table, specific gravity and magnetic techniques. Crystal fractions for analysis were picked by hand under a binocular microscope; all analysed fractions consisted of single grains. Some zircon crystals were subjected to air abrasion (Krogh, 1982), whist others used a modified chemical abrasion technique (Mattinson, 2005). The zircon crystals were ultrasonically washed in 4N HNO_3, rinsed in ultra-pure water, then further washed in warm 4N HNO_3 prior to rinsing with distilled water, all of which aimed to remove surface contamination. A mixed ^{205}Pb - ^{235}U tracer was used to spike all fractions. Dissolved, spike equilibrated samples were not subjected to ion-exchange procedures but were converted to chloride and loaded onto degassed rhenium filaments in silica gel following a procedure modified after Mundil et al. (2004). Isotope data were collected using a Thermo Electron Triton with SEM for ion counting, and faraday cups for voltage measurement when ion counts exceeded 800,000 per second. Errors were calculated using numerical error propagation (Ludwig, 1980). Isotope ratios were plotted using Isoplot version 3 (Ludwig, 1993, 2003), and error ellipses reflect 2σ (95% confidence level) uncertainty. Mean Squared Weighted Deviates (MSWD) are calculated by dividing the sum of the squares of the mis-fits to the regression line by the number of data points minus two, and are a measure of the scatter of points. If scatter is limited to that caused by analytical errors, MSWD should = 1, too much scatter results in MSWD > 1 and too little (less than expected from analytical errors) results in MSWD <1. MSWD values near 1 give a high level of confidence that a true isochron is indicated by the data (McIntyre et al., 1966).

Lead blanks recorded during three separate batches of analysis ranged from 1.2pg and 0.2pg. Samples were blank corrected using the blank ^{204}Pb:^{206}Pb:^{207}Pb ratio measured during the analysis. Correction for common lead in all samples was carried out using the Stacey-Kramers common lead evolutionary model (Stacey and Kramers, 1975), however the amount of common lead in the analysed zircons was negligible, as the correction was dominated by the Pb blank.

4.2 Oyut Ulaan Intrusion

4.2.1 Field data and petrography

The Oyut Ulaan intrusion crops-out in the southeast corner of the Saykhandulaan inlier, within a belt of Carboniferous volcanic and sedimentary rocks called the Oyut Ulaan Volcanic Group (OUVG; Fig. 3.2; Chapter 3). The base formation of the OUVG (the Yasun Eliy-e formation; YEF) forms the country rock to the Oyut Ulaan intrusion. Two roof-pendants of basaltic and andesitic lithologies crop-out in direct contact with the intrusion in the south and east. The western roof pendant divides the intrusion into east and west lobes (Fig. 4.2). Lithologies within these roof pendants are all but obscured by thermal metamorphism, dykes, and intense hydrothermal alteration. Several generations of dykes cut the intrusion, and a cluster of tourmaline breccia pipes form prominent topographic features in the western lobe of the pluton's outcrop area.

The intrusion is elongate, measuring around 10 km in the E-W orientation, and around 3 km N-S. No emplacement-related ductile fabrics were observed, but there are fractures trending 045 and faults with apparent dextral offsets (<1 m), trending 135, throughout the outcrop area (Fig. 4.2). The contact of the intrusion with the country rock is generally not exposed, and the distribution of outcrop and major drainage channels suggests it is fault bound on most margins. Where the intrusion's contact with the country rock is exposed, in the southeast, it is irregular, has a 1-2 cm chilled margin, and follows topographic contours, suggesting that it is a relatively low-angle surface. Small (<1 m wide) apophyses of the intrusive lithology occur in the country rock, and xenoliths of country rock are seen within 5 m of the granitoid margin.

Whilst the there are only limited exposures of the intrusion's contact with surrounding rocks, some further details of its nature and morphology can be observed on satellite imagery. The pluton's southern boundary is parallel with a major E-W crustal lineament that marks the southern margin of the Saykhandulaan inlier. The western margins of both roof pendants are obscured by major drainages, but the northern and eastern margins appear to be intrusive contacts. Further observations of drainage patterns within the outcrop area show a drainage-divide approximately parallel with, and proximal to, the sharply defined northeastern margin of the intrusion, suggesting the body has been tilted to the south in relatively recent times.

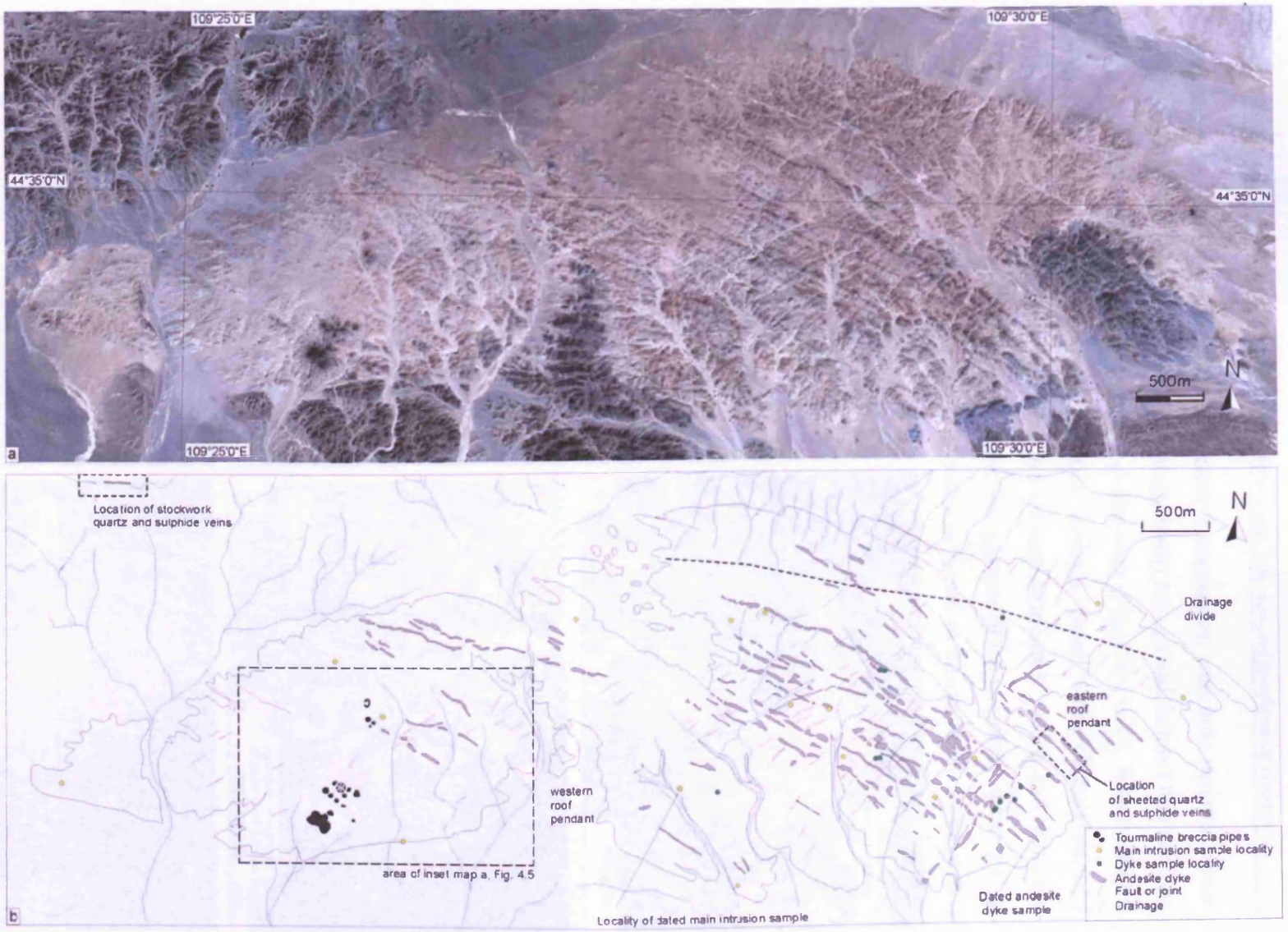

Fig. 4.2 a) Quickbird satellite image of Oyut Ulaan Intrusion. b) Interpretation of satellite image showing outline of the granite and the main andesite dyke swarm. Locations of geochemical analyses from the granite and the dykes shown.

The lithology of the intrusion is remarkably homogenous, with little variation across the outcrop area. The main mineral phase is plagioclase (An_{25-30}) and, in most thin sections, forms a framework of euhedral phenocrysts 1-5 mm long (Fig. 4.3, a to c). Small euhedral hornblende phenocrysts of 1-3 mm occur in some sections. Small biotite phenocrysts (of 1 to 2 mm length) are seen in all sections, but are sparsely distributed. Quartz and orthoclase feldspar form interstitial phases and myrmekitic intergrowths of the two occur sparsely (Fig. 4.3 d). Biotite also occurs as secondary growths proximal to quartz veins, along with a

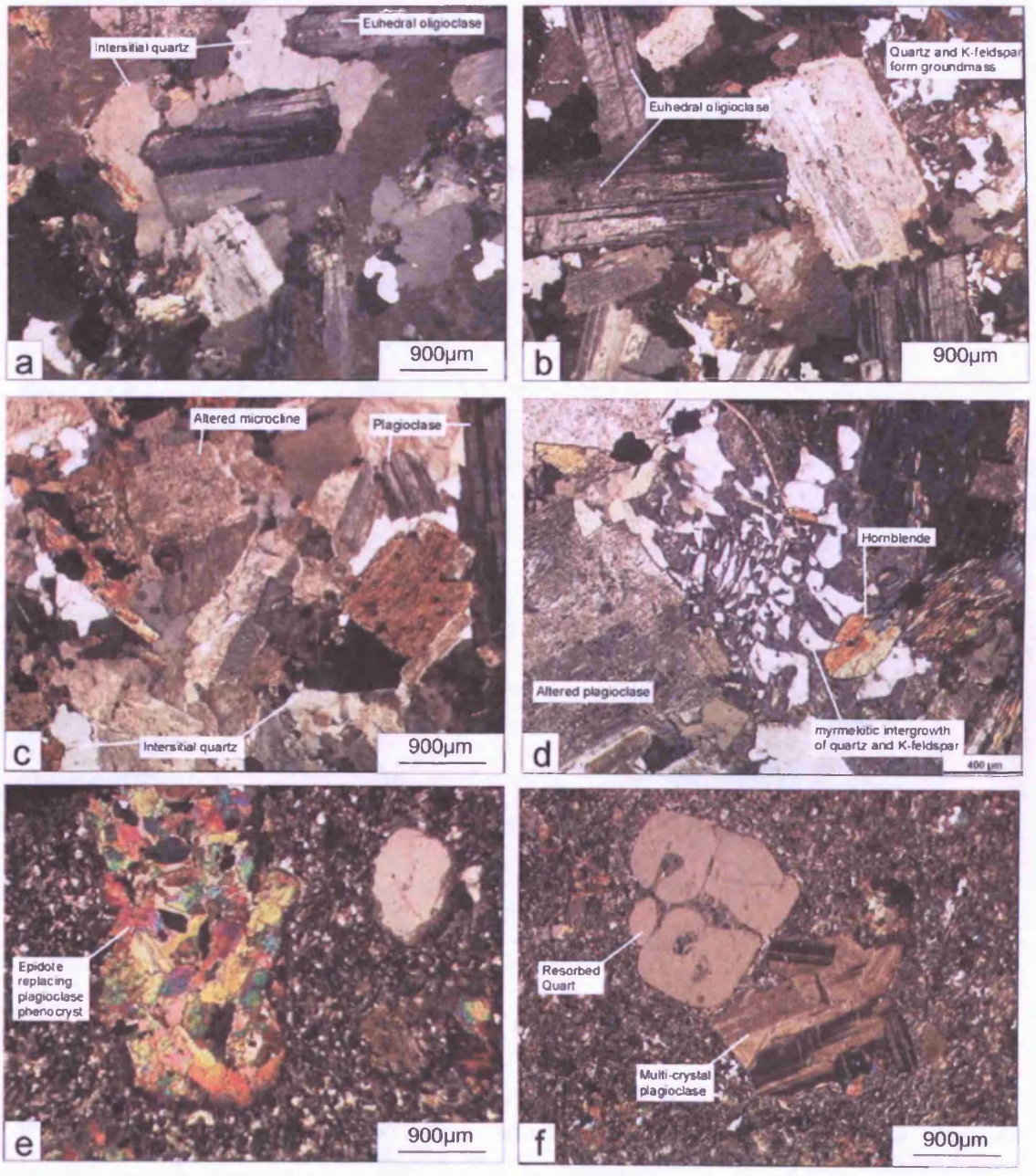

Fig. 4.3 Photomicrographs of the Oyut Ulaan main intrusion (a, b, c and d) and the andesite dykes (e and f).

higher concentration of opaque phases. Accessory phases, such as zircon and apatite, are also present.

Three sets of dykes of various lithologies cut the intrusion, each with a distinctive orientation (Fig. 4.4). Pink fine-grained aphyric dykes crop out in all areas. Locally these bodies branch and bifurcate, and appear to be randomly orientated, but rose diagrams of all recorded dykes show that ENE-trends occur more commonly than any other orientation (Fig. 4.4 a). These dykes were not observed in the surrounding country rock. The felsic dykes

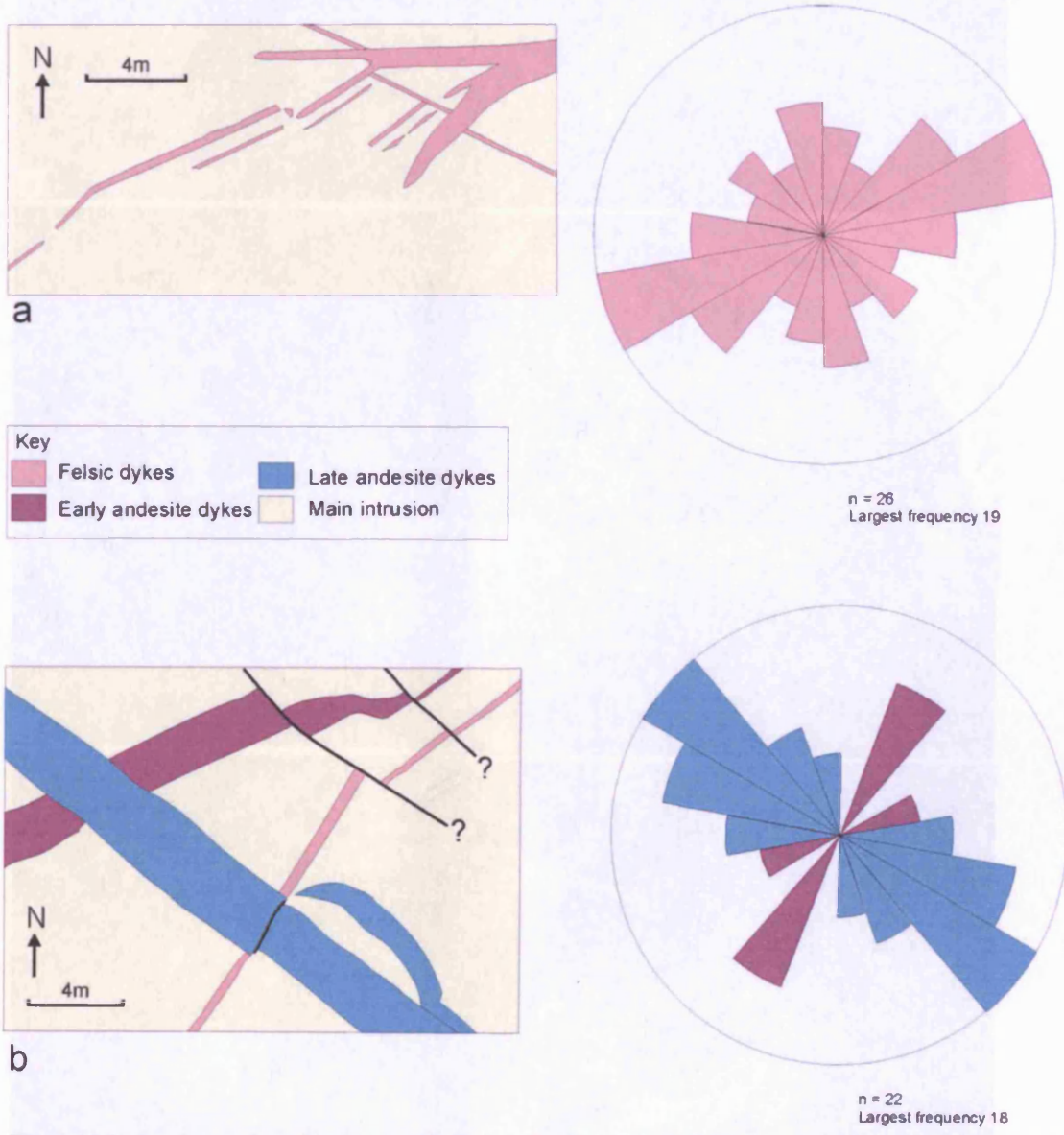

Fig. 4.4 Maps and rose plots showing morphology and cross-cutting relationships of 3 separate dyke swarms identified in the Oyut Ulaan intrusion. a) Earliest phase rhyolite dykes branch and crosscut each other and have diverse orientation, but are dominantly ENE trending. b) andesite dyke, which is part of large NW trending swarm cross-cuts earlier NE trending andesite dyke, and NE trending rhyolite dyke, rose plot showings orientations of the two sets of andesite dykes.

Special Note

Page 89 missing from the original

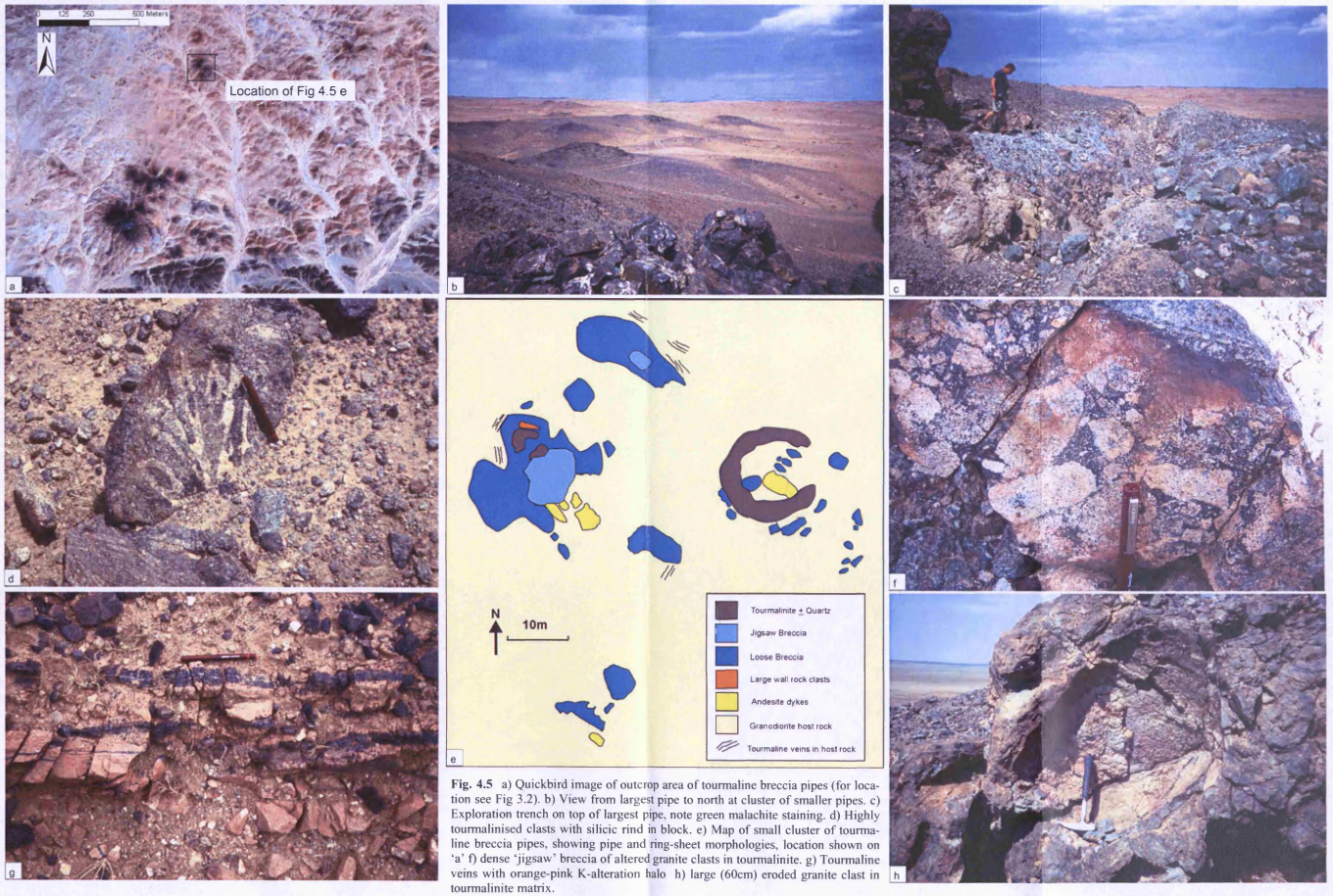

Fig. 4.5 a) Quickbird image of outcrop area of tourmaline breccia pipes (for location see Fig 3.2). b) View from largest pipe to north at cluster of smaller pipes. c) Exploration trench on top of largest pipe, note green malachite staining. d) Highly tourmalinised clasts with silicic rind in block. e) Map of small cluster of tourmaline breccia pipes, showing pipe and ring-sheet morphologies, location shown on 'a' f) dense 'jigsaw' breccia of altered granite clasts in tourmalinite. g) Tourmaline veins with orange-pink K-alteration halo h) large (60cm) eroded granite clast in tourmalinite matrix.

scree makes true pipe-margins indistinct. Other pipes have average apparent widths of 25-40m (Fig. 4.5 e). Circular morphologies are the most common, although one mapped pipe, and another observed on satellite imagery, have ring-sheet morphologies. The tourmaline breccia pipes locally cross cut the youngest dyke set.

Various textures that occur within the tourmalinite suggest several phases of fluid flow, and brecciation. Tight jigsaw breccias, loose breccias, massive tourmalinite, granite with pervasive tourmaline alteration and tourmaline vein stockworks with orange-pink potassic halos all occur in the vicinity of the pipes (Fig 4.5). Thin 1 to 5 cm tourmaline/ quartz veins, with 1 to 2 cm potassic alteration halos, cut the Oyut Ulaan intrusion across its whole outcrop area. These veins increase in number and thickness near the breccia pipes .

4.2.2 Geochemistry

The Oyut Ulaan intrusion is metaluminous, and has an alumina saturation index (ASI) of less than 1.1, which indicates it is either A- or I-type (Chappell and White, 1974; Wu et al., 2000; Results - Appendix A). The primacy of plagioclase over K-feldspar, and relatively high Na_2O abundances suggests that the intrusion is I-type rather than A-type (Fig. 4.6; Chappell and White, 1974; Eby, 1990; Chappell and White, 2001).

Major element abundances of the Oyut Ulaan intrusion indicate a quartz-monzonite composition (Fig. 4.6 a). Harker variation diagrams for analyses of the main intrusion show typical inverse correlations between major elements and SiO_2, with the exception of K_2O which shows a positive, incompatible trend (Fig. 4.7) suggesting increasing amounts of K-feldspar and mica in more evolved samples. Of the trace elements, Sr and Y show a decrease with silica, which is interpreted to be controlled by plagioclase fractionation, whereas Rb shows a positive trend, matching that of K_2O. Other elemental abundances do not display discernable trends for the main intrusion samples.

Major element abundances of the early, pink, felsic-dykes show they are rhyolites. The NE trending dark dykes are trachy-andesites, and the more prolific, late, NW-trending swarm has a range of compositions from andesites and trachyandesites to dacites (Fig. 4.6 a). Harker diagrams featuring all the lithologies from the Oyut Ulaan plutonic complex, show simple, single trends with silica (Fig. 4.7). These trends parallel those established for the main intrusion, suggesting that, as a whole, the complex was derived from the same magma source, which was evolving and being replenished at depth. The NE-trending andesite dykes have the most mafic compositions, and the later NW-trending swarm have a range of compo-

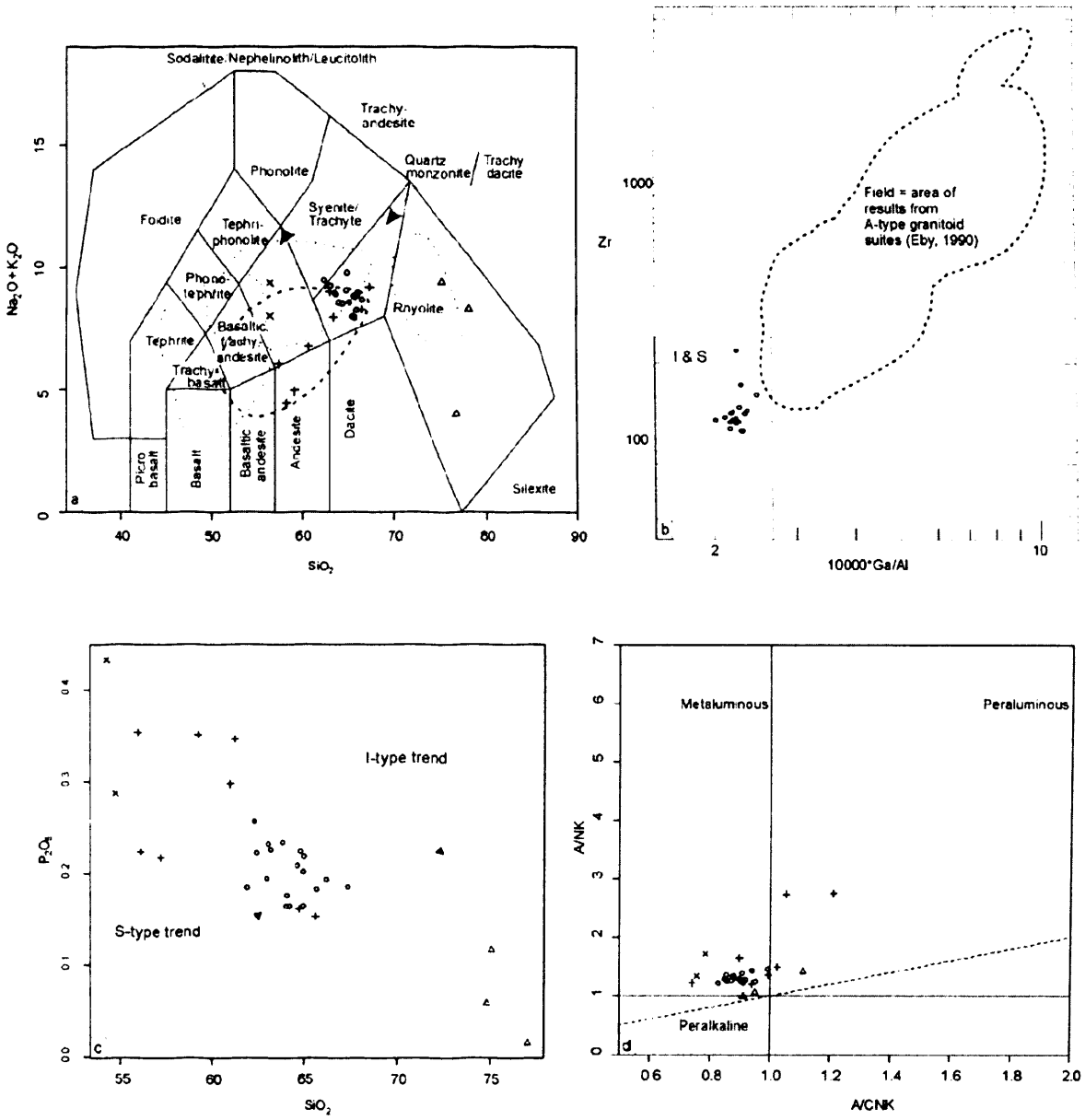

Fig. 4.6 a) Composite volcanic/plutonic Total Alkalis Silica (TAS) diagram after Middlemost (1985), for Oyut Ulaan Intrusive Complex rocks. Plot shows quartz-monzonite compositions of main intrusion, rhyolitic and andesitic composition, respectively, for early- and late-stage dykes. Note overlap between late-stage andesite dykes and field of analytical results from Shargyn Moghai Formation (Chapter 3). Graphs produced using GCDKit software (Janoušek et al., 2006). b) Diagram of Zr vs 10000*Ga/Al after Eby (1990) to differentiate I & S type granitoids from A-type granitoids. c) Diagram of SiO_2 vs P_2O_5 showing inverse trend typical of I-type granitoids and indicative of the fractionation of apatite in the absence of Y-bearing accessory minerals (Wu et al., 2000). d) A/CNK-ANK plot of Shand (1943) showing predominantly metaluminous signature of Oyut Ulaan intrusive complex.

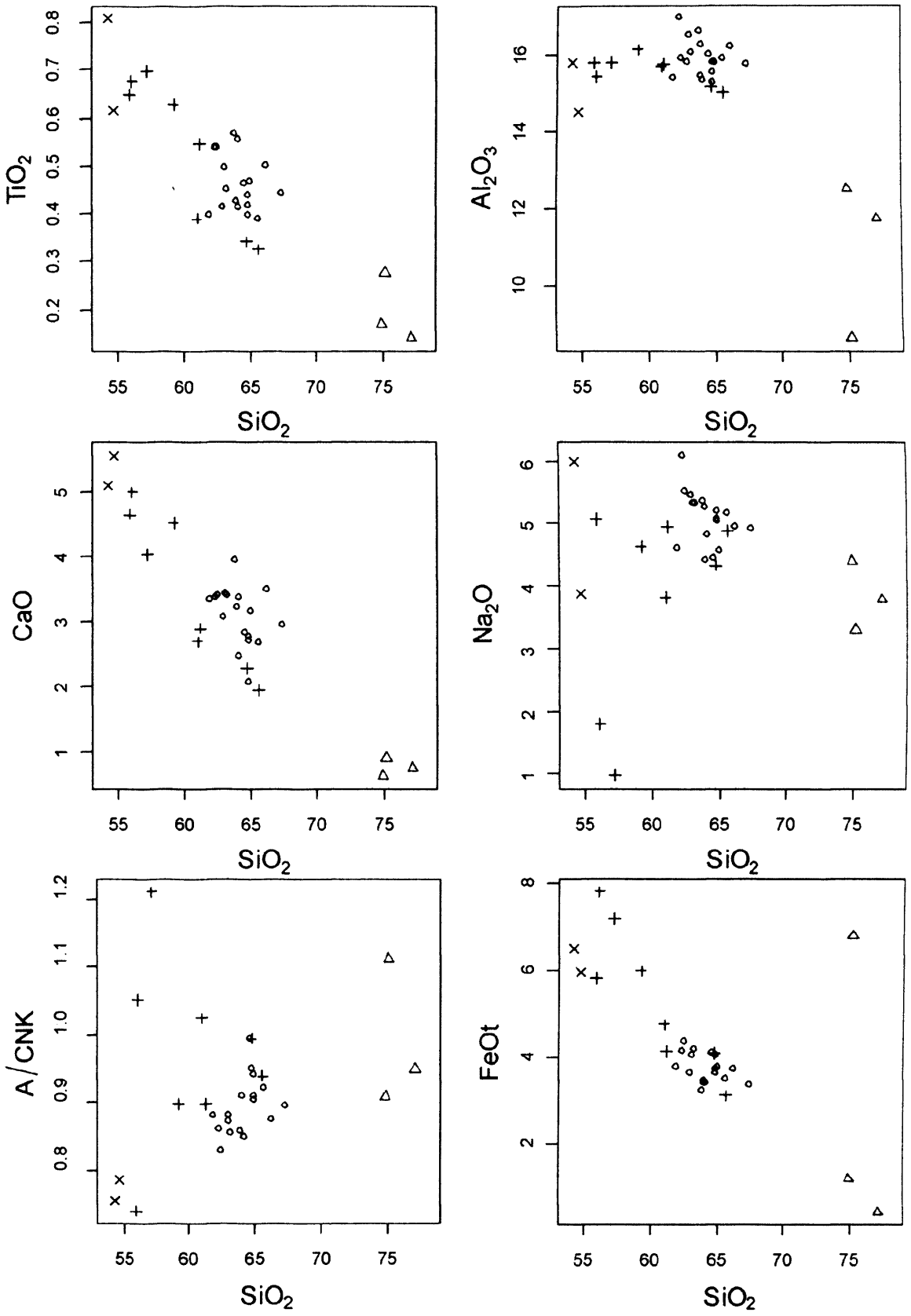

Fig. 4.7 Harker variation diagrams of major (Wt%) and trace elements (PPM) vs SiO_2 for the Oyut Ulaan intrusive complex (continued over next two pages).

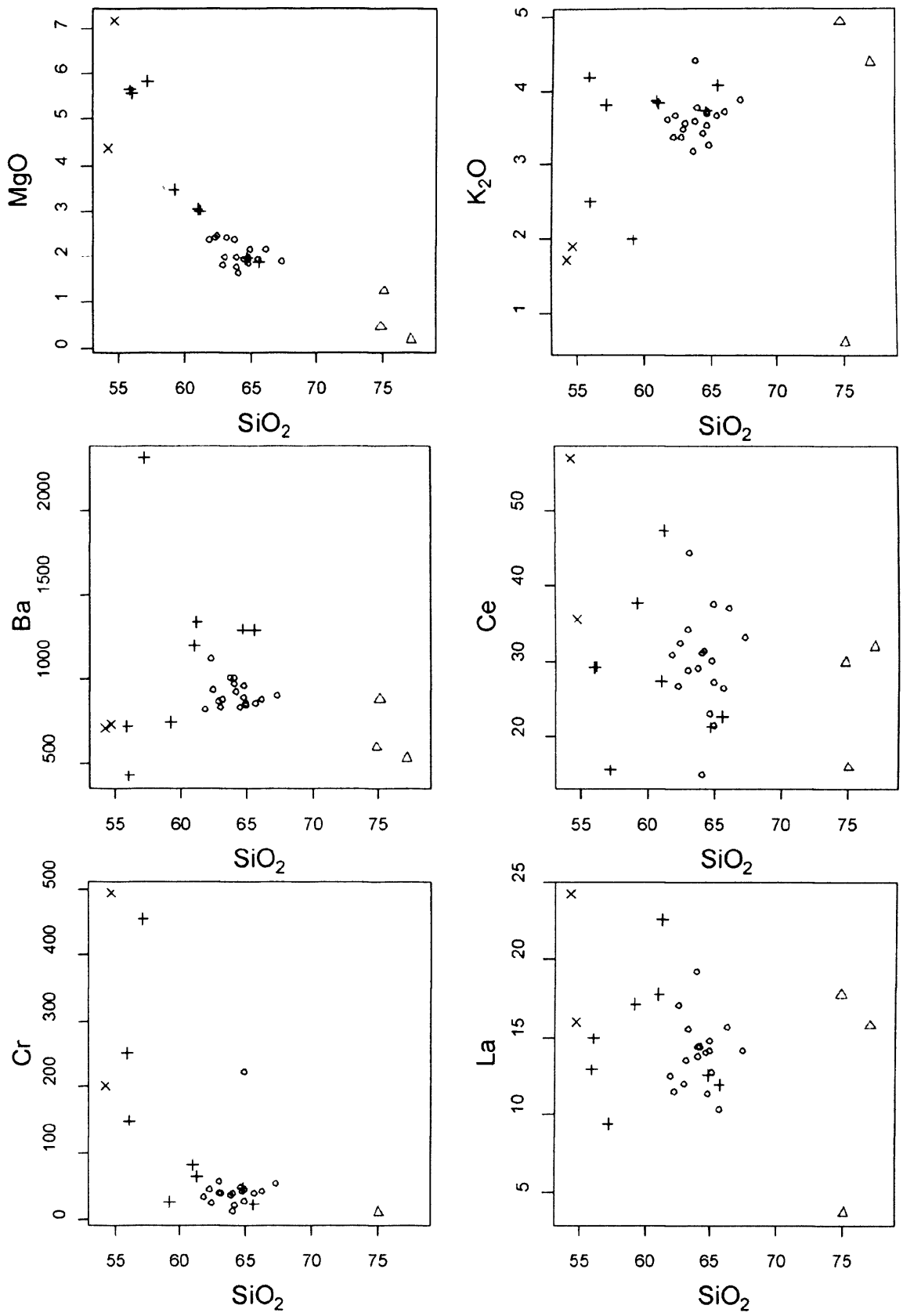
MgO
SiO_2
K_2O
SiO_2
Ba
SiO_2
Ce
SiO_2
Cr
SiO_2
La
SiO_2
Oyut Ulaan Intrusion
Early-stage dykes
NE-trending andesite dykes
NW trending andesite dykes

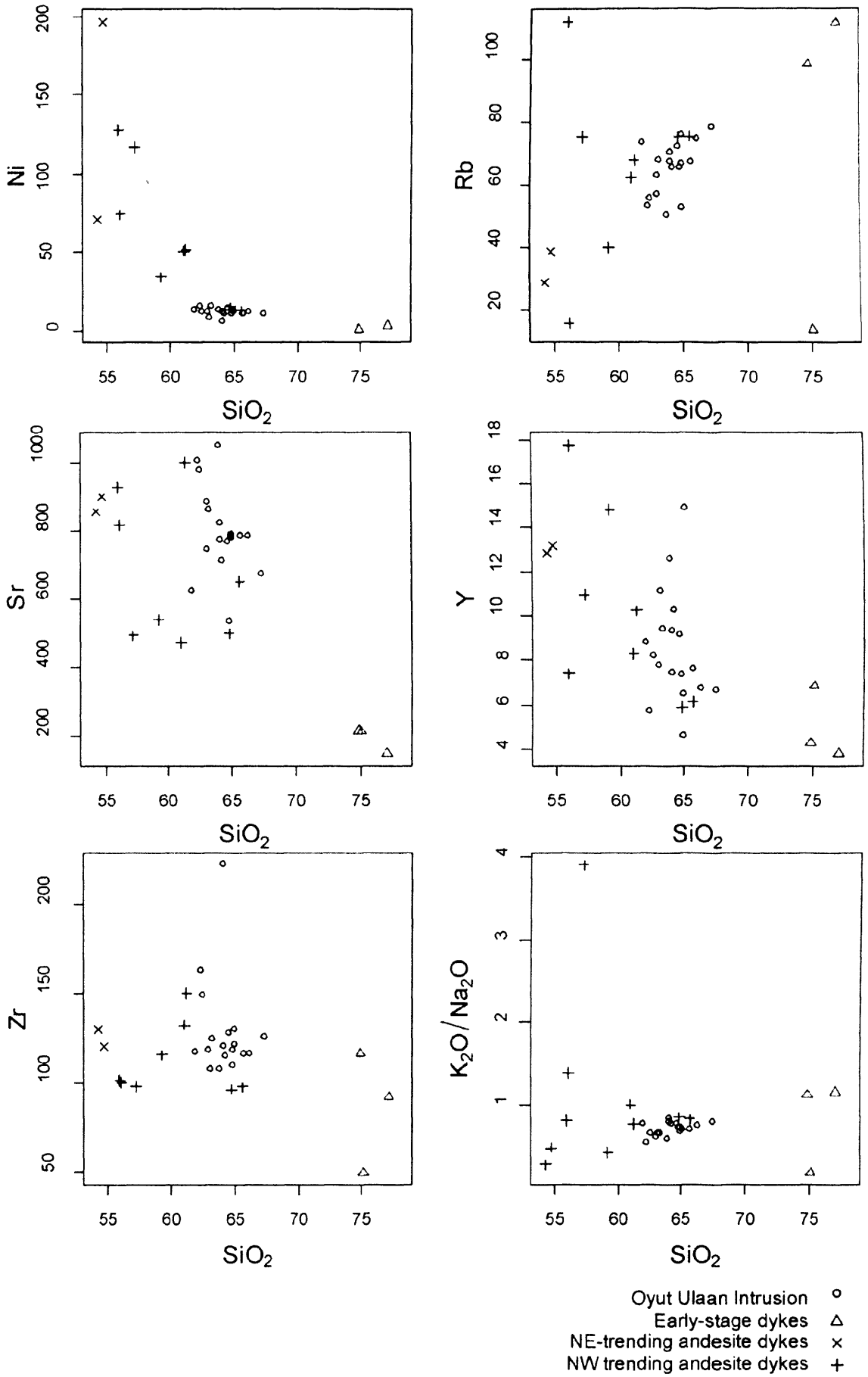
Ni
Rb
Sr
Y
Zr
K_2O/Na_2O
SiO_2
Oyut Ulaan Intrusion
Early-stage dykes
NE-trending andesite dykes
NW trending andesite dykes

sitions from those similar to the NE-trending dykes to those similar to the intrusion. The compositional range in the NW trending dykes does not seem to vary systematically with location.

Geochemically, the Oyut Ulaan intrusive complex has many similarities with its host rocks, the Oyut Ulaan Volcanic Group (Chapter 3). However, it is hosted by the Yasun Eliy-e formation, the least evolved formation of the OUVG, which lies at the base of this group, and is also considerably more mafic than any parts of the intrusive complex (Fig. 3.15). The late-stage andesite and trachyandesite dykes show a geochemical similarity to the Shargyn Moghai formation, the third formation of the group (Fig. 4.6 a). When considered *in toto*, chemical analyses of the intrusive rocks and host volcanic rocks show simple, single trends, characteristic of an evolving magma body, which was perhaps the ultimate source of both the intrusive and extrusive components of an 'Oyut Ulaan volcano-plutonic suite'.

Barium and strontium abundances of the whole Oyut Ulaan intrusive complex, show that the early-stage rhyolite dykes have a composition not inconsistent with magmatic evolution from a source chemically similar to the main intrusion, predominantly via fractional crystallisation of plagioclase, and, to a lesser degree, K-feldspar (Fig. 4.8). Petrographic analysis reveals that these are the main mineral constituents of the intrusion (Appendix D - mineral modal abundances; Fig. 4.3). The andesite dykes do not represent a continuation of this trend, and their signature in Ba-Sr space suggests plagioclase and hornblende fractionation from a source chemically similar to the early, NE-trending andesite dykes.

Geo-spatial analysis of the distribution of trace and minor element abundances across the Oyut Ulaan intrusion was carried out by applying standard interpolation techniques (kriging; Oliver and Webster, 1990) to analytical results from seventeen sample locations using surfer (Fig. 4.9). The results should be interpreted conservatively due to the relatively low number of samples compared to the area of outcrop. The intrusion shows a relatively homogenous chemistry across its outcrop area for most elements. However, NaO_2, Fe_2O_3 and Sr abundances are elevated in the western lobe of the body, suggesting this part of the intrusion is relatively enriched in plagioclase and magnetite. The most silicic and evolved part of the intrusion is situated to the NE. Tourmalinisation may have produced elevated levels of Cu, Zr and As in the west lobe.

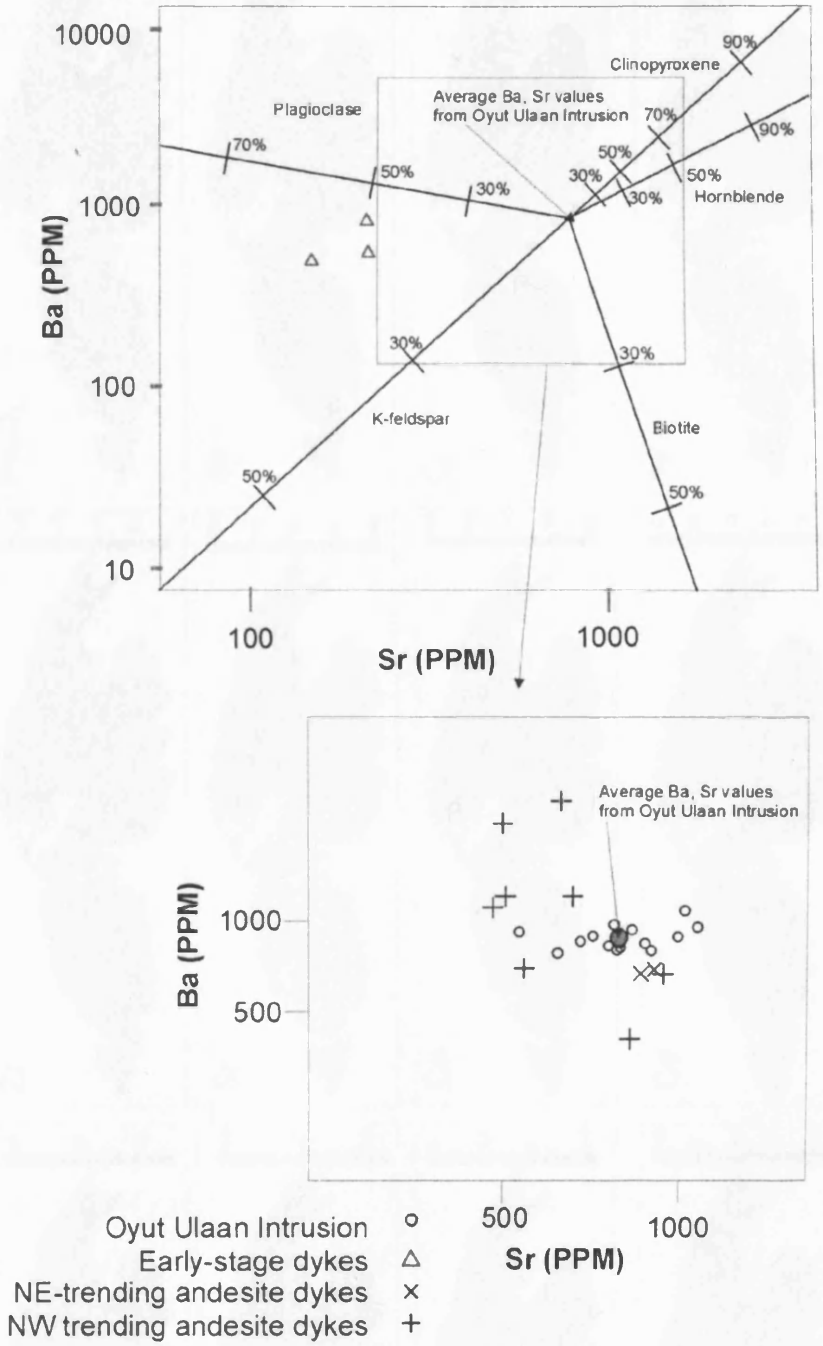

Fig. 4.8 Log Ba versus log Sr diagram for Oyut Ulaan Intrusive Complex rocks. Fractional crystallisation vectors for plagioclase, K-feldspar, biotite, orthopyroxene, clinopyroxene and hornblende calculated from average values for Ba and Sr from Oyut Ulaan Granite, using partition coefficients for rhyolitic liquids from Rollinson (1993).

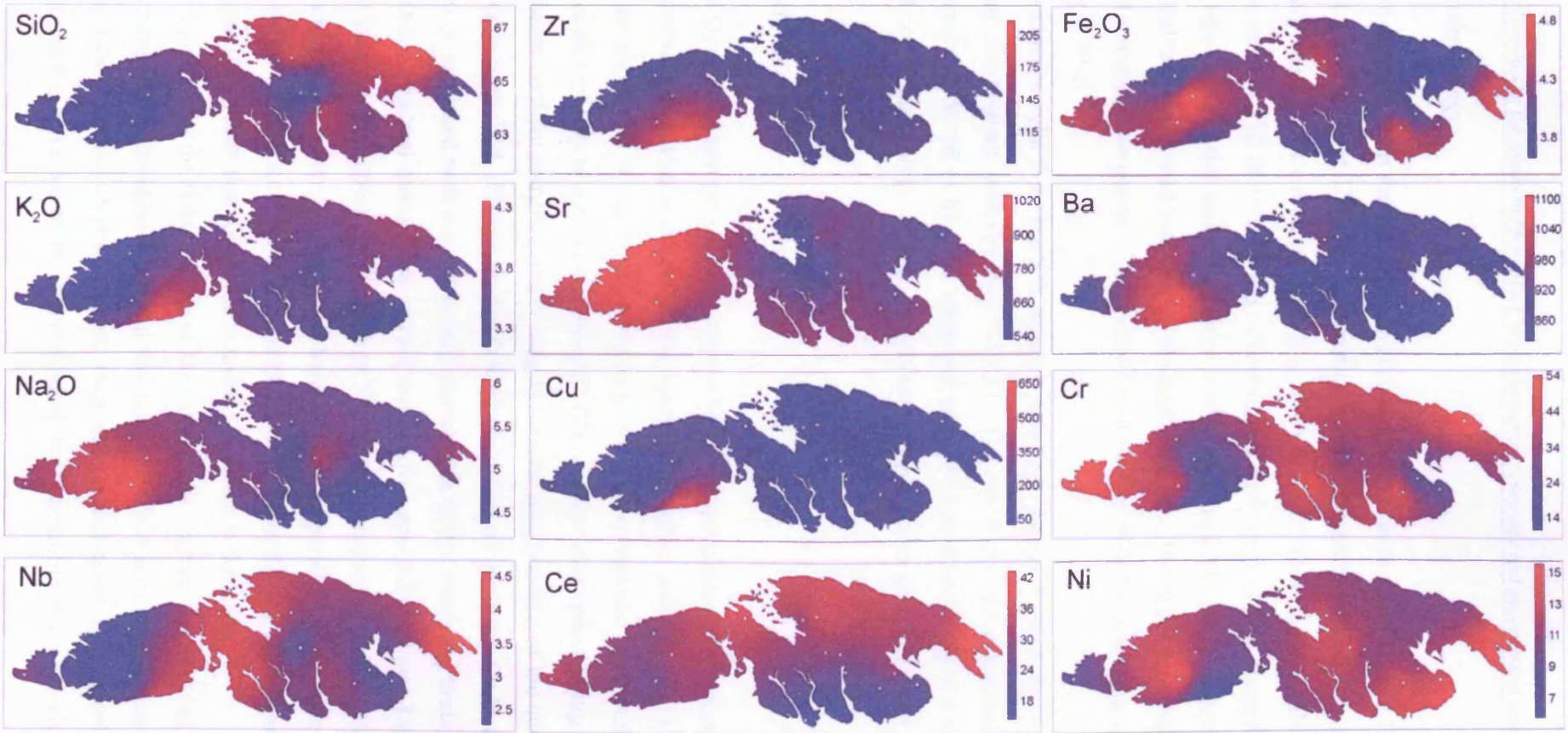

Fig. 4.9 Geospatial contour plots for various elemental abundances, created by interpolation of 17 geochemical analyses across the Oyut Ulaan Intrusion outcrop area.

4.2.3 Geochronology

Two samples from the Oyut Ulaan intrusive system were dated (Fig. 4.10; Results - Appendix B). The Oyut Ulaan main intrusion quartz-monzonite yielded five overlapping, concordant, single-grain zircon analyses (Fig. 4.10 a). The concordia age calculated from these five points is 330.02 +/- 0.53 Ma. Three further analyses plot with discordant younger ages, a likely cause of this being the failure to remove completely the outer portions of zircon that had undergone lead-loss during chemical abrasion. The upper-intercept of the line of best-fit through these points is coincident (within error) with the concordia age as calculated (Fig. 4.10 a).

An andesite dyke from the NW trending late-stage swarm yielded three overlapping, concordant, single-grain analyses (Fig. 4.10 b). The concordia age calculated from these three points is 327.86 ±0.44 Ma. An additional analysis plots discordantly and older than the cluster of concordant points. This is interpreted to represent an older inherited zircon core-zone.

4.2.4 Discussion

The Oyut Ulaan complex is interpreted to represent two phases of intrusion; the first is the emplacement of a relatively homogenous quartz-monzonite body (Fig. 4.11 a). The lobate outcrop expression of the intrusion suggests that it was emplaced as two adjacent, connected bodies, probably as a result of roof uplift. The shallow roof zone dipping to the south and the abrupt northern margin together suggest that the emplacement of the quartz monzonite was fault controlled. Plutons in the Coastal Cordillera of the north Chilean Andes are thought to be emplaced with similar vertical movements of the overlying strata; both compressive and extensional models can explain these movements (Grocott and Taylor, 2002). At Oyut Ulaan the roof uplift could relate to N-S compression or extension within an EW trending arc, or transtension in a step-over between two arc-parallel faults. More work is required to define the structural controls on emplacement, especially the attitude and kinematics of the postulated fault that appears to bound the intrusion to the north.

The lithology in the western lobe of the intrusion is slightly less evolved than in the east, suggesting that it solidified first and that incompatible elements were concentrated in the eastern lobe. As the intrusion cooled, fractional crystallisation of plagioclase and K-feldspar appears to have driven the compositional development of the relatively small vol-

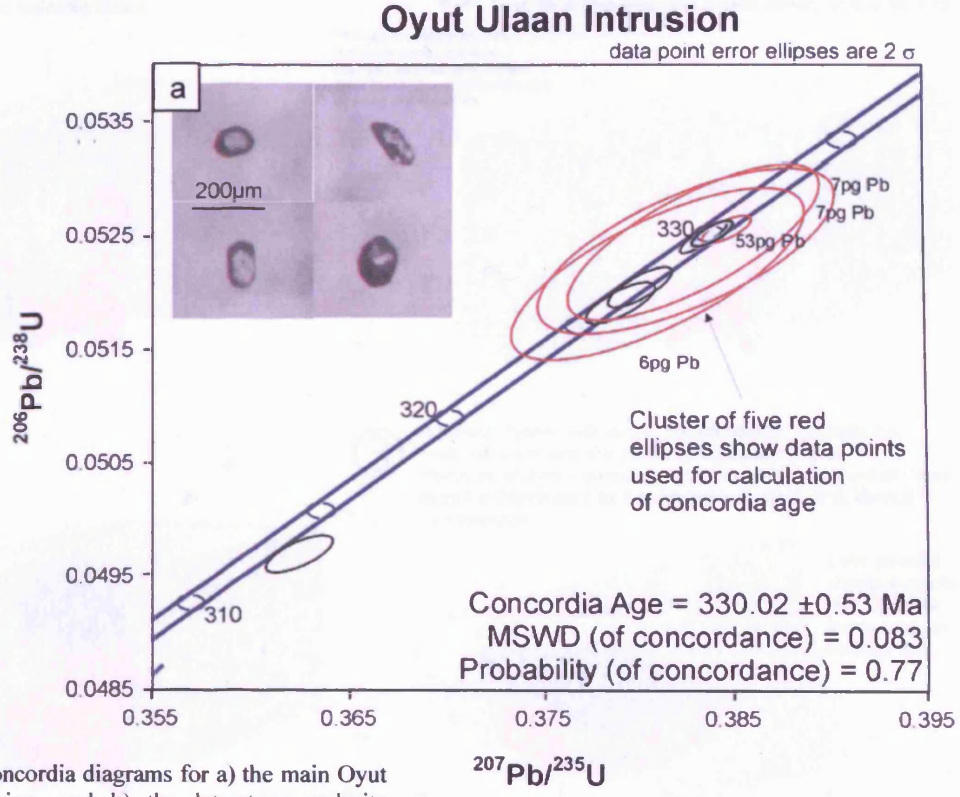

Fig. 4.10 Concordia diagrams for a) the main Oyut Ulaan Intrusion, and b) the late-stage andesite dykes. Ellipses with fine outlines show the data points, and corresponding errors. Grey-filled ellipses show the calculated concordia age. See text for explanation of MSWD.

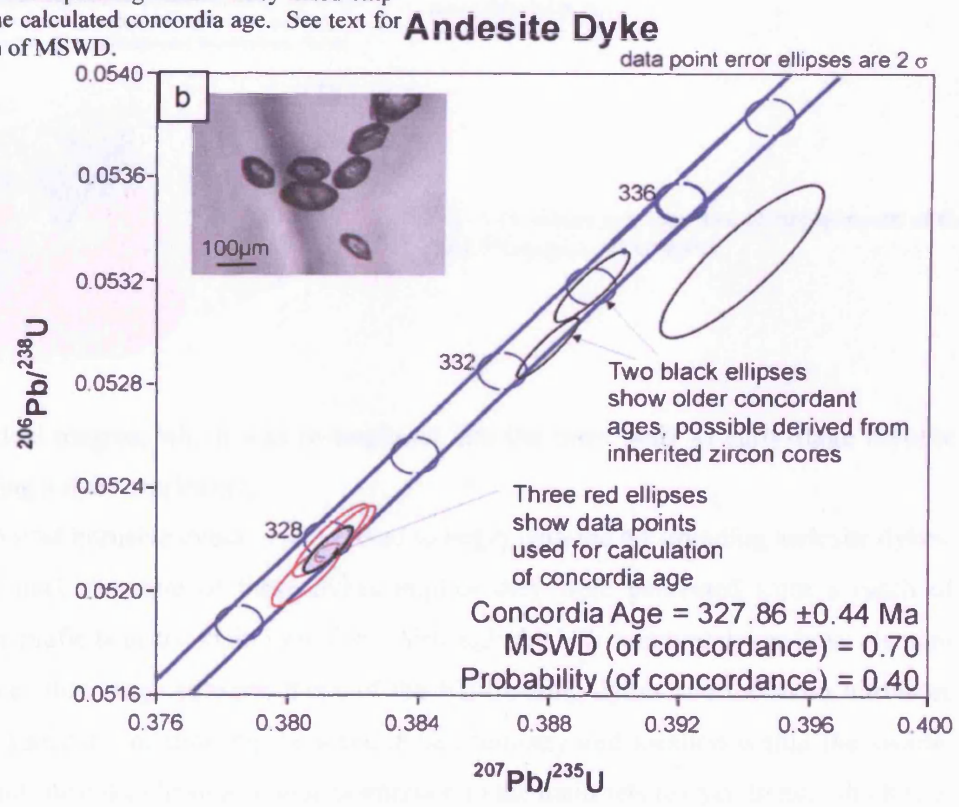

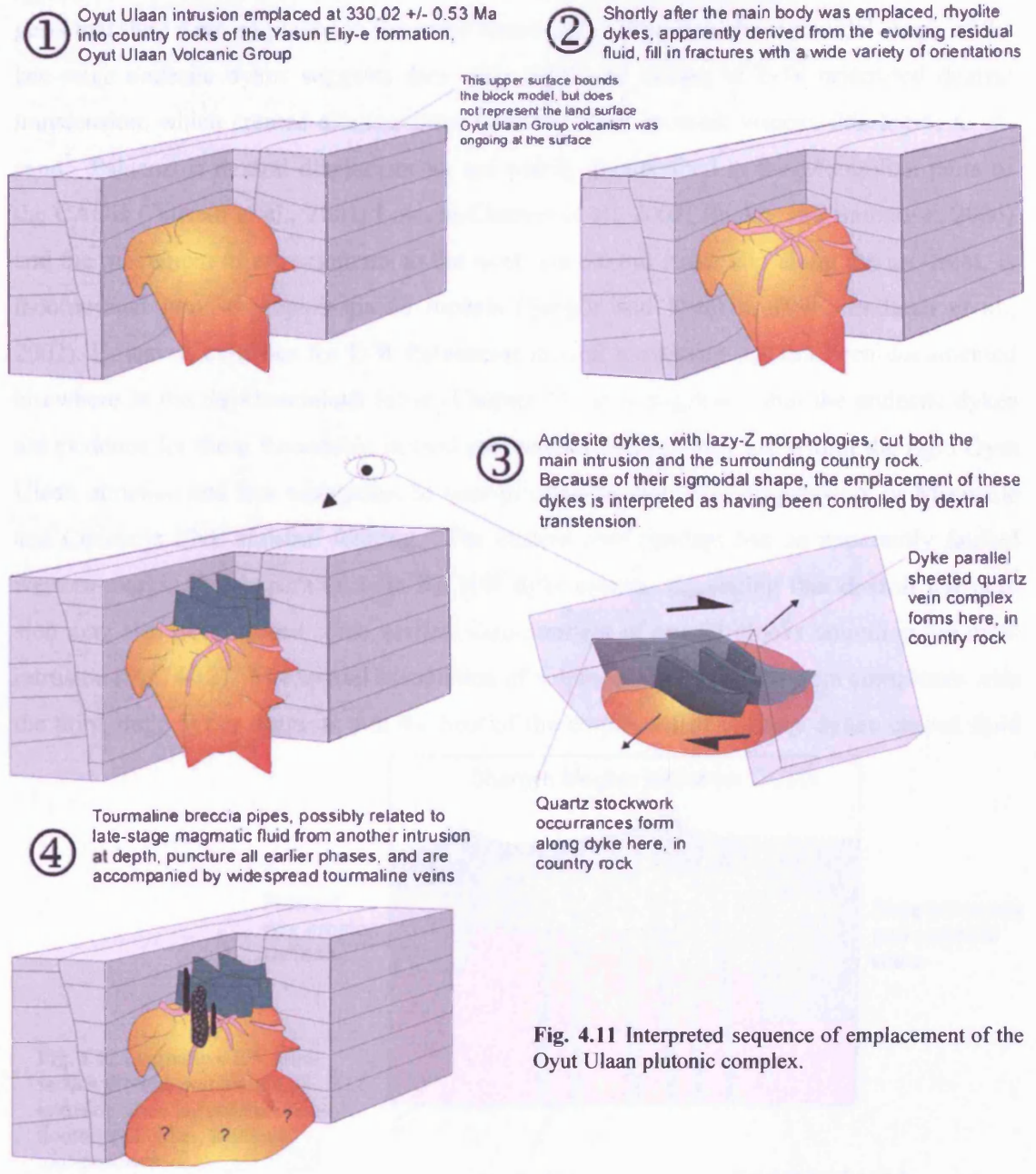

Fig. 4.11 Interpreted sequence of emplacement of the Oyut Ulaan plutonic complex.

ume of residual magma, which was re-emplaced into the main body as early-stage rhyolite dykes, forming a dyke-stockwork.

The second intrusive event is interpreted to begin with the NE-trending andesite dykes. The geochemical signature of these dykes implies they were generated from a batch of magma more mafic than the main intrusion. Although the NW trending dykes have elemental abundances that range between those of the NE-trending dykes and the main intrusion, there is no systematic relationship between dyke chemistry and location within the swarm. The early andesite dykes have a similar orientation to the main felsite dyke trend, which sug-

gests that they were emplaced in the same stress-field. However, the sigmoidal shape of the late-stage andesite dykes suggests they were emplaced during of E-W orientated dextral transtension, which created dilation sites, allowing more evolved, viscous lithologies to ascend. Palaeozoic dextral displacements are widely documented in the Mongolian parts of the CAOB (Buchan et al., 2001; Laurent-Charvet et al., 2002; Buslov and Safonova, 2006) and the movement of arc segments to the west, via dextral strike slip along the arc-front, is incorporated into some palinspastic models (Şengör and Natal'in, 1996; Badarch et al., 2002). However, evidence for E-W Palaeozoic dextral movement has not been documented elsewhere in the Saykhandulaan Inlier (Chapter 1). It is suggested that the andesite dykes are evidence for these Palaeozoic dextral movements because they are within the rigid Oyut Ulaan intrusion and less susceptible to over-printing by later NS compression, or Mesozoic and Cenozoic ENE sinistral faulting. The eastern roof pendant has an apparently faulted western-margin that is parallel with the NW dyke swarm, suggesting that dextral transtension may also have caused some vertical displacement of crustal-blocks bounding the main intrusion (Fig. 4.12). The spatial association of sulphide bearing quartz vein complexes with the third stage dykes suggests that the heat of the emplacement of these dykes caused fluid

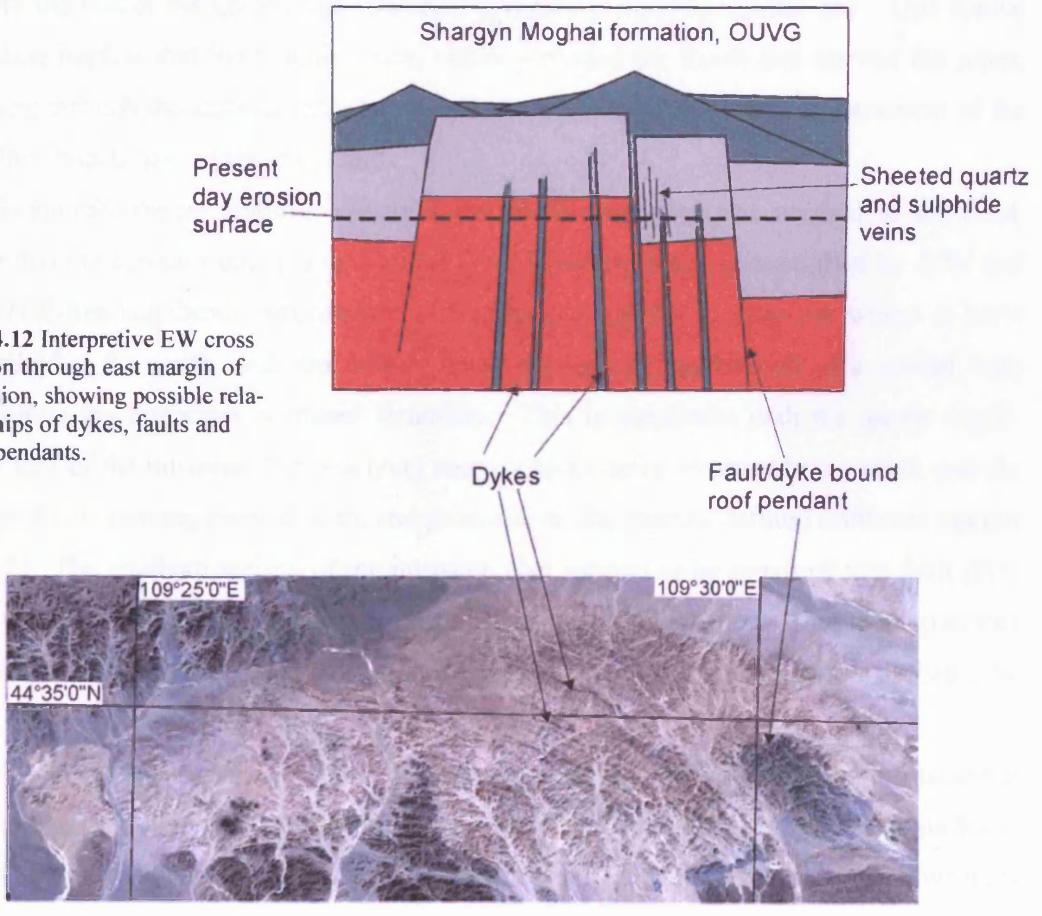

Fig. 4.12 Interpretive EW cross section through east margin of intrusion, showing possible relationships of dykes, faults and roof-pendants.

convection, and the action of their emplacement fractured the surrounding rocks generating space for the hydrothermal deposition of minerals. The sheeted vein complex in the eastern roof pendant, in particular, appears to have been formed in an identical stress regime to the third stage dykes. The associations of the stockwork vein zone in the northwest are less clear. The dyke that crops out in contact with the vein zone appears to be of a similar lithology to the late stage dykes, and has a similar orientation to the dextral tail zones of the dykes in the NW of the intrusion outcrop area. The slight deviation in the stockwork-zone-proximal dyke's orientation (E-W rather than WNW-ESE) can be explained by the N-S directed deformation that has affected the country rock (Chapter 3).

Finally, the solidification of a later magma body at depth and the resultant increase in fluid pressure due to the generation of Boron-rich magmatic fluid, caused the emplacement of the tourmaline breccia pipes into the overlying strata, cross-cutting both the Oyut Ulaan intrusion and the late-stage andesite dykes. This interpreted magma batch may be related to the andesite dykes, as they show an increasingly silicic trend with time. There are no geochemical or absolute age data from the tourmaline breccia pipes, meaning that their association with the rest of the Oyut Ulaan intrusive complex is a purely spatial one. This spatial association implies that the magma batch, which provided the fluids that formed the pipes, was rising through the same crustal plumbing system that controlled the emplacement of the rest of the Oyut Ulaan intrusive complex.

Geomorphological features, observed on satellite imagery and verified in the field, suggest that the current outcrop shape of the Oyut Ulaan intrusion is controlled by E-W and ESE-WNW-trending brittle structures. The intrusion appears to crop-out within a horst block, tilted to the south, with the deepest levels exposed in the footwall of a normal fault that delimits the intrusions northeast boundary. This is consistent with the gently south-sloping roof of the intrusion, the overlying country rocks being exposed to the south and the drainage divide running parallel with, and proximal to, the sharply defined northeast margin (Fig. 4.2). The southern margin of the intrusion also appears to be proximal to a fault (Fig. 4.2), although an intrusive contact was documented in some localities. This fault truncates the NW trending andesite dykes, so that their terminations are not visible, unlike at their NW ends.

The Oyut Ulaan intrusion is considerably younger than other mineralised intrusions in the region. Oyu Tolgoi and Tsagaan Suvarga both record Devonian ages (411+/-3 Ma K-Ar and 364.9+/- 3.5 Ma Ar-Ar respectively; Lamb and Cox, 1998; Perello et al., 2001), whereas

post-mineralisation dykes at Tsagaan Suvarga have an age and composition much closer to that of Oyut Ulaan (313 +/- 2.9 Ma Ar-Ar; monzonite).

The age of the Oyut Ulaan intrusion also indirectly provides a minimum age for its host rocks - the basal formation of the Oyut Ulaan Volcanic Group. Upper parts of this volcano-sedimentary succession have been dated at 323.12 ±0.64 Ma (Chapter 3) giving a minimum duration of volcanism in the OUVG of 6.9 M.y., with a maximum range of 8.07 M.y. and a minimum range of 5.73 M.y., when error values are taken into account.

The time gap between ages of emplacement of the main quartz monzonite and the late-stage andesite dykes is 2.16 M.y., or a range of 1.19-3.31 M.y., considering errors. Furthermore, the volcanic model proposed for the Oyut Ulaan Volcanic Group (Chapter 3) suggests a period of higher effusion and more mafic lava types, related to increased extension, during the Shargyn Moghai Formation volcanism. Therefore, these dykes, with their chemical similarity to the SMF and their interpreted emplacement during crustal transtension, provide an age for the SMF, which, although indirect, is the best available.

4.3 Other granites in southeast Mongolia

4.3.1 Field data and petrography

Samples from the Mandakh and Shuteen intrusions were collected as part of a reconnaissance transect during summer of 2004 (Fig. 4.13). Ivanhoe Mines Ltd provided samples from the Bronze Fox and Narin Hudag intrusions, which were exploration targets at the time of sampling. The country rock for these four intrusions was not investigated; it is assumed to be arc volcanic and sedimentary rocks of a similar age and type to those that occur along strike in the Saykhandulaan inlier (Chapters 2 and 3). This assumption is supported by available literature (Badarch et al., 2002; Bignall et al., 2005). Mineral modal abundances for the lithologies discussed here are available in Appendix D.

The Narin Hudag and Mandakh samples come from a large area in the north of the Mandakh inlier, dominated by multiple intrusions (Fig. 4.1; Fig. 4.13). Two separate intrusive bodies were sampled near the town of Mandakh. The North Mandakh granite has an outcrop area of approximately 220 km^2, dominating the northeast of the Mandakh inlier (Fig. 4.13). It is very coarse-grained and is predominantly composed of large sub- and anhedral K-feldspars with microperthitic textures (Fig. 4.14, a and b). Plagioclase (An_{25}) is present as

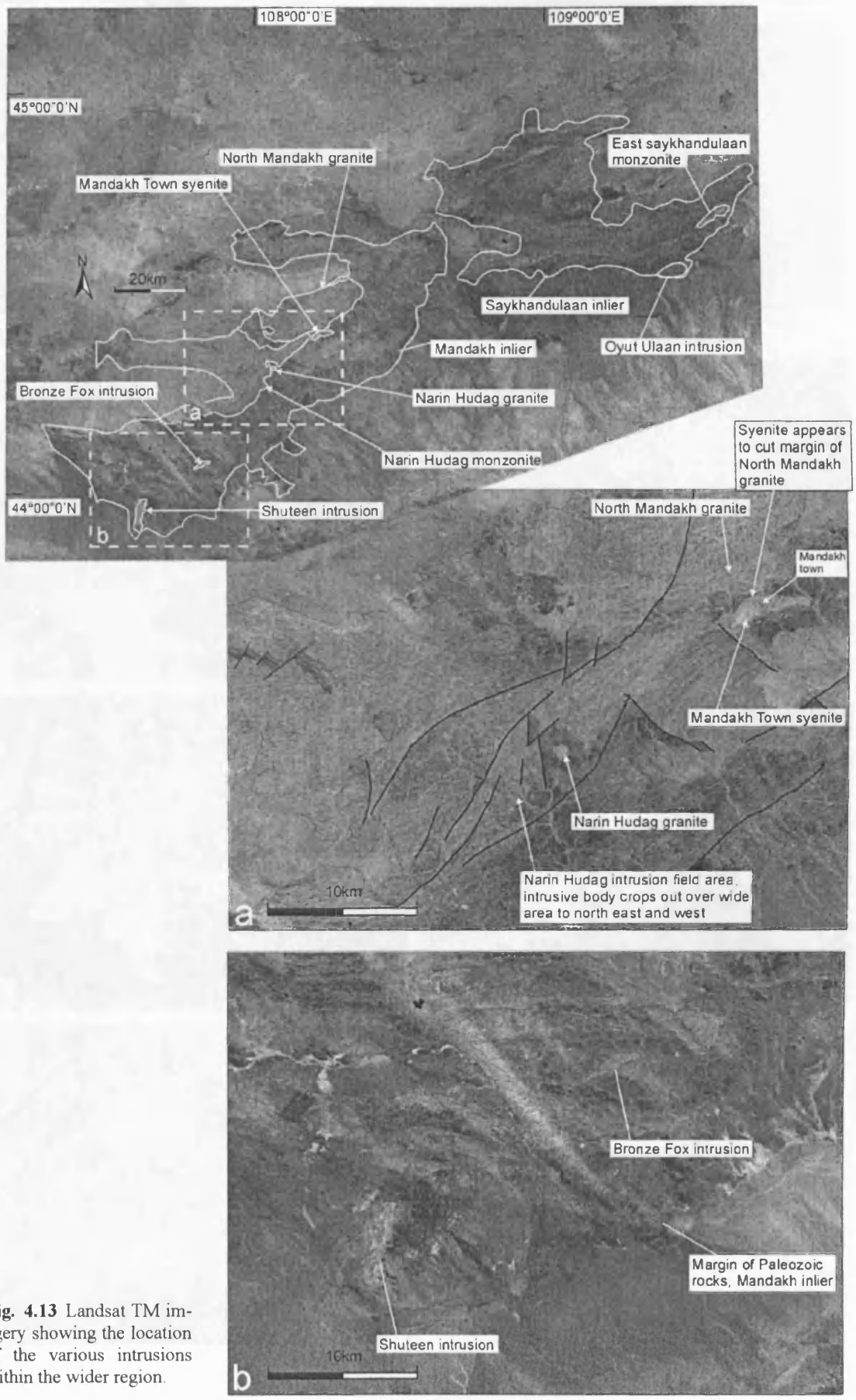

Fig. 4.13 Landsat TM imagery showing the location of the various intrusions within the wider region.

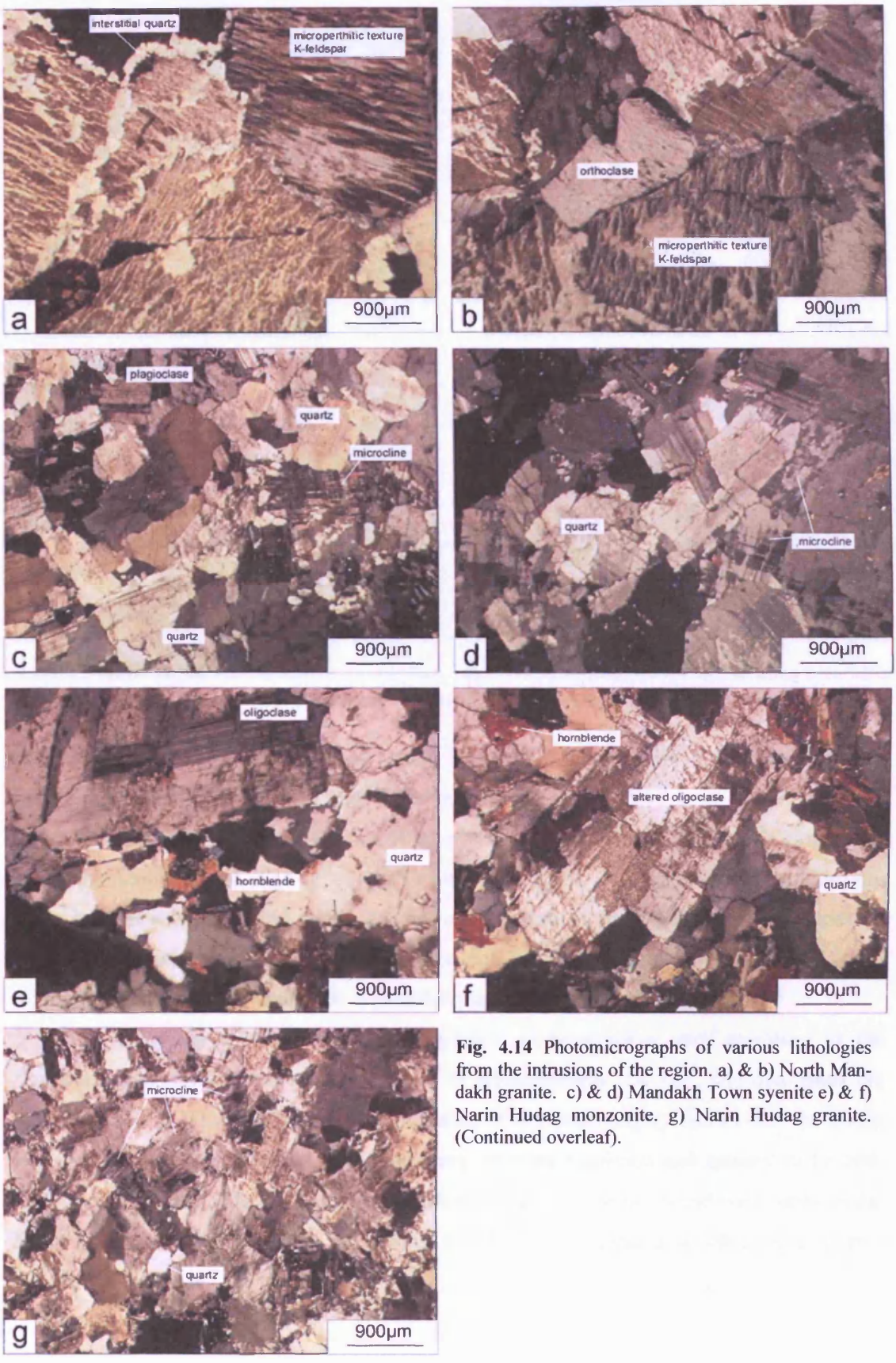

Fig. 4.14 Photomicrographs of various lithologies from the intrusions of the region. a) & b) North Mandakh granite. c) & d) Mandakh Town syenite e) & f) Narin Hudag monzonite. g) Narin Hudag granite. (Continued overleaf).

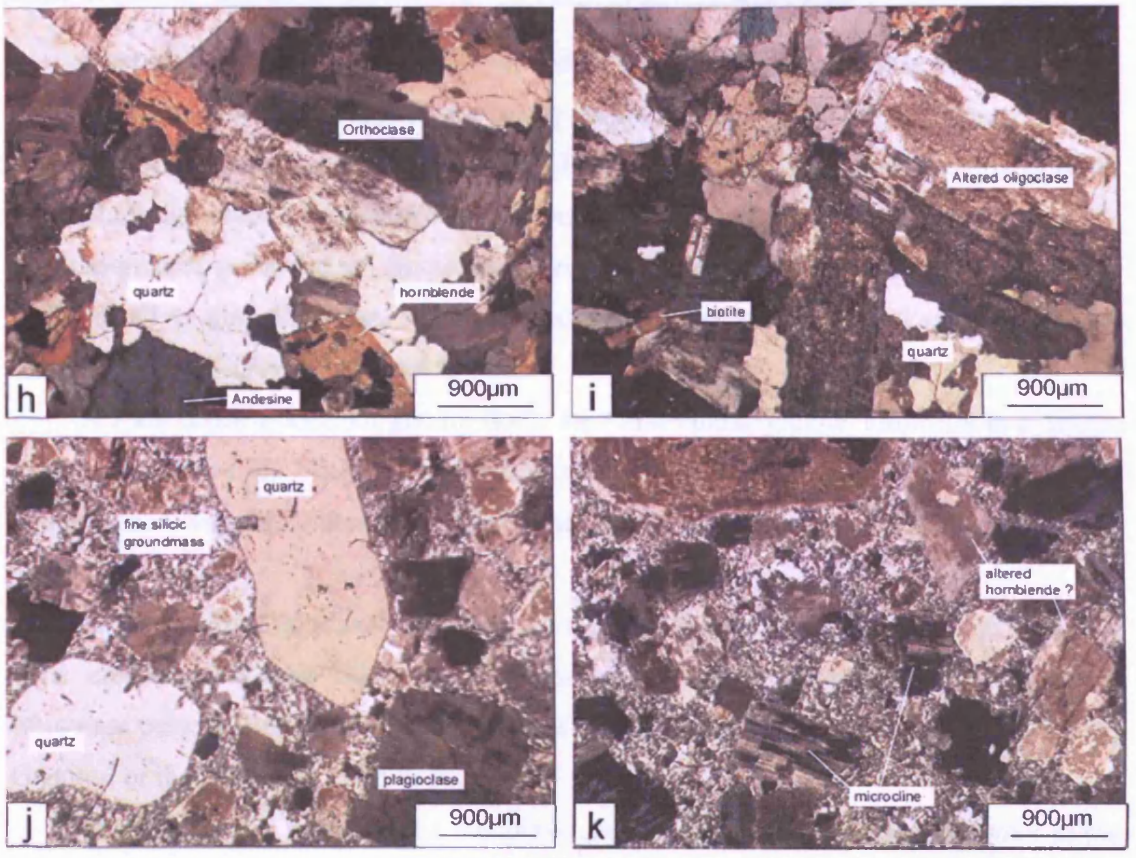

Fig. 4.14 (continued from previous page) h) and i) Shuteen intrusion. j) and i) East Saykhandulaan intrusion

rims and cores to these large crystals, whilst interstitial quartz, euhedral to subhedral hornblende, biotite and opaques form minor mineral phases.

The Mandakh Town syenite is a relatively small stock (5.5 km^2) which is elongate in the E-W orientation and slightly arcuate in form (Fig. 4.13). Its expression on satellite imagery suggest it is associated with a 25 km^2 outcrop area of apparently similar material directly to the south. It is almost entirely composed of 1-3 mm long plagioclase (An_{21-28}) and microcline phenocrysts, with minor interstitial quartz (Fig. 4.14, d and e).

The main Narin Hudag monzonite (referred to by Ivanhoe staff members as the 'Pudwake granodiorite') has an outcrop area of approximately 500 km^2, and dominates the northwest of the Mandakh inlier. Interpretation of satellite imagery shows that the Narin Hudag monzonite has several fault-bound margins in the southeast and appears to be contiguous with intrusions to the southwest of Mandakh town. The north and west limits of the Narin Hudag monzonite seem to be defined by Mesozoic sediments which lie unconformably on the intrusion.

Samples from the Narin Hudag monzonite were taken from a relatively small area near its southeast margin (Fig. 4.13). It is a coarse porphyritic intrusive body, composed primarily of 3 to 6 mm long euhedral plagioclase phenocrysts (An_{22-25}), in which zoning is common. Lozenge-shaped subhedral hornblendes of 1 to 2 mm length occur in the fine-to-medium grained groundmass. Some hornblendes have an apparently poikilitic texture, encasing small <1 mm plagioclase laths. The groundmass also contains 2 to 3 mm biotites and interstitial quartz. (Fig. 4.14, e and f).

A 1 km diameter circular granite stock, the Narin Hudag granite, crops-out in country-rock to the east of the Narin Hudag monzonite's margin. The granite is fine to medium-grained, and composed primarily of microcline with a fine-grained quartz groundmass (Fig. 4.14 g).

Dyke swarms, trending E and NE, are a visible feature of intrusions in the Mandakh inlier including the main Narin Hudag intrusion. However, these dark coloured dykes, which are pervasive elsewhere, do not appear to cut the North Mandakh and Narin Hudag Granites, or the Mandakh Town Syenite.

The Bronze Fox intrusion is a complexly zoned monzo-granodiorite stockwork to the southwest of the large-volume intrusive rocks at Narin Hudag and Mandakh (Fig. 4.13). This body features an asymmetrically zoned sequence of intrusive lithologies including an outer shell of hornblende monzodiorite, a middle-zone of hornblende-biotite quartz-monzonite, and a core of biotite-hornblende granodiorite. Gold-copper mineralisation is strongly associated with the core zone of the intrusive system here (Stewart, 2005, pers comm.).

The Shuteen volcano-plutonic complex is at the southwest end of the belt of intrusions studied here. Shuteen is unique amongst the intrusions investigated here, in having been the subject of some previous work: Korim et al. (1984) report that the Shuteen intrusion has a typical ring-structure with circular normal-faults. Bignall et al. (2005) show that the Shuteen volcano-plutonic complex is comprised of the Dusiin Ovoo Volcanic formation and the Shuteen pluton, which is formed of a variety of granitoid lithologies, and previously dated via Rb/Sr whole rock methods at 321+/- 9 Ma (Batkhishig and Iizumi, 2001; Batkhishig et al., 2003). The part of the pluton sampled for this study consisted primarily of a medium-grained granitoid densely packed with subhedral 2-4 mm K-feldspar phenocrysts, and euhedral plagioclase laths (An_{22-34}) of similar size (Fig. 4.14, h and i). Supplementary phases include euhedral biotite and sparsely distributed hornblende. Microgranite dykes that cut the

pluton are sparsely populated with quartz xenocrysts and plagioclase phenocrysts in a fine grained groundmass of quartz plagioclase and biotite. Some zoned plagioclase phenocrysts show a clear variation in composition from inner to outer zones (An_{60} to An_{26}). Myrmekitic intergrowths of quartz and K-feldspar occur in one sample.

The East Saykhandulaan intrusion lies at the eastern edge of the Saykhandulaan inlier, 10 km to the northeast of the Oyut Ulaan intrusion. This body consists of two lobes, elongate to the north-east, parallel to the structural grain of the area. It is a fine- to medium-grained felsic body, composed of K-feldspar and quartz phenocrysts in a fine-grained felsic groundmass (Fig. 4.14, j and k). Its distinctive porphyritic texture suggests that it is a large hypabyssal intrusion rather than a pluton. The central zone, between the two lobes, contains a complex stockwork of overlapping hypabyssal intrusions of various mafic lithologies, which appear to postdate the main intrusion; 1-2 m thick basalt dykes cut the felsic body, and xenoliths of granite occur within larger volumes of mafic material.

4.3.2 Geochemistry of intrusions from the region, and comparison with Oyut Ulaan

The TAS diagram of Middlemost (1985) was used for determination of intrusive lithologies (Fig. 4.15; Results - Appendix A). Two analysed samples from Bronze Fox plot as monzonites and two as quartz-monzonites. All analysed samples from the Narin Hudag monzonite plot as quartz-monzonites. All samples from the Narin Hudag granite plot within the granite field. The one sample that was analysed from the East Saykhandulaan intrusion plot in the monzonite field. Four analyses from Shuteen plot as a cluster near the quartz monzonite-granite boundary, with two analyses falling either side of the line. One sample from Shuteen plots as a granite. This represents a mircrogranite dyke that cuts the main intrusion there.

Harker diagrams for all samples show typical inverse differentiation trends of compatiable elemental abundances with SiO_2 (Fig. 4.16). Samples from Bronze Fox and the Narin Hudag Monzonite define the more mafic end of this trend on most diagrams, whereas the true granitic lithologies are most evolved, and have the highest abundances of incompatible

Fig. 4.15 (next page) a) Total Alkalis Silica (TAS) diagram after Middlemost (1985), for all intrusions. Field shows area of Oyut Ulaan intrusion samples. Analyses of granitoid cobbles from Oyut Ulaan Volcanic Group also shown. b) Diagram of A/CNK (Alkali saturation index; $Al_2O_3/[K_2O + Na_2O + CaO]$) vs A/NK ($Al_2O_3/[K_2O + Na_2O]$) after Shand (1943) c) Diagram of SiO_2 vs P_2O_5 showing inverse trend typical of I-type granitoids and indicative of the fractionation of apatite in the absence of Y-bearing accessory minerals (Wu et al., 2000) d) Diagram of Zr vs 10000*Ga/Al after Eby (1990), to differentiate I & S type granitoids from A-type granitoids. e) diagram of Y/Nb vs Sc/Nb after Eby (1992) to differentiate A1 and A2 type granitoids, note North Mandakh granite plotting nearer to A2 field than other intrusions, fields represent data as cited in Appendix C.

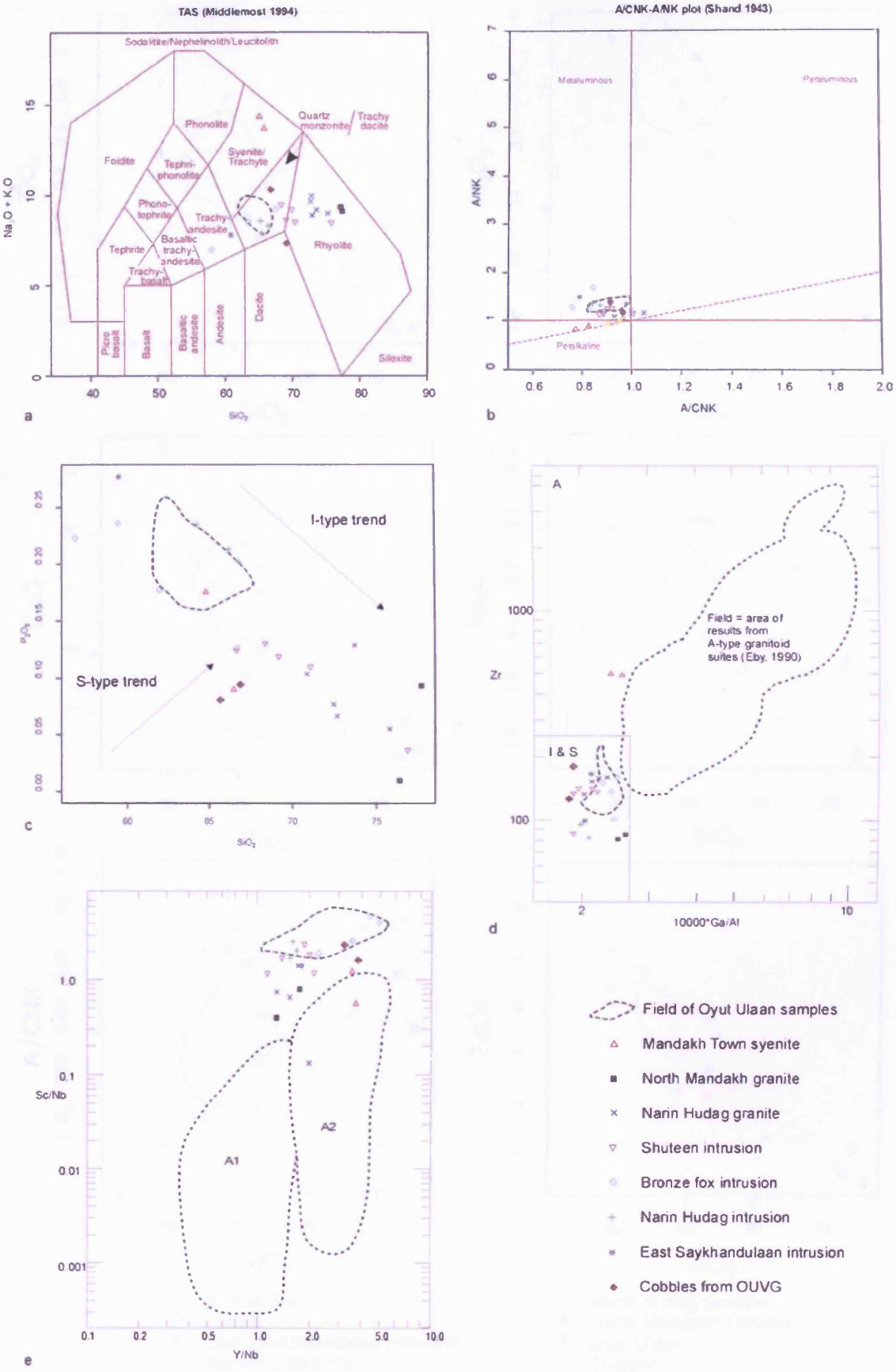
TAS (Middlemost 1994)
Sodalite/Nepheline/Leucitolith
Phonolite
Quartz monzonite
Trachy dacite
Foidite
Tephri-phonolite
Syenite/ Trachyte
Phono-tephrite
Trachy-andesite
Tephrite
Basaltic trachy-andesite
Rhyolite
Trachy-basalt
Picro basalt
Basalt
Basaltic andesite
Andesite
Dacite
Silexite
Na2O + K2O
SiO2
a
A/CNK-A/NK plot (Shand 1943)
Metaluminous
Peraluminous
Peralkaline
A/NK
A/CNK
b
I-type trend
S-type trend
P2O5
SiO2
c
A
Field = area of results from A-type granitoid suites (Eby, 1990)
I & S
Zr
10000*Ga/Al
d
Sc/Nb
Y/Nb
A1
A2
e
Field of Oyut Ulaan samples
Mandakh Town syenite
North Mandakh granite
Narin Hudag granite
Shuteen intrusion
Bronze fox intrusion
Narin Hudag intrusion
East Saykhandulaan intrusion
Cobbles from OUVG

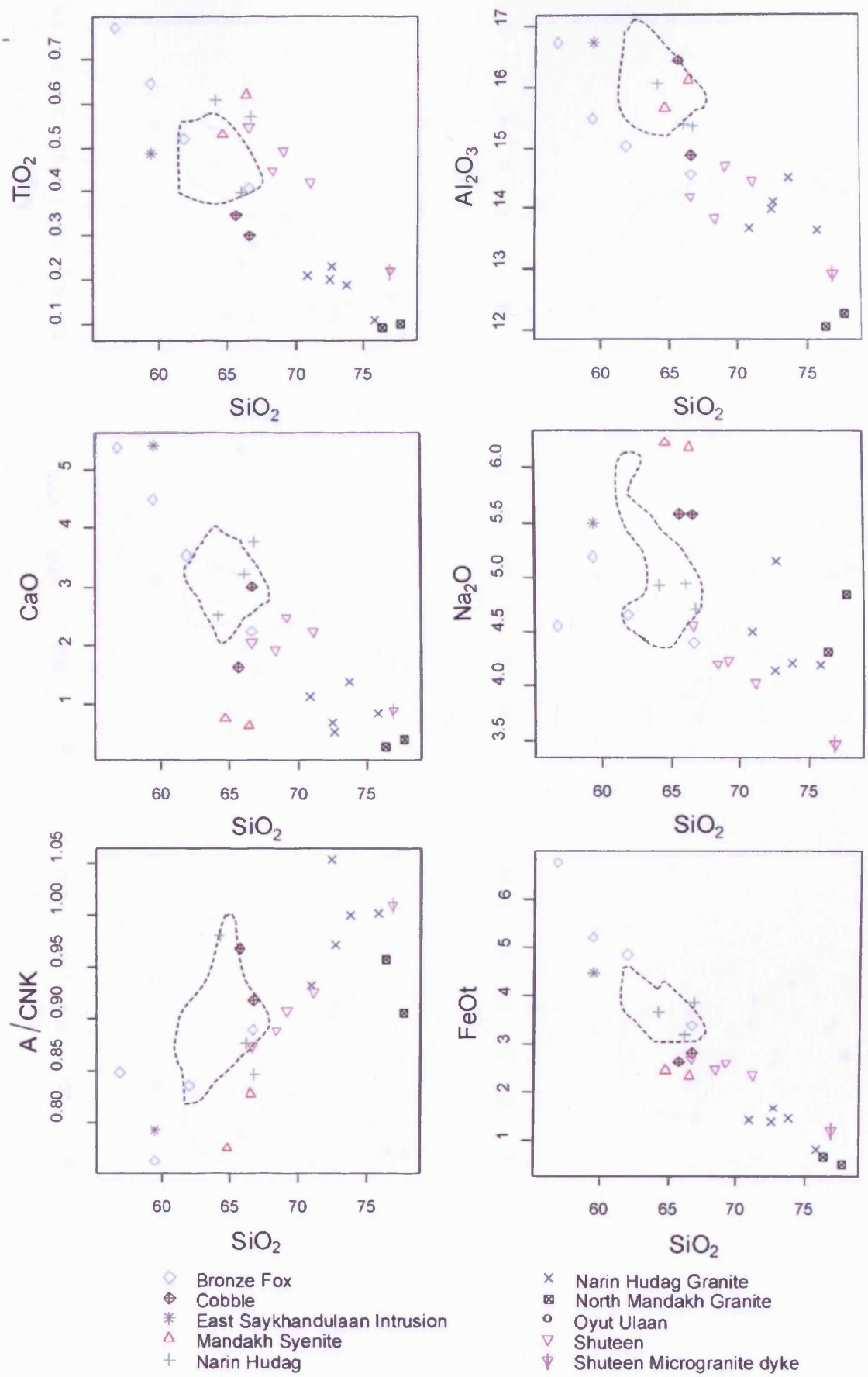

Fig. 4.16 Harker variation diagrams of major and trace elements vs SiO_2 for intrusions of the region. (continued over next two pages)

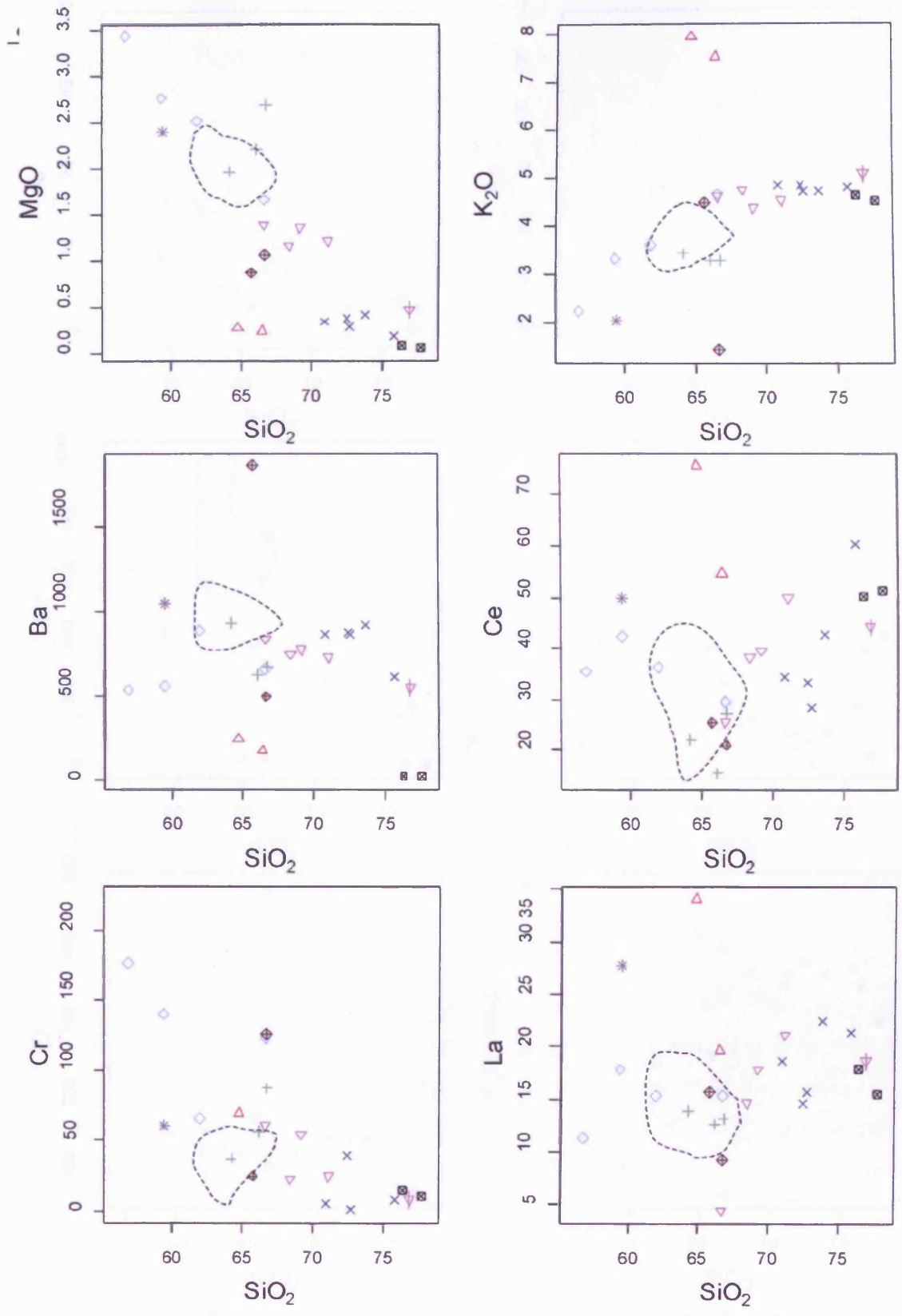
MgO
SiO_2
K_2O
SiO_2
Ba
SiO_2
Ce
SiO_2
Cr
SiO_2
La
SiO_2
Bronze Fox
Cobble
East Saykhandulaan Intrusion
Mandakh Syenite
Narin Hudag
Narin Hudag Granite
North Mandakh Granite
Oyut Ulaan
Shuteen
Shuteen Microgranite dyke

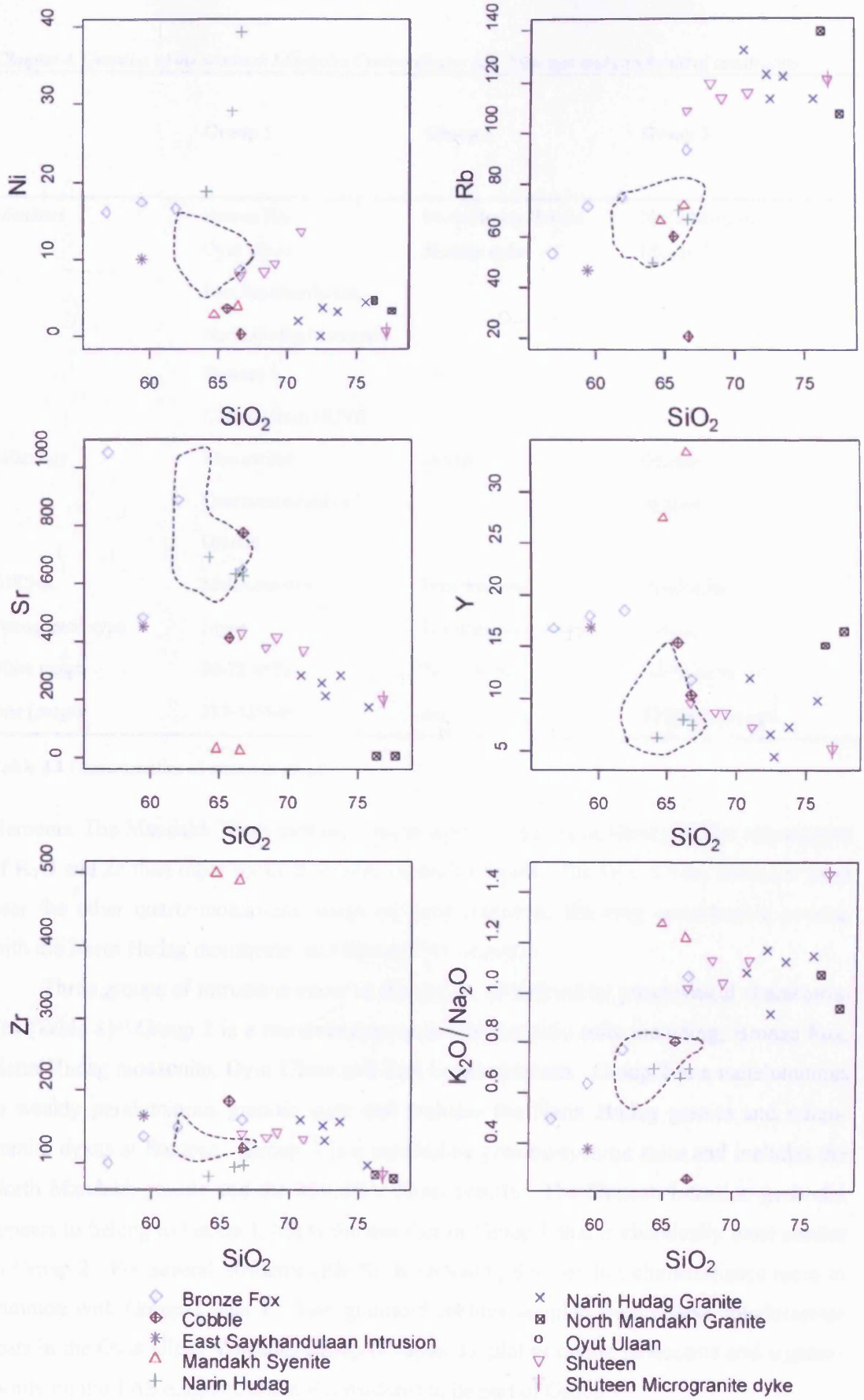
Ni
Rb
Sr
Y
Zr
K_2O/Na_2O
SiO_2
Bronze Fox
Cobble
East Saykhandulaan Intrusion
Mandakh Syenite
Narin Hudag
Narin Hudag Granite
North Mandakh Granite
Oyut Ulaan
Shuteen
Shuteen Microgranite dyke

	Group 1	**Group 2**	**Group 3**
Members	Bronze Fox	Narin Hudag Granite	North Mandakh
	Oyut Ulaan	Shuteen dyke	Mandakh Town
	East Saykhandulaan		
	Narin Hudag Monzonite		
	Shuteen		
	Cobbles from OUVG		
Lithology	Monzonites	Granite	Granite
	Quartz-monzonites		Syenite
	Granite		
Al/CNK	Metaluminous	Peraluminous	Peralkaline
Petrogenetic type	I-type	I or aluminous A-type	A-type
Silica range	56-72 wt %	71-77 wt %	65-79 wt %
Age (range)	339-325Ma	n/a	329Ma (max age)

Table 4.1 Characteristics of intrusion groups.

elements. The Mandakh Town syenite is an exception to this rule, having higher abundances of K_2O and Zr than other rocks at similar values for silica. The Oyut Ulaan intrusion plots near the other quartz-monzonitic rocks on most diagrams, showing considerable overlap with the Narin Hudag monzonite, and Bronze Fox intrusion.

Three groups of intrusions occur in the region, as defined by geochemical characteristics (Table 1). Group 1 is a metaluminous quartz-monzonitic suite including; Bronze Fox, Narin Hudag monzonite, Oyut Ulaan and East Saykhandulaan. Group 2 is a metaluminous to weakly peraluminous granitic suite and includes the Narin Hudag granite and micro-granite dykes at Shuteen. Group 3 is a peralkaline granitic-syenitic suite and includes the North Mandakh granite and the Mandakh Town syenite. The Shuteen intrusion generally appears to belong to Group 1, but is the member of Group 1 that is chemically most similar to Group 2. For several elements (Rb, Sr, K_2O/Na_2O), Shuteen has characteristics more in common with Group 2 than 1. Two granitoid cobbles sampled from coarse conglomerate units in the Oyut Ulaan Volcanic Group (Chapter 3), plot as quartz monzonite and a granodiorite on the TAS diagram, and are considered to be part of Group 1.

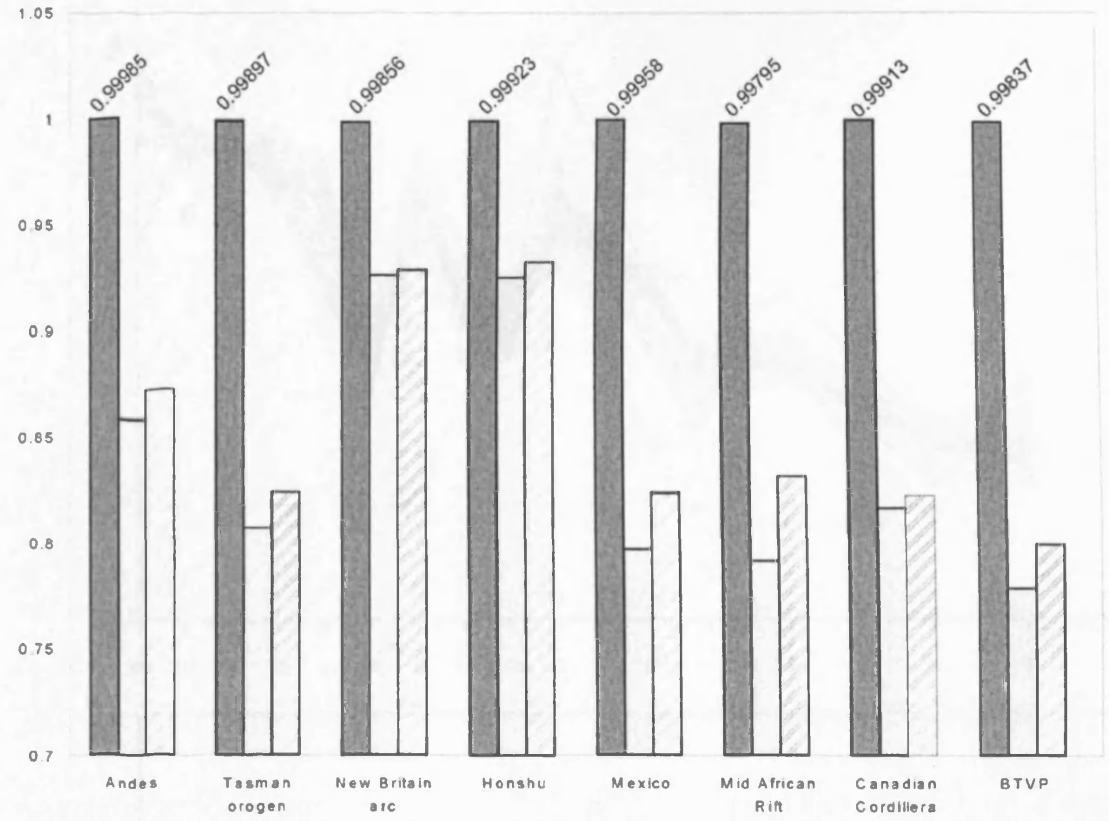

Fig. 4.17 Bar chart of correlation coefficients for average elemental abundaces from Group 1 versus average elemental abundances from various plutons from locations worldwide. The silica range of comparative suites was selected to match that of in Group 1 (60-70wt%). Note the high correlation between major element values alone indicating close fit of lithologies being compared. Closest comparators are Honshu and the New Britain arc, followed by the Andes. Intrusions of British Tertiary Volcanic Province (BTVP) are the least geochemically similar to Group 1 rocks.

Group 1 rocks are I-type granitoids (Fig. 4.15; Chappell and White, 1974; Wu et al., 2000). Group 2 rocks plot as I-type on a range of diagrams, but from their high silica content, it is possible that they are part of the aluminous A-type association defined by King et al. (1997). This association does not have the tectono-magmatic implications of the standard A-type classification, and the potential source region is infra-crustal, overlapping with the I-type source regions. A variation of physical properties at source, such as limited H_2O and high temperatures during partial melting, is thought to generate aluminous A-type magmas (King et al., 1997). It is noted that the more evolved aluminous A-type granites are difficult to distinguish from I-type granites, and that, ideally, suites containing less evolved rocks would be compared.

The Mandakh Town syenite is the only intrusion that appears conclusively to be of peralkaline A-type character (Fig. 4.15), whilst the peralkaline North Mandakh granite plots closer to A-type fields than other intrusions from the region (Fig. 4.15). The A-type signa-

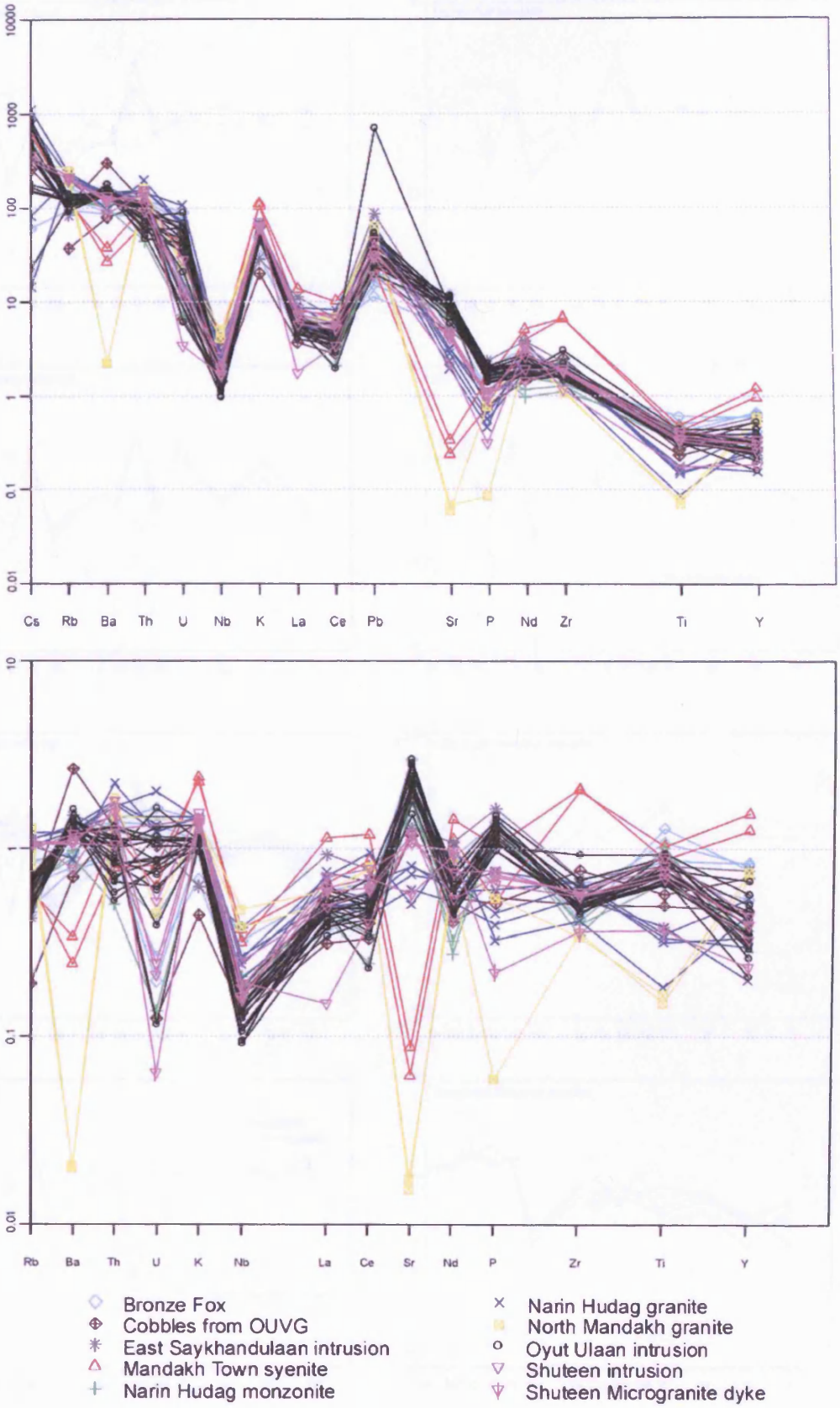

Fig. 4.18 Spidergrams of trace element abundances from all analysed samples; a) normalised to NMORB (Sun and McDonough, 1989); b) normalised to average upper crustal values (Taylor and McLennan, 1985); c) (next page) normalised to average upper crustal values, plotted separately, by intrusive body, for clarity.

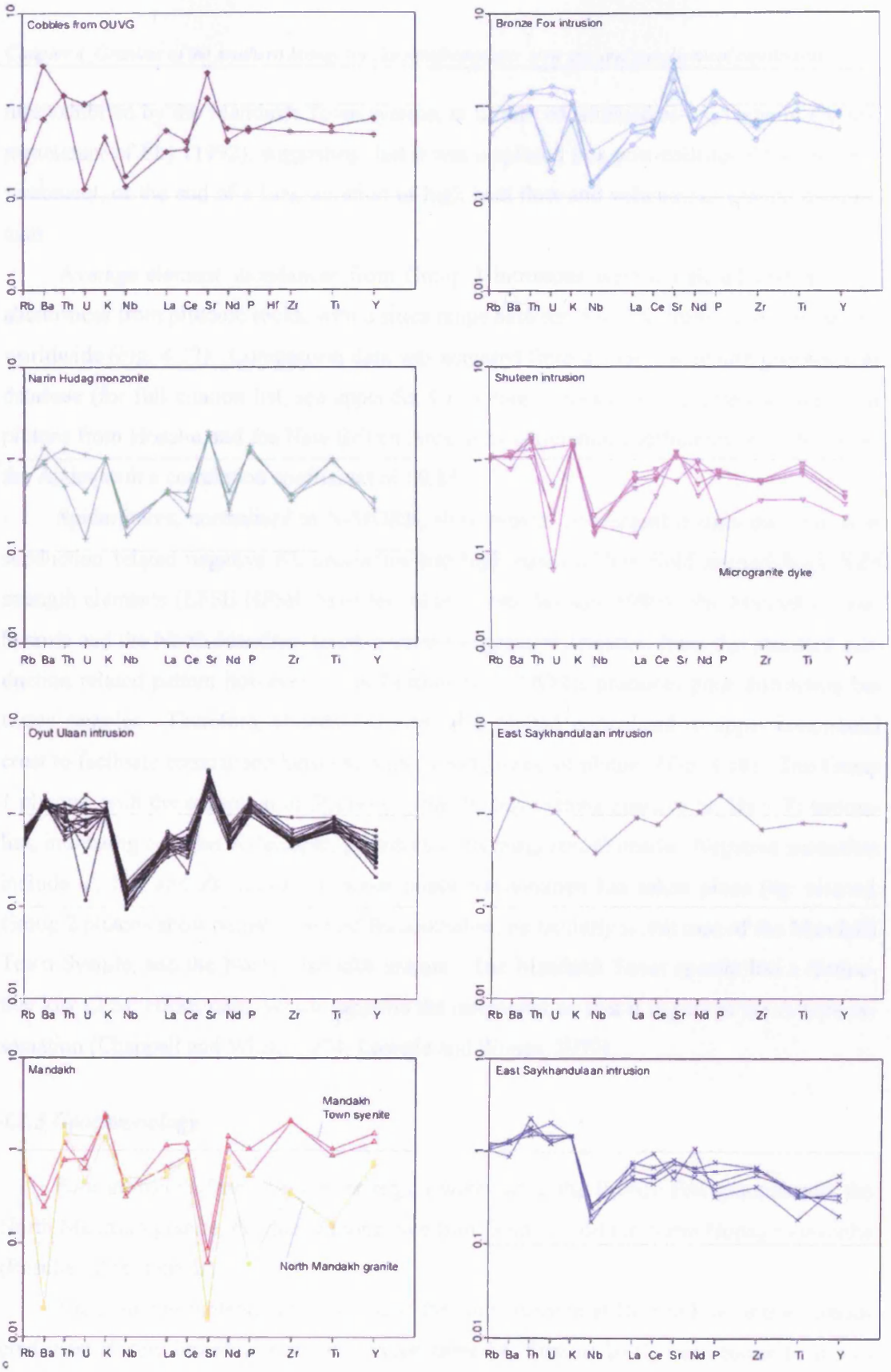

Fig. 4.18c (continued from previous page)

ture exhibited by the Mandakh Town syenite, is further constrained as 'A_2' type in the nomenclature of Eby (1992), suggesting that it was emplaced in a post-collisional tectonic environment, or the end of a long duration of high heat flow and voluminous granite magmatism.

Average element abundances from Group 1 intrusions were correlated with average abundances from plutonic rocks, with a silica range between 60-70%, from various locations worldwide (Fig. 4.17). Comparison data was acquired from the Georoc online geochemical database (for full citation list, see appendix C). Group 1 rocks show greatest similarity to plutons from Honshu and the New Britain Arcs, with correlation coefficients of >0.9, and to the Andes with a correlation coefficient of >0.85.

Spidergrams, normalised to N-MORB, show typical convergent margin patterns, with subduction related negative Nb anomalies and high ratios of low field strength/high field strength elements (LFSE:HFSE; Saunders et al., 1980; Wilson, 1989), the Mandakh Town Syenite and the North Mandakh Granite show the greatest deviation from this standard subduction related pattern however, normalisation by N-MORB produces poor distinction between samples. Therefore, abundances were also plotted normalised to upper continental crust to facilitate comparison between plutons and groups of plutons (Fig. 4.18). The Group 1 plutons, with the exception of Shuteen, generally have strong positive Sr, Ba + Ti anomalies, indicating cumulus K-feldspar, plagioclase and magnetite/ilmenite. Negative anomalies include U, Nd, and Zr indicating minor phase fractionation has taken place (eg. zircon). Group 2 plutons show negative Sr and Ba anomalies, particularly in the case of the Mandakh Town Syenite, and the North Mandakh granite. The Mandakh Town syenite has a distinctive low LFSE:HFSE ratio, which supports the interpretation that it is part of the A-type association (Chappell and White, 1974; Loiselle and Wones, 1979).

4.3.3 Geochronology

Four intrusions from the greater region were dated, the Bronze Fox granodiorite, the North Mandakh granite, the quartz monzonite from Shuteen and the Narin Hudag monzonite (Results - Appendix B).

The biotite-hornblende granodiorite is the core intrusion at Bronze Fox, and is considered most closely linked with mineralisation there (A. Stewart 2005, pers. comm.). It was geochemically determined to be of quartz monzonitic composition in this study and yielded two overlapping, concordant, single-grain zircon analyses. The concordia age calculated

from these two points is 333.60 +/- 0.60 Ma (Fig. 4.19 a). Four further analyses plotted with younger discordant ages, relating to incomplete removal of parts of the zircon that had suffered lead loss. A discordia line through all data points gives an upper intercept of 331.9 +/- 5.7 Ma, which falls within error of the two point concordia age (Fig. 4.19 a).

The Narin Hudag monzonite yielded three, overlapping, concordant, single-grain zircon analyses. The concordia age calculated from these three points is 333.22 ±0.63 Ma (Fig. 4.19 b). Three further analyses plotted with younger discordant ages are likely to have been caused by lead loss.

The Shuteen quartz-monzonite yielded three, overlapping concordant, single-grain zircon analyses. The concordia age calculated from these three points is 325.47 ±0.95 Ma (Fig. 4.19 c). Two other analyses plotted with strong negative discordance, and were disregarded.

The north Mandakh granite yielded three, overlapping, concordant, single-grain zircon analyses. The concordia age calculated from these three points is 292.34 +/- 0.50 Ma (Fig. 4.19 d). One further analysis plotted with a younger discordant age, which again is likely to have been caused by lead loss.

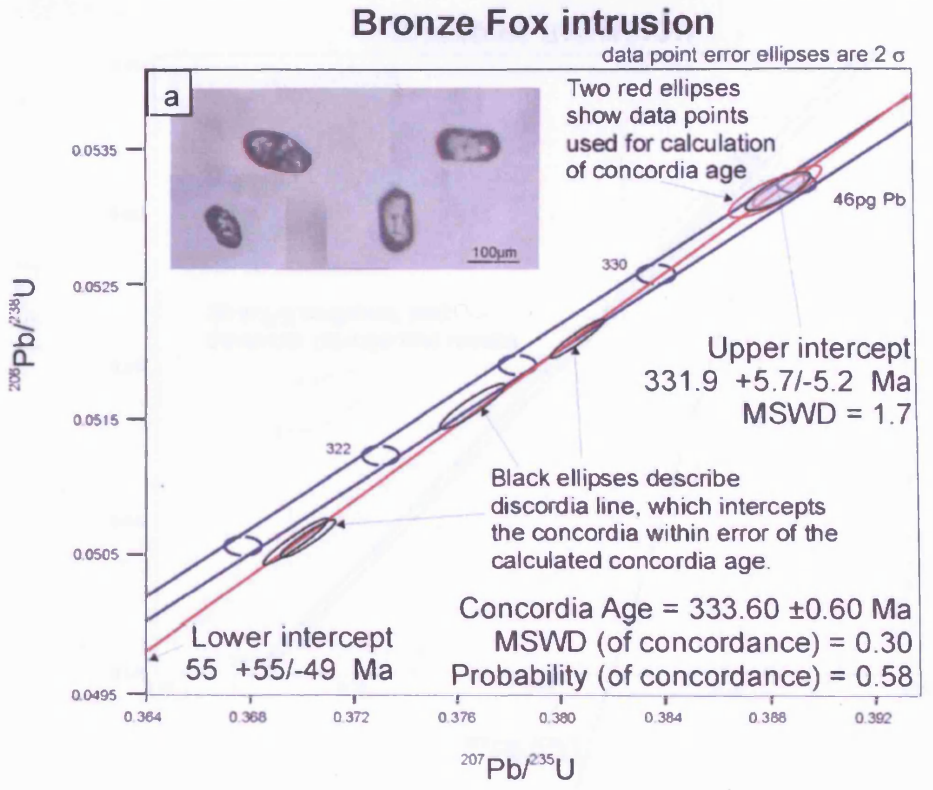

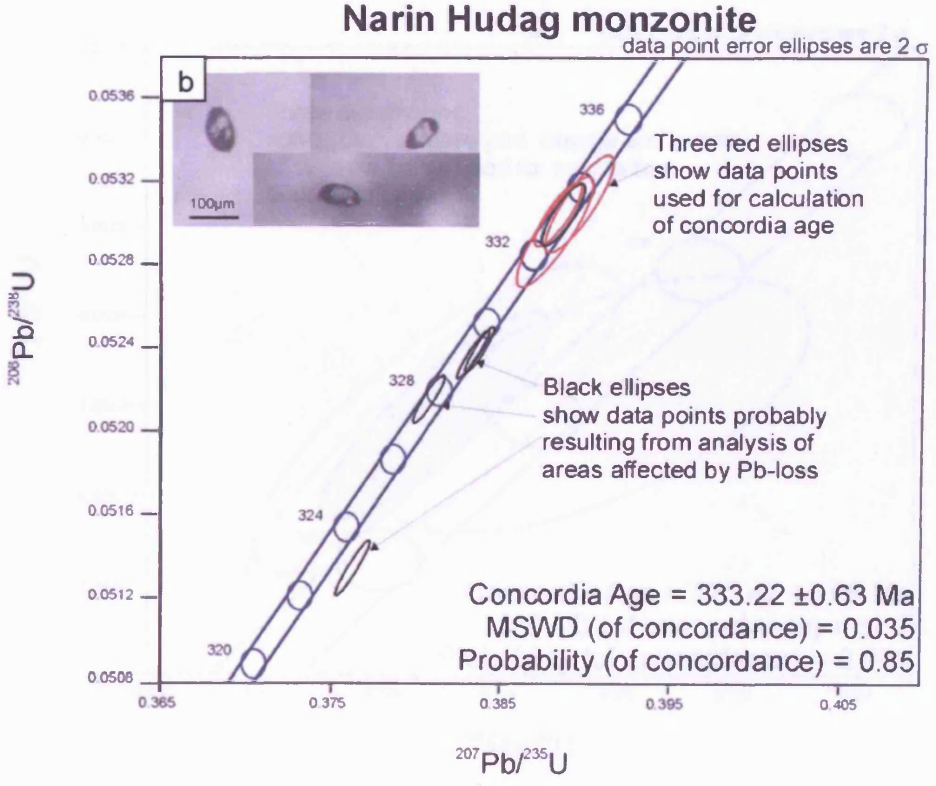

Fig. 4.19 Concorda diagrams for dated intrusions from the region. Ellipses with fine outlines show the data points, and corresponding errors. Grey-filled ellipses show the calculated concordia age. (continued over next two pages). See text for explanation of MSWD.

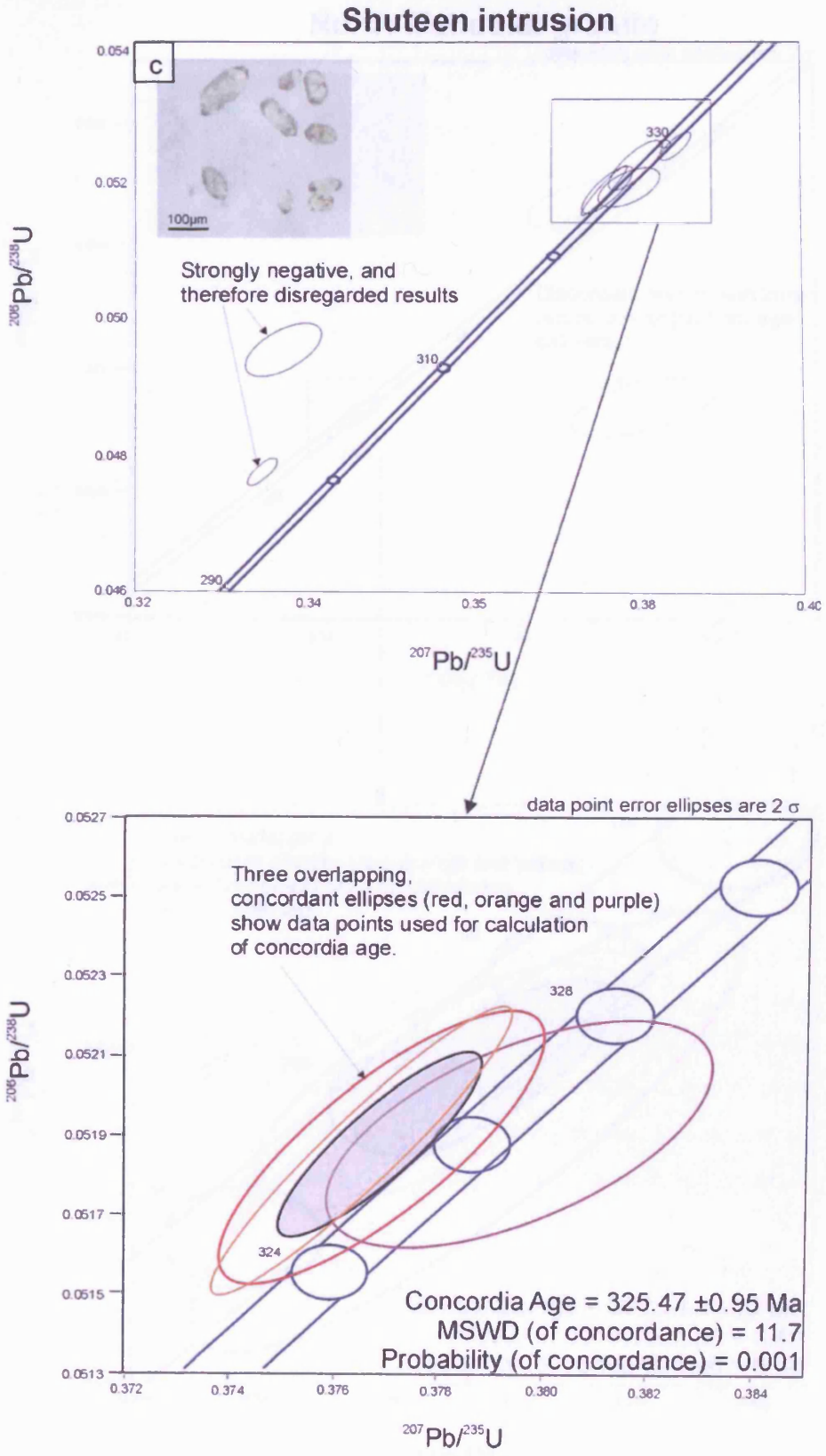
Shuteen intrusion
C
100µm
Strongly negative, and
therefore disregarded results
330
310
290
0.054
0.052
0.050
0.048
0.046
0.32
0.34
0.35
0.38
0.40
$^{206}Pb/^{238}U$
$^{207}Pb/^{235}U$
data point error ellipses are 2 σ
Three overlapping,
concordant ellipses (red, orange and purple)
show data points used for calculation
of concordia age.
328
324
Concordia Age = 325.47 ±0.95 Ma
MSWD (of concordance) = 11.7
Probability (of concordance) = 0.001
0.0527
0.0525
0.0523
0.0521
0.0519
0.0517
0.0515
0.0513
0.372
0.374
0.376
0.378
0.380
0.382
0.384
$^{206}Pb/^{238}U$
$^{207}Pb/^{235}U$

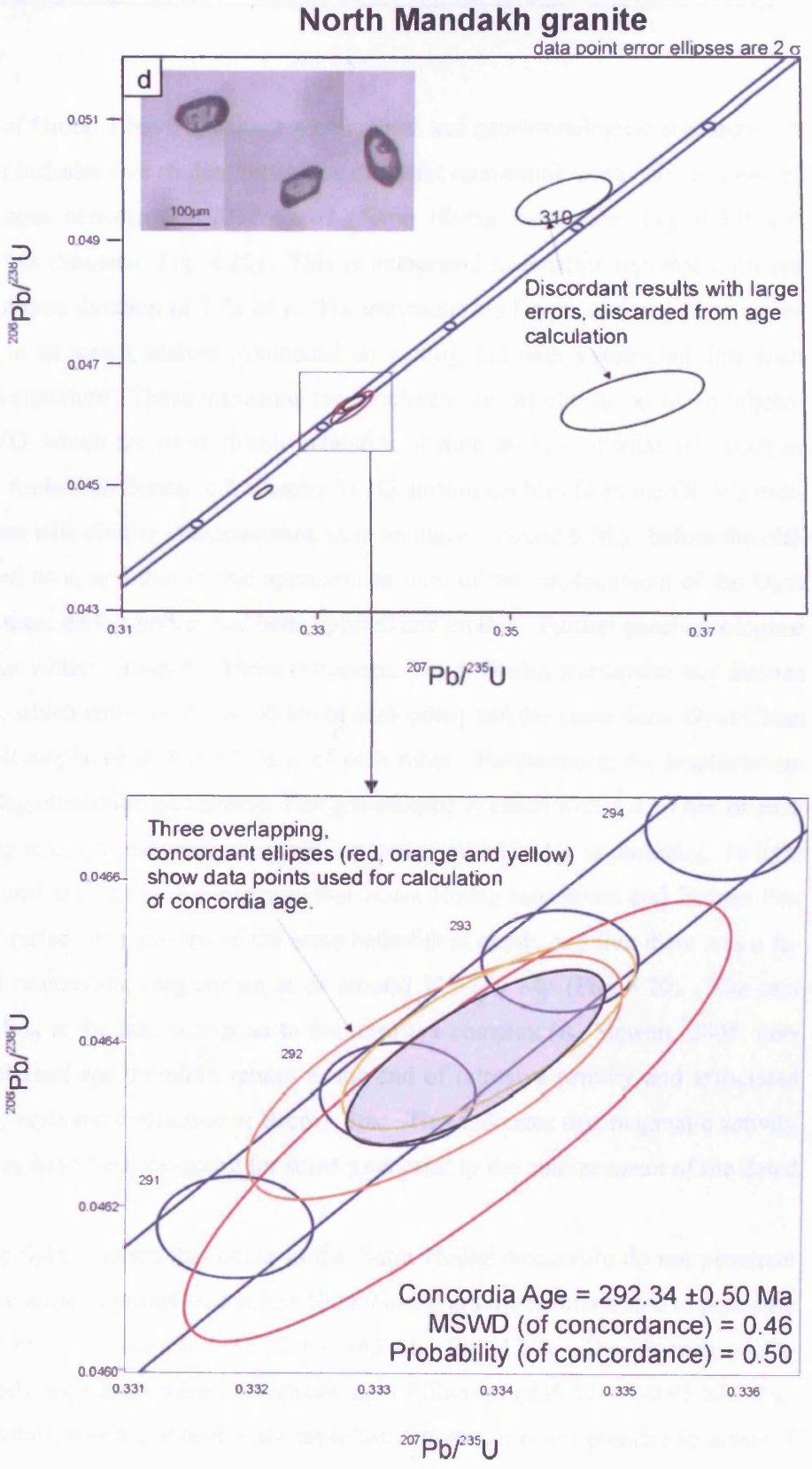
North Mandakh granite
data point error ellipses are 2 σ
d
100µm
310
Discordant results with large errors, discarded from age calculation
0.051
0.049
0.047
0.045
0.043
0.31
0.33
0.35
0.37
206Pb/238U
207Pb/235U
Three overlapping, concordant ellipses (red, orange and yellow) show data points used for calculation of concordia age.
294
293
292
291
0.0466
0.0464
0.0462
0.0460
0.331
0.332
0.333
0.334
0.335
0.336
Concordia Age = 292.34 ±0.50 Ma
MSWD (of concordance) = 0.46
Probability (of concordance) = 0.50
206Pb/238U
207Pb/235U

4.3.4 Discussion

Intrusions of Group 1 have a distinct geochemical and geochronological signature. A 180 km long belt includes five studied intrusions of quartz monzonitic composition, three of which returned ages between 333.22 +/- 0.63 (Narin Hudag monzonite; Fig. 4.20) and 325.47 +/- 0.95 Ma (Shuteen; Fig. 4.20). This is interpreted to indicate regional intrusive activity with minimum duration of 7.75 M.y. The intrusions are I-type, and appear to represent magmatism in an active, mature continental-arc setting, but with a restricted time span and geochemical signature. These intrusions are geochemically similar to extrusive lithologies of the OUVG, which are most closely related to mature arcs/continental arcs such as Honshu, Central Andes and Sunda (c.f. Chapter 3). Granitoid cobbles from the OUVG indicate that intrusions with similar characteristics were emplaced around 6 M.y. before the oldest intrusion dated here, and that by the approximate time of the emplacement of the Oyut Ulaan Intrusion, these earlier bodies had been uplifted and eroded. Further geochronological associations occur within Group 1. Three intrusions; Narin Hudag monzonite and Bronze Fox granodiorite, which crop out within 40 km of each other, and the more distal Oyut Ulaan intrusion, were all emplaced within 3.5 M.y. of each other. Furthermore, the emplacement of the Narin Hudag monzonite and Bronze Fox granodiorite occured within 0.14 My of each other (considering errors, a maximum temporal separation of 1.37 M.y. is possible). In light of their geochemical similarity, this suggests that Narin Hudag monzonite and Bronze Fox complex may be surface expressions of the same batholith at depth, and that there was a focussed period of monzonitic magmatism at or around 333-330 My (Fig. 4.20). The unit dated at Bronze Fox is the late core-zone to the intrusive complex (A. Stewart, 2005. pers comm.). The obtained age therefore relates to the end of intrusive activity and associated primary porphyry-style mineralisation at Bronze Fox. This indicates that magmatic activity at Bronze Fox may have been on-going for some time prior to the emplacement of the dated unit.

The prolific dyke swarms that occur in the Narin Hudag monzonite do not penetrate the Narin Hudag granite. For this reason, the Narin Hudag granite is interpreted to post-date the emplacement of the monzonite (333.22 +/- 0.63 Ma; Fig. 4.20). The Shuteen microgranite dyke clearly post-dates the emplacement age of Shuteen (325.47 +/- 0.95 Ma; Fig. 4.20). As no absolute ages are available for these two features, it is not possible to assess if their compositional similarity is purely coincidental, or if there was some regional granite emplacement activity that took place towards the end of, or after the emplacement of the

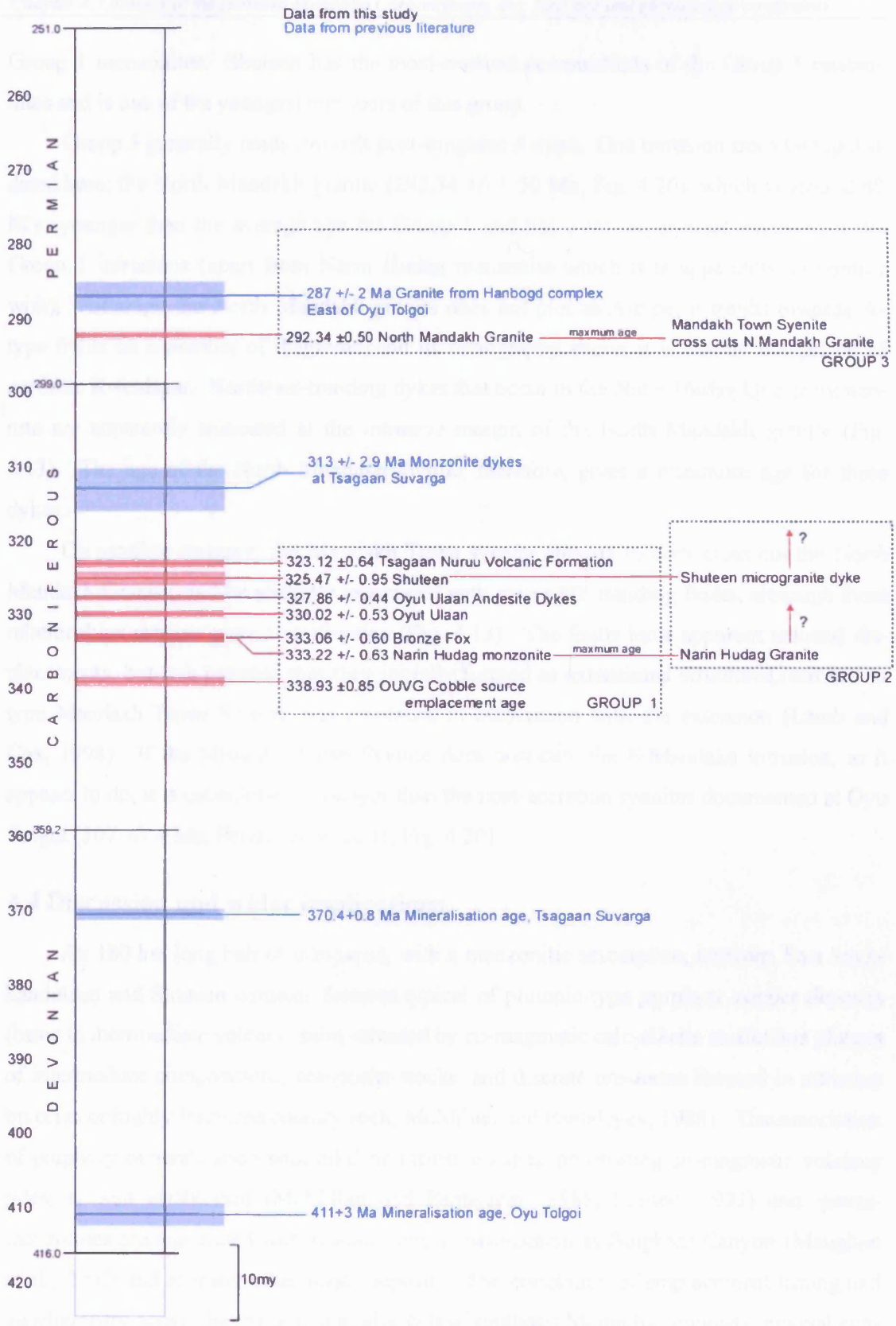

Fig. 4.20 Summary of ages from this chapter, chapter 3 and published literature (blue) marked on the the International Stratigraphic Chart geological time scale (2004). Undated intrusions are marked with maximum ages interpreted from cross-cutting relationships

Group 1 monzonites. Shuteen has the most-evolved compositions of the Group 1 monzonites and is one of the youngest members of this group.

Group 3 generally tends towards post-orogenic A-type. One intrusion from Group 3 is dated here; the North Mandakh granite (292.34 +/- 0.50 Ma; Fig. 4.20), which is around 40 M.y. younger than the average age for Group 1 and has a far larger areal extent than the Group 1 intrusions (apart from Narin Hudag monzonite which it is apparently in contact with). Although the North Mandakh granite does not plot as A-type, it trends towards A-type fields on a number of diagrams, and its petrography shows it is mainly comprised of perthitic K-feldspar. Northeast-trending dykes that occur in the Narin Hudag Quartz monzonite are apparently truncated at the intrusive margin of the North Mandakh granite (Fig. 4.13). The age of the North Mandakh granite, therefore, gives a minimum age for these dykes.

On satellite imagery, the Mandakh Town syenite appears to both cross-cut the North Mandakh Granite, and be spatially associated with major NE trending faults, although these relationships require ground-verification (Fig. 4.13). The faults have apparent sinistral displacements, but it is possible that they initially formed as extensional structures, and the A-type Mandakh Town Syenite was emplaced in association with the extension (Lamb and Cox, 1998). If the Mandakh Town Syenite does post-date the N.Mandakh intrusion, as it appears to do, it is considerably younger than the post-accretion syenites documented at Oyu Tolgoi (307 +/- 4 Ma, Perello et al. 2001; Fig. 4.20).

4.4 Discussion and wider implications

An 180 km long belt of intrusions, with a monzonitic association, between East Saykhandulaan and Shuteen contains features typical of plutonic-type porphyry copper deposits (basic to intermediate volcanic piles intruded by co-magmatic calc-alkalic to alkaline plutons of intermediate compositions; composite stocks; and discrete ore-zones focused in intrusive breccias or highly fractured country rock; McMillan and Pantaleyev, 1988). The association of porphyry mineralisation with alkaline intrusive suites, penetrating co-magmatic volcanic piles, is well established (McMillan and Pantaleyev, 1988; Sillitoe, 1997) and quartz-monzonites are associated with Cu-porphyry mineralisation at Bingham Canyon (Maughan et al., 2002) and at many other major deposits. The correlation of emplacement timing and geochemistry across the regional intrusive belt of southeast Mongolia, suggests regional controls on emplacement and mineralisation. This chronological and geochemical association

may extend beyond the confines of the belt as studied here, along-strike in both directions, and may define a common association of mineral prospectivity.

There is a great volume of post-orogenic granite (North Mandakh granite) in close proximity to the Oyut Ulaan-Shuteen belt and A-type syenites also occur in this region (Group 3). Generally, these bodies are emplaced to the north of the Group 1 belt, and considerably later (Permian vs Carboniferous). At other mineral deposits in the region, similar intrusions were emplaced post-mineralisation and are apparently barren. The Hanbogd pluton to the east of Oyu Tolgoi is a multi-stage granitoid complex, consisting of two phases of alkaline granite and multiple dyke swarms with concentric and radial morphologies, composed of various alkaline lithologies. It is peraluminous, has an A-type signature, and was formed in a post-collisional setting (Gerel et al., 2005). The emplacement age of the Hanbogd pluton is very similar to that of the North Mandakh granite (287+2Ma and 292.34 +/- 0.50 Ma respectively; Fig. 4.20).

It is conceivable that porphyry mineralisation occurrences will be found in association with Group 3 bodies, although none have been reported as yet from Mongolia. Such deposits are likely to be of the classic (stock related) type defined by McMillan and Pantaleyev (1988; associated with post-orogenic stocks intruding unrelated host rocks). The substantial outcrop area of the Group 3 intrusions (specifically the North Mandakh granite) and the Hanbogd pluton, suggests that the upper levels of these plutons have been removed by erosion, and so mineralised volumes may have been lost.

To the south of the belt, mineralisation (and therefore emplacement) at Oyu Tolgoi and Tsgaan Suvarga took place earlier than the emplacement ages for Group 1. The ages available in the literature for these deposits are largely based on K/Ar and Ar/Ar techniques, and so must be treated with caution, although the Re/Os date from Tsagaan Suvarga should be more reliable, and confers relatively well with the Ar/Ar age from the same deposit (Rundle, 1981; Watanabe and Stein, 2000; Stein et al., 2000; Selby et al., 2002). The locus of emplacement of mineralised bodies appears, in the first instance, to have moved north with time. However, this does not take into account tectonic models that suggest parts of the arc have moved dextrally along the arc front (Şengör and Natal'in, 1996; Badarch et al., 2002). If these models are correct, crust that hosts Tsagaan Suvarga and Oyu Tolgoi originally formed as a contiguous section of arc, along-strike to the east of the Oyut Ulaan-Shuteen belt, and moved laterally to the west via dextral strike-slip faulting. Whilst this movement is poorly constrained in time and space, it is generally regarded as Devonian-

Carboniferous by Badarch et al. (2002) and early Carboniferous by Şengör and Natal'in (1996). If the dextral translation occurred at an earlier time (prior to the 411+3 Ma Oyu Tolgoi age; Perello et al., 2001), the arc segments could have been in their present-day position prior to emplacement of any of the region's mineralised intrusions, and a northward-movement of the magmatic arc with time would be a viable interpretation. However, it seems unlikely that the arc segments assumed their current juxtaposition so early. Evidence for dextral transtension only occurs in the andesite dykes of the Oyut Ulaan Intrusive Complex, and this event now has a well-constrained 327.86 +/- 0.44 date. Whilst this date constitutes neither a minimum or maximum age for dextral motion, it does suggest that a dextral transtensional stress field was in place during the Mid-Carboniferous, and that the only observable evidence for this (in the Saykhandulaan inlier) post-dates the emplacement of the Group 1 monzonitic-quartz-monzonitic suite. This further supports the notion of progressively southwards-directed accretion in southeast Mongolia by removing its counter argument (i.e. the apparent northward younging of volcanic and intrusive lithologies).

Discussion and conclusions 5

5.1 The Saykhandulaan inlier

The Saykhandulaan inlier contains evidence for a wide range of depositional environments, magmatic episodes and deformation events. North-south transects across the inlier reveal that rock types can be logically subdivided into five lithotectonic domains. The analysis of lithologies and structures in these domains elucidates the large-scale evolution of the crust in the upper Palaeozoic. However, the domains are fault-bound and the exact relationships between domains are poorly constrained.

On a large scale, across the whole inlier from north to south, the original depositional environment changes from siliciclastic deep turbiditic-basin sedimentation to a terrestrial volcanic and fluvial environment, whereas the sedimentary provenance changes from a cratonal source in the north, to a dissected arc, with a further change to an un-dissected arc in the youngest Molasse Succession. Deformation and metamorphism generally are more intense in the north than the south, but reach a peak at the Saykhandulaan Valley Lineament Zone.

The four-dimensional development of the Saykhandulaan inlier began with sediment, eroded from a cratonal terrane probably to the north, being deposited in a basin, that would later become the Northern Slate Belt. In the south, volcanic arc lithologies were also being eroded. The protolith to the High Strain Belt, and the coarse conglomerates in the Oyut Ulaan Volcanic Group were both derived from uplifted arc segments. The protolith to the High Strain Belt likely formed distally from the eroding arc, as the HSB is predominantly composed of meta-psammites and pelites with turbiditic grading. The HSB is interpreted to represent deep levels of the southern, arc-dominated margin of the back arc basin, and to have been exhumed by thrusting along the Saykhandulaan Valley Lineament Zone. This also explains the sharp break in lithologies at the SVLZ, and the change in provenance.

Two phases of Palaeozoic ductile deformation are recorded in the inlier. The first resulted in ENE-WNW orientated largely upright folds in the Northern Slate Belt and High Strain Belts. The second deformation resulted in E-W orientated folds in the Oyut Ulaan Volcanic Group, and the Molasse Succession, and is interpreted to have tightened and modified earlier structures, and to have folded pre-existing cleavage in the Northern Slate Belt. The first deformation is interpreted to have occurred during back-arc basin inversion as a response to changing subduction-zone stresses to the south of the area, whereas the

second is interpreted to be related to final closure of the Palaeo-Asian Ocean along the Solonker Suture to the south.

The inlier appears to have been tilted, with deeper stratigraphic levels generally exposed in the east (Fig. 5.1); The most metamorphosed parts of the Northern Slate Belt and the High Strain Belt occur in the east; the deepest parts of the Oyut Ulaan Volcanic Group also crops-out in the east, where it is intruded by the Oyut Ulaan intrusive complex; the unconformable contact at the base of the Molasse sucession with the High Strain Belt, defines the eastern margin of the Molasse succession out-crop area. This tilting may be due to crustal extension associated with Jurassic-Cretaceous rifting (Graham et al., 2001), on normal faults running N-S or NW-SE, parallel to the western edge of the inlier, and the eastern edge of the Northern Slate Belt (Fig. 5.1). The westward plunge of folds in the inlier exposes stratigraphic variation within individual domains, and so comparison of eastern and western areas gives a more detailed view of the changing palaeo-environment within each domain, e.g. the evolving volcanic environment that formed the OUVG.

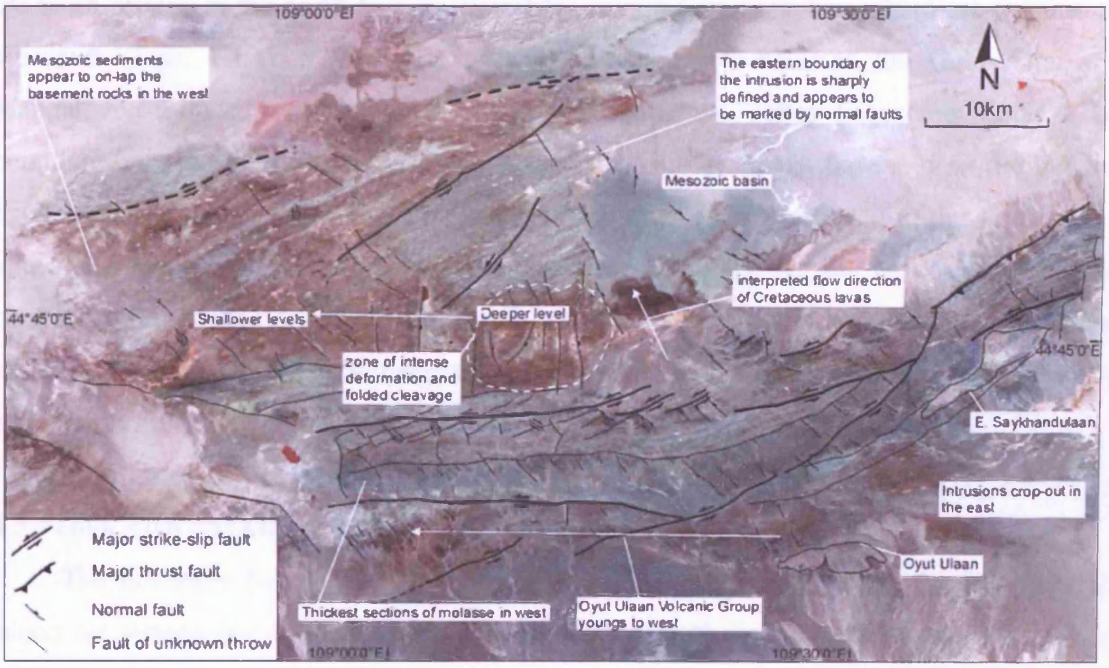

Fig. 5.1 Landsat satellite image showing the Saykhandulaan inlier, annotated with features that show westward down-tilt of whole inlier.

5.2 The evolving volcano-sedimentary environment

The Oyut Ulaan Volcanic Group records a predominantly andesitic, subduction-related volcanic arc environment, active between 330-323 Ma. The OUVG appears to represent a co-magmatic eruptive sequence to the Oyut Ulaan intrusive complex. Clear lithological,

geochemical, and geochronological associations suggest that the late-stage andesite dykes of the Oyut Ulaan intrusive complex fed parts of the OUVG (Fig. 3.4 e, 4.6 a and 4.12). Increasing effusion rates, changing magma chemistry and the preservation of a thick volcanic sequence suggest increased arc extension during OUVG volcanism. Rhyolitic units of the uppermost formation have an A-type signature, but the timing of these units significantly predates the Permian ages of the post-orogenic granites and A-type syenites of the Mandakh inlier and elsewhere (Figs. 3.19 and 4.20). The changing geochemical signature of the OUVG may be the earliest evidence of a transition from volcanic-arc to A-type post-collision magmatism in south east Mongolia.

5.3 Terrane models

The terrane model of Badarch et al. (2002) is the most detailed available. The areas studied here span three of the terranes described in this model, the Gobi Altai back-arc/fore-arc basin terrane in the north and the Mandalovoo and Gurvansayhan island arc terranes to the south (Figs. 1.1 & 5.2). In Chapter 2, the boundary between the Gobi Altai and Mandalovoo terranes was identified in the Saykhandulaan Valley Lineament Zone. The boundary between the Mandalovoo terrane and the Gurvansayhan terrane does not cut the Saykhandulaan inlier. The terrane map of Badarch et al. (2002) shows it to the south of the inlier, and cutting the Mandakh inlier to the west (Fig. 5.2). In the Mandakh inlier, the boundary divides the northern areas, which are dominated by granitoid out-crops, from the southern areas, which are predominantly country rock, with some small intrusions (Shuteen and Bronze Fox).

5.3.1 Gobi Altai and Mandalovoo terrane boundary.

The boundary between the Gobi-Altai back-arc basin terrane, and the Mandalovoo island arc terrane is important, because it marks the northern limit of Altaid volcanic-arc lithologies in southeast Mongolia (Figs. 1.1 and 5.2). The structural and tectonic significance of this boundary, as it is expressed in the SVLZ, has not previously been documented. The SVLZ is interpreted to have first formed when a compressive event, possibly related to the accretion of an arc terrane at the subduction zone to the south during one stage of the closure of the Palaeoasian Ocean (Fig. 2.1), caused the overthrusting of lithologies of the HSB over those of the NSB (Fig. 2.21). The reason for the exact location of the boundary is unclear, and it is difficult to estimate the volume of 'lost strata' that might

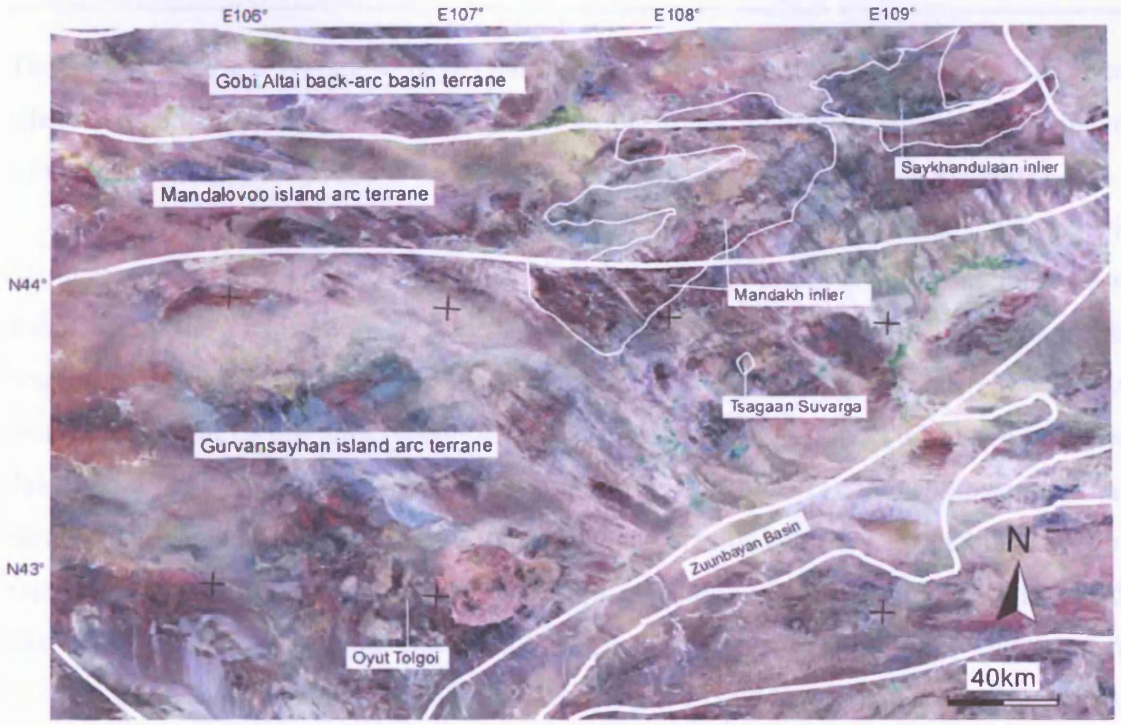

Fig. 5.2 Landsat Satellite image showing the southeast Gobi region with the inliers studied here marked, and the terrane model of Badarch et al. 2002 superimposed as (thick white lines).

have existed between the NSB and the HSB. The existence of volcanic 'slivers' within the SVLZ suggests that a sequence of volcanics became entrained in the thrust-zone. The status of the SVLZ as a major crustal fault zone is further confirmed by the focussing of subsequent deformation and dyke emplacement within the zone. Oblique shear zones crop out at the surface with silicified, striated slip surfaces, suggesting that oblique-slip movements (with a strong strike slip component; Figs. 2.19 and 2.20) took place along the zone, some time after initial north-directed thrusting. Basalt dykes run parallel within the zone, and the lobate outcrop expression of the Cretaceous lavas that unconformably overlie basement rocks suggest that they flowed to the north, away from the SVLZ (Fig. 5.1). This implies that the SVLZ provided a crustal conduit for these lavas. Finally, at the southern margin of the SVLZ, in the far east corner of the inlier, greenschist-grade conglomerates of the HSB are thrust over unconsolidated sediments, suggesting Cenozoic reactivation (Fig. 2.19).

5.3.2 Mandalovoo and Gurvansayhan terrane boundary

The tectonic relationship between the Mandalovoo and Gurvansayhan terranes should be of particular interest to mineral explorationists, because the Gurvansayhan terrane contains both the Oyu Tolgoi Au-Cu porphyry and the Tsagaan Suvarga Cu-Mo porphyry.

The two terranes are thought to have been previously along-strike components of the same island arc, and then during Devonian-Carboniferous times, the Gurvansayhan terrane moved southwest to its current location, via dextral shear along the arc (Badarch et al., 2002).

This study calls into question the positioning of the terrane boundary between the Mandalovoo and Gurvansayhan terranes. Members of the Group 1 intrusions crop-out on either side of the lineament (as it is currenly positioned; Figs. 5.2 and 5.3). Furthermore, the boundary divides the Bronze Fox intrusion (south of the line) from the Narin Hudag monzonite (north of the line), which share the closest age association of all the intrusions dated here. There are three possible explanations for this; (1) the compositional and chronological association between the intrusions is coincidental; they formed distally from each other and were brought into their current juxtaposition via the dextral movement of the Gurvansayhan terrane; (2) by the time that the Group 1 intrusions were emplaced the terranes were at, or near, their current position; (3) the boundary between the Mandalovoo and Gurvansayhan terranes is too far north, as it is previously defined (Badarch et al. 2002; Fig. 5.2 and 5.4). The third option appears to be the most likely here; the boundary between the Gurvansayhan and Mandalovoo terranes, along which an arc segment is supposed to have migrated (Fig. 2.1), is marked, in the Mandakh inlier, by the southerly margin of the large area of granite outcrop, a boundary that appears to be largely intrusive in nature (Fig. 5.2). By comparison, the Gobi Altai-Mandalovoo boundary, as exposed in the Saykkhandulaan inlier (Figs. 2.6 and 5.1), is a multiply reactivated belt of deformation, alteration and metamorphism (Figs. 2.19 and 2.20), and yet, in previously-published terrane models, no major Palaeozoic strike-slip motion has been suggested for this boundary.

Whilst explanation (1) appears far-fetched, and is contradicted by the available evidence, explanations (2) and (3) are not denied by the available evidence and neither need they be mutually exclusive. It is plausible that the correct position of the boundary is to the south beneath basin fill *and* the dextral movement of the Gurvansayhan terrane took place along this boundary. This scenario seems to be further supported by the post-mineralisation monzonite dykes at Tsagaan Suvarga, which are of a reasonably similar age and composition to be considered part of the Group 1 Carboniferous monzonite association that occurs to the north.

In Badarch et al. (2002), the text states that the Mandalovoo terrane contains only Devonian plutons, however, stratigraphic columns for the whole terrane show a

Fig. 5.3 (next page) Three satellite image maps to show the time periods of emplacement of different groups of intrusions a) the Porphyry deposits of the Gurvansayhan terrane, b) the Group 1 monzonite association of this study, c) the post-orogenic granitoids.

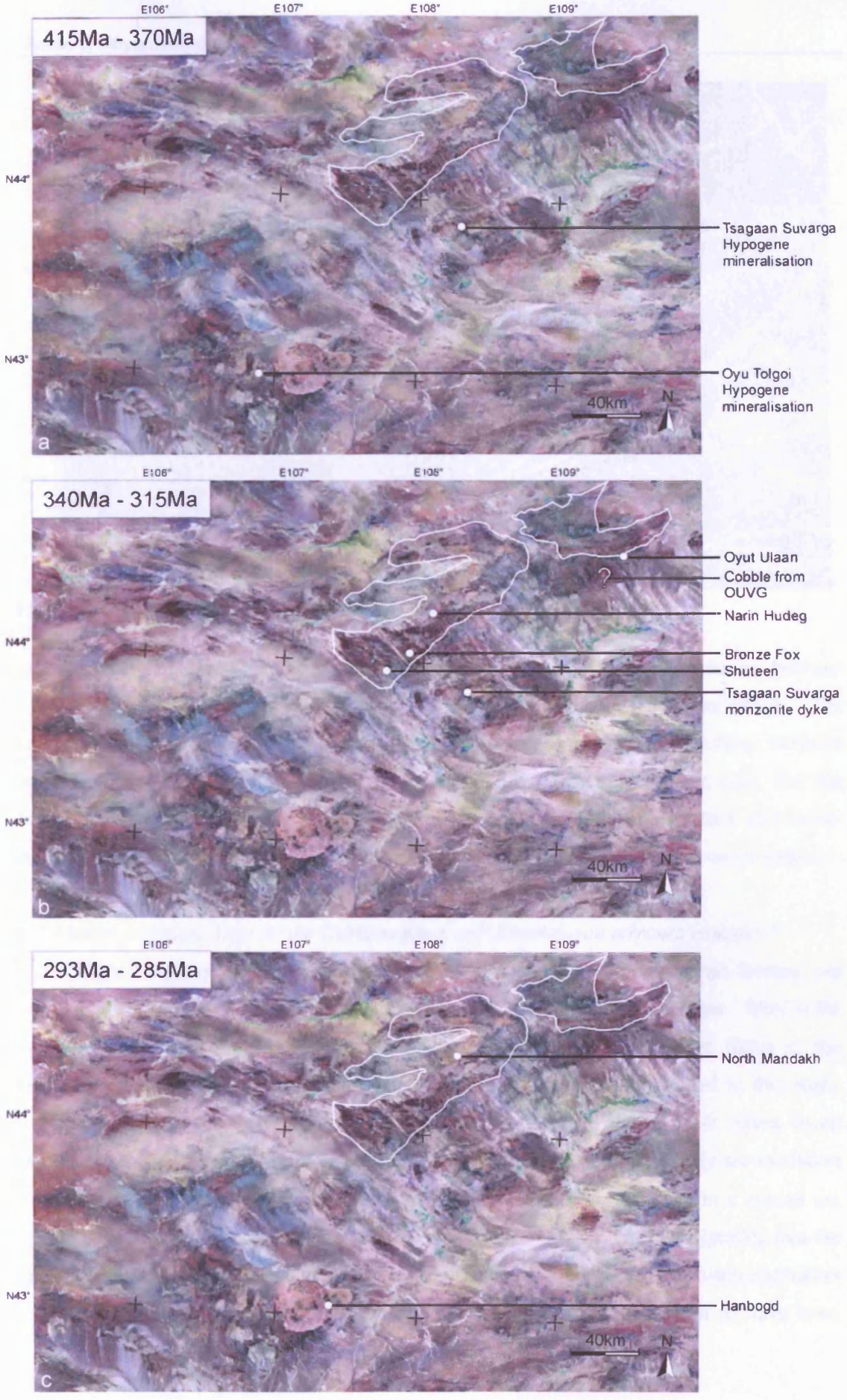
E106°
E107°
E108°
E109°
415Ma - 370Ma
N44°
N43°
Tsagaan Suvarga
Hypogene
mineralisation
Oyu Tolgoi
Hypogene
mineralisation
40km
N
a
340Ma - 315Ma
Oyut Ulaan
?
Cobble from
OUVG
Narin Hudeg
Bronze Fox
Shuteen
Tsagaan Suvarga
monzonite dyke
b
293Ma - 285Ma
North Mandakh
Hanbogd
c

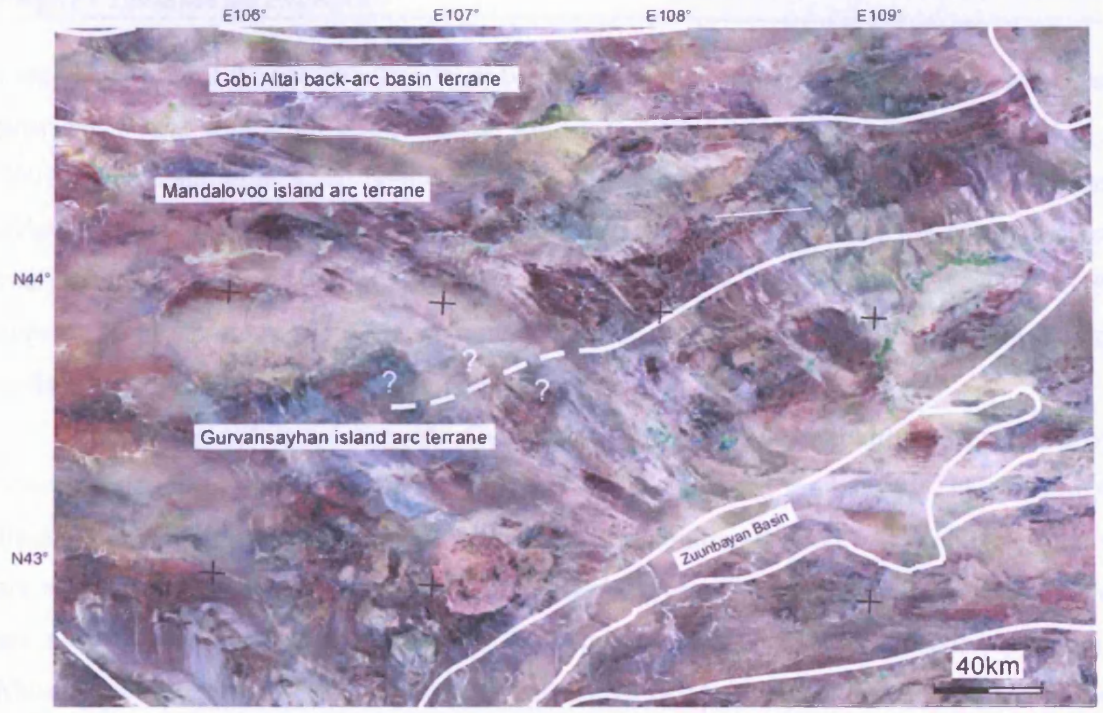

Fig. 5.4 Proposed new path of the Mandalovoo-Gurvansayhan boundary.

granodioritic-tonalitic magmatic phase from 400-355 Ma and two granitic phases, between 315-300 Ma and 270-290 Ma with no absolute age data to support these assertions. The Group 1 monzonitic suite of this study does not fit in with any of these postulated intrusive episodes. It is suggested, in light of the new absolute age data presented here, that the Mandalovoo terrane definition is wrong, and that a clear distinguishing feature, and along-strike characteristic of the terrane is the existance of mid-Carboniferous monzonitic plutons.

5.3.3 Mineralisation: How do the Gurvansayhan and Mandalovoo terranes compare?

Major porphyry mineral deposits have been found in the Gurvansayhan terrane, yet nothing on a similar scale has so far been discovered in the Mandalovoo terrane. What is the key difference between the two areas? Those intrusions that have been dated in the Gurvansayhan terrane have Devonian ages, whereas all the intrusions dated in this study were emplaced during the mid-upper Carboniferous. Oyu Tolgoi is the oldest dated intrusive body in the region, and is interpreted as having formed during early arc-evolution in the upper-Silurian to Devonian, whereas Tsagaan Suvarga formed later in a mature arc setting in the upper Devonian (Lamb and Cox, 1998; Perello et al., 2001), suggesting that the age of formation relative to arc maturity is not a controlling factor. Syn-mineralisation telescoping enhanced the mineralisation at Oyu Tolgoi, and is interpreted to have been

caused by uplift at the Silurian-Devonian boundary, whilst intra- and late-mineral intrusions provided a heat source for hydrothermal fluid circulation during this time (Perello et al., 2001). The main mineralised features at Oyut Ulaan are associated with late-stage andesite dykes and tourmaline breccia pipes, and evidence for uplift occurs in the plutonic-clast bearing voluminous conglomerates within the co-magmatic volcanic section. This uplift appears to be approximately contemporaneous with the emplacement of Oyut Ulaan into underlying parts of the volcanic stratigraphy.

An essential difference between Oyut Tolgoi and Ouyt Ulaan could be the number of concurrent and subsequent magmatic episodes, which provided the heat for hydrothermal fluid circulation during uplift-related telescoping of the mineralisation. At Oyu Tolgoi there are multiple phases of inter- and late-mineral dyke intrusions, whereas, at Oyut Ulaan there are only three phases of dyke activity, and the first two of these are relatively minor. Mineralised features at Oyut Ulaan are spatially associated with the latest stage of dyke activity and tourmaline breccia pipes, and there are no younger local intrusions.

5.4 Granite magmatism

Jahn et al. (2001) give an overview of granitoids within the Central Asian Orogenic Belt. They divide the CAOB into two gigantic granitic belts, (1) a northern belt from N Mongolia to Transbaikalia, and (2) a southern belt from Kazakhstan, Xinjiang and Southern Mongolia to NE China. The intrusions in southeast Mongolia are situated in the southern belt. Jahn et al. (2001) note a younging-to-the-south trend in the granites of the CAOB. However, one of the interesting features of southeast Mongolia is the juxtaposition of older intrusions to the south (Oyu Tolgoi and Tsagaan Suvarga) and younger intrusions to the north (Group 1). This has been explained by along strike re-arrangement of the arc, and it shows that greater detail and complexity occurs within the southeast Gobi region, than can be described by generalised CAOB trends.

Granites with an A-type post-collision signatures, and very similar ages to the North Mandakh granite and Hanbogd Plutons (Fig. 5.3), have been documented from as far-afield as west Junngar, Xinjiang Province, China and Transbaikalia, Russia. (Fig. 1.2; Zhou et al., 2006; Litvinovsky et al., 2002). This illustrates the change in tectonic environment from a subduction related along-strike intrusive belt, active in the mid-Carboniferous, to a whole-CAOB post-collisional A-type event in the early Permian.

The geochemical signature and age of the granites studied here correspond closely with that of granites which crop out in northeast China, (Fig. 5.5; Zhu et al., 2001; Wu et al., 2002; Wu et al., 2003) and it is likely that they formed during similar regional tectonic processes. Indeed, the arc terranes in southern Mongolia may be traceable into NE China, with a greater level of accuracy than has thus far been accomplished, by the large-scale comparison of granite chemistry, emplacement timing and volcanic host rocks across the region. This has clear implications for mineral exploration in the region, as the along-strike continuation of the Carboniferous volcanic-arc is likely to be prospective for mineralisation.

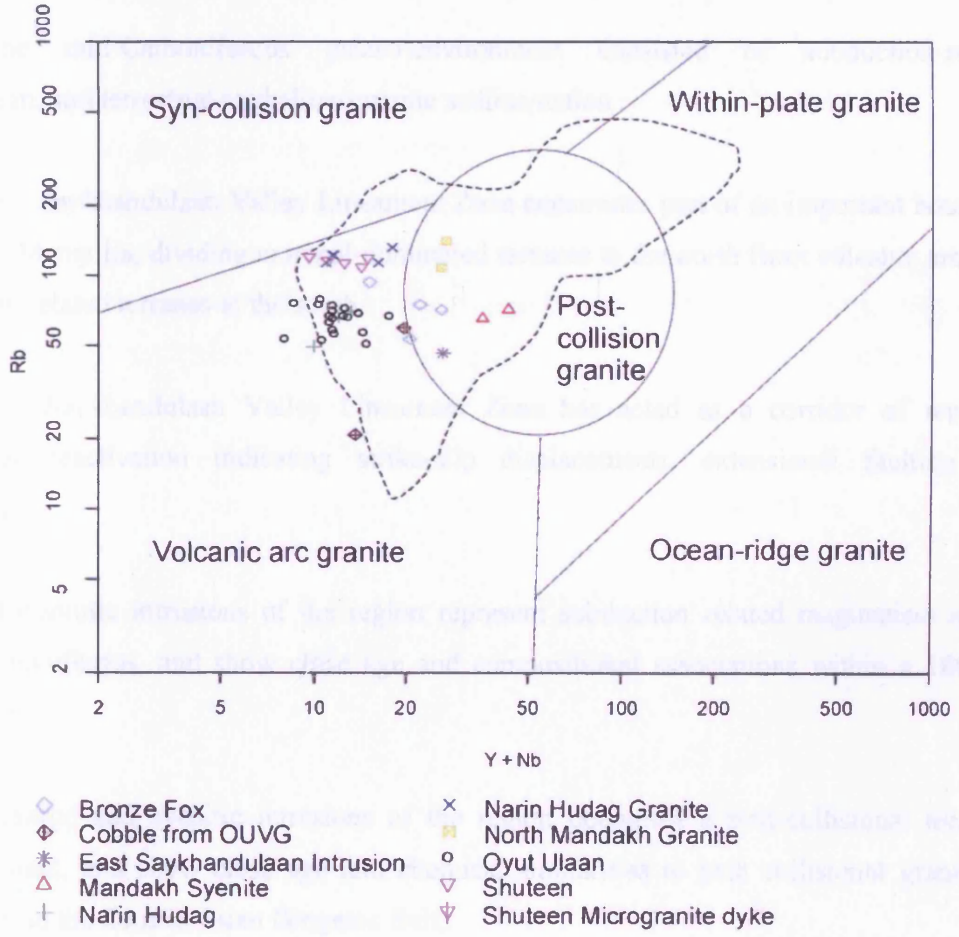

Fig. 5.5 Y+Nb vs Rb diagram after Pearce (1996), dashed line shows field of results from granites of NE China (Wu et al., 2000).

5.5 Conclusions

The Saykhandulaan inlier is a key area of Palaeozoic basement outcrop, within a region in which the basement is mostly obscured by Mesozoic basins. It records the geological evolution of part of the Palaeo-Asian Ocean's northern margin.

The Devonian - Early Carboniferous palaeo-environment consisted of basin sedimentation in a back-arc environment supplied by a cratonal source in the north, and an eroding volcanic arc in the south.

The mid-Carboniferous palaeo-environment consisted of subduction-related volcanism, and terrestrial to shallow-marine sedimentation.

The Saykhandulaan Valley Lineament Zone constitutes part of an important boundary in south Mongolia, dividing cratonal-dominated terranes to the north from volcanic arcs and accretion related terranes to the south.

The Saykhandulaan Valley Lineament Zone has acted as a corridor of repeated structural reactivation indicating strike-slip displacements, extensional faulting and thrusting.

Monzonitic intrusions of the region represent subduction related magmatism in the mid-Carboniferous, and show close age and compositional associations within a 180 km long belt.

Granitic and syenitic intrusions of the region document a post-collisional tectonic environment, and show close age and chemical similarities to post collisional granitoids from across the Central Asian Orogenic Belt.

5.6 Recommendations for future work

This project represents an island of detailed work in an unstudied frontier region. Only through further detailed work in adjacent areas will the terrane boundaries, regional structure, magmatic events and mineralisation setting of the region be fully understood. Specifically, a similar geological survey of the neighbouring Mandakh inlier would provide many points of comparison with this study, and build on information presented here.

Within the Saykhandulaan inlier, pressure-temperature work and mica dating would help establish and date the metamorphic and deformation histories of the Nothern Slate Belt and the High Strain Belt. Isotope age data from the volcanic lithologies in the SVLZ is also desirable, to compare its age with the surrounding lithotectonic domains and the OUVG to the south. A full and detailed sedimentological survey and mapping of the molasse succession would more effectively document the Permian palaeo-environment.

Post-Palaeozoic lithologies and events have been touched on here, but there is scope for more work, especially in the basin to the northeast, which includes several basalt lava sequences and unconsolidated sediments. Badland topography and drainage channels expose the stratigraphy of the unconsolidated sediments, and detailed sedimentological analysis would elucidate not only the depositional environment, but also periods of tectonic activity.

Appendix A

Part 1 XRF geochemical results
Part 2 locations of samples

Sample number	BFD002F	BFD024B	BFD024C	BFD024D	51.1A	51.1A	51.2B	51.4A
Bead	LF25998	LF25993	LF25995	LF26000	LF25623	LF25624	LF25640	LF25633
field area	Bronze Fox	Bronze Fox	Bronze Fox	Bronze Fox	Mandakh	Mandakh	Mandakh	Mandakh
formation	n/a	n/a	n/a	n/a	n/a	n/a	n/a	n/a
SiO2	61.97	56.84	59.43	66.67	76.74	77.57	78.75	66.49
TiO2	0.52	0.77	0.64	0.40	0.10	0.11	0.11	0.62
Al2O3	15.03	16.72	15.48	14.55	12.54	12.71	12.25	16.10
Fe2O3	5.37	7.50	5.78	3.74	0.60	0.57	0.43	2.58
MnO	0.08	0.12	0.09	0.03	0.04	0.04	0.00	0.10
MgO	2.51	3.43	2.76	1.66	0.12	0.10	0.08	0.25
CaO	3.54	5.38	4.49	2.24	0.42	0.41	0.40	0.62
Na2O	4.66	4.55	5.19	4.39	4.27	4.23	4.09	6.19
K2O	3.61	2.26	3.33	4.68	4.69	4.65	4.53	7.53
P2O5	0.18	0.22	0.24	0.13	0.02	0.02	0.03	0.09
SO3	0.29	0.24	0.89	0.96	0.01	0.02	0.03	0.05
LOI	1.97	1.97	2.47	1.25	0.33	0.47	0.25	0.23
As	19.70	10.28	14.75	2.77	8.22	6.68	116.04	3.50
Ba	885.98	533.89	553.30	654.82	66.66	87.09	67.32	168.71
Ce	36.45	35.41	42.37	29.65	40.89	35.76	15.26	54.76
Co	17.08	25.20	20.54	12.90	0.07	n/a	n/a	3.12
Cr	65.07	176.25	140.16	123.02	4.89	4.31	4.74	n/a
Cs	2.85	0.42	n/a	3.39	0.36	3.96	2.81	4.99
Cu	116.47	161.87	1930.64	4694.96	n/a	n/a	n/a	n/a
Ga	18.22	21.69	19.79	19.20	15.17	15.75	13.85	21.98
La	15.31	11.23	17.79	15.27	18.99	19.98	9.56	19.61
Mo	1.63	4.75	1.86	1.39	1.91	0.85	0.74	1.39
Nb	3.70	3.77	8.00	3.38	14.36	14.82	15.69	9.21
Nd	18.07	12.84	23.07	13.03	8.43	9.16	4.46	29.09
Ni	16.52	15.98	17.34	8.52	4.10	3.63	5.74	3.94
Pb	5.35	6.14	3.41	4.55	20.81	20.22	16.58	6.94
Rb	75.07	53.17	71.30	93.55	144.12	141.87	138.91	71.58
Sc	17.20	20.76	17.45	10.08	n/a	9.94	3.14	5.77
Sr	884.88	1048.24	479.77	646.02	26.03	23.65	29.84	21.61
Th	14.33	9.34	10.06	14.73	25.88	26.25	24.41	8.25
U	3.34	0.66	0.49	4.10	n/a	1.40	n/a	2.02
V	145.10	225.60	169.79	110.52	6.42	1.62	4.09	5.83
Y	18.50	16.78	17.93	11.86	7.32	8.24	4.20	33.77
Zn	35.38	76.57	51.71	33.62	14.76	15.69	6.80	40.37
Zr	150.17	100.90	137.02	159.70	80.52	80.64	65.36	489.34
Total	99.72	98.04	100.79	100.71	99.55	100.43	100.70	100.84

Sample number	54.20A	54.3A	54.6A	55.12A	55.13A	55.14A	55.17A	55.18A
Bead	LF25094	LF25057	LF25063	LF25083	LF25472	LF25086	LF25068	LF25055
field area	OUVG	OUVG	OUVG	OUVG	OUVG	OUVG	OUVG	OUVG
	Gurvan Morin	Gurvan Morin	Gurvan Morin	Gurvan Morin	Gurvan Morin	Gurvan Morin	Gurvan Morin	Gurvan Morin
formation	Hondiy	Hondiy	Hondiy	Hondiy	Hondiy	Hondiy	Hondiy	Hondiy
SiO2	56.77	58.07	61.15	55.18	54.61	56.73	55.49	53.13
TiO2	0.75	0.65	0.66	0.92	0.73	0.82	0.56	0.68
Al2O3	18.45	16.89	16.10	17.68	17.75	16.74	17.13	17.44
Fe2O3	5.90	5.99	5.03	7.44	8.65	7.09	7.13	9.13
MnO	0.09	0.09	0.07	0.12	0.18	0.18	0.12	0.13
MgO	1.99	2.93	2.53	2.80	2.17	2.95	3.10	2.96
CaO	3.56	4.82	2.12	6.21	2.81	3.33	6.82	4.44
Na2O	7.44	4.69	7.53	4.92	9.53	8.10	4.76	5.69
K2O	2.36	3.02	1.10	2.99	0.18	0.84	2.02	2.63
P2O5	0.33	0.29	0.27	0.33	0.62	0.31	0.32	0.21
SO3	0.04	0.08	0.07	0.02	0.04	0.03	0.04	0.02
LOI	2.80	1.50	3.24	1.87	2.59	3.47	1.53	2.58
As	5.57	6.15	7.41	6.05	10.61	8.34	10.13	27.22
Ba	677.95	1027.70	524.03	950.74	63.18	323.62	719.16	713.44
Ce	34.81	30.35	30.02	46.46	70.47	47.73	47.24	79.85
Co	18.60	18.28	14.60	20.65	26.75	22.86	22.65	33.58
Cr	n/a	70.00	55.94	18.32	n/a	87.28	24.54	51.06
Cs	2.49	n/a	n/a	3.54	6.21	n/a	n/a	2.54
Cu	94.30	118.21	43.61	191.79	169.19	111.20	128.71	36.22
Ga	17.83	21.69	17.84	21.31	17.67	16.43	21.16	24.35
La	14.04	13.49	14.06	16.82	29.04	18.56	21.01	20.63
Mo	1.30	2.13	1.28	2.12	1.88	1.69	2.23	1.05
Nb	2.02	3.45	3.56	3.08	12.55	2.72	4.77	4.00
Nd	14.46	17.24	15.57	21.73	33.34	18.15	25.72	25.19
Ni	3.98	10.54	5.52	1.53	n/a	5.87	4.81	10.73
Pb	11.35	6.11	9.37	8.74	7.23	8.95	10.48	12.96
Rb	39.26	45.44	14.80	50.76	1.82	14.23	42.37	55.01
Sc	21.64	16.10	15.92	15.02	12.57	14.74	17.19	17.46
Sr	1541.07	1187.51	781.80	1228.83	277.14	858.04	1178.72	997.39
Th	2.99	3.04	5.71	11.30	7.29	6.10	6.87	8.15
U	0.12	n/a	1.20	2.87	n/a	2.43	2.65	3.30
V	208.72	180.05	168.92	221.91	159.77	180.61	194.71	249.09
Y	9.64	11.42	13.56	15.21	20.55	14.39	19.23	17.39
Zn	53.79	60.59	58.55	68.16	98.57	78.15	73.38	92.83
Zr	102.47	122.54	143.45	143.27	128.17	153.12	181.11	162.97
Total	100.47	99.00	99.87	100.46	99.84	100.59	99.01	99.04

Sample number	51.4B	51.5A	51.6A	51.7A	11/08_2	17/08_6	78.3A	JBSP001	JBSP003
Bead	LF25642	LF25684	LF25632	LF25641	LF22797	LF22796	LF25986	LF25647	LF25649
field area	Mandakh	Mandakh	Mandakh	Mandakh	Mesozoic basalts	Mesozoic basalts	Molasse Sucession Dyke	Narin Hudag	Narin Hudag
formation	n/a	n/a	n/a	n/a	n/a	n/a	n/a	n/a	n/a
SiO2	78.71	64.78	77.69	76.35	55.25	51.24	57.83	72.68	73.72
TiO2	0.10	0.53	0.10	0.09	2.22	2.74	1.43	0.23	0.19
Al2O3	12.38	15.65	12.27	12.05	14.28	14.09	16.69	14.09	14.50
Fe2O3	0.69	2.71	0.57	0.71	9.16	10.31	6.69	1.86	1.63
MnO	0.05	0.11	0.05	0.07	0.14	0.16	0.10	0.02	0.04
MgO	0.07	0.28	0.06	0.08	3.00	3.16	2.32	0.30	0.42
CaO	0.32	0.75	0.38	0.26	5.78	7.80	1.90	0.51	1.36
Na2O	4.58	6.23	4.84	4.32	3.47	3.98	5.96	5.15	4.21
K2O	4.27	7.94	4.53	4.64	2.78	2.34	3.75	4.73	4.73
P2O5	0.01	0.18	0.09	0.01	1.17	1.67	0.64	0.07	0.13
SO3	0.02	0.03	0.05	0.03	0.03	0.08	0.04	0.03	0.02
LOI	0.17	0.31	0.16	0.20	2.73	2.38	2.60	0.68	0.52
As	0.44	1.62	0.88	376.71	7.22	n/a	0.02	0.80	1.68
Ba	8.51	235.35	14.30	13.92	782.57	1210.50	677.46	855.89	919.08
Ce	41.48	75.74	51.31	50.16	90.02	204.07	65.86	28.32	42.55
Co	0.51	4.08	n/a	n/a	8.41	28.52	23.53	3.19	1.92
Cr	8.47	69.33	10.27	14.95	8.07	0.47	123.96	0.29	n/a
Cs	2.21	4.37	n/a	2.42	4.13	0.75	2.37	0.57	5.37
Cu	n/a	n/a	n/a	8.83	5.03	30.81	23.13	9.01	4.46
Ga	13.89	19.92	16.29	16.75	22.18	23.61	19.06	15.24	17.19
La	24.48	34.11	15.43	17.88	37.72	96.16	26.83	15.65	22.46
Mo	1.18	3.10	2.04	1.36	3.69	2.40	1.06	1.64	0.72
Nb	9.19	7.86	9.48	11.79	14.17	36.01	12.00	6.62	4.30
Nd	12.44	37.14	21.74	17.43	41.16	95.20	34.58	13.55	16.85
Ni	3.72	2.76	3.34	4.62	n/a	5.51	8.09	3.62	3.20
Pb	14.87	11.19	15.29	19.16	12.04	26.97	8.17	19.94	19.81
Rb	108.17	65.77	107.49	139.76	82.52	99.47	53.12	113.41	122.23
Sc	3.86	10.96	8.58	5.22	5.13	17.12	19.75	n/a	6.94
Sr	3.62	30.50	5.37	6.13	80.87	708.58	267.49	211.69	281.91
Th	13.99	12.62	15.76	19.44	15.58	14.23	5.41	17.39	18.61
U	2.51	1.57	n/a	1.13	3.52	1.19	1.60	5.02	3.32
V	4.27	6.16	3.15	8.99	13.67	152.29	167.65	24.07	23.90
Y	14.51	27.41	16.49	15.16	68.04	41.94	30.67	4.38	7.34
Zn	17.53	37.69	21.94	24.40	61.90	143.93	64.64	12.11	25.71
Zr	80.11	498.98	80.98	85.45	520.44	632.78	240.00	132.47	158.01
Total	101.19	99.48	100.79	98.61	100.01	99.96	99.96	100.35	100.95

Sample number	55.18B	55.19A	55.19A	55.1A	55.1B	55.1B	55.1B	55.1C	55.20A
Bead	LF25464	LF25555	LF25556	LF25041	LF25105	LF25108	LF25109	LF25104	LF25091
field area	OUVG Gurvan Morin	OUVG Gurvan Morin	OUVG Gurvan Morin	OUVG Gurvan Morin	OUVG Gurvan Morin	OUVG Gurvan Morin	OUVG Gurvan Morin	OUVG Gurvan Morin	OUVG Gurvan Morin
formation	Hondiy	Hondiy	Hondiy	Hondiy	Hondiy	Hondiy	Hondiy	Hondiy	Hondiy
SiO2	54.07	51.81	56.29	63.52	53.48	53.18	53.66	52.85	57.38
TiO2	0.92	0.69	0.57	0.59	0.89	0.76	0.89	0.77	0.96
Al2O3	18.38	20.38	17.81	16.72	17.15	17.18	17.19	17.29	15.87
Fe2O3	7.75	8.44	8.20	4.09	8.08	8.03	8.08	8.05	6.05
MnO	0.13	0.23	0.11	0.03	0.15	0.15	0.15	0.14	0.09
MgO	3.20	2.39	2.03	1.58	5.98	5.79	5.85	6.12	4.01
CaO	2.77	3.91	2.48	1.42	2.82	2.72	2.78	4.60	4.17
Na2O	6.07	8.05	6.75	5.45	6.39	6.47	6.40	4.36	5.44
K2O	4.29	0.78	3.61	3.52	0.75	0.72	0.75	1.16	2.27
P2O5	0.37	0.41	0.27	0.16	0.22	0.22	0.22	0.22	0.33
SO3	0.03	0.06	0.03	0.24	0.05	0.04	0.05	0.22	0.05
LOI	2.01	3.02	1.81	2.25	4.38	4.38	4.36	3.38	2.25
As	16.01	21.88	6.31	38.47	53.64	55.13	51.54	11.43	24.31
Ba	1606.78	708.81	258.23	1798.76	365.31	342.93	348.51	573.91	989.31
Ce	49.89	58.15	36.43	18.50	32.02	41.93	40.37	41.80	34.18
Co	25.30	25.92	26.99	11.19	26.67	25.51	26.89	28.95	22.43
Cr	0.85	20.11	8.93	867.78	337.37	311.96	337.86	367.84	195.16
Cs	2.91	1.61	n/a	2.88	3.50	4.02	3.77	1.66	n/a
Cu	26.66	96.35	173.52	79.39	80.89	81.77	82.14	83.60	71.35
Ga	19.08	19.76	22.69	15.36	18.14	19.55	19.41	19.20	17.91
La	24.74	22.07	13.12	11.39	12.80	13.10	11.62	13.46	16.04
Mo	1.26	1.77	1.76	3.90	2.36	1.64	2.31	1.26	2.34
Nb	5.26	3.76	7.34	4.04	4.92	3.65	2.99	3.01	6.77
Nd	24.58	29.42	17.93	13.84	14.75	17.32	16.27	16.61	17.18
Ni	6.84	3.76	n/a	5.26	112.31	112.71	111.88	106.74	64.43
Pb	9.16	8.13	2.13	11.08	n/a	0.23	2.10	6.27	6.93
Rb	93.07	71.94	9.72	56.80	10.85	10.90	11.23	15.98	32.35
Sc	18.91	16.19	17.46	16.19	31.43	17.37	21.36	26.62	14.02
Sr	957.48	910.97	1021.51	1270.68	1062.66	1070.58	1068.13	1172.45	1277.62
Th	10.63	7.59	1.68	4.44	3.11	0.88	3.05	5.74	1.13
U	1.35	1.97	4.42	0.47	0.79	2.05	2.28	3.18	n/a
V	222.82	234.50	170.46	204.10	211.45	207.13	215.04	220.35	147.35
Y	19.66	25.58	23.83	12.94	13.06	13.41	14.55	14.88	14.24
Zn	87.16	75.76	88.61	32.29	72.53	73.78	75.74	64.65	69.33
Zr	191.31	177.83	104.78	123.33	81.61	102.85	93.07	87.78	160.99
Total	100.00	100.16	99.95	99.57	100.33	99.66	100.39	99.14	98.88

Sample number	JBSP004	JBSP004	JBSP004	JBSP005	JBSP006	JBSP007	JBSP008
Bead	LF25629	LF25630	LF25631	LF25648	LF25637	LF25652	LF25651
field area	Narin Hudag	Narin Hudag	Narin Hudag	Narin Hudag	Narin Hudag	Narin Hudag	Narin Hudag
formation	n/a	n/a	n/a	n/a	n/a	n/a	n/a
SiO2	73.02	73.96	72.45	70.89	75.80	66.15	64.24
TiO2	0.24	0.21	0.20	0.21	0.11	0.40	0.61
Al2O3	13.95	14.16	13.99	13.68	13.65	15.38	16.04
Fe2O3	1.51	1.52	1.55	1.58	0.91	3.53	4.05
MnO	0.04	0.04	0.04	0.05	0.03	0.06	0.08
MgO	0.38	0.36	0.37	0.35	0.19	2.20	1.97
CaO	0.68	0.66	0.67	1.10	0.84	3.23	2.50
Na2O	4.51	4.57	4.15	4.50	4.19	4.94	4.93
K2O	5.15	4.90	4.85	4.86	4.81	3.28	3.44
P2O5	0.08	0.07	0.08	0.10	0.06	0.21	0.23
SO3	0.05	0.04	0.01	0.02	0.02	0.02	0.02
LOI	0.64	0.63	0.63	0.44	0.36	0.85	2.19
As	0.87	0.10	n/a	2.75	3.43	n/a	0.68
Ba	903.40	873.37	875.56	859.50	608.27	620.32	932.35
Ce	29.04	23.78	33.36	34.50	60.37	15.54	22.12
Co	3.11	1.00	2.79	2.90	1.20	10.57	13.25
Cr	14.26	15.88	39.22	4.78	7.72	55.75	37.05
Cs	2.48	0.59	0.10	7.71	n/a	n/a	3.10
Cu	n/a	n/a	n/a	0.76	n/a	19.63	31.69
Ga	15.64	16.03	15.90	17.06	14.88	16.33	17.91
La	17.65	18.22	14.65	18.57	21.35	12.63	13.84
Mo	1.57	1.26	1.45	0.41	2.58	1.88	2.26
Nb	6.33	6.93	5.03	6.03	6.42	5.18	3.72
Nd	14.99	13.74	17.27	15.32	27.70	8.38	7.12
Ni	n/a	n/a	0.07	2.01	4.53	29.00	18.71
Pb	15.06	16.25	16.15	17.63	15.71	10.49	8.59
Rb	124.42	124.73	122.55	132.18	112.86	70.00	49.73
Sc	2.23	n/a	4.22	0.87	4.68	10.03	8.76
Sr	258.44	262.93	254.84	283.46	175.94	629.22	689.51
Th	16.24	17.91	15.55	18.24	23.42	5.25	7.47
U	1.00	0.63	n/a	3.04	3.05	0.34	1.07
V	23.62	24.64	21.20	19.70	11.26	77.39	93.47
Y	6.41	8.91	6.52	11.94	9.82	8.03	6.27
Zn	19.61	18.56	19.00	20.34	6.02	33.90	50.20
Zr	157.16	152.46	152.64	160.35	98.94	95.05	82.22
Total	100.24	101.12	98.36	98.78	100.61	100.25	100.30

Sample number	55.22A	55.3A	55.4A	55.6A	55.8A	55.8B	55.9A
Bead	LF25675	LF25099	LF25092	LF25468	LF25053	LF25473	LF25465
field area	OUVG Gurvan Morin	OUVG Gurvan Morin	OUVG Gurvan Morin	OUVG Gurvan Morin	OUVG Gurvan Morin	OUVG Gurvan Morin	OUVG Gurvan Morin
formation	Hondiy	Hondiy	Hondiy	Hondiy	Hondiy	Hondiy	Hondiy
SiO2	65.73	52.76	57.39	55.83	56.30	56.38	53.47
TiO2	0.35	0.83	0.74	0.71	0.66	0.79	1.07
Al2O3	16.43	16.80	17.92	17.77	17.50	17.73	19.91
Fe2O3	2.92	7.56	6.35	5.91	6.60	6.40	7.81
MnO	0.06	0.11	0.10	0.09	0.08	0.11	0.11
MgO	0.87	2.97	2.55	2.46	2.64	2.79	2.69
CaO	1.62	4.09	3.51	3.97	3.26	5.35	3.23
Na2O	5.58	7.69	6.38	6.27	7.04	5.94	7.56
K2O	4.50	0.72	2.72	2.72	1.94	2.09	1.78
P2O5	0.09	0.28	0.34	0.31	0.31	0.31	0.41
SO3	0.03	0.03	0.08	0.01	0.03	0.02	0.02
LOI	1.30	5.05	2.20	3.01	2.47	2.25	2.39
As	8.83	26.45	30.56	30.12	28.58	27.92	33.75
Ba	1861.71	325.61	740.33	659.72	790.20	602.47	774.03
Ce	25.53	39.28	41.67	40.35	38.27	36.07	62.15
Co	6.95	24.97	20.47	18.64	21.28	18.79	25.42
Cr	24.59	17.90	134.75	26.16	167.90	n/a	57.70
Cs	1.81	4.37	n/a	n/a	1.88	n/a	n/a
Cu	17.84	121.10	85.76	93.55	99.90	87.64	160.32
Ga	16.80	20.96	21.49	21.51	20.33	21.22	23.55
La	15.67	12.91	16.21	18.09	14.54	13.84	21.53
Mo	1.10	1.76	2.49	1.21	2.23	1.22	0.96
Nb	4.25	3.83	3.58	1.70	3.78	2.48	3.70
Nd	14.21	17.42	17.23	20.03	17.61	20.92	25.66
Ni	3.62	4.95	5.81	2.36	5.08	5.64	4.60
Pb	6.38	4.62	7.38	7.10	6.45	9.60	8.93
Rb	59.50	10.51	49.47	51.17	35.08	38.49	35.01
Sc	7.44	26.08	17.01	12.29	15.47	12.48	19.28
Sr	409.82	838.72	1591.24	1451.84	1182.09	1622.37	2024.03
Th	13.35	2.94	4.37	5.79	5.28	5.36	4.12
U	2.57	n/a	n/a	0.50	1.74	3.62	1.46
V	47.40	126.02	227.62	207.03	211.22	200.79	234.06
Y	15.41	14.30	10.92	14.97	14.49	15.32	22.47
Zn	27.47	73.18	72.24	58.60	66.80	77.67	92.02
Zr	185.32	112.06	125.20	119.33	121.24	120.74	167.76
Total	99.47	98.89	100.27	99.07	98.85	100.17	100.46

Sample number	JBSP010	JBSP010	JBSP010	27/07_5	22/08_11	22/08_11	22/08_11	22/08_13
Bead	LF25676	LF25677	LF25678	LF22804	LF22775	LF22786	LF22789	LF22779
field area	Narin Hudag	Narin Hudag	Narin Hudag	East Sykhandulaan Intrusion	Oyut Ulaan	Oyut Ulaan	Oyut Ulaan	Oyut Ulaan
formation	n/a	n/a	n/a	n/a	n/a	n/a	n/a	n/a
SiO2	66.80	65.36	64.49	59.48	64.64	64.39	54.96	62.41
TiO2	0.57	0.55	0.51	0.49	0.46	0.45	0.71	0.55
Al2O3	15.34	15.02	14.62	16.73	16.02	16.10	17.19	15.67
Fe2O3	4.26	4.20	4.27	4.97	4.55	4.56	7.34	5.64
MnO	0.08	0.07	0.08	0.12	0.09	0.09	0.14	0.10
MgO	2.69	2.69	2.63	2.40	1.93	1.96	3.91	3.06
CaO	3.75	3.70	3.30	5.42	2.83	2.86	5.08	3.69
Na2O	4.71	4.66	5.04	5.50	4.43	4.57	5.00	4.69
K2O	3.29	3.28	3.60	2.07	3.41	3.32	0.98	3.10
P2O5	0.20	0.20	0.20	0.28	0.21	0.20	0.24	0.19
SO3	0.03	0.03	0.01	0.08	0.03	0.15	0.08	0.01
LOI	0.79	0.80	0.74	2.73	1.48	1.50	4.42	0.85
As	3.38	2.79	3.83	14.22	3.90	3.83	13.43	2.57
Ba	672.93	652.06	653.14	1041.18	832.51	276.74	372.42	882.15
Ce	27.36	34.45	32.42	49.84	22.90	23.02	15.63	22.30
Co	11.75	10.79	13.32	15.46	13.89	10.85	27.32	15.83
Cr	86.81	88.68	75.52	60.45	47.44	38.24	92.36	106.25
Cs	n/a	4.15	4.42	n/a	2.84	n/a	0.90	n/a
Cu	34.61	36.82	36.10	23.12	211.18	22.90	51.86	131.63
Ga	16.61	16.41	15.91	18.90	18.78	16.52	18.55	19.95
La	13.13	17.25	16.54	27.72	14.04	14.49	5.24	11.88
Mo	2.14	1.82	1.63	0.14	2.26	0.66	n/a	1.35
Nb	4.64	5.41	3.26	9.42	3.46	4.96	0.76	3.03
Nd	11.43	14.96	11.14	27.95	12.97	17.22	8.26	14.66
Ni	39.30	40.44	37.84	9.99	13.81	1.56	15.93	21.64
Pb	6.17	6.67	5.55	25.96	11.72	9.82	3.15	9.00
Rb	66.13	64.58	66.27	46.44	72.04	17.24	17.52	64.63
Sc	13.55	8.74	12.62	15.05	9.57	5.59	24.41	16.26
Sr	624.23	612.34	620.68	447.58	765.49	456.12	491.57	798.52
Th	13.69	12.50	7.60	13.08	13.59	5.80	4.46	12.06
U	2.78	0.90	2.84	2.72	2.56	1.63	n/a	0.96
V	95.29	93.32	95.70	112.42	96.59	49.29	202.54	138.23
Y	7.46	10.10	7.47	16.93	9.11	26.67	22.57	13.03
Zn	33.05	32.61	33.70	86.53	43.23	76.21	69.87	47.27
Zr	98.32	107.52	112.27	165.77	127.89	120.97	76.06	102.91
Total	101.72	99.76	99.47	100.27	100.07	100.15	100.04	99.94

Sample number	3/08_6	55.24B	56.2A	91.2A	91.3A	91.3B	91.4C	91.4D
Bead	LF22772	LF25567	LF25557	LF25469	LF25477	LF25554	LF25553	LF25064
field area	OUVG	OUVG	OUVG	OUVG	OUVG	OUVG	OUVG	OUVG
formation	Tsagaan Nuruu	Tsagaan Nuruu	Tsagaan Nuruu	Tsagaan Nuruu	Tsagaan Nuruu	Tsagaan Nuruu	Tsagaan Nuruu	Tsagaan Nuruu
SiO2	64.01	72.41	74.24	69.98	60.30	50.89	74.73	52.80
TiO2	0.72	0.28	0.24	0.24	1.59	1.97	0.18	1.57
Al2O3	16.96	13.20	11.88	11.81	14.82	17.25	12.47	16.21
Fe2O3	2.89	3.67	3.84	3.21	8.27	11.36	3.23	9.82
MnO	0.04	0.11	0.06	0.09	0.16	0.28	0.03	0.15
MgO	1.54	0.07	0.11	0.19	1.48	2.34	0.12	1.64
CaO	2.83	0.34	0.32	3.02	2.51	3.40	0.29	3.14
Na2O	4.52	5.75	3.91	3.93	5.46	6.97	4.35	7.41
K2O	2.39	2.94	4.70	3.22	2.02	0.36	2.81	1.29
P2O5	0.33	0.03	0.04	0.01	0.60	0.77	0.06	0.77
SO3	0.02	0.10	0.04	0.08	0.08	0.02	0.03	0.07
LOI	3.43	1.55	1.31	3.64	3.03	3.50	1.46	4.44
As	6.01	62.37	24.86	15.36	146.02	38.54	8.32	15.37
Ba	1000.39	466.60	165.10	199.31	921.01	181.64	145.14	716.78
Ce	34.26	143.78	190.43	140.22	63.80	80.74	151.39	80.04
Co	9.83	8.08	7.23	6.37	21.36	39.01	6.82	25.95
Cr	85.50	0.88	14.19	12.84	6.23	61.53	12.60	36.18
Cs	0.26	5.32	4.67	3.17	4.10	5.64	3.81	n/a
Cu	30.96	n/a	4.03	0.69	17.39	102.16	n/a	48.18
Ga	17.43	26.72	27.88	23.79	21.44	23.14	27.69	24.40
La	21.41	56.36	68.98	62.53	25.21	30.13	58.50	29.58
Mo	1.63	3.65	3.95	2.72	2.24	2.66	2.79	2.13
Nb	6.43	21.45	27.12	26.33	11.69	9.83	22.89	15.28
Nd	21.24	74.28	87.72	73.06	36.61	40.65	71.79	43.69
Ni	34.73	n/a	n/a	n/a	n/a	32.32	n/a	n/a
Pb	10.10	15.77	32.68	12.71	18.80	5.03	19.93	11.72
Rb	43.35	42.42	109.06	63.52	27.09	7.66	61.54	16.92
Sc	9.19	3.68	1.59	8.40	19.10	30.98	2.32	21.45
Sr	1038.80	76.89	33.64	133.58	303.95	654.84	26.31	326.81
Th	7.39	15.61	17.96	12.62	7.52	4.49	14.88	7.56
U	0.63	5.09	4.87	3.76	1.80	1.92	2.18	4.12
V	93.04	4.18	7.09	3.01	90.15	266.68	3.40	97.14
Y	9.81	116.83	141.28	115.64	61.82	58.39	117.79	66.17
Zn	38.23	101.47	159.93	109.25	112.76	156.56	99.88	121.45
Zr	89.84	958.15	1169.38	1031.23	460.07	330.84	1095.56	547.39
Total	99.68	100.45	100.69	99.42	100.33	99.12	99.75	99.32

Sample number	22/08_13	22/08_13	22/08_15	22/08_15	22/08_15	22/08_9	22/08_9
Bead	LF22782	LF22783	LF22776	LF22777	LF22780	LF22771	LF22773
field area	Oyut Ulaan	Oyut Ulaan	Oyut Ulaan	Oyut Ulaan	Oyut Ulaan	Oyut Ulaan	Oyut Ulaan
formation	n/a	n/a	n/a	n/a	n/a	n/a	n/a
SiO2	64.66	64.09	63.54	63.92	63.89	64.74	65.04
TiO2	0.50	0.43	0.59	0.59	0.57	0.45	0.47
Al2O3	14.99	15.46	16.63	16.93	16.66	16.03	15.81
Fe2O3	4.56	3.81	4.01	3.67	3.58	3.93	4.18
MnO	0.07	0.06	0.06	0.05	0.05	0.05	0.06
MgO	2.37	1.96	2.38	2.26	2.34	1.98	2.15
CaO	3.34	3.23	3.97	3.98	3.95	3.07	3.15
Na2O	4.18	4.42	5.30	5.50	5.36	4.65	4.57
K2O	3.60	3.56	3.17	3.06	3.16	3.36	3.25
P2O5	0.19	0.16	0.23	0.23	0.23	0.22	0.22
SO3	0.02	0.02	0.02	0.01	0.01	0.02	0.02
LOI	0.72	0.68	0.48	0.46	0.51	0.90	0.86
As	2.84	1.29	11.94	11.81	12.13	6.20	5.36
Ba	931.70	975.21	974.46	959.75	1001.52	868.88	838.36
Ce	19.73	14.78	19.90	22.21	28.93	14.62	21.46
Co	12.87	9.61	9.29	8.82	7.55	11.59	10.34
Cr	32.50	38.30	24.66	32.19	33.47	29.24	24.91
Cs	n/a	1.08	n/a	1.82	2.46	n/a	4.85
Cu	114.20	92.99	176.23	195.06	222.31	140.08	145.67
Ga	17.94	18.45	21.31	20.51	20.56	19.61	19.96
La	12.49	13.77	17.59	15.36	19.20	13.49	12.73
Mo	1.27	1.48	2.18	2.55	2.61	1.05	1.19
Nb	3.33	3.11	2.56	2.26	2.29	3.41	2.78
Nd	13.71	11.62	15.03	14.11	16.01	12.43	15.02
Ni	16.94	11.34	14.49	11.03	12.69	14.02	13.69
Pb	8.09	8.40	10.36	9.28	7.66	3.85	5.83
Rb	67.47	67.28	48.58	49.43	50.52	69.08	66.57
Sc	8.93	10.06	11.86	12.35	10.66	10.92	12.01
Sr	756.20	823.05	1048.36	1045.46	1050.73	822.50	777.46
Th	12.74	12.10	11.94	12.43	8.70	9.40	13.83
U	0.79	0.29	1.55	3.63	n/a	2.42	n/a
V	112.52	90.33	128.63	111.06	120.29	89.49	89.59
Y	12.02	9.32	10.93	9.92	12.55	10.55	14.86
Zn	38.22	32.87	44.62	42.15	43.96	30.91	33.30
Zr	128.87	120.62	114.68	104.24	108.27	134.53	129.90
Total	99.21	97.88	100.37	100.68	100.30	99.41	99.78

Sample number	95.10A	95.11A	95.1A	95.3A	95.5A	95.7A	3/08_1
Bead	LF25559	LF25562	LF25561	LF25054	LF25563	LF25067	LF22785
field area	OUVG	OUVG	OUVG	OUVG	OUVG	OUVG	OUVG
formation	Tsagaan Nuruu	Tsagaan Nuruu	Tsagaan Nuruu	Tsagaan Nuruu	Tsagaan Nuruu	Tsagaan Nuruu	Shargyn Moghai
SiO2	73.07	69.84	73.68	71.90	71.99	73.19	62.53
TiO2	0.31	0.30	0.27	0.24	0.35	0.34	0.57
Al2O3	14.05	13.94	12.97	11.76	14.00	13.76	16.21
Fe2O3	0.58	3.67	1.38	4.18	1.09	0.16	4.85
MnO	0.01	0.20	0.01	0.04	0.01	0.00	0.08
MgO	0.14	0.11	0.07	0.09	0.08	0.11	2.47
CaO	0.44	0.31	0.88	0.85	1.04	0.72	3.62
Na2O	5.15	5.19	5.16	6.75	5.44	5.03	4.88
K2O	5.59	5.54	4.31	1.05	5.55	4.51	2.44
P2O5	0.05	0.05	0.03	0.01	0.11	0.07	0.22
SO3	0.02	0.02	0.05	0.06	0.06	0.05	0.02
LOI	0.75	1.21	1.49	1.89	1.19	1.16	1.93
As	16.21	71.79	28.93	27.54	8.37	25.64	4.96
Ba	333.66	630.98	394.95	197.69	592.83	326.16	807.52
Ce	144.25	134.74	401.50	30.05	126.99	125.00	19.93
Co	n/a	7.23	0.88	7.92	0.69	n/a	13.50
Cr	14.50	n/a	n/a	45.67	n/a	29.28	35.38
Cs	n/a	4.74	11.62	3.48	1.15	3.50	n/a
Cu	n/a	n/a	n/a	n/a	n/a	n/a	201.26
Ga	30.90	28.26	26.46	26.27	26.78	27.33	18.81
La	48.24	59.52	177.11	6.20	53.42	59.58	12.03
Mo	1.81	3.12	3.04	3.69	2.90	1.78	2.13
Nb	25.05	24.63	24.72	23.26	24.61	23.11	2.93
Nd	65.38	72.31	211.13	19.92	71.83	73.81	11.75
Ni	n/a	2.70	3.60	0.01	2.45	n/a	13.16
Pb	16.01	20.37	25.34	16.81	15.85	6.62	10.91
Rb	100.85	90.60	75.04	19.74	98.08	85.95	69.53
Sc	3.41	10.12	6.31	8.76	5.86	9.48	8.67
Sr	24.96	59.12	39.84	71.48	62.68	31.53	765.07
Th	11.43	14.03	13.96	13.77	14.18	15.73	12.97
U	4.03	4.70	4.71	2.79	5.80	0.95	3.09
V	9.59	6.40	4.38	14.47	7.63	4.59	93.72
Y	117.75	116.24	133.58	90.72	119.77	123.39	9.82
Zn	38.01	138.48	59.67	135.39	59.76	9.64	44.08
Zr	992.54	1000.95	909.10	988.70	964.17	1000.30	113.62
Total	100.15	100.36	100.30	98.81	100.91	99.09	99.82

Sample number	22/08_9	60.13B	61.7A	62.10A	62.16A	62.3A	62.5A	62.7A
Bead	LF22803	LF25671	LF25683	LF25667	LF25665	LF25666	LF25669	LF25664
field area	Oyut Ulaan	Oyut Ulaan	Oyut Ulaan	Oyut Ulaan	Oyut Ulaan	Oyut Ulaan	Oyut Ulaan	Oyut Ulaan
formation	n/a	n/a	n/a	n/a	n/a	n/a	n/a	n/a
SiO2	64.08	64.85	62.34	65.72	63.02	67.41	63.26	64.24
TiO2	0.44	0.39	0.54	0.39	0.41	0.44	0.45	0.41
Al2O3	15.93	15.30	16.99	15.92	15.81	15.77	16.09	15.37
Fe2O3	3.79	4.47	4.57	3.87	4.05	3.72	4.62	3.79
MnO	0.05	0.14	0.08	0.07	0.13	0.12	0.10	0.08
MgO	1.89	1.94	2.38	1.93	1.79	1.87	2.39	1.63
CaO	3.06	2.06	3.37	2.66	3.05	2.93	3.41	3.36
Na2O	4.64	5.08	6.09	5.16	5.45	4.91	5.34	4.81
K2O	3.36	3.68	3.35	3.65	3.35	3.87	3.53	3.77
P2O5	0.20	0.22	0.26	0.18	0.19	0.19	0.23	0.16
SO3	0.03	0.02	0.03	0.03	0.02	0.03	0.03	0.03
LOI	0.97	1.43	0.62	0.70	1.95	0.56	0.36	1.81
As	4.80	8.31	4.41	3.38	21.18	3.72	10.26	2.86
Ba	838.04	957.44	1120.75	856.79	864.02	894.85	875.95	923.11
Ce	14.42	30.07	26.58	26.34	28.77	32.97	44.15	31.35
Co	10.63	12.89	11.88	9.40	12.00	8.83	13.50	8.25
Cr	32.49	39.86	42.57	36.65	36.60	53.12	36.81	20.02
Cs	n/a	1.04	2.47	1.17	n/a	1.23	n/a	3.45
Cu	133.98	33.95	70.32	51.94	102.34	108.42	83.61	155.06
Ga	20.32	16.51	20.80	19.23	18.57	18.36	20.04	18.39
La	13.11	11.34	11.48	10.24	11.91	14.07	15.44	14.31
Mo	0.86	2.13	2.68	1.30	1.54	2.39	2.65	2.63
Nb	4.07	4.09	2.31	3.62	3.45	3.78	4.62	2.65
Nd	7.58	11.00	11.25	12.95	13.24	15.94	19.16	13.41
Ni	12.30	12.98	15.39	10.97	11.32	10.60	15.65	11.12
Pb	6.23	10.10	10.17	7.74	211.44	16.00	12.96	9.17
Rb	66.73	65.33	53.54	67.12	62.81	78.42	68.21	65.74
Sc	11.63	13.46	13.73	8.92	12.99	13.27	9.48	12.16
Sr	826.24	533.87	1005.83	784.19	746.13	674.42	861.39	709.53
Th	8.24	11.62	6.95	9.21	6.14	10.63	12.15	7.47
U	0.03	n/a	1.57	1.80	n/a	0.97	2.12	2.17
V	84.61	103.50	141.59	90.05	109.74	84.77	111.95	91.18
Y	10.25	7.37	5.74	7.61	7.77	6.69	9.44	10.29
Zn	30.59	71.70	43.69	30.03	416.27	51.56	70.49	38.88
Zr	113.07	118.94	163.58	116.62	118.75	126.07	125.31	115.54
Total	98.45	99.59	100.62	100.28	99.23	101.25	99.81	99.46

Sample number	3/08_1	3/08_2	3/08_2	31/07_1	31/07_2	31/07_3	56.10A	56.13A
Bead	LF22801	LF22767	LF22781	LF22778	LF22794	LF22792	LF25558	LF25065
field area	OUVG	OUVG	OUVG	OUVG	OUVG	OUVG	OUVG	OUVG
formation	Shargyn Moghai	Shargyn Moghai	Shargyn Moghai	Shargyn Moghai	Shargyn Moghai	Shargyn Moghai	Shargyn Moghai	Shargyn Moghai
SiO2	61.95	62.65	64.62	59.42	53.57	47.24	55.78	48.05
TiO2	0.70	0.51	0.51	0.71	0.90	0.69	0.66	0.73
Al2O3	16.69	16.34	16.89	15.09	18.64	17.27	16.90	13.50
Fe2O3	5.10	4.27	4.27	6.32	8.31	7.80	7.19	5.89
MnO	0.06	0.06	0.06	0.09	0.10	0.23	0.12	0.12
MgO	2.24	1.17	1.24	2.49	4.34	2.31	3.85	4.58
CaO	2.47	1.81	1.85	5.97	7.77	11.73	4.16	10.30
Na2O	6.37	5.36	5.40	4.55	3.44	4.01	5.80	4.69
K2O	2.15	3.01	3.02	0.88	0.65	1.14	2.69	0.40
P2O5	0.30	0.22	0.23	0.32	0.26	0.28	0.48	0.40
SO3	0.06	0.02	0.01	0.02	0.03	0.14	0.02	0.05
LOI	2.23	1.30	1.48	3.70	2.37	7.40	1.93	10.49
As	4.54	3.93	2.83	58.63	7.94	12.12	6.43	5.90
Ba	738.27	947.24	964.35	611.07	953.54	347.70	1198.01	133.41
Ce	65.44	25.99	21.25	29.55	25.87	43.08	50.97	57.63
Co	9.08	13.08	13.02	19.12	10.61	19.03	23.93	24.22
Cr	n/a	45.40	35.64	47.89	11.51	4.83	201.28	307.41
Cs	0.57	0.11	1.00	n/a	2.14	n/a	n/a	7.28
Cu	2.13	48.02	48.39	43.75	151.99	2.70	33.33	95.40
Ga	16.08	18.98	18.77	14.96	21.47	14.06	20.30	18.83
La	31.07	14.00	15.83	14.31	15.86	19.35	22.61	23.76
Mo	1.15	1.00	0.54	1.48	2.12	0.52	2.12	1.77
Nb	8.34	1.97	2.91	4.31	2.65	7.20	7.16	7.53
Nd	34.72	14.61	13.57	19.39	15.25	25.26	24.69	26.63
Ni	n/a	24.82	26.97	22.08	6.94	n/a	111.27	129.54
Pb	19.49	4.23	6.71	5.04	11.67	7.60	8.40	6.40
Rb	114.55	55.72	54.97	13.76	63.44	14.79	38.65	7.08
Sc	5.28	7.46	6.94	16.26	14.15	15.17	18.37	20.82
Sr	99.53	928.82	927.56	981.23	1113.07	103.65	1932.21	747.18
Th	14.83	9.49	6.98	5.07	7.44	8.86	0.13	4.84
U	4.11	0.35	1.68	0.25	2.11	1.28	n/a	1.21
V	17.39	86.15	93.56	143.61	125.07	60.41	185.15	149.39
Y	37.20	10.62	10.73	17.68	11.69	34.78	12.49	12.54
Zn	61.84	51.88	53.70	55.36	42.50	81.09	79.58	72.79
Zr	255.27	115.56	120.40	137.79	141.31	226.02	159.38	128.58
Total	100.32	96.71	99.58	99.57	100.36	100.23	99.57	99.21

Sample number	65.12A	65.14A	65.14A	65.14A	65.1A	65.3A	65.6A	66.20A
Bead	LF25673	LF25686	LF25689	LF25690	LF25663	LF25685	LF25661	LF25656
field area	Oyut Ulaan	Oyut Ulaan	Oyut Ulaan	Oyut Ulaan	Oyut Ulaan	Oyut Ulaan	Oyut Ulaan	Oyut Ulaan
formation	n/a	n/a	n/a	n/a	n/a	n/a	n/a	n/a
SiO2	66.23	64.96	66.78	65.01	62.00	63.12	61.92	64.79
TiO2	0.50	0.42	0.51	0.42	0.55	0.49	0.40	0.53
Al2O3	16.21	15.57	16.00	15.68	16.27	16.55	15.43	15.74
Fe2O3	4.16	4.14	4.31	4.19	4.94	4.49	4.16	3.89
MnO	0.08	0.07	0.07	0.07	0.08	0.07	0.14	0.08
MgO	2.12	1.86	1.98	1.90	2.13	1.95	2.33	1.98
CaO	3.49	2.71	3.24	2.73	3.34	3.44	3.33	2.89
Na2O	4.96	5.05	5.05	5.19	5.58	5.33	4.60	5.35
K2O	3.70	3.69	3.48	3.73	3.64	3.47	3.59	3.96
P2O5	0.19	0.20	0.21	0.20	0.24	0.23	0.18	0.19
SO3	0.04	0.03	0.03	0.02	0.05	0.04	0.01	0.02
LOI	0.79	0.73	0.72	0.63	0.47	1.27	3.19	0.62
As	6.56	4.64	0.00	0.00	4.02	5.96	5.65	4.78
Ba	873.69	885.22	0.00	0.00	921.60	834.85	814.77	920.68
Ce	36.97	37.46	27.96	29.36	33.19	34.01	30.81	30.39
Co	10.83	11.30	0.00	0.00	11.98	12.23	11.48	9.26
Cr	40.24	42.26	0.00	0.00	48.58	54.96	30.81	24.43
Cs	6.06	5.23	1.72	3.20	0.16	2.66	3.24	2.07
Cu	148.64	153.58	0.00	0.00	160.66	137.07	90.83	144.01
Ga	18.79	18.06	0.00	0.00	19.73	20.31	18.44	20.08
La	15.64	14.69	13.28	14.19	18.03	13.52	12.44	14.62
Mo	2.13	2.68	0.00	0.00	2.40	2.93	1.89	2.51
Nb	3.63	4.10	0.00	0.00	2.38	3.39	2.67	2.18
Nd	15.79	17.14	15.46	14.56	20.28	18.55	12.65	13.98
Ni	11.49	10.29	0.00	0.00	9.73	8.78	13.67	10.35
Pb	14.95	10.12	0.00	0.00	15.57	16.40	10.37	8.87
Rb	74.80	75.84	0.00	0.00	58.40	57.03	73.54	71.84
Sc	12.53	10.49	0.00	0.00	13.27	16.14	16.60	11.23
Sr	782.97	784.90	0.00	0.00	883.30	881.44	619.71	818.88
Th	10.54	7.09	0.00	0.00	9.65	8.78	11.76	10.57
U	2.74	2.88	0.00	0.00	4.11	1.50	n/a	3.64
V	93.85	93.98	0.00	0.00	145.10	121.72	111.14	118.69
Y	6.73	4.56	0.00	0.00	9.20	11.13	8.79	9.30
Zn	49.55	42.49	0.00	0.00	69.37	66.58	80.23	38.16
Zr	116.58	110.15	0.00	0.00	133.28	108.00	117.57	214.64
Total	101.68	99.42	101.66	99.78	99.31	100.44	99.28	100.03

Sample number	56.14A	56.15A	56.15B	56.16A	56.17A	56.3A	56.3B	56.4A
Bead	LF25043	LF25044	LF25050	LF25040	LF25061	LF25552	LF25096	LF25095
field area	OUVG	OUVG	OUVG	OUVG	OUVG	OUVG	OUVG	OUVG
formation	Shargyn Moghai	Shargyn Moghai	Shargyn Moghai	Shargyn Moghai	Shargyn Moghai	Shargyn Moghai	Shargyn Moghai	Shargyn Moghai
SiO2	57.09	52.74	52.94	59.94	53.78	57.57	54.37	62.22
TiO2	0.81	0.71	0.53	0.56	0.66	0.56	0.79	0.66
Al2O3	14.42	16.23	13.38	16.10	16.61	17.34	16.12	16.07
Fe2O3	6.97	7.58	5.67	6.02	6.56	6.80	8.46	4.90
MnO	0.07	0.14	0.17	0.07	0.14	0.12	0.24	0.08
MgO	3.39	5.20	2.35	2.43	4.67	3.29	4.58	2.90
CaO	3.65	3.54	8.47	2.44	6.91	6.65	7.31	4.25
Na2O	6.38	5.29	6.64	4.87	5.40	4.32	3.53	4.80
K2O	1.26	2.44	0.85	3.33	1.45	0.73	1.45	2.04
P2O5	0.41	0.49	0.56	0.32	0.24	0.25	0.21	0.22
SO3	0.20	0.02	0.09	0.18	0.07	0.04	0.02	0.04
LOI	4.47	4.81	7.22	2.81	2.69	1.75	2.31	1.29
As	9.53	25.29	9.66	19.68	8.78	4.75	1.93	16.17
Ba	780.43	2823.01	553.09	1687.09	1312.96	526.92	797.41	1330.12
Ce	51.26	51.62	38.22	36.91	26.51	35.98	25.57	33.71
Co	23.36	29.95	17.61	19.09	26.52	23.75	32.28	16.00
Cr	209.81	537.45	155.58	130.92	404.85	94.48	79.57	81.18
Cs	n/a	1.40	n/a	0.53	n/a	2.84	n/a	1.52
Cu	41.59	56.96	197.79	63.38	77.13	174.20	15.17	23.48
Ga	16.82	18.15	13.41	19.64	17.71	19.20	18.34	17.84
La	24.40	30.03	26.71	19.55	10.24	16.90	10.95	16.63
Mo	1.35	2.34	1.43	1.81	2.43	0.00	1.25	1.06
Nb	6.77	5.45	4.68	5.49	2.48	3.76	3.70	4.92
Nd	26.82	26.75	27.25	20.61	13.47	18.50	15.87	17.71
Ni	86.63	114.35	71.73	56.06	115.55	28.15	30.24	37.72
Pb	6.17	11.42	9.93	9.72	2.57	0.74	8.04	8.50
Rb	19.21	31.15	19.68	62.07	19.81	14.29	30.14	56.08
Sc	16.19	22.36	26.26	9.39	29.71	28.35	26.89	15.11
Sr	732.89	1700.60	1137.75	1449.48	1278.96	978.00	993.60	1035.60
Th	4.85	4.49	4.35	3.22	4.41	3.00	0.03	7.99
U	0.02	n/a	n/a	2.92	1.23	1.15	1.27	0.12
V	139.92	216.77	146.33	148.55	186.25	222.77	213.31	113.37
Y	15.64	13.57	15.34	11.91	12.56	17.26	16.65	12.57
Zn	61.63	78.50	50.75	71.05	60.76	61.49	91.25	60.46
Zr	142.47	140.07	123.65	148.87	82.81	113.82	105.51	148.37
Total	99.11	99.19	98.87	99.08	99.16	99.43	99.38	99.47

Sample number	66.20A	66.21A	88.2A	88.3A	88.3A	88.3A	22/08_10	22/08_10
Bead	LF25657	LF25660	LF25659	LF25653	LF25654	LF25655	LF22791	LF25611
field area	Oyut Ulaan	Oyut Ulaan	Oyut Ulaan	Oyut Ulaan	Oyut Ulaan	Oyut Ulaan	Oyut Ulaan	Oyut Ulaan
formation	n/a	n/a	n/a	n/a	n/a	n/a	dyke	dyke
SiO2	64.06	64.10	62.50	64.80	64.97	65.70	56.09	56.11
TiO2	0.47	0.55	0.54	0.39	0.44	0.49	0.68	0.61
Al2O3	15.61	16.26	15.90	15.80	15.83	16.05	15.47	15.61
Fe2O3	3.91	3.77	4.83	4.08	4.05	4.09	8.69	8.59
MnO	0.08	0.05	0.09	0.06	0.06	0.06	0.31	0.32
MgO	2.00	1.76	2.42	2.02	1.97	2.10	5.58	5.35
CaO	2.83	2.45	3.40	2.73	2.76	3.19	4.98	4.19
Na2O	5.32	5.25	5.51	5.31	5.21	4.95	1.79	2.17
K2O	3.95	4.39	3.63	3.46	3.50	3.24	2.49	2.61
P2O5	0.21	0.18	0.22	0.16	0.16	0.17	0.22	0.21
SO3	0.02	0.02	0.01	0.03	0.03	0.05	0.27	0.07
LOI	1.13	1.33	0.52	1.03	1.00	1.01	3.28	3.30
As	4.56	6.61	3.85	4.19	3.75	3.77	5.01	13.02
Ba	883.90	1007.68	929.60	884.77	854.18	878.60	430.94	1284.80
Ce	33.66	30.97	32.41	34.27	27.02	33.77	29.27	24.71
Co	9.18	8.93	11.76	10.37	10.72	12.18	31.28	33.64
Cr	41.23	9.41	20.91	25.11	223.07	58.18	148.69	316.21
Cs	0.71	5.31	n/a	2.10	5.59	2.63	0.43	1.98
Cu	142.77	684.68	165.72	72.14	69.60	66.81	79.57	2.50
Ga	20.19	19.54	21.04	19.87	17.92	18.62	19.23	17.65
La	15.29	14.40	17.01	14.20	14.13	11.90	14.93	9.43
Mo	2.07	2.24	3.06	1.29	2.55	2.49	0.84	1.49
Nb	4.34	4.03	3.37	3.25	4.08	3.79	3.74	3.08
Nd	13.70	12.72	16.14	13.44	12.03	12.33	15.48	11.37
Ni	9.79	5.69	11.66	12.74	12.12	11.73	73.94	116.09
Pb	9.71	7.13	11.35	8.69	10.13	8.47	6.54	11.02
Rb	72.94	70.35	55.99	53.63	52.79	53.55	15.79	48.96
Sc	14.75	9.94	14.94	15.77	13.55	15.12	25.31	14.02
Sr	828.58	769.17	978.79	795.76	786.33	785.82	816.14	626.65
Th	9.51	10.62	5.54	13.16	8.69	7.20	6.16	9.20
U	7.97	3.22	2.00	2.46	2.16	2.27	1.24	0.85
V	123.55	122.00	146.59	102.96	108.96	99.91	193.84	151.95
Y	7.62	7.45	8.23	7.90	6.51	6.05	17.73	11.44
Zn	38.30	120.35	44.83	32.57	30.92	30.86	53.31	142.55
Zr	226.57	222.18	148.98	109.34	121.81	110.05	100.36	104.75
Total	99.58	100.10	99.58	99.89	99.98	100.09	99.83	99.13

Sample number	56.4B	56.5A	56.5A	56.5A	56.6A	56.7A	56.8A	56.9A
Bead	LF25090	LF25546	LF25547	LF25548	LF25070	LF25089	LF25566	LF25088
field area	OUVG	OUVG	OUVG	OUVG	OUVG	OUVG	OUVG	OUVG
formation	Shargyn Moghai	Shargyn Moghai	Shargyn Moghai	Shargyn Moghai	Shargyn Moghai	Shargyn Moghai	Shargyn Moghai	Shargyn Moghai
SiO2	62.27	55.17	55.46	55.26	54.36	58.64	60.45	59.27
TiO2	0.61	0.57	0.61	0.56	0.61	0.87	0.40	0.76
Al2O3	16.96	16.85	16.80	16.96	16.87	15.59	15.22	16.33
Fe2O3	5.79	7.06	7.01	6.98	7.50	7.33	4.82	5.73
MnO	0.05	0.14	0.13	0.14	0.11	0.13	0.06	0.07
MgO	1.37	4.84	4.74	4.76	4.78	4.71	2.16	2.29
CaO	3.36	5.24	5.28	5.09	5.50	5.87	3.09	2.98
Na2O	4.93	5.05	4.93	4.94	4.06	4.16	4.74	5.89
K2O	3.17	1.87	1.82	1.83	1.62	0.71	3.29	2.34
P2O5	0.23	0.24	0.24	0.24	0.27	0.28	0.22	0.31
SO3	0.03	0.05	0.05	0.05	0.08	0.03	0.04	0.03
LOI	0.96	2.54	2.54	2.54	3.65	2.16	5.27	4.00
As	6.39	11.17	8.88	8.81	9.63	3.00	15.95	6.38
Ba	891.52	632.00	663.72	641.10	844.73	259.94	960.76	739.19
Ce	34.88	29.66	27.43	38.98	39.49	39.64	55.61	47.20
Co	18.01	27.06	26.44	25.26	25.51	26.83	31.43	18.61
Cr	75.67	203.45	105.69	212.49	95.27	86.11	262.94	233.61
Cs	3.94	2.16	7.86	0.56	7.52	4.18	n/a	1.41
Cu	33.32	10.88	8.71	9.94	5.04	15.89	46.48	44.22
Ga	19.51	18.46	18.31	18.11	20.15	16.85	19.96	19.08
La	17.72	11.61	11.39	11.17	10.77	12.35	25.79	20.13
Mo	1.66	1.69	2.05	1.50	1.14	2.09	2.15	1.89
Nb	3.27	3.25	3.52	2.26	2.34	3.07	6.27	6.21
Nd	15.29	17.06	16.17	15.46	17.76	17.60	30.90	23.70
Ni	36.96	33.95	34.58	33.56	29.42	31.49	207.56	51.97
Pb	8.81	3.42	6.18	7.44	2.99	3.51	8.43	8.97
Rb	58.31	46.55	47.37	47.26	56.55	14.25	21.94	33.13
Sc	11.57	24.72	29.80	31.88	26.62	31.07	22.72	16.65
Sr	832.99	882.97	889.83	878.39	860.49	922.70	1069.80	1029.04
Th	3.54	3.17	5.86	3.54	3.92	5.50	5.22	4.33
U	2.70	n/a	0.55	1.36	3.32	2.40	2.12	1.41
V	120.58	203.31	202.10	206.94	213.88	188.30	186.49	140.16
Y	13.57	21.25	16.38	17.58	20.68	19.25	16.78	10.01
Zn	57.93	71.09	72.55	73.12	71.30	49.17	71.53	63.81
Zr	152.98	114.21	120.61	113.80	116.22	111.38	122.68	154.84
Total	99.73	99.61	99.61	99.34	99.41	100.47	99.76	100.00

Sample number	22/08_12	60.12A	60.12B	60.22A	60.7A	60.9A	60.9A	67.4A
Bead	LF22770	LF25618	LF25614	LF25620	LF25609	LF25607	LF25608	LF25610
field area	Oyut Ulaan	Oyut Ulaan	Oyut Ulaan	Oyut Ulaan	Oyut Ulaan	Oyut Ulaan	Oyut Ulaan	Oyut Ulaan
formation	dyke	dyke	dyke	dyke	dyke	dyke	dyke	dyke
SiO2	59.24	65.63	57.20	74.85	61.00	64.77	66.10	55.93
TiO2	0.63	0.32	0.70	0.17	0.39	0.34	0.40	0.65
Al2O3	16.15	15.03	15.80	12.52	15.69	15.20	15.59	15.82
Fe2O3	6.65	3.45	7.99	1.31	5.29	4.54	4.72	6.46
MnO	0.14	0.06	0.24	0.05	0.16	0.08	0.07	0.22
MgO	3.47	1.89	5.82	0.48	3.05	1.98	2.08	5.64
CaO	4.51	1.95	4.04	0.65	2.69	2.27	2.76	4.65
Na2O	4.63	4.88	0.98	4.41	3.81	4.33	4.39	5.09
K2O	1.99	4.07	3.81	4.93	3.85	3.72	3.59	4.19
P2O5	0.35	0.15	0.22	0.06	0.30	0.16	0.17	0.35
SO3	0.04	0.02	0.06	0.01	0.16	0.09	0.05	0.09
LOI	2.18	1.70	3.23	0.53	2.63	2.64	2.62	1.77
As	9.55	8.38	21.82	14.86	7.53	3.03	4.27	16.96
Ba	747.95	1295.89	2315.44	600.67	1202.38	1298.67	1290.70	722.72
Ce	37.78	22.66	15.56	29.82	27.41	21.26	20.42	29.22
Co	21.82	10.42	27.26	0.89	17.30	12.96	12.74	24.44
Cr	25.06	21.43	455.77	n/a	82.10	46.04	65.98	251.42
Cs	0.05	n/a	n/a	0.53	n/a	0.38	n/a	n/a
Cu	70.55	280.37	367.87	57.88	317.52	155.28	154.17	2.05
Ga	21.15	16.14	17.21	15.48	18.49	17.93	17.36	19.29
La	17.11	11.92	9.44	17.74	17.78	12.58	14.02	12.90
Mo	2.13	1.68	2.21	2.86	2.84	1.87	2.40	1.91
Nb	5.94	2.86	3.66	4.90	4.46	3.89	3.68	2.08
Nd	17.60	10.44	7.50	11.65	15.53	10.84	11.79	18.61
Ni	34.35	12.72	116.66	1.05	51.00	15.13	18.08	127.36
Pb	2.31	4.83	7.69	11.23	10.38	8.97	9.23	9.24
Rb	39.89	75.53	75.25	98.55	62.68	75.14	73.30	112.44
Sc	12.54	12.75	14.92	1.87	14.20	12.57	10.12	22.63
Sr	538.02	649.34	492.31	216.13	473.43	497.53	492.09	926.12
Th	8.51	10.99	6.30	22.94	1.27	10.35	9.95	8.99
U	1.49	1.44	n/a	3.25	3.41	0.07	0.32	n/a
V	134.36	87.11	153.79	30.74	137.74	98.16	100.40	216.01
Y	14.82	6.16	10.95	4.27	8.27	5.88	5.57	7.39
Zn	37.86	42.23	47.39	34.75	69.36	40.85	40.70	115.09
Zr	115.92	97.85	98.07	116.64	132.56	96.49	100.51	101.27
Total	99.97	99.15	100.08	99.96	99.00	100.11	99.92	100.87

Sample number	56.9A	56.9A	56.9B	8/07_3	93.10A	93.10A	93.10A	93.12A
Bead	LF25110	LF25111	LF25093	LF22774	LF25071	LF25074	LF25069	LF25549
field area	OUVG	OUVG	OUVG	OUVG	OUVG	OUVG	OUVG	OUVG
formation	Shargyn Moghai	Shargyn Moghai	Shargyn Moghai	Shargyn Moghai	Shargyn Moghai	Shargyn Moghai	Shargyn Moghai	Shargyn Moghai
SiO2	59.60	59.04	59.55	60.72	60.59	60.08	60.74	59.10
TiO2	0.75	0.84	0.86	0.57	0.66	0.54	0.66	0.58
Al2O3	16.50	16.15	16.74	16.25	16.82	16.54	16.81	16.79
Fe2O3	5.66	5.64	5.97	5.15	5.67	5.64	5.74	5.95
MnO	0.08	0.07	0.08	0.07	0.07	0.07	0.06	0.10
MgO	2.27	2.30	1.98	3.03	1.71	1.81	1.78	2.68
CaO	3.03	3.05	2.41	3.99	1.95	1.83	1.97	4.31
Na2O	5.88	5.88	6.72	4.91	7.67	7.53	7.79	5.46
K2O	2.25	2.38	3.12	2.05	2.81	2.65	2.79	3.17
P2O5	0.31	0.31	0.32	0.23	0.27	0.27	0.28	0.28
SO3	0.04	0.03	0.03	0.01	0.04	0.03	0.04	0.03
LOI	4.24	4.24	2.71	2.37	2.27	2.26	2.26	1.41
As	4.73	2.37	6.08	14.02	18.59	21.44	20.72	7.33
Ba	744.05	750.19	1271.02	1069.95	926.90	892.46	892.22	920.99
Ce	42.56	44.98	34.87	29.04	27.17	26.06	27.43	38.46
Co	19.16	17.83	19.03	18.44	16.81	17.88	15.84	17.54
Cr	83.62	126.67	90.18	60.99	12.52	32.42	58.74	10.35
Cs	n/a	n/a	2.05	n/a	n/a	0.12	0.42	0.68
Cu	46.17	42.05	61.86	275.98	246.17	248.71	240.36	139.74
Ga	17.91	18.97	20.24	20.07	18.80	17.86	18.40	22.13
La	19.57	20.71	16.93	14.34	16.75	14.78	15.82	16.04
Mo	2.10	1.99	2.37	0.81	0.95	0.89	1.49	1.31
Nb	6.81	5.94	6.12	3.58	1.43	3.39	3.37	2.77
Nd	19.93	19.74	16.32	15.31	17.48	19.75	16.54	17.10
Ni	50.40	48.62	44.40	32.79	3.43	5.97	6.31	5.32
Pb	8.83	11.34	5.72	9.23	7.82	5.40	4.91	11.55
Rb	34.44	32.79	48.08	34.49	33.12	33.69	32.09	46.96
Sc	13.84	15.74	14.20	11.60	13.11	17.65	14.47	15.11
Sr	1008.83	988.91	1054.24	1293.84	654.91	650.65	653.33	1186.36
Th	7.27	5.08	5.35	9.93	6.05	7.70	6.85	5.48
U	n/a	2.03	2.47	n/a	n/a	1.68	2.55	1.11
V	120.33	111.33	143.11	120.50	169.26	165.17	163.94	187.11
Y	10.36	10.59	12.74	12.58	16.17	12.02	13.25	12.10
Zn	65.39	65.01	61.26	66.75	50.34	51.76	49.97	65.33
Zr	154.53	145.17	155.85	142.16	140.50	131.45	143.71	139.42
Total	100.60	99.94	100.49	99.36	100.54	99.25	100.91	99.87

Sample number	67.4B	67.5A	67.5B	67.7A	90.9B	68.1A	88.10A	88.12A
Bead	LF25621	LF25613	LF25615	LF25612	LF25616	LF25680	LF25047	LF25058
field area	Oyut Ulaan	Oyut Ulaan	Oyut Ulaan	Oyut Ulaan	Oyut Ulaan	Oyut Ulaan	OUVG	OUVG
formation	dyke	dyke	dyke	dyke	dyke	dyke	Yasun Eliy-e	Yasun Eliy-e
SiO2	77.09	54.72	61.25	75.10	54.28	60.42	49.05	46.82
TiO2	0.14	0.62	0.54	0.28	0.81	0.57	1.01	0.96
Al2O3	11.76	14.54	15.77	8.63	15.84	15.55	18.15	17.34
Fe2O3	0.45	6.60	4.60	7.55	7.21	5.26	10.72	13.15
MnO	0.02	0.13	0.09	0.05	0.31	0.11	0.10	0.15
MgO	0.19	7.15	3.01	1.24	4.38	3.34	3.71	4.66
CaO	0.77	5.55	2.89	0.92	5.09	3.58	7.67	8.02
Na2O	3.80	3.89	4.95	3.30	6.00	5.83	4.11	3.13
K2O	4.39	1.89	3.82	0.62	1.70	2.89	2.83	2.78
P2O5	0.02	0.29	0.35	0.12	0.43	0.30	0.48	0.42
SO3	0.09	0.08	0.11	0.08	0.10	0.02	0.03	0.08
LOI	0.63	3.69	2.94	1.45	3.83	1.39	1.50	1.66
As	64.13	33.91	15.19	2.85	33.41	17.63	16.15	15.16
Ba	537.29	737.26	1343.55	887.34	712.75	1327.70	596.22	724.08
Ce	31.98	35.72	47.37	16.00	56.95	34.44	48.06	42.27
Co	n/a	27.72	15.09	16.89	26.33	16.82	32.65	36.39
Cr	n/a	493.54	64.81	9.27	201.15	61.48	14.87	37.02
Cs	1.78	1.06	n/a	n/a	n/a	3.27	4.23	2.17
Cu	269.30	53.47	7.01	4388.42	734.25	133.55	832.29	116.21
Ga	14.77	18.11	19.50	13.27	19.17	17.50	20.94	20.16
La	15.78	16.03	22.56	3.66	24.23	13.64	17.77	11.39
Mo	3.13	1.55	2.13	6.99	1.35	1.25	1.83	1.49
Nb	4.81	4.79	7.49	0.28	5.19	3.99	4.96	6.37
Nd	13.88	19.89	22.67	5.85	23.51	15.92	24.24	20.40
Ni	3.28	196.36	51.55	n/a	71.23	26.15	6.95	14.38
Pb	6.53	26.10	10.35	3.40	27.97	5.58	4.48	1.80
Rb	111.73	38.83	67.89	13.92	28.82	57.15	48.35	81.19
Sc	n/a	16.19	9.12	6.49	15.65	16.14	28.71	37.05
Sr	149.74	897.40	999.36	212.77	852.36	878.56	859.47	791.04
Th	38.67	6.64	4.63	2.80	6.27	7.12	3.67	2.58
U	5.18	0.36	0.49	7.48	n/a	3.63	0.99	n/a
V	14.84	166.18	134.73	102.68	173.98	160.75	254.39	385.64
Y	3.83	13.16	10.23	6.84	12.82	7.81	27.22	26.68
Zn	6.51	91.03	137.70	55.53	434.90	60.77	43.23	90.46
Zr	91.99	120.79	150.21	49.70	130.25	91.52	104.70	91.04
Total	99.32	99.14	100.33	99.33	99.97	99.25	99.37	99.17

Sample number	93.12A	93.12A	93.15A	93.15A	93.15A	93.15C	96.2A	96.2B
Bead	LF25550	LF25551	LF25543	LF25544	LF25545	LF25564	LF25573	LF25458
field area	OUVG	OUVG	OUVG	OUVG	OUVG	OUVG	OUVG	OUVG
formation	Shargyn Moghai	Shargyn Moghai	Shargyn Moghai	Shargyn Moghai	Shargyn Moghai	Shargyn Moghai	Shargyn Moghai	Shargyn Moghai
SiO2	59.13	58.81	67.79	67.56	67.02	52.20	63.57	63.38
TiO2	0.51	0.56	0.40	0.35	0.38	0.45	0.40	0.51
Al2O3	16.82	16.80	13.63	13.66	13.51	15.04	16.49	16.30
Fe2O3	5.84	5.82	3.85	3.76	3.83	8.30	4.33	4.82
MnO	0.10	0.10	0.08	0.09	0.08	0.16	0.06	0.05
MgO	2.66	2.70	1.09	1.05	1.05	2.87	1.74	1.24
CaO	4.15	4.23	2.23	2.18	2.23	6.92	3.07	3.05
Na2O	5.33	5.45	7.60	7.65	7.45	4.06	5.43	6.16
K2O	2.93	3.02	0.43	0.42	0.42	1.05	2.85	2.38
P2O5	0.28	0.28	0.14	0.14	0.13	0.27	0.21	0.22
SO3	0.03	0.03	0.05	0.05	0.04	0.12	0.07	0.03
LOI	1.41	1.41	2.86	2.85	2.88	8.36	1.28	1.71
As	9.07	6.96	5.99	9.14	6.00	10.59	0.77	5.18
Ba	935.80	928.51	122.44	114.53	105.75	1259.44	1278.72	954.73
Ce	35.02	37.30	74.23	73.77	76.87	28.11	24.46	27.10
Co	17.71	16.78	9.78	11.93	10.68	30.27	15.22	13.21
Cr	1.63	31.52	19.18	153.32	12.34	253.83	23.70	44.16
Cs	n/a	n/a	1.63	n/a	4.94	1.11	n/a	n/a
Cu	143.34	142.32	8.79	8.74	7.93	77.93	26.56	12.52
Ga	22.41	21.69	19.82	20.31	20.42	17.08	18.83	19.05
La	16.97	15.93	30.73	31.53	32.46	9.97	10.97	15.95
Mo	0.78	1.76	1.67	1.85	2.31	1.91	1.88	1.87
Nb	2.21	3.40	13.51	14.49	12.41	2.93	5.40	3.81
Nd	19.12	18.56	35.67	36.84	38.34	15.05	16.29	13.60
Ni	6.44	6.13	5.26	6.71	5.52	67.14	19.21	15.75
Pb	10.23	13.15	7.59	6.19	7.62	3.32	12.35	6.90
Rb	45.81	46.45	8.36	8.56	9.84	17.56	39.04	39.20
Sc	13.11	17.28	11.21	5.95	14.74	23.99	14.83	7.49
Sr	1206.85	1198.30	364.24	365.01	370.22	621.00	1240.71	945.44
Th	5.14	10.80	13.16	12.06	12.92	4.00	2.55	5.08
U	2.16	0.27	2.49	1.97	3.49	1.63	1.20	2.52
V	178.32	193.23	42.74	57.10	47.61	213.79	92.94	95.16
Y	11.87	11.95	57.13	56.22	55.08	16.49	7.55	10.99
Zn	65.85	66.50	72.21	72.33	72.92	69.90	55.25	47.14
Zr	138.12	137.85	423.47	412.57	424.25	75.48	122.31	125.42
Total	99.20	99.21	100.14	99.74	99.02	99.80	99.51	99.84

Sample number	88.12A	88.12A	88.17A	88.7A	88.9A	89.10A	89.10A	89.10A
Bead	LF25072	LF25075	LF25049	LF25042	LF25046	LF25079	LF25106	LF25107
field area	OUVG	OUVG	OUVG	OUVG	OUVG	OUVG	OUVG	OUVG
formation	Yasun Eliy-e	Yasun Eliy-e	Yasun Eliy-e	Yasun Eliy-e	Yasun Eliy-e	Yasun Eliy-e	Yasun Eliy-e	Yasun Eliy-e
SiO2	47.22	46.97	51.67	49.18	49.15	49.52	49.78	49.53
TiO2	0.96	1.15	0.77	0.84	0.88	1.02	1.15	1.30
Al2O3	17.53	17.47	15.70	18.87	15.87	19.33	19.18	19.02
Fe2O3	13.15	13.11	8.11	11.05	12.25	8.50	8.45	8.51
MnO	0.15	0.14	0.17	0.17	0.23	0.13	0.15	0.14
MgO	4.47	4.48	3.42	3.74	5.29	1.95	1.94	1.95
CaO	7.94	8.04	5.27	8.69	10.16	8.37	7.70	7.86
Na2O	3.17	3.17	3.43	2.64	2.85	4.58	4.65	4.68
K2O	2.83	2.95	4.98	1.83	0.59	1.12	1.20	1.30
P2O5	0.42	0.42	0.37	0.48	0.22	0.50	0.49	0.49
SO3	0.04	0.04	0.02	0.19	0.02	0.03	0.02	0.02
LOI	1.70	1.67	5.14	1.63	1.10	5.09	5.36	5.33
As	14.94	15.83	25.79	19.75	13.03	32.54	32.93	32.89
Ba	740.41	715.38	772.93	362.96	159.01	517.58	532.83	526.73
Ce	41.15	38.64	43.11	49.87	30.82	43.28	46.71	43.95
Co	40.53	36.53	24.31	37.04	45.35	25.00	27.95	25.46
Cr	57.67	22.29	588.82	67.93	34.27	18.29	n/a	n/a
Cs	4.54	n/a	3.72	1.48	2.83	0.53	0.61	0.98
Cu	112.34	113.85	29.77	70.84	43.97	145.65	145.96	144.24
Ga	21.55	19.68	15.85	21.30	19.55	20.60	20.48	20.15
La	10.81	10.54	17.50	14.12	4.81	14.74	14.14	16.12
Mo	2.53	0.16	3.02	1.78	2.29	2.22	2.02	2.31
Nb	4.88	3.59	5.76	5.27	2.47	7.12	6.97	6.77
Nd	18.79	18.33	18.77	23.12	9.29	22.97	19.60	20.94
Ni	13.72	13.10	54.30	1.76	21.74	2.05	2.42	2.02
Pb	2.16	n/a	6.11	7.05	3.07	8.29	6.57	6.96
Rb	83.04	82.21	85.54	41.78	20.06	20.62	20.79	21.05
Sc	31.70	38.41	27.80	22.18	37.96	20.18	28.25	22.45
Sr	794.87	796.28	405.44	596.19	499.71	667.37	670.14	665.50
Th	3.38	6.06	5.13	5.60	5.17	4.02	9.46	1.77
U	3.42	1.59	1.51	3.16	0.02	2.88	0.46	1.16
V	399.30	395.64	257.72	256.22	361.94	171.35	181.52	170.23
Y	24.67	25.16	25.17	30.38	28.60	33.02	37.34	33.56
Zn	93.36	93.37	112.64	129.68	125.10	82.35	84.58	82.93
Zr	94.30	94.01	117.56	103.20	93.81	134.64	137.30	133.07
Total	99.58	99.61	99.06	99.29	98.62	100.13	100.07	100.14

Sample number	96.4A	96.5A	96.6A	96.7A	96.8B	96.9A	96.9B	18/08_2
Bead	LF25459	LF25570	LF25568	LF25565	LF25572	LF25569	LF25571	LF22788
field area	OUVG	OUVG	OUVG	OUVG	OUVG	OUVG	OUVG	SVLZ
formation	Shargyn Moghai	Shargyn Moghai	Shargyn Moghai	Shargyn Moghai	Shargyn Moghai	Shargyn Moghai	Shargyn Moghai	n/a
SiO2	55.66	55.20	56.19	53.83	61.30	55.80	59.98	76.40
TiO2	0.77	0.51	0.53	0.70	0.50	0.56	0.61	0.03
Al2O3	16.00	15.66	16.52	15.78	15.31	15.65	16.86	13.96
Fe2O3	8.01	6.77	7.99	8.14	4.99	6.97	6.85	0.56
MnO	0.16	0.17	0.13	0.14	0.08	0.10	0.10	0.02
MgO	4.74	3.54	3.66	4.92	2.91	4.09	1.49	n/a
CaO	7.32	7.91	5.50	4.37	2.81	4.80	1.61	0.09
Na2O	3.52	3.74	4.53	7.58	6.14	5.10	9.93	5.06
K2O	1.79	2.11	2.11	2.14	1.24	0.90	0.40	3.05
P2O5	0.25	0.27	0.24	0.48	0.18	0.22	0.42	0.04
SO3	0.04	0.16	0.08	0.07	0.07	0.10	0.32	0.13
LOI	1.76	2.86	1.75	1.71	3.54	4.55	1.64	0.65
As	1.90	1.13	0.22	2.20	13.30	21.12	10.20	4.35
Ba	597.29	983.28	723.35	909.24	635.55	972.30	294.84	806.04
Ce	40.36	38.17	35.89	28.98	33.57	35.28	55.44	14.58
Co	28.78	26.58	24.94	13.52	16.89	28.78	22.94	12.50
Cr	102.23	94.91	57.18	86.30	124.82	236.90	86.41	26.96
Cs	n/a	0.54	2.48	0.01	1.64	n/a	0.95	n/a
Cu	74.46	55.37	62.98	115.49	73.99	60.26	16.72	195.98
Ga	18.49	16.31	18.96	16.94	17.56	18.53	19.87	17.94
La	12.20	14.20	12.59	16.51	12.57	14.14	25.69	11.63
Mo	1.21	1.20	2.03	2.00	1.77	2.49	0.91	1.46
Nb	0.83	5.08	4.32	5.93	5.96	3.86	5.76	2.76
Nd	18.86	19.01	16.76	13.59	16.08	18.05	31.07	9.15
Ni	41.47	40.39	36.08	35.66	68.89	101.74	61.84	11.97
Pb	7.39	5.37	6.72	9.33	9.13	5.82	6.50	11.85
Rb	29.12	34.25	38.68	61.69	30.19	15.87	8.29	69.07
Sc	24.26	25.17	22.54	13.47	16.01	21.64	10.03	10.09
Sr	874.93	926.36	1005.20	813.95	1090.52	1090.54	743.21	767.53
Th	3.12	1.74	3.94	n/a	2.62	0.68	8.79	11.95
U	n/a	0.03	3.16	n/a	3.06	0.19	2.13	1.14
V	213.55	195.40	202.66	111.86	111.11	148.96	121.84	94.24
Y	18.01	16.73	15.00	11.39	8.22	12.67	19.88	8.00
Zn	73.38	74.21	76.51	58.99	61.76	71.11	81.41	41.22
Zr	109.07	112.75	107.55	135.27	146.26	121.42	146.49	109.41
Total	100.00	98.93	99.24	99.88	99.07	98.85	100.21	99.98

Sample number	89.11A	89.12A	89.14A	89.15A	89.1A	89.3A	89.4A	89.6B
Bead	LF25475	LF25470	LF25087	LF25471	LF25082	LF25080	LF25474	LF25467
field area	OUVG	OUVG	OUVG	OUVG	OUVG	OUVG	OUVG	OUVG
formation	Yasun Eliy-e	Yasun Eliy-e	Yasun Eliy-e	Yasun Eliy-e	Yasun Eliy-e	Yasun Eliy-e	Yasun Eliy-e	Yasun Eliy-e
SiO2	49.57	51.37	52.86	68.31	49.80	61.05	54.30	50.30
TiO2	1.48	0.77	1.17	0.46	1.05	0.47	1.37	1.36
Al2O3	16.30	17.30	19.80	16.16	18.06	16.08	14.63	19.87
Fe2O3	10.61	8.39	8.13	2.46	10.77	5.04	9.31	8.94
MnO	0.24	0.17	0.13	0.06	0.22	0.15	0.31	0.15
MgO	4.22	3.87	2.25	0.18	4.39	1.71	3.15	2.27
CaO	6.46	7.28	6.74	1.28	5.93	4.52	6.80	4.17
Na2O	3.69	4.16	4.65	5.94	4.17	5.77	4.14	6.27
K2O	1.88	0.79	2.58	3.53	2.23	1.26	1.26	2.80
P2O5	0.39	0.19	0.40	0.13	0.33	0.22	0.32	0.50
SO3	0.03	0.03	0.03	0.12	0.08	0.01	0.04	0.02
LOI	4.14	4.27	1.65	2.07	2.46	2.66	4.24	3.63
As	7.64	10.47	9.92	17.00	13.25	7.46	9.33	15.20
Ba	469.36	411.23	667.18	1173.46	773.88	617.45	410.95	954.61
Ce	37.14	29.75	32.77	35.19	35.06	19.54	29.31	47.03
Co	33.17	28.19	24.57	4.43	36.18	13.74	32.70	27.65
Cr	20.91	7.81	8.99	15.48	106.59	39.92	15.84	11.85
Cs	1.66	2.76	1.23	2.32	n/a	2.77	n/a	3.24
Cu	34.76	76.92	63.14	11.30	118.30	7.27	10.24	41.62
Ga	19.78	19.48	20.62	18.75	21.03	16.73	16.36	19.99
La	14.60	4.59	14.17	17.08	7.02	12.98	11.95	16.14
Mo	1.95	1.32	1.35	2.58	1.20	0.65	2.63	1.07
Nb	7.21	0.74	7.87	5.75	3.29	7.94	6.48	9.11
Nd	21.41	11.68	17.39	19.57	16.46	11.76	13.37	19.80
Ni	11.76	4.69	1.17	n/a	18.13	2.62	4.44	4.49
Pb	5.98	1.86	4.91	8.98	n/a	6.54	5.44	8.59
Rb	30.35	13.14	41.51	65.19	53.41	24.58	19.92	38.13
Sc	42.94	32.79	16.10	7.58	24.17	16.83	28.89	24.90
Sr	424.37	719.63	750.50	202.59	657.43	524.41	352.75	753.73
Th	5.77	3.45	5.31	10.69	6.49	6.56	8.55	8.20
U	1.01	n/a	0.28	1.32	2.18	0.70	0.94	2.89
V	274.85	258.23	151.77	36.42	280.08	116.40	270.45	146.67
Y	42.33	16.70	32.42	26.89	34.17	24.33	32.34	35.64
Zn	90.53	75.01	73.37	34.30	116.78	51.54	182.47	93.06
Zr	148.16	75.17	122.69	299.62	120.55	133.99	116.59	142.40
Total	98.99	98.60	100.40	100.69	99.50	98.94	99.86	100.31

Sample number	18/08_3	18/08_5	19/08_1	79.11A	79.12A	8/08_1	8/08_2	8/08_5
Bead	LF22784	LF22787	LF22790	LF25989	LF25979	LF22793	LF22802	LF22798
field area	SVLZ	SVLZ	SVLZ	SVLZ	SVLZ	SVLZ	SVLZ	SVLZ
formation	n/a	n/a	n/a	n/a	n/a	n/a	n/a	n/a
SiO2	48.73	64.09	54.93	65.89	67.31	65.83	72.95	68.17
TiO2	0.64	0.53	0.69	0.82	0.78	0.92	0.18	0.40
Al2O3	17.13	16.37	17.24	15.55	16.46	11.84	13.21	15.46
Fe2O3	8.01	4.18	7.38	3.98	1.84	7.22	3.36	3.58
MnO	0.12	0.15	0.14	0.03	0.03	0.11	0.10	0.03
MgO	9.09	1.06	3.94	0.11	0.13	0.60	0.26	0.35
CaO	8.16	3.27	5.00	0.74	0.70	2.56	0.27	0.32
Na2O	3.58	6.66	5.02	6.22	6.46	4.29	3.31	5.21
K2O	0.79	1.26	0.96	4.83	5.19	0.87	4.41	4.40
P2O5	0.09	0.23	0.24	0.33	0.43	0.46	0.06	0.26
SO3	0.02	0.14	0.16	0.05	0.03	0.30	0.03	0.05
LOI	3.88	2.57	4.44	1.08	0.66	3.37	1.18	1.40
As	5.02	89.98	12.52	15.10	41.15	26.41	2.19	9.67
Ba	817.97	120.51	1281.88	794.24	725.49	536.58	236.10	977.47
Ce	33.91	0.45	14.10	65.19	88.85	20.16	15.48	27.89
Co	17.08	n/a	35.67	8.83	3.81	29.70	33.25	11.04
Cr	74.43	2.16	332.59	3.13	83.67	18.09	356.09	25.96
Cs	n/a	0.41	n/a	n/a	n/a	n/a	n/a	n/a
Cu	64.38	3.25	5.81	2.60	0.39	61.38	39.91	161.39
Ga	19.13	22.80	18.00	16.80	17.14	20.07	16.49	20.93
La	20.30	2.98	10.15	29.61	39.27	16.16	2.71	15.48
Mo	1.17	0.63	0.58	1.11	1.18	0.80	n/a	1.69
Nb	5.25	48.02	1.73	11.95	12.86	3.63	n/a	3.42
Nd	16.14	4.55	8.10	32.03	43.45	13.73	8.78	15.49
Ni	38.84	n/a	115.42	2.09	2.47	30.25	144.06	8.23
Pb	8.13	29.32	11.45	13.00	11.70	3.68	n/a	6.80
Rb	52.63	106.54	50.98	89.37	94.68	8.36	23.01	66.16
Sc	10.70	3.56	17.31	8.22	7.62	28.13	34.41	8.82
Sr	804.65	73.65	619.43	213.93	194.78	922.82	517.57	1106.50
Th	9.23	16.85	6.29	14.97	9.80	8.32	2.69	11.67
U	1.75	2.53	1.81	1.47	1.37	1.71	0.14	1.26
V	105.67	4.24	133.86	41.10	31.79	208.16	221.54	128.82
Y	12.85	45.94	15.72	49.15	55.74	18.53	17.76	10.32
Zn	63.36	23.11	139.29	46.74	44.91	76.35	62.02	43.79
Zr	144.66	62.17	101.18	470.54	1252.98	107.72	44.00	123.31
Total	100.25	100.50	100.12	99.64	100.02	98.37	99.32	99.63

Sample number	89.6C	89.8A	89.9A	89.9B	89.9B	89.9B	52.12A	52.3A
Bead	LF25085	LF25476	LF25081	LF25451	LF25452	LF25453	LF25457	LF25456
field area	OUVG	OUVG	OUVG	OUVG	OUVG	OUVG	OUVG Gurvan Morin	OUVG Gurvan Morin
formation	Yasun Eliy-e	Yasun Eliy-e	Yasun Eliy-e	Yasun Eliy-e	Yasun Eliy-e	Yasun Eliy-e	Hondiy	Hondiy
SiO2	51.47	59.45	44.95	41.65	41.55	42.44	55.97	49.14
TiO2	1.26	0.55	0.75	1.28	1.41	1.27	0.99	1.06
Al2O3	18.78	17.70	11.03	17.33	17.26	17.62	17.87	18.32
Fe2O3	8.06	5.79	10.46	10.86	10.68	10.63	6.99	11.05
MnO	0.16	0.15	0.21	0.25	0.24	0.25	0.09	0.25
MgO	2.32	2.49	7.83	4.10	4.21	4.15	2.20	3.76
CaO	5.15	3.93	16.02	8.78	8.92	8.70	2.19	6.11
Na2O	5.33	5.89	1.39	5.36	5.41	5.47	8.85	4.69
K2O	2.72	1.54	0.54	1.51	1.59	1.50	1.29	2.87
P2O5	0.48	0.18	0.12	0.24	0.24	0.24	0.12	0.41
SO3	0.04	0.07	0.02	0.03	0.03	0.03	0.15	0.02
LOI	3.82	2.10	6.38	7.95	7.90	7.95	2.25	1.90
As	20.66	14.59	6.33	17.12	16.64	16.16	10.47	2.03
Ba	840.06	1064.01	301.24	817.60	792.31	791.26	408.72	512.31
Ce	37.48	13.50	26.78	25.11	30.14	32.38	20.11	43.24
Co	22.82	16.89	43.26	37.61	39.93	37.23	22.80	38.16
Cr	11.21	80.75	533.63	47.54	36.46	39.38	28.15	19.06
Cs	1.57	0.68	1.18	2.61	0.06	0.74	n/a	1.79
Cu	7.86	42.31	85.64	215.57	213.44	218.25	70.34	261.62
Ga	18.22	19.95	13.76	19.85	17.84	19.95	16.74	21.61
La	18.07	6.28	0.51	5.00	6.73	5.99	6.77	12.92
Mo	1.36	1.68	1.14	1.03	1.41	2.23	0.95	1.78
Nb	8.05	3.48	1.61	5.09	3.58	3.78	2.49	6.15
Nd	19.31	12.56	8.53	10.72	9.35	13.07	11.32	18.90
Ni	1.34	7.43	137.47	34.41	34.76	35.01	7.58	2.61
Pb	4.78	7.50	4.24	5.39	6.75	6.39	5.97	5.05
Rb	39.87	21.99	10.18	19.37	19.40	19.81	14.67	44.17
Sc	14.20	17.74	47.21	24.54	36.87	36.14	19.64	18.01
Sr	675.10	986.82	259.90	826.47	836.62	835.85	438.30	812.65
Th	1.19	1.01	3.16	3.85	2.66	1.31	7.32	1.53
U	0.63	0.19	0.43	0.91	n/a	2.74	2.18	n/a
V	174.08	135.90	279.95	312.71	315.05	300.75	223.79	303.29
Y	33.40	16.15	19.81	26.15	29.15	28.09	16.39	24.21
Zn	69.57	57.68	74.48	105.02	105.86	108.85	71.08	101.02
Zr	129.81	97.84	50.99	97.05	91.80	94.03	83.79	87.10
Total	99.59	99.83	99.70	99.34	99.43	100.26	98.95	99.57

Sample number	80.13A	80.1A	80.5A	81.10A	81.11A	81.13A	81.19A	81.7A
Bead	LF25978	LF25981	LF25980	LF25982	LF25983	LF25999	LF25991	LF25988
field area	SVLZ	SVLZ	SVLZ	SVLZ	SVLZ	SVLZ	SVLZ	SVLZ
formation	n/a	n/a	n/a	n/a	n/a	n/a	n/a	n/a
SiO2	74.89	79.71	74.02	75.50	69.77	79.54	63.15	63.86
TiO2	0.29	0.07	0.06	0.16	0.32	0.14	1.58	1.11
Al2O3	13.22	10.31	12.09	12.70	15.11	9.79	14.29	15.34
Fe2O3	1.82	0.17	0.89	1.19	2.29	0.52	6.46	6.61
MnO	0.02	0.00	0.09	0.02	0.05	0.01	0.15	0.15
MgO	0.06	0.07	0.10	0.05	0.19	0.11	0.72	0.38
CaO	0.20	0.27	0.26	0.30	0.49	0.31	1.14	0.81
Na2O	5.22	1.23	0.88	4.69	5.41	1.42	5.66	6.41
K2O	4.13	7.43	10.51	5.31	5.97	6.36	4.06	2.12
P2O5	0.08	0.02	0.01	0.05	0.14	0.02	0.58	0.75
SO3	0.03	0.03	0.03	0.04	0.07	0.14	0.05	0.05
LOI	0.87	0.60	0.76	0.77	0.78	0.75	1.66	2.29
As	10.19	32.16	20.90	7.84	1.85	7.29	6.65	36.88
Ba	322.25	414.87	254.19	436.74	110.69	411.38	752.21	641.75
Ce	129.70	57.28	28.87	69.71	50.32	46.47	85.52	58.41
Co	3.65	n/a	n/a	0.22	0.26	n/a	19.63	20.18
Cr	21.66	4.91	21.09	92.75	35.45	0.12	5.12	10.72
Cs	4.58	1.96	n/a	4.17	2.24	1.90	1.19	0.07
Cu	4.58	4.74	6.09	2.57	7.14	4.54	15.21	0.85
Ga	21.90	11.75	13.87	13.91	9.66	11.47	16.52	17.88
La	49.93	28.15	12.05	32.47	23.66	24.67	38.07	28.07
Mo	1.19	6.90	3.20	0.86	2.05	0.98	1.12	3.09
Nb	18.10	6.93	10.22	9.85	8.02	7.59	13.55	8.13
Nd	63.26	24.73	14.80	32.08	23.70	22.94	45.35	30.26
Ni	0.20	3.51	2.87	2.70	3.97	3.33	2.30	4.87
Pb	19.53	12.41	20.67	14.65	14.33	9.20	13.73	13.56
Rb	62.20	117.21	162.67	103.54	20.98	120.76	61.68	33.59
Sc	6.02	3.96	3.06	5.12	4.66	0.80	12.38	12.48
Sr	48.68	65.40	94.51	48.29	107.89	56.19	311.78	153.61
Th	13.96	11.92	10.48	11.85	16.44	11.48	9.04	6.72
U	1.99	2.90	3.82	0.53	3.88	1.98	2.77	0.81
V	17.91	7.00	10.97	10.18	8.71	9.07	103.38	82.72
Y	93.39	10.83	22.91	36.65	23.67	27.40	54.85	38.61
Zn	85.54	9.76	26.63	18.85	30.52	12.74	74.64	69.31
Zr	1017.65	171.95	121.40	266.47	188.49	189.81	486.70	277.60
Total	100.83	99.92	99.71	100.78	100.58	99.10	99.50	99.90

Sample number	52.5A	52.6A	53.12A	53.12A	53.12A	53.17A	53.18A	53.20A
Bead	LF25462	LF25575A	LF25445	LF25446	LF25447	LF25461	LF25466	LF25454
field area	OUVG	OUVG	OUVG	OUVG	OUVG	OUVG	OUVG	OUVG
formation	Gurvan Morin Hondiy	Gurvan Morin Hondiy	Gurvan Morin Hondiy	Gurvan Morin Hondiy	Gurvan Morin Hondiy	Gurvan Morin Hondiy	Gurvan Morin Hondiy	Gurvan Morin Hondiy
SiO2	47.01	53.24	50.70	50.15	50.10	53.93	54.56	53.35
TiO2	0.87	0.74	0.66	0.75	0.68	1.09	0.88	0.89
Al2O3	14.91	19.43	15.73	15.32	15.57	19.63	18.14	17.62
Fe2O3	6.90	7.99	6.61	6.85	6.54	8.63	8.08	7.01
MnO	0.24	0.17	0.09	0.09	0.09	0.25	0.16	0.13
MgO	2.02	2.46	1.60	1.58	1.57	2.17	2.17	3.67
CaO	10.46	4.60	7.70	7.94	7.64	2.91	4.11	6.31
Na2O	4.32	6.72	8.80	8.73	9.04	8.39	7.00	6.86
K2O	4.10	1.66	0.79	0.74	0.81	0.86	1.22	1.38
P2O5	0.77	0.39	0.25	0.25	0.25	0.59	0.41	0.27
SO3	0.05	0.08	0.03	0.03	0.04	0.03	0.04	0.04
LOI	8.33	2.91	6.88	6.85	7.33	2.02	2.75	2.55
As	14.43	17.32	10.25	9.45	10.61	6.42	2.72	2.60
Ba	695.97	675.50	288.09	288.80	302.31	381.74	364.01	1004.74
Ce	46.68	41.94	20.45	24.58	20.56	61.62	37.17	20.16
Co	21.30	24.36	17.70	17.37	17.20	24.83	24.04	22.43
Cr	3.70	n/a	4.48	15.79	14.46	0.24	n/a	77.91
Cs	0.24	n/a	0.92	5.52	n/a	n/a	0.42	n/a
Cu	213.71	169.90	54.88	53.25	55.34	156.57	179.61	39.14
Ga	16.11	20.59	12.65	12.52	13.59	22.96	17.62	21.67
La	15.37	14.15	6.89	6.31	7.06	22.69	14.62	6.64
Mo	1.82	2.08	1.65	0.23	0.98	1.96	1.75	0.69
Nb	7.10	4.72	2.61	2.54	2.05	9.55	6.90	1.83
Nd	24.03	20.06	14.00	15.12	13.51	30.66	18.65	11.60
Ni	n/a	0.13	1.15	3.61	0.92	n/a	n/a	49.27
Pb	1.31	2.03	0.49	3.40	0.58	4.80	2.92	6.08
Rb	54.53	18.64	5.30	6.79	8.29	7.65	9.46	19.69
Sc	20.73	16.01	23.45	22.18	20.00	13.93	13.75	20.27
Sr	824.90	868.86	444.17	443.67	450.56	762.96	283.07	1283.76
Th	7.47	2.90	10.34	4.23	3.38	4.65	2.57	2.51
U	0.97	2.48	0.26	2.01	n/a	n/a	0.36	0.88
V	192.16	160.89	193.97	198.91	195.49	142.09	149.04	219.79
Y	28.32	24.28	21.01	18.83	19.83	36.46	25.54	11.31
Zn	85.95	76.00	59.44	59.04	60.03	101.64	88.11	70.86
Zr	95.98	107.58	77.62	76.05	79.10	152.58	109.11	81.47
Total	99.98	100.38	99.85	99.30	99.67	100.49	99.52	100.08

Sample number	82.11A	82.11A	82.11A	82.5A	83.3A	97.2A	97.3A	97.5A
Bead	LF26005	LF26006	LF26007	LF25984	LF25996	LF25679	LF25635	LF25634
field area	SVLZ	SVLZ	SVLZ	SVLZ	SVLZ	Shuteen	Shuteen	Shuteen
formation	n/a	n/a	n/a	n/a	n/a	n/a	n/a	n/a
SiO2	74.48	73.16	74.61	69.69	60.02	69.19	66.65	76.87
TiO2	0.23	0.26	0.23	0.33	0.81	0.49	0.55	0.22
Al2O3	13.02	12.98	13.06	15.11	16.34	14.70	14.18	12.93
Fe2O3	1.69	1.72	1.68	2.28	6.30	2.90	2.98	1.33
MnO	0.04	0.04	0.04	0.05	0.06	0.05	0.06	0.02
MgO	0.30	0.31	0.26	0.20	1.57	1.36	1.39	0.48
CaO	0.38	0.40	0.37	0.47	1.34	2.48	2.05	0.89
Na2O	7.36	7.95	7.35	5.16	6.56	4.23	4.55	3.46
K2O	1.09	1.21	1.06	5.86	4.24	4.38	4.63	5.09
P2O5	0.25	0.25	0.25	0.14	0.48	0.12	0.12	0.04
SO3	0.12	0.20	0.10	0.06	0.14	0.04	0.05	0.03
LOI	1.19	1.10	1.12	0.89	1.57	0.54	0.79	0.53
As	2.19	1.77	2.07	21.26	1.99	7.66	4.74	2.79
Ba	211.49	218.54	230.85	1545.45	1093.67	776.04	835.52	546.98
Ce	82.00	85.56	86.94	53.87	66.39	39.59	25.64	44.28
Co	2.78	2.97	2.64	2.63	20.59	7.94	8.29	1.64
Cr	37.96	10.08	5.22	27.59	96.86	53.80	60.51	8.37
Cs	1.71	1.81	n/a	0.04	1.05	2.25	n/a	2.51
Cu	4.68	6.47	6.18	3.92	17.27	13.24	5.70	1.06
Ga	24.00	25.39	23.42	15.20	16.85	15.39	16.15	13.16
La	33.57	31.87	33.23	27.90	34.18	17.83	4.45	18.59
Mo	0.73	1.03	1.89	2.78	1.37	1.18	1.20	1.76
Nb	22.35	24.60	24.19	10.92	10.35	4.06	4.79	4.54
Nd	46.16	46.98	46.03	30.00	31.42	14.12	10.55	23.98
Ni	2.23	3.12	2.39	1.84	25.30	9.47	7.92	n/a
Pb	12.73	13.64	11.67	10.08	10.03	13.26	9.48	8.89
Rb	40.95	42.17	41.05	69.58	76.02	113.44	108.52	120.88
Sc	10.13	6.32	5.92	3.06	13.79	5.50	10.12	6.04
Sr	77.30	77.21	76.85	79.68	734.72	412.76	425.61	200.59
Th	18.51	17.99	19.78	8.18	11.50	16.16	13.25	17.58
U	1.12	1.66	2.61	1.45	2.68	0.53	n/a	1.31
V	0.00	3.62	2.36	7.57	127.01	61.79	65.14	21.05
Y	120.96	118.61	120.70	36.49	23.61	8.57	9.59	5.16
Zn	89.15	89.45	88.50	43.48	67.93	38.91	29.28	14.32
Zr	730.79	746.22	728.35	513.98	242.60	141.80	141.74	86.10
Total	100.14	99.56	100.12	100.24	99.42	99.94	98.01	101.36

Sample number	53.9B	54.10A	54.12A	54.13A	54.14A	54.17A	54.18A	54.1A
Bead	LF25463	LF25060	LF25103	LF25102	LF25097	LF25101	LF25098	LF25674
field area	OUVG Gurvan Morin Hondiy	OUVG Gurvan Morin Hondiy	OUVG Gurvan Morin Hondiy	OUVG Gurvan Morin Hondiy	OUVG Gurvan Morin Hondiy	OUVG Gurvan Morin Hondiy	OUVG Gurvan Morin Hondiy	OUVG Gurvan Morin Hondiy
formation								
SiO2	47.37	51.53	57.93	59.34	52.40	53.80	58.60	66.72
TiO2	1.04	0.61	0.76	0.68	0.80	0.94	0.69	0.30
Al2O3	16.58	14.99	16.42	17.37	17.72	18.31	17.03	14.86
Fe2O3	11.54	7.38	6.01	5.52	6.09	7.79	6.50	3.10
MnO	0.16	0.11	0.06	0.10	0.08	0.13	0.10	0.07
MgO	4.84	6.17	3.05	2.44	2.71	3.60	2.79	1.06
CaO	8.09	6.62	3.39	2.89	4.87	2.91	2.50	3.01
Na2O	3.30	4.20	5.69	5.65	8.24	7.10	6.04	5.57
K2O	0.53	0.56	1.73	3.27	0.72	1.98	3.54	1.46
P2O5	0.08	0.28	0.27	0.28	0.28	0.30	0.28	0.09
SO3	0.02	0.12	0.02	0.03	0.03	0.04	0.04	0.03
LOI	6.68	6.09	4.82	2.04	5.93	2.92	2.36	3.28
As	11.48	4.47	3.70	9.14	23.11	13.44	14.15	2.67
Ba	259.96	703.51	673.48	1607.98	173.44	792.03	1204.01	493.02
Ce	27.34	39.94	32.45	30.57	43.47	39.35	39.28	21.06
Co	37.82	27.26	19.01	15.14	18.92	26.76	20.35	9.81
Cr	4.70	575.35	145.96	19.09	72.70	31.98	120.54	125.50
Cs	3.35	6.91	2.53	n/a	n/a	0.79	0.73	n/a
Cu	39.45	70.18	26.18	22.55	166.95	172.42	65.83	4.05
Ga	18.42	17.28	20.12	19.06	21.79	22.80	19.95	15.02
La	5.76	13.93	13.50	14.15	15.63	14.15	13.39	9.31
Mo	1.82	2.24	2.27	0.57	1.17	2.13	1.83	2.55
Nb	0.55	2.75	3.77	3.21	2.66	3.82	1.08	3.31
Nd	8.63	17.61	16.43	16.18	15.35	18.69	14.26	10.54
Ni	5.82	125.13	8.74	7.90	12.40	9.44	16.07	0.36
Pb	2.87	2.37	8.42	7.82	12.56	7.02	8.47	7.37
Rb	8.49	11.58	33.73	53.80	13.04	30.06	47.19	20.86
Sc	29.34	26.71	12.93	8.49	15.92	18.10	17.10	8.83
Sr	430.36	1036.16	835.65	1987.42	494.47	1130.79	756.09	772.21
Th	5.18	6.67	5.36	3.66	5.83	5.83	4.03	13.33
U	1.05	1.13	0.05	0.86	1.74	n/a	2.25	0.31
V	305.25	204.20	185.77	174.47	188.35	197.72	191.38	80.23
Y	17.60	11.97	11.79	9.89	16.20	11.14	12.71	10.32
Zn	89.51	66.91	64.43	56.59	74.03	85.93	61.63	28.93
Zr	61.41	113.63	111.52	115.83	116.50	113.03	106.68	121.68
Total	100.23	98.69	100.14	99.60	99.87	99.82	100.48	99.56

Sample number	97.6A	97.6A	97.7A	97.8A	70.11A	22/08_14	22/08_14	22/08_14
Bead	LF25626	LF25628	LF25636	LF25638	LF25987	LF22795	LF22799	LF22800
field area	Shuteen	Shuteen	Shuteen	Shuteen	Dyke in Northern Slate Belt	Sheeted quartz vein complex	Sheeted quartz vein complex	Sheeted quartz vein complex
formation	n/a	n/a	n/a	n/a	n/a	n/a	n/a	n/a
SiO2	77.37	75.29	71.10	68.41	52.51	63.26	63.17	63.74
TiO2	0.23	0.22	0.42	0.45	2.29	0.60	0.60	0.58
Al2O3	12.97	12.73	14.44	13.83	14.77	16.31	16.37	16.65
Fe2O3	1.28	1.31	2.62	2.75	10.85	4.55	4.62	4.54
MnO	0.02	0.02	0.05	0.05	0.19	0.07	0.08	0.07
MgO	0.48	0.48	1.21	1.16	5.52	2.37	2.37	2.32
CaO	0.91	0.93	2.24	1.92	5.66	3.59	3.59	3.57
Na2O	3.39	3.53	4.03	4.21	4.39	4.86	4.85	4.94
K2O	5.09	5.12	4.53	4.76	1.95	3.46	3.40	3.39
P2O5	0.04	0.04	0.11	0.13	0.35	0.23	0.23	0.22
SO3	0.00	0.01	0.00	0.02	0.13	0.24	0.01	0.05
LOI	0.45	0.48	0.49	0.72	2.30	0.54	0.50	0.52
As	2.61	3.28	5.20	3.13	2.69	5.15	8.20	5.64
Ba	571.02	566.94	728.28	744.59	435.25	1338.88	970.18	812.13
Ce	5.07	11.71	50.03	38.42	67.32	207.14	25.22	32.37
Co	2.55	2.69	6.56	5.49	42.30	31.16	11.20	15.61
Cr	1.99	38.55	24.67	22.48	150.85	n/a	12.28	51.44
Cs	4.83	4.59	n/a	n/a	n/a	1.11	4.49	n/a
Cu	7.04	6.66	26.36	13.99	26.57	36.72	152.27	43.05
Ga	13.55	13.24	14.70	16.23	19.60	24.56	19.99	18.87
La	6.85	4.93	21.13	14.64	19.86	90.78	16.24	19.27
Mo	2.62	2.02	2.07	1.69	1.03	2.78	2.05	1.19
Nb	4.35	4.88	3.90	6.27	9.99	29.07	2.49	5.41
Nd	6.41	6.34	25.23	19.49	36.47	100.48	15.13	17.70
Ni	n/a	n/a	13.52	8.35	40.06	10.17	8.69	31.13
Pb	9.36	8.36	10.52	5.79	1.86	15.73	6.80	5.20
Rb	120.77	121.53	115.55	119.40	43.94	69.44	64.46	37.31
Sc	n/a	0.87	10.75	12.29	36.45	15.54	11.15	12.20
Sr	199.87	202.92	369.60	377.02	454.83	1123.28	1112.63	1166.94
Th	18.50	16.63	18.74	10.97	7.33	12.39	13.39	4.90
U	0.27	1.56	0.16	0.61	n/a	3.14	2.78	1.35
V	27.59	26.46	54.88	59.89	226.86	190.89	129.04	106.60
Y	1.51	2.40	7.25	8.67	62.43	34.93	7.95	10.27
Zn	15.45	13.42	52.73	21.94	99.17	152.05	43.85	70.60
Zr	95.74	90.40	133.73	136.23	406.44	527.13	139.11	159.94
Total	101.78	99.68	100.75	98.39	100.90	100.07	99.78	100.59

Sample locality	Sample number	field area	Sample formation or secondary descriptor	UTM	EASTING	NORTHING
BFD024	BFD024B	Bronze Fox	n/a	48T	727700	4883000
BFD024	BFD024C	Bronze Fox	n/a	48T	727700	4883000
BFD002	BFD002F	Bronze Fox	n/a	48T	727700	4883000
BFD024	BFD024D	Bronze Fox	n/a	48T	727700	4883000
BFD002	BFD002G	Bronze Fox	n/a	48T	727700	4883000
51.1	51.1A	Mandakh	n/a	48T	730145	4906700
51.1	51.1A	Mandakh	n/a	48T	730145	4906700
51.6	51.6A	Mandakh	n/a	49T	282756	4925067
51.4	51.4A	Mandakh	n/a	49T	279566	4919940
51.2	51.2B	Mandakh	n/a	48T	730238	4906697
51.7	51.7A	Mandakh	n/a	49T	282789	4925132
51.4	51.4B	Mandakh	n/a	49T	279566	4919940
51.5	51.5A	Mandakh	n/a	49T	281056	4921196
41.4	17/08_6	Mesozoic basalts	n/a	49T	329450	4960446
36.8	11/08_2	Mesozoic basalts	n/a	49T	332239	4961451
78.3	78.3A	Molasse	n/a	49T	371370	4945604
JBSP004	JBSP004	Narin Hudag	n/a	49T	267843	4910997
JBSP004	JBSP004	Narin Hudag	n/a	49T	267843	4910997
JBSP004	JBSP004	Narin Hudag	n/a	49T	267843	4910997
JBSP006	JBSP006	Narin Hudag	n/a	49T	267576	4910916
JBSP001	JBSP001	Narin Hudag	n/a	49T	267960	4911116
JBSP005	JBSP005	Narin Hudag	n/a	49T	267834	4910968
JBSP003	JBSP003	Narin Hudag	n/a	49T	267844	4910998
JBSP008	JBSP008	Narin Hudag	n/a	49T	263912	4902566
JBSP007	JBSP007	Narin Hudag	n/a	49T	266779	4911450
JBSP010	JBSP010	Narin Hudag	n/a	49T	264232	4902759
JBSP010	JBSP010	Narin Hudag	n/a	49T	264232	4902759
JBSP010	JBSP010	Narin Hudag	n/a	49T	264232	4902759
23.10	27/07_5	North Eastern Intrusion	n/a	49T	389947	4953141
46.4	22/08_9	Oyut Ulaan	n/a	49T	380649	4936829
46.4	22/08_9	Oyut Ulaan	n/a	49T	380649	4936829
46.7	22/08_11	Oyut Ulaan	n/a	49T	379899	4936765
46.12	22/08_15	Oyut Ulaan	n/a	49T	375316	4937921
46.12	22/08_15	Oyut Ulaan	n/a	49T	375316	4937921
46.9	22/08_13	Oyut Ulaan	n/a	49T	378399	4936135
46.12	22/08_15	Oyut Ulaan	n/a	49T	375316	4937921
46.9	22/08_13	Oyut Ulaan	n/a	49T	378399	4936135
46.9	22/08_13	Oyut Ulaan	n/a	49T	378399	4936135
46.7	22/08_11	Oyut Ulaan	n/a	49T	379899	4936765
46.7	22/08_11	Oyut Ulaan	n/a	49T	379899	4936765
46.4	22/08_9	Oyut Ulaan	n/a	49T	380649	4936829
88.3	88.3A	Oyut Ulaan	n/a	49T	377966	4936864
88.3	88.3A	Oyut Ulaan	n/a	49T	377966	4936864
88.3	88.3A	Oyut Ulaan	n/a	49T	377966	4936864
66.20	66.20A	Oyut Ulaan	n/a	49T	377017	4937003
66.20	66.20A	Oyut Ulaan	n/a	49T	377017	4937003
88.2	88.2A	Oyut Ulaan	n/a	49T	375708	4937420
66.21	66.21A	Oyut Ulaan	n/a	49T	375857	4936480
65.6	65.6A	Oyut Ulaan	n/a	49T	378807	4937481
65.1	65.1A	Oyut Ulaan	n/a	49T	373695	4939189
62.7	62.7A	Oyut Ulaan	n/a	49T	380196	4937050
62.16	62.16A	Oyut Ulaan	n/a	49T	379101	4937440
62.3	62.3A	Oyut Ulaan	n/a	49T	381155	4938241
62.10	62.10A	Oyut Ulaan	n/a	49T	379350	4937055
62.5	62.5A	Oyut Ulaan	n/a	49T	381786	4937507
60.13	60.13B	Oyut Ulaan	n/a	49T	380599	4936958
65.12	65.12A	Oyut Ulaan	n/a	49T	378627	4938181
61.7	61.7A	Oyut Ulaan	n/a	49T	375388	4936878
65.3	65.3A	Oyut Ulaan	n/a	49T	373261	4936907
65.14	65.14A	Oyut Ulaan	n/a	49T	377179	4938161
65.14	65.14A	Oyut Ulaan	n/a	49T	377179	4938161
65.14	65.14A	Oyut Ulaan	n/a	49T	377179	4938161
46.8	22/08_12	Oyut Ulaan	dyke	49T	379278	4936793
46.5	22/08_10	Oyut Ulaan	dyke	49T	380578	4936774
60.9	60.9A	Oyut Ulaan	dyke	49T	380496	4936742
60.9	60.9A	Oyut Ulaan	dyke	49T	380496	4936742
60.7	60.7A	Oyut Ulaan	dyke	49T	380577	4936833
67.4	67.4A	Oyut Ulaan	dyke	49T	379457	4937059
46.5	22/08_10	Oyut Ulaan	dyke	49T	380578	4936774
67.7	67.7A	Oyut Ulaan	dyke	49T	380995	4936882
67.5	67.5A	Oyut Ulaan	dyke	49T	379491	4937736
60.12	60.12B	Oyut Ulaan	dyke	49T	380362	4936670
67.5	67.5B	Oyut Ulaan	dyke	49T	379491	4937736

Sample locality	Sample number	field area	Sample formation or secondary descriptor	UTM	EASTING	NORTHING
90.9	90.9B	Oyut Ulaan	dyke	49T	378246	4936839
60.12	60.12A	Oyut Ulaan	dyke	49T	380362	4936670
60.22	60.22A	Oyut Ulaan	dyke	49T	380423	4938124
67.4	67.4B	Oyut Ulaan	dyke	49T	379457	4937059
68.1	68.1A	Oyut Ulaan Contact Zone	n/a	49T	380683	4936351
88.7	88.7A	Oyut Ulaan Volcanic Group	Dead vulture	49T	372340	4937358
88.9	88.9A	Oyut Ulaan Volcanic Group	Dead vulture	49T	372350	4937426
88.10	88.10A	Oyut Ulaan Volcanic Group	Dead vulture	49T	372374	4937646
88.17	88.17A	Oyut Ulaan Volcanic Group	Dead vulture	49T	372376	4938362
88.12	88.12A	Oyut Ulaan Volcanic Group	Dead vulture	49T	372360	4937748
88.12	88.12A	Oyut Ulaan Volcanic Group	Dead vulture	49T	372360	4937748
88.12	88.12A	Oyut Ulaan Volcanic Group	Dead vulture	49T	372360	4937748
89.10	89.10A	Oyut Ulaan Volcanic Group	Dead vulture	49T	371615	4939093
89.3	89.3A	Oyut Ulaan Volcanic Group	Dead vulture	49T	372301	4938518
89.9	89.9A	Oyut Ulaan Volcanic Group	Dead vulture	49T	371700	4938972
89.1	89.1A	Oyut Ulaan Volcanic Group	Dead vulture	49T	372357	4938407
89.6	89.6C	Oyut Ulaan Volcanic Group	Dead vulture	49T	371917	4938701
89.14	89.14A	Oyut Ulaan Volcanic Group	Dead vulture	49T	371417	4939330
89.10	89.10A	Oyut Ulaan Volcanic Group	Dead vulture	49T	371615	4939093
89.10	89.10A	Oyut Ulaan Volcanic Group	Dead vulture	49T	371615	4939093
89.9	89.9B	Oyut Ulaan Volcanic Group	Dead vulture	49T	371700	4938972
89.9	89.9B	Oyut Ulaan Volcanic Group	Dead vulture	49T	371700	4938972
89.9	89.9B	Oyut Ulaan Volcanic Group	Dead vulture	49T	371700	4938972
89.6	89.6B	Oyut Ulaan Volcanic Group	Dead vulture	49T	371917	4938701
89.12	89.12A	Oyut Ulaan Volcanic Group	Dead vulture	49T	371562	4939128
89.15	89.15A	Oyut Ulaan Volcanic Group	Dead vulture	49T	371656	4940207
89.4	89.4A	Oyut Ulaan Volcanic Group	Dead vulture	49T	372028	4938638
89.11	89.11A	Oyut Ulaan Volcanic Group	Dead vulture	49T	371544	4939144
89.8	89.8A	Oyut Ulaan Volcanic Group	Dead vulture	49T	371872	4938794
55.1	55.1A	Oyut Ulaan Volcanic Group	Three Horse Valley	49T	355577	4939715
55.8	55.8A	Oyut Ulaan Volcanic Group	Three Horse Valley	49T	355522	4939545
55.18	55.18A	Oyut Ulaan Volcanic Group	Three Horse Valley	49T	355612	4939296
54.3	54.3A	Oyut Ulaan Volcanic Group	Three Horse Valley	49T	355315	4940510
54.1	54.10A	Oyut Ulaan Volcanic Group	Three Horse Valley	49T	355338	4940928
54.7i	54.6A	Oyut Ulaan Volcanic Group	Three Horse Valley	49T	355378	4940335
55.12	55.12A	Oyut Ulaan Volcanic Group	Three Horse Valley	49T	355505	4939423
55.17	55.17A	Oyut Ulaan Volcanic Group	Three Horse Valley	49T	355567	4939312
55.14	55.14A	Oyut Ulaan Volcanic Group	Three Horse Valley	49T	355525	4939392
55.2	55.20A	Oyut Ulaan Volcanic Group	Three Horse Valley	49T	355580	4939734
55.4	55.4A	Oyut Ulaan Volcanic Group	Three Horse Valley	49T	355529	4939589
54.20	54.20A	Oyut Ulaan Volcanic Group	Three Horse Valley	49T	355571	4939741
54.14	54.14A	Oyut Ulaan Volcanic Group	Three Horse Valley	49T	355331	4939942
54.18	54.18A	Oyut Ulaan Volcanic Group	Three Horse Valley	49T	355544	4939796
55.3	55.3A	Oyut Ulaan Volcanic Group	Three Horse Valley	49T	355560	4939631
54.17	54.17A	Oyut Ulaan Volcanic Group	Three Horse Valley	49T	355532	4939858
54.13	54.13A	Oyut Ulaan Volcanic Group	Three Horse Valley	49T	355309	4939960
54.12	54.12A	Oyut Ulaan Volcanic Group	Three Horse Valley	49T	355285	4939959
55.1	55.1C	Oyut Ulaan Volcanic Group	Three Horse Valley	49T	355577	4939715
55.1	55.1B	Oyut Ulaan Volcanic Group	Three Horse Valley	49T	355577	4939715
55.1	55.1B	Oyut Ulaan Volcanic Group	Three Horse Valley	49T	355577	4939715
55.1	55.1B	Oyut Ulaan Volcanic Group	Three Horse Valley	49T	355577	4939715
53.12	53.12A	Oyut Ulaan Volcanic Group	Three Horse Valley	49T	355343	4941288
53.12	53.12A	Oyut Ulaan Volcanic Group	Three Horse Valley	49T	355343	4941288
53.12	53.12A	Oyut Ulaan Volcanic Group	Three Horse Valley	49T	355343	4941288
53.20	53.20A	Oyut Ulaan Volcanic Group	Three Horse Valley	49T	355338	4940861
52.3	52.3A	Oyut Ulaan Volcanic Group	Three Horse Valley	49T	355358	4941838
52.12	52.12A	Oyut Ulaan Volcanic Group	Three Horse Valley	49T	355538	4941699
53.17	53.17A	Oyut Ulaan Volcanic Group	Three Horse Valley	49T	355374	4941015
52.5	52.5A	Oyut Ulaan Volcanic Group	Three Horse Valley	49T	355554	4941857
53.9	53.9B	Oyut Ulaan Volcanic Group	Three Horse Valley	49T	355354	4941406
55.18	55.18B	Oyut Ulaan Volcanic Group	Three Horse Valley	49T	355612	4939296
55.9	55.9A	Oyut Ulaan Volcanic Group	Three Horse Valley	49T	355512	4939466
53.18	53.18A	Oyut Ulaan Volcanic Group	Three Horse Valley	49T	355325	4940978
55.6	55.6A	Oyut Ulaan Volcanic Group	Three Horse Valley	49T	355507	4939594
55.13	55.13A	Oyut Ulaan Volcanic Group	Three Horse Valley	49T	355518	4939400
55.8	55.8B	Oyut Ulaan Volcanic Group	Three Horse Valley	49T	355522	4939545
55.19	55.19A	Oyut Ulaan Volcanic Group	Three Horse Valley	49T	355612	4939276
55.19	55.19A	Oyut Ulaan Volcanic Group	Three Horse Valley	49T	355612	4939276
52.6	52.6A	Oyut Ulaan Volcanic Group	Three Horse Valley	49T	355574	4941844
54.1	54.1A	Oyut Ulaan Volcanic Group	Three Horse Valley	49T	355338	4940928
55.23	55.22A	Oyut Ulaan Volcanic Group	Three Horse Valley	49T	355801	4939019
28.9	3/08_6	Oyut Ulaan Volcanic Group	Tsagaan Nuruu	49T	343895	4941174
95.3	95.3A	Oyut Ulaan Volcanic Group	Tsagaan Nuruu	49T	342609	4941517

Sample locality	Sample number	field area	Sample formation or secondary descriptor	UTM	EASTING	NORTHING
91.4	91.4D	Oyut Ulaan Volcanic Group	Tsagaan Nuruu	49T	341463	4942031
95.7	95.7A	Oyut Ulaan Volcanic Group	Tsagaan Nuruu	49T	342301	4941709
91.2	91.2A	Oyut Ulaan Volcanic Group	Tsagaan Nuruu	49T	341464	4941974
91.3	91.3A	Oyut Ulaan Volcanic Group	Tsagaan Nuruu	49T	341465	4941999
91.4	91.4C	Oyut Ulaan Volcanic Group	Tsagaan Nuruu	49T	341463	4942031
91.3	91.3B	Oyut Ulaan Volcanic Group	Tsagaan Nuruu	49T	341465	4941999
56.2	56.2A	Oyut Ulaan Volcanic Group	Tsagaan Nuruu	49T	341866	4940639
95.10	95.10A	Oyut Ulaan Volcanic Group	Tsagaan Nuruu	49T	341923	4941715
95.1	95.1A	Oyut Ulaan Volcanic Group	Tsagaan Nuruu	49T	342612	4941497
95.11	95.11A	Oyut Ulaan Volcanic Group	Tsagaan Nuruu	49T	341874	4941780
95.5	95.5A	Oyut Ulaan Volcanic Group	Tsagaan Nuruu	49T	342558	4941588
55.25	55.24B	Oyut Ulaan Volcanic Group	Tsagaan Nuruu	49T	342303	4941710
28.4	3/08_2	Oyut Ulaan Volcanic Group	Yellow Snake	49T	343612	4939628
6.6	8/07_3	Oyut Ulaan Volcanic Group	Yellow Snake	49T	341758	4938930
26.2	31/07_1	Oyut Ulaan Volcanic Group	Yellow Snake	49T	344542	4937513
28.4	3/08_2	Oyut Ulaan Volcanic Group	Yellow Snake	49T	343612	4939628
28.1	3/08_1	Oyut Ulaan Volcanic Group	Yellow Snake	49T	343139	4938787
26.2	31/07_3	Oyut Ulaan Volcanic Group	Yellow Snake	49T	344542	4937513
26.2	31/07_2	Oyut Ulaan Volcanic Group	Yellow Snake	49T	344542	4937513
28.1	3/08_1	Oyut Ulaan Volcanic Group	Yellow Snake	49T	343139	4938787
56.16	56.16A	Oyut Ulaan Volcanic Group	Yellow Snake	49T	342401	4939328
56.14	56.14A	Oyut Ulaan Volcanic Group	Yellow Snake	49T	342432	4939309
56.15	56.15A	Oyut Ulaan Volcanic Group	Yellow Snake	49T	342424	4939313
56.15	56.15B	Oyut Ulaan Volcanic Group	Yellow Snake	49T	342424	4939313
56.17	56.17A	Oyut Ulaan Volcanic Group	Yellow Snake	49T	343535	4937498
56.6	56.6A	Oyut Ulaan Volcanic Group	Yellow Snake	49T	341932	4940096
93.10	93.10A	Oyut Ulaan Volcanic Group	Yellow Snake	49T	349960	4939739
93.10	93.10A	Oyut Ulaan Volcanic Group	Yellow Snake	49T	349960	4939739
56.13	56.13A	Oyut Ulaan Volcanic Group	Yellow Snake	49T	342450	4939258
93.10	93.10A	Oyut Ulaan Volcanic Group	Yellow Snake	49T	349960	4939739
56.9	56.9A	Oyut Ulaan Volcanic Group	Yellow Snake	49T	342553	4939235
56.7	56.7A	Oyut Ulaan Volcanic Group	Yellow Snake	49T	341917	4940138
56.4	56.4B	Oyut Ulaan Volcanic Group	Yellow Snake	49T	341860	4940373
56.9	56.9B	Oyut Ulaan Volcanic Group	Yellow Snake	49T	342553	4939235
56.4	56.4A	Oyut Ulaan Volcanic Group	Yellow Snake	49T	341860	4940373
56.3	56.3B	Oyut Ulaan Volcanic Group	Yellow Snake	49T	342017	4940248
56.9	56.9A	Oyut Ulaan Volcanic Group	Yellow Snake	49T	342553	4939235
56.9	56.9A	Oyut Ulaan Volcanic Group	Yellow Snake	49T	342553	4939235
96.2	96.2B	Oyut Ulaan Volcanic Group	Yellow Snake	49T	343759	4939686
96.4	96.4A	Oyut Ulaan Volcanic Group	Yellow Snake	49T	343698	4939787
93.15	93.15A	Oyut Ulaan Volcanic Group	Yellow Snake	49T	348955	4941952
93.15	93.15A	Oyut Ulaan Volcanic Group	Yellow Snake	49T	348955	4941952
93.15	93.15A	Oyut Ulaan Volcanic Group	Yellow Snake	49T	348955	4941952
56.5	56.5A	Oyut Ulaan Volcanic Group	Yellow Snake	49T	341913	4940074
56.5	56.5A	Oyut Ulaan Volcanic Group	Yellow Snake	49T	341913	4940074
56.5	56.5A	Oyut Ulaan Volcanic Group	Yellow Snake	49T	341913	4940074
93.12	93.12A	Oyut Ulaan Volcanic Group	Yellow Snake	49T	349684	4939171
93.12	93.12A	Oyut Ulaan Volcanic Group	Yellow Snake	49T	349684	4939171
93.12	93.12A	Oyut Ulaan Volcanic Group	Yellow Snake	49T	349684	4939171
56.3	56.3A	Oyut Ulaan Volcanic Group	Yellow Snake	49T	342017	4940248
56.10	56.10A	Oyut Ulaan Volcanic Group	Yellow Snake	49T	342399	4939133
93.15	93.15C	Oyut Ulaan Volcanic Group	Yellow Snake	49T	348955	4941952
96.7	96.7A	Oyut Ulaan Volcanic Group	Yellow Snake	49T	343651	4939934
56.8	56.8A	Oyut Ulaan Volcanic Group	Yellow Snake	49T	342532	4939190
96.6	96.6A	Oyut Ulaan Volcanic Group	Yellow Snake	49T	343663	4939840
96.9	96.9A	Oyut Ulaan Volcanic Group	Yellow Snake	49T	343478	4940309
96.5	96.5A	Oyut Ulaan Volcanic Group	Yellow Snake	49T	343683	4939809
96.9	96.9B	Oyut Ulaan Volcanic Group	Yellow Snake	49T	343478	4940309
96.8	96.8B	Oyut Ulaan Volcanic Group	Yellow Snake	49T	343493	4940269
96.2	96.2A	Oyut Ulaan Volcanic Group	Yellow Snake	49T	343759	4939686
42.9	18/08_3	Saykhandulaan valley	n/a	49T	352612	4950925
42.16	18/08_5	Saykhandulaan valley	n/a	49T	351946	4950405
42.3	18/08_2	Saykhandulaan valley	n/a	49T	353099	4951063
43.1	19/08_1	Saykhandulaan valley	n/a	49T	351971	4949613
33.1	8/08_1	Saykhandulaan valley	n/a	49T	342776	4949066
33.9	8/08_5	Saykhandulaan valley	n/a	49T	343163	4942475
33.2	8/08_2	Saykhandulaan valley	n/a	49T	342591	4949144
80.13	80.13A	Saykhandulaan valley	n/a	49T	354599	4950867
79.12	79.12A	Saykhandulaan valley	n/a	49T	341310	4948749
80.5	80.5A	Saykhandulaan valley	n/a	49T	341679	4948911
80.1	80.1A	Saykhandulaan valley	n/a	49T	341457	4948837
81.10	81.10A	Saykhandulaan valley	n/a	49T	342489	4949052
81.11	81.11A	Saykhandulaan valley	n/a	49T	342576	4949143

Sample locality	Sample number	field area	Sample formation or secondary descriptor	UTM	EASTING	NORTHING
82.5	82.5A	Saykhandulaan valley	n/a	49T	343212	4949942
81.7	81.7A	Saykhandulaan valley	n/a	49T	342100	4949041
79.11	79.11A	Saykhandulaan valley	n/a	49T	341277	4948660
81.19	81.19A	Saykhandulaan valley	n/a	49T	344018	4949922
83.3	83.3A	Saykhandulaan valley	n/a	49T	346260	4950536
81.13	81.13A	Saykhandulaan valley	n/a	49T	342493	4949079
82.11	82.11A	Saykhandulaan valley	n/a	49T	345342	4950506
82.11	82.11A	Saykhandulaan valley	n/a	49T	345342	4950506
82.11	82.11A	Saykhandulaan valley	n/a	49T	345342	4950506
97.6	97.6A	Shuteen	n/a	48T	715785	4867022
97.6	97.6A	Shuteen	n/a	48T	715785	4867022
97.5	97.5A	Shuteen	n/a	48T	714578	4866098
97.3	97.3A	Shuteen	n/a	48T	714149	4866052
97.7	97.7A	Shuteen	n/a	48T	713625	4865861
97.8	97.8A	Shuteen	n/a	48T	713332	4865612
97.2	97.2A	Shuteen	n/a	48T	714092	4865539
70.11	70.11A	Slate Belt	n/a	49T	342024	4955444
46.1	22/08_14	South East Target	n/a	49T	381062	4937003
46.1	22/08_14	South East Target	n/a	49T	381062	4937003
46.1	22/08_14	South East Target	n/a	49T	381062	4937003

Appendix B

U-Pb isotopic analyses results

Sample Number	88:3A	88:3A	88:3A	88:3A	51:7A
Unique ID	1992	1993	1994	1995	2006
Fraction Code	Z-1	Z-2	Z-3	Z-4	Z-6
chemistry code	148-01	148-02	148-03	148-04	148-05
Sample Weight (µg)	6.3	3.7	7.5	4.0	5.0
Spike Weight (g)	0.0025	0.0025	0.0025	0.0025	0.0025
$^{206}Pb/^{208}Pb$	2.5872	2.6500	2.4956	3.4303	4.3494
2σ % error	0.043	0.055	0.020	0.043	0.031
$^{206}Pb/^{207}Pb$	7.2195	7.1843	6.8372	9.8690	12.7973
2σ % error	0.074	0.078	0.040	0.049	0.039
$^{206}Pb/^{205}Pb$	0.6181	0.6461	0.6927	1.1191	1.7150
2σ % error	0.035	0.035	0.020	0.022	0.018
$^{206}Pb/^{204}Pb$	164.6010	163.6560	151.4908	291.6760	550.4980
2σ % error	0.152	0.188	0.100	0.147	0.175
$^{238}U/^{235}U$	0.0919	0.0951	0.1070	0.1789	0.2076
2σ % error	0.184	0.258	0.110	0.181	0.076
Pb Blank	2.0	2.0	2.0	2.0	2.0
U Blank	4.5	4.5	4.5	4.5	4.5
Stacey & Kramer, 1975					
model Pb age	328	329	329	329	300
64c	18.1949	18.1933	18.1933	18.1933	18.2393
74c	15.6019	15.6018	15.6018	15.6018	15.6046
84c	38.0278	38.0260	38.0260	38.0260	38.0797
BlankUsed	2.0000	2.0000	2.0000	2.0000	2.0000
Common Pb	2.0849	2.4385	3.5870	2.2346	0.9095
Total Pb C	4.0849	4.4385	5.5870	4.2346	2.9095
Pb ppm	2.8340	5.0795	2.8170	8.3435	10.1180
U ppm	45.1631	79.6622	44.3574	140.2306	130.4238
Pb206U238	0.0520	0.0526	0.0497	0.0524	0.0724
Pb206U238err	0.3251	0.3680	0.2676	0.2658	0.1913
Pb206U238errA	16.8935	19.3521	13.2982	13.9311	13.8570
Pb206U238age	326.5876	330.4117	312.6667	329.3681	450.7178
Pb207U235	0.3817	0.3865	0.3626	0.3845	0.5279
Pb207U235err	0.4538	0.5156	0.3904	0.3156	0.2170
Pb207U235errA	17.3232	19.9284	14.1543	12.1340	11.4583
Pb207U235age	328.2968	331.7977	314.1552	330.3325	430.4305
Pb207Pb206	0.0533	0.0533	0.0529	0.0532	0.0529
Pb207Pb206err	0.3073	0.3486	0.2744	0.1655	0.1006
Pb207Pb206errA	16.3694	18.5819	14.5225	8.8043	5.3200
Pb207Pb206age	340.4370	341.5342	325.2212	337.1383	323.2444
Pb207Pb206ageerr	6.9575	7.8925	6.2309	3.7497	2.2853
Pb206Pb204	464.5249	418.2556	308.2676	846.3067	3290.6546
Pb208Pb206	0.1861	0.1730	0.1801	0.1776	0.1698
Rho	0.7362	0.7372	0.7116	0.8515	0.8861
Description	U from Pb fraction	U from Pb fraction	U from Pb fraction	U from Pb fraction	U from Pb fractios

Sample Number	JBSP010	JBSP010	JBSP010	JBSP010	97.2A
Unique ID	2015	2016	2017	2018	2023
Fraction Code	Z-9	Z-10	Z-11	Z-12	Z-13
chemistry code	148-09	148-10	148-11	148-12	148-13
Sample Weight (µg)	14.4	11.6	18.0	11.0	3.8
Spike Weight (g)	0.0025	0.0025	0.0025	0.0025	0.0025
$^{206}Pb/^{208}Pb$	5.5447	5.3950	5.7205	5.7015	2.1773
2σ % error	0.027	0.034	0.041	0.094	0.064
$^{206}Pb/^{207}Pb$	16.3820	15.7812	16.5984	16.6039	6.8878
2σ % error	0.060	0.041	0.074	0.930	0.081
$^{206}Pb/^{205}Pb$	6.1720	5.1343	5.3126	4.9472	0.5811
2σ % error	0.023	0.017	0.053	0.090	0.030
$^{206}Pb/^{204}Pb$	1761.2140	1290.8170	1945.3750	150.1020	150.1020
2σ % error	0.285	0.112	0.402	0.357	0.154
$^{238}U/^{235}U$	0.8858	0.8817	0.9242	0.0860	0.0923
2σ % error	0.161	0.060	0.236	0.127	0.300
Pb Blank	2.0	2.0	2.0	2.0	2.0
U Blank	4.5	4.5	4.5	4.5	4.2
Stacey & Kramer, 1975					
model Pb age	330	333	334	326	236
64c	18.1917	18.1869	18.1854	18.1981	18.3401
74c	15.6017	15.6014	15.6013	15.6021	15.6104
84c	38.0241	38.0186	38.0167	38.0315	38.1979
BlankUsed	2.0000	2.0000	2.0000	2.0000	2.0000
Common Pb	1.6234	2.4928	0.2013	55.7824	2.3085
Total Pb C	3.6234	4.4928	2.2013	57.7824	4.3085
Pb ppm	12.9912	13.4128	8.8512	13.5252	4.6331
U ppm	195.6985	241.8099	163.4045	24.1810	75.2828
Pb206U238	0.0630	0.0523	0.0519	0.4735	0.0477
Pb206U238err	0.2287	0.1717	0.2916	0.2467	0.4098
Pb206U238errA	14.4012	8.9906	15.1410	116.8426	19.5345
Pb206U238age	393.6725	328.9226	326.3105	2499.0066	300.1628
Pb207U235	0.4614	0.3789	0.3807	0.0000	0.3363
Pb207U235err	0.2459	0.1884	0.3081	1.4733	0.5564
Pb207U235errA	11.3453	7.1374	11.7301	0.0000	18.7137
Pb207U235age	385.2218	326.2322	327.5825	0.0000	294.3740
Pb207Pb206	0.0531	0.0525	0.0532	-0.0500	0.0512
Pb207Pb206err	0.0898	0.0770	0.0990	1.4824	0.3651
Pb207Pb206errA	4.7741	4.0446	5.2645	-74.1832	18.6827
Pb207Pb206age	334.7696	307.0870	336.6365	0.0000	248.6967
Pb207Pb206ageerr	2.0363	1.7549	2.2429	0.0000	8.4033
Pb206Pb204	6897.3312	3724.4647	47752.9673	160.3172	391.7250
Pb208Pb206	0.1615	0.1594	0.1579	-0.0894	0.2520
Rho	0.9309	0.9125	0.9470	0.0469	0.7549

Description	U from Pb fraction	U from Pb fraction	U from Pb fraction	U from Pb fraction	U from Pb fraction

Sample Number	97.2A	97.2A	97.2A	95.3A	95.3A
Unique ID	2054	2055	2056	2024	2025
Fraction Code	Z-14	Z-15	Z-16	Z-17	Z-18
chemistry code	148-14	148-15	148-16	148-17	148-18
Sample Weight (µg)	0.0	0.7	0.0	2.8	1.0
Spike Weight (g)	0.0025	0.0025	0.0025	0.0025	0.0025
$^{206}Pb/^{208}Pb$	2.3357	2.4437	1.7870	2.9087	0.9372
2σ % error	0.122	0.105	0.103	0.041	0.123
$^{206}Pb/^{207}Pb$	6.6422	7.1617	4.9341	10.5687	2.3057
2σ % error	0.118	0.148	0.148	0.078	0.154
$^{206}Pb/^{205}Pb$	0.3326	0.3483	0.2106	0.8583	0.0896
2σ % error	0.050	0.061	0.062	0.033	0.123
$^{206}Pb/^{204}Pb$	141.6210	157.8420	91.5560	332.5710	35.2090
2σ % error	0.232	0.334	0.289	0.216	0.286
$^{238}U/^{235}U$	0.0454	0.0487	0.0242	0.1399	0.0024
2σ % error	0.069	0.178	0.281	0.093	0.900
Pb Blank	2.0	2.0	2.0	2.0	2.0
U Blank	4.5	4.5	4.5	4.5	4.5
Stacey & Kramer, 1975					
model Pb age	330	338	321	323	
64c	18.1917	18.1790	18.2060	18.2028	
74c	15.6017	15.6009	15.6026	15.6024	
84c	38.0241	38.0093	38.0408	38.0371	
BlankUsed	1.0000	1.0000	1.0000	1.0000	
Common Pb	0.4966	0.2355	0.4072	0.9237	
Total Pb C	1.4966	1.2355	1.4072	1.9237	
Pb ppm	27622.1624	12.3485	6293.2507	9.3493	
U ppm	456870.0761	210.9113	99927.9439	156.0678	
Pb206U238	0.0524	0.0523	0.0520	0.0514	
Pb206U238err	0.3222	0.3548	0.6223	0.2063	
Pb206U238errA	16.8849	18.5483	32.3643	10.5947	
Pb206U238age	329.3135	328.4856	326.8320	322.8677	
Pb207U235	0.3877	0.3809	0.3762	0.3760	
Pb207U235err	0.4796	0.5219	0.9528	0.2624	
Pb207U235errA	18.5920	19.8778	35.8438	9.8659	
Pb207U235age	332.6844	327.7071	324.2465	324.0641	
Pb207Pb206	0.0536	0.0528	0.0525	0.0531	
Pb207Pb206err	0.3462	0.3729	0.6993	0.1590	
Pb207Pb206errA	18.5738	19.7080	36.6873	8.4424	
Pb207Pb206age	356.3289	322.1894	305.7305	332.6761	
Pb207Pb206ageerr	7.8171	8.4716	15.9315	3.6056	
Pb206Pb204	928.4518	2080.0271	580.6126	1547.7060	
Pb208Pb206	0.2064	0.2130	0.2244	0.2540	
Rho	0.6922	0.6998	0.6797	0.7955	
Description	U and Pb from separate fractions	U from U fraction - .dat files for U from Pb won't open	U from U fraction - .dat files for U from Pb won't open	U from Pb fraction	U from Pb fraction

Sample Number	95.3A	55.22A	55.22A	55.22A	55.22A	68.3A
Unique ID	2026	2027	2058	2059	2060	2061
Fraction Code	Z-19	Z-20	Z-21	Z-22	Z-23	Z-24
chemistry code	148-19	148-20	148-21	148-22	148-23	148-24
Sample Weight (µg)	206.0	3.0	5.7	0.7	0.7	0.3
Spike Weight (g)	0.0025	0.0025	0.0025	0.0025	0.0025	0.0025
$^{206}Pb/^{208}Pb$	3.5232	5.9562	5.8814	5.3063	5.5874	3.9561
2σ % error	0.065	0.030	0.028	0.062	0.024	0.054
$^{206}Pb/^{207}Pb$	8.4995	13.0107	14.7650	12.4748	13.9223	10.5763
2σ % error	0.086	0.044	0.039	0.055	0.028	0.054
$^{206}Pb/^{205}Pb$	0.6305	1.4445	3.3450	1.7405	2.0925	0.9198
2σ % error	0.028	0.021	0.028	0.031	0.012	0.018
$^{206}Pb/^{204}Pb$	214.7700	585.0450	972.4610	528.4590	748.9930	335.2800
2σ % error	0.194	0.150	0.215	0.188	0.129	0.153
$^{238}U/^{235}U$	0.1098	0.2335	0.7200	0.2880	0.3424	0.1455
2σ % error	0.184	0.059	0.208	0.228	0.105	0.062
Pb Blank	2.0	2.1	2.0	2.0	2.0	2.0
U Blank	4.5	0.4	4.5	4.5	4.5	0.1
Stacey & Kramer, 1975						
model Pb age	310	340	330	364	342	334
64c	18.2235	18.1758	18.1917	18.1375	18.1726	18.1854
74c	15.6036	15.6007	15.6017	15.5984	15.6006	15.6013
84c	38.0612	38.0056	38.0241	37.9611	38.0019	38.0167
BlankUsed	2.0000	1.0500	2.0000	2.0000	2.0000	2.0000
Common Pb	0.5786	0.6678	1.5044	1.2337	0.3166	0.2240
Total Pb C	2.5786	1.7178	3.5044	3.2337	2.3166	2.2240
Pb ppm	0.0793	13.4268	17.2548	69.9843	84.4786	74.3592
U ppm	1.6572	246.1689	401.1642	1278.3311	1522.1082	1350.2376
Pb206U238	0.0456	0.0537	0.0414	0.0528	0.0541	0.0526
Pb206U238err	0.3179	0.1748	0.2662	0.2888	0.1987	0.2101
Pb206U238errA	14.5125	9.3849	11.0320	15.2340	10.7479	11.0536
Pb206U238age	287.7542	337.2063	261.7467	331.4030	339.5254	330.5085
Pb207U235	0.3337	0.3950	0.3051	0.3915	0.3981	0.3869
Pb207U235err	0.4054	0.1960	0.2795	0.3125	0.2128	0.2508
Pb207U235errA	13.5285	7.7428	8.5284	12.2346	8.4720	9.7061
Pb207U235age	292.3725	338.0428	270.3614	335.4651	340.2861	332.1279
Pb207Pb206	0.0530	0.0534	0.0534	0.0538	0.0534	0.0533
Pb207Pb206err	0.2458	0.0879	0.0842	0.1174	0.0755	0.1349
Pb207Pb206errA	13.0326	4.6915	4.4945	6.3189	4.0301	7.1955
Pb207Pb206age	329.4422	343.8065	345.6459	363.7290	345.4921	343.4930
Pb207Pb206ageerr	5.5771	1.9899	1.9042	2.6472	1.7076	3.0525
Pb206Pb204	1714.8185	3753.4162	3981.9926	2456.4016	11626.5269	6802.1869
Pb208Pb206	0.1222	0.1080	0.1348	0.1228	0.1334	0.1527
Rho	0.7953	0.8937	0.9536	0.9268	0.9350	0.8431
Description	U from U fraction	U from Pb fraction	U from U fraction	U from U fraction	U from U fraction	U from U fraction

Sample Number	68.3A	BLANK05	68.3A	55.22A	BLANK05	BLANK05
Unique ID	2062	1917	2063	2064	1918	1919
Fraction Code	Z-25	B-1	Z-26	Z-28	B-2	B-3
chemistry code	148-25	148-25	148-26	148-28	148-28	148-29
Sample Weight (µg)	0.5	1.0	0.3	0.5	1.0	1.0
Spike Weight (g)	0.0025	0.0025	0.0025	0.0025	0.0025	0.0025
$^{206}Pb/^{208}Pb$	4.4543	0.9311	3.9348	0.7965	0.5797	0.9312
2σ % error	0.066	0.073	0.030	0.029	0.031	0.146
$^{206}Pb/^{207}Pb$	13.6339	2.3024	11.2680	1.9601	1.3974	2.2797
2σ % error	0.078	0.056	0.030	0.038	0.019	0.305
$^{206}Pb/^{205}Pb$	2.0639	0.0914	1.0800	0.1086	0.2420	0.0899
2σ % error	0.044	0.058	0.014	0.021	0.026	0.056
$^{206}Pb/^{204}Pb$	690.9860	36.1568	288.3670	30.7278	24.2327	34.5995
2σ % error	0.374	0.111	0.700	0.078	0.021	0.579
$^{238}U/^{235}U$	0.3443	1.0000	0.1764	0.0020	1.0000	1.0000
2σ % error	0.272	1.000	0.422	0.422	0.100	1.000
Pb Blank	2.4	0.0	2.0	2.0	0.0	0.0
U Blank	0.1	0.0	0.1	4.5	0.0	0.0
Stacey & Kramer, 1975						
model Pb age	330	0	322	0	0	0
64c	18.1917	18.7033	18.2044	18.7033	18.7033	18.7033
74c	15.6017	15.6288	15.6025	15.6288	15.6288	15.6288
84c	38.0241	38.6305	38.0390	38.6305	38.6305	38.6305
BlankUsed	2.4000	0.0000	2.0000	2.0000	0.0000	0.0000
Common Pb	0.2727	1.8519	2.0669	1.7020	15.7711	1.9843
Total Pb C	2.6727	1.8519	4.0669	3.7020	15.7711	1.9843
Pb ppm	132.9426	1.8452	113.4387	3.3247	17.3229	1.7623
U ppm	2372.4464	3192.8035	2063.5865	-0.9997	3192.8035	3192.8035
Pb206U238	0.0527	0.0000	0.0508	0.0449	0.0001	0.0000
Pb206U238err	0.3245	3.7214	0.4642	46.2171	1.3304	5.8313
Pb206U238errA	17.0995	0.0264	23.5826	2076.1837	0.1491	-0.1086
Pb206U238age	331.0247	0.0458	319.4750	283.2727	0.7226	-0.1201
Pb207U235	0.3872	-0.0001	0.2702	-0.7264	0.0219	-0.0018
Pb207U235err	0.3541	39.7996	0.8094	70.4269	0.9219	7.6406
Pb207U235errA	13.7111	-0.3266	21.8692	-5115.7216	2.0192	-1.3787
Pb207U235age	332.3563	-0.0833	242.8475	-1315.9801	21.9994	-1.8338
Pb207Pb206	0.0533	-0.0838	0.0386	-0.1173	1.4171	0.7027
Pb207Pb206err	0.1388	43.0083	0.6350	61.1389	0.7089	3.4545
Pb207Pb206errA	7.3982	-3602.3523	24.4909	-7170.0394	1004.4883	2427.4564
Pb207Pb206age	341.6940	0.0000	-445.8908	0.0000	5722.6323	4736.2510
Pb207Pb206ageerr	3.1420	0.0000	16.7173	0.0000	9.7808	49.6256
Pb206Pb204	13287.6856	19.4863	880.4029	17.8600	20.1539	16.7879
Pb208Pb206	0.1771	-1.2437	0.1344	1.1632	2.5978	2.6146
Rho	0.9200	-0.8502	0.6220	0.5158	0.8632	0.9028
Description	U from U fraction	Zircon chemistry blank No U	U from U fraction	U from U fraction	Zircon Chemistry blank	Zircon Chemistry Blank

Sample Number	51.7A	91500	91500	91500	91500
Unique ID	2065	1920	1921	1922	1930
Fraction Code	Z-30	Z	Z	Z	Z-31
chemistry code	148-30	148-31	148-31	148-31	148-31
Sample Weight (µg)	0.4	60.0	60.0	60.0	80.0
Spike Weight (g)	0.0025	0.0025	0.0025	0.0025	0.0025
$^{206}Pb/^{208}Pb$	2.6129	8.7922	8.7757	8.8437	8.8738
2σ % error	0.532	0.024	0.029	0.016	0.070
$^{206}Pb/^{207}Pb$	6.1407	12.7961	12.7760	12.9077	12.9453
2σ % error	0.539	0.015	0.014	0.023	0.110
$^{206}Pb/^{205}Pb$	0.3026	13.6900	13.6710	13.7341	13.7275
2σ % error	0.386	0.031	0.219	0.029	0.070
$^{206}Pb/^{204}Pb$	126.2350	4824.9250	4870.4413	4870.4413	4875.5688
2σ % error	0.679	0.234	0.219	0.219	1.103
$^{238}U/^{235}U$	0.0450	0.7025	0.7025	0.7019	0.7019
2σ % error	0.174	0.009	0.009	0.020	0.020
Pb Blank	2.0	1.8	1.8	1.8	1.8
U Blank	4.5	4.3	4.3	4.3	4.3
Stacey & Kramer, 1975 model Pb age	330	1065	1065	1065	1064
64c	18.1917	16.9536	16.9536	16.9536	16.9554
74c	15.6017	15.4978	15.4978	15.4978	15.4980
84c	38.0241	36.6374	36.6374	36.6374	36.6393
BlankUsed	1.0000	1.8000	1.8000	1.8000	1.8000
Common Pb	0.5861	0.5585	0.5047	0.5276	0.5200
Total Pb C	1.5861	2.3585	2.3047	2.3276	2.3200
Pb ppm	16.2802	6.7548	6.7473	6.7691	5.0717
U ppm	323.6258	37.2192	37.2192	37.1888	27.8916
Pb206U238	0.0462	0.1782	0.1780	0.1790	0.1789
Pb206U238err	0.6501	0.1621	0.2719	0.1627	0.1749
Pb206U238errA	30.0384	28.8910	48.3906	29.1201	31.2871
Pb206U238age	291.1709	1057.3126	1055.9916	1061.2948	1060.8281
Pb207U235	0.3448	1.8561	1.8573	1.8476	1.8412
Pb207U235err	1.5504	0.1707	0.2770	0.1722	0.2150
Pb207U235errA	53.4637	31.6817	51.4422	31.8124	39.5856
Pb207U235age	300.8367	1065.6121	1066.0405	1062.5604	1060.2776
Pb207Pb206	0.0541	0.0755	0.0757	0.0749	0.0747
Pb207Pb206err	1.3826	0.0534	0.0530	0.0563	0.1248
Pb207Pb206errA	74.8435	4.0363	4.0089	4.2147	9.3136
Pb207Pb206age	376.5195	1082.6442	1086.6639	1065.1611	1059.1449
Pb207Pb206ageerr	31.1072	1.0718	1.0618	1.1319	2.5111
Pb206Pb204	692.4725	43187.2145	47722.4196	45863.7338	46514.5085
Pb208Pb206	0.1034	0.1067	0.1070	0.1061	0.1058
Rho	0.4537	0.9497	0.9815	0.9451	0.8144
Description	U from U fraction	91500 SOLN Pb_SEM_1	91500 2nd run (possible organics)	Pb collected statically on Faradays (6/4 fro, SEM_2)	Pb MIC_2

Sample Number	91500	91500	51.7A	91500	91500	91500
Unique ID	1929	1927	2066	1924	1928	1925
Fraction Code	Z-31	Z-31	Z	Z-32	Z	
chemistry code	148-31	148-31	148-31	148-32	148-32	148-32
Sample Weight (µg)	80.0	60.0	0.3	80.0	80.0	80.0
Spike Weight (g)	0.0025	0.0025	0.0020	0.0025	0.0025	0.0025
$^{206}Pb/^{208}Pb$	8.8693	8.8096	5.1471	8.9193	8.9396	8.9211
2σ % error	0.060	0.010	0.385	0.032	0.010	0.029
$^{206}Pb/^{207}Pb$	12.8741	12.8034	12.6490	12.9000	12.8926	12.9021
2σ % error	0.060	0.014	0.456	0.015	0.010	0.018
$^{206}Pb/^{205}Pb$	13.7515	13.8684	1.5366	21.9470	22.2285	21.8947
2σ % error	0.090	0.020	0.226	0.040	0.020	0.047
$^{206}Pb/^{204}Pb$	4969.6195	4892.6986	522.3120	6331.1192	6378.7661	6326.6110
2σ % error	1.300	0.260	1.161	0.260	0.228	0.230
$^{238}U/^{235}U$	0.7019	0.7025	0.2690	1.1230	1.1230	1.1230
2σ % error	0.020	0.010	0.124	0.009	0.010	0.009
Pb Blank	1.8	1.8	2.0	1.8	1.8	1.8
U Blank	4.3	4.3	4.5	4.3	4.3	4.3
Stacey & Kramer, 1975						
model Pb age	1065	1065	312	1065	1065	1065
64c	16.9536	16.9536	18.2203	16.9536	16.9536	16.9536
74c	15.4978	15.4978	15.6034	15.4978	15.4978	15.4978
84c	36.6374	36.6374	38.0575	36.6374	36.6374	36.6374
BlankUsed	1.8000	1.8000	2.0000	1.8000	1.8000	1.8000
Common Pb	0.4342	0.5535	0.0723	1.6714	1.7037	1.6611
Total Pb C	2.2342	2.3535	2.0723	3.4714	3.5037	3.4611
Pb ppm	5.0828	6.8425	137.1169	8.1496	8.2535	8.1297
U ppm	27.8916	37.2192	2707.9599	44.8089	44.8089	44.8089
Pb206U238	0.1792	0.1806	0.0497	0.1784	0.1807	0.1780
Pb206U238err	0.1839	0.1604	0.3293	0.1637	0.1600	0.1656
Pb206U238errA	32.9636	28.9620	16.3785	29.2033	28.9145	29.4645
Pb206U238age	1062.6094	1070.1014	312.9540	1058.1383	1070.6885	1055.8055
Pb207U235	1.8565	1.8803	0.3601	1.8574	1.8828	1.8526
Pb207U235err	0.2019	0.1690	0.7561	0.1722	0.1683	0.1742
Pb207U235errA	37.4748	31.7803	27.2267	31.9829	31.6872	32.2803
Pb207U235age	1065.7537	1074.1764	312.2762	1066.0507	1075.0421	1064.3516
Pb207Pb206	0.0751	0.0755	0.0525	0.0755	0.0756	0.0755
Pb207Pb206err	0.0826	0.0533	0.6712	0.0534	0.0521	0.0543
Pb207Pb206errA	6.2064	4.0229	35.2393	4.0291	3.9360	4.0975
Pb207Pb206age	1072.1964	1082.4581	307.2277	1082.2795	1083.8831	1081.9130
Pb207Pb206ageerr	1.6593	1.0684	15.2886	1.0702	1.0443	1.0886
Pb206Pb204	55792.9398	44150.4067	29346.6649	23191.4431	23045.4165	23278.7440
Pb208Pb206	0.1060	0.1066	0.1284	0.1069	0.1067	0.1068
Rho	0.9124	0.9490	0.4611	0.9508	0.9509	0.9503

Description	Pb from MIC	91500 SEM Integration experiment	U from U fraction	SEM_1	91500 SEM Integration Experiment	SEM_2

Sample Number	91500	BFD	BFD	BFD	BFD	
Unique ID	1923	1926	2095	2096	2097	2098
Fraction Code	Z	Z-1	Z-2	Z-3	Z-4	
chemistry code	148-32	148-32	154-06	154-07	154-08	154-09
Sample Weight (µg)	0.0	80.0	2.0	2.0	2.0	2.0
Spike Weight (g)	0.0000	0.0025	0.0025	0.0025	0.0025	0.0025
$^{206}Pb/^{208}Pb$	0.0000	8.9855	4.3547	4.2895	5.0386	4.9932
2σ % error	0.000	0.014	0.030	0.020	0.030	0.026
$^{206}Pb/^{207}Pb$	0.0000	13.0039	12.7766	12.2844	14.2292	13.7510
2σ % error	0.000	0.020	0.060	0.030	0.030	0.040
$^{206}Pb/^{205}Pb$	0.0000	22.0174	1.7169	2.0727	2.0258	1.7606
2σ % error	0.000	0.029	0.020	0.010	0.020	0.020
$^{206}Pb/^{204}Pb$	0.0000	6326.6110	548.6800	497.3139	802.7013	702.5165
2σ % error	0.000	0.230	0.180	0.130	0.120	0.160
$^{238}U/^{235}U$	0.0000	1.1239	0.2855	0.3494	0.3431	0.3047
2σ % error	0.000	0.011	0.030	0.030	0.080	0.030
Pb Blank	0.0	1.8	1.3	1.3	1.3	1.3
U Blank	0.0	4.3	0.1	0.1	0.1	0.1
Stacey & Kramer, 1975 model Pb age	0	1065	328	325	327	0
64c	0.0000	16.9536	18.1949	18.1997	18.1965	18.7033
74c	0.0000	15.4978	15.6019	15.6022	15.6020	15.6288
84c	0.0000	36.6374	38.0278	38.0334	38.0297	38.6305
BlankUsed		1.8000	1.3000	1.3000	1.3000	1.3000
Common Pb		1.6954	1.6078	3.5174	0.4948	0.4697
Total Pb C		3.4954	2.9078	4.8174	1.7948	1.7697
Pb ppm		8.1658	25.6840	31.7367	29.7594	25.6144
U ppm		44.8479	452.6589	554.4505	544.4182	483.2766
Pb206U238		0.1788	0.0522	0.0515	0.0520	0.0506
Pb206U238err		0.1615	0.2312	0.2104	0.2259	0.2280
Pb206U238errA		28.8706	12.0752	10.8453	11.7517	11.5360
Pb206U238age		1060.4197	328.2430	323.9773	326.9785	318.1337
Pb207U235		1.8463	0.3821	0.3783	0.3823	0.3718
Pb207U235err		0.1706	0.2696	0.2427	0.2448	0.2540
Pb207U235errA		31.4958	10.3021	9.1792	9.3585	9.4428
Pb207U235age		1062.1124	328.5716	325.7515	328.6993	320.9969
Pb207Pb206		0.0749	0.0530	0.0532	0.0533	0.0533
Pb207Pb206err		0.0550	0.1407	0.1214	0.0975	0.1122
Pb207Pb206errA		4.1196	7.4649	6.4630	5.1931	5.9796
Pb207Pb206age		1065.5927	330.9070	338.4566	340.9077	341.8301
Pb207Pb206ageerr		1.1061	3.1916	2.7504	2.2066	2.5393
Pb206Pb204		22936.2203	1869.3516	1040.9950	7224.4779	6672.2860
Pb208Pb206		0.1060	0.1699	0.1660	0.1577	0.1533
Rho		0.9466	0.8530	0.8658	0.9174	0.8972
Description	FARADAYS (6/4 FROM SEM 2)	CA 120	CA 120	CA 120	CA 120	

Sample Number	BFD	88:3A	88:3A	88:3A	88:3A	51:7A
Unique ID	2099	2302	2301	2300	2299	2298
Fraction Code	Z-5	Z-5	Z-6	Z-7	Z-8	Z-5
chemistry code	154-10	159-01	159-02	159-03	159-04	159-06
Sample Weight (µg)	2.0	3.1	0.5	1.3	0.6	22.9
Spike Weight (g)	0.0025	0.0025	0.0025	0.0025	0.0025	0.0025
$^{206}Pb/^{208}Pb$	4.4183	4.9961	2.3386	2.1584	2.4677	5.1004
2σ % error	0.040	0.061	0.114	0.165	0.203	0.100
$^{206}Pb/^{207}Pb$	12.8768	13.7409	6.1484	5.7768	6.7413	10.9197
2σ % error	0.040	0.128	0.247	0.191	0.280	0.120
$^{206}Pb/^{205}Pb$	1.2661	1.9041	0.3073	0.2597	0.3226	1.0371
2σ % error	0.020	0.040	0.105	0.065	0.117	0.045
$^{206}Pb/^{204}Pb$	557.9304	702.9070	124.7970	113.5480	142.6480	351.9810
2σ % error	0.170	0.420	0.744	0.704	0.620	0.321
$^{238}U/^{235}U$	0.2158	0.3179	0.0391	0.0314	0.0424	0.1874
2σ % error	0.020	0.100	0.039	0.108	0.058	0.056
Pb Blank	1.3	0.2	1.2	1.0	1.2	0.9
U Blank	0.1	0.1	0.1	0.1	0.1	0.1
Stacey & Kramer, 1975 model Pb age	320	330	329	329	334	320
64c	18.2076	18.1917	18.1933	18.1933	18.1854	18.2076
74c	15.6027	15.6017	15.6018	15.6018	15.6013	15.6027
84c	38.0427	38.0241	38.0260	38.0260	38.0167	38.0427
BlankUsed	1.3000	0.2000	1.2000	1.0000	1.2000	0.9000
Common Pb	0.0272	1.9528	0.4836	0.3645	0.1146	1.6788
Total Pb C	1.3272	2.1528	1.6836	1.3645	1.3146	2.5788
Pb ppm	18.1777	18.3663	14.3527	4.4349	12.4766	1.2581
U ppm	341.6693	325.2910	243.7196	74.9459	220.4415	25.8937
Pb206U238	0.0506	0.0526	0.0524	0.0522	0.0524	0.0464
Pb206U238err	0.2785	0.1932	1.1363	1.1875	1.0679	0.2616
Pb206U238errA	14.0821	10.1545	59.5057	61.9481	56.0052	12.1279
Pb206U238age	317.9698	330.2262	329.0427	327.8133	329.5172	292.1281
Pb207U235	0.3720	0.3849	0.3828	0.3813	0.3832	0.3335
Pb207U235err	0.3080	0.2662	1.6390	1.6258	1.3859	0.3668
Pb207U235errA	11.4581	10.2445	62.7387	61.9940	53.1032	12.2315
Pb207U235age	321.1678	330.6441	329.0806	327.9966	329.3681	292.2201
Pb207Pb206	0.0534	0.0531	0.0530	0.0530	0.0530	0.0522
Pb207Pb206err	0.1379	0.1810	1.1815	1.1197	0.9100	0.2548
Pb207Pb206errA	7.3589	9.6118	62.6340	59.3553	48.2181	13.2913
Pb207Pb206age	344.4312	333.5931	329.3560	329.3046	328.3215	292.9558
Pb207Pb206ageerr	3.1200	4.1027	26.8046	25.4022	20.6484	5.8175
Pb206Pb204	79992.0141	1726.1829	848.6378	895.7016	3825.7321	1049.1232
Pb208Pb206	0.1687	0.1527	0.1659	0.1819	0.1820	0.0955
Rho	0.8942	0.7333	0.6931	0.7251	0.7544	0.7194
Description	CA 120	single zircon no chem CA 180 (57pg Pb)	single zircon no chemistry CA 180	single zircon no chem CA 180	single zircon no chem CA 180	single zircon no chem CA 180 concordant

Sample Number	51:7A	51.7A	BFD	BFD	BFD	68:1A
Unique ID	2296	2295	2294	2293	2292	2291
Fraction Code	Z-7	Z-8	Z-8	Z-9	Z-10	Z-1
chemistry code	159-08	159-09	159-11	159-12	159-13	159-14
Sample Weight (µg)	9.5	7.9	2.2	0.7	0.5	2.3
Spike Weight (g)	0.0025	0.0025	0.0025	0.0025	0.0025	0.0025
$^{208}Pb/^{208}Pb$	4.2807	4.0819	4.0686	4.0694	3.0139	2.9532
2σ % error	0.073	0.060	0.058	0.055	0.088	0.039
$^{206}Pb/^{207}Pb$	10.4199	9.8291	13.6581	13.8207	9.2045	8.9812
2σ % error	0.103	0.084	0.120	0.088	0.227	0.070
$^{206}Pb/^{205}Pb$	0.7849	0.6034	1.5140	1.5463	0.6317	0.5239
2σ % error	0.030	0.032	0.036	0.035	0.041	0.029
$^{206}Pb/^{204}Pb$	315.5150	274.9510	672.6440	703.3830	243.8160	235.5760
2σ % error	0.293	0.267	0.614	0.453	0.828	0.276
$^{238}U/^{235}U$	0.1389	0.1041	0.2486	0.2540	0.0948	0.0767
2σ % error	0.110	0.040	0.053	0.062	0.056	0.050
Pb Blank	0.2	1.1	1.2	1.1	1.9	0.9
U Blank	0.1	0.1	0.1	0.1	0.1	0.1
Stacey & Kramer, 1975						
model Pb age	292	300	333	333	330	330
64c	18.2520	18.2393	18.1869	18.1869	18.1917	18.1917
74c	15.6053	15.6046	15.6014	15.6014	15.6017	15.6017
84c	38.0945	38.0797	38.0186	38.0186	38.0241	38.0241
BlankUsed	0.2000	1.1000	1.2000	1.1000	1.9000	0.9000
Common Pb	1.5492	0.0931	0.0949	0.1002	0.0088	0.3500
Total Pb C	1.7492	1.1931	1.2949	1.2002	1.9088	1.2500
Pb ppm	2.3318	1.9522	20.5384	66.1745	34.2011	6.2168
U ppm	46.1712	41.5292	358.0627	1150.0795	597.3564	104.8749
Pb206U238	0.0464	0.0463	0.0531	0.0532	0.0529	0.0533
Pb206U238err	0.2042	0.4679	0.2436	0.2331	0.7482	0.4531
Pb206U238errA	9.4763	21.6687	12.9335	12.3929	39.5932	24.1405
Pb206U238age	292.4428	291.8029	333.4482	333.8697	332.3933	334.6018
Pb207U235	0.3339	0.3337	0.3883	0.3891	0.3838	0.3942
Pb207U235err	0.2904	0.5356	0.3096	0.2759	1.0095	0.5217
Pb207U235errA	9.6978	17.8712	12.0233	10.7366	38.7469	20.5639
Pb207U235age	292.5594	292.3668	333.1576	333.7462	329.8559	337.3999
Pb207Pb206	0.0522	0.0523	0.0531	0.0531	0.0526	0.0537
Pb207Pb206err	0.2023	0.2743	0.1913	0.1489	0.6819	0.2702
Pb207Pb206errA	10.5561	14.3379	10.1503	7.9047	35.8724	14.4977
Pb207Pb206age	293.4899	296.8844	331.1359	332.8920	312.0018	356.7341
Pb207Pb206ageerr	4.6188	6.2604	4.3391	3.3755	15.5174	6.1001
Pb206Pb204	846.6543	10301.7538	27742.4105	26895.6956	113423.2743	2328.7185
Pb208Pb206	0.1245	0.1209	0.1998	0.2020	0.2040	0.2076
Rho	0.7177	0.8590	0.7862	0.8419	0.7374	0.8556
Description	single zircon no chem CA 180 concordant	single zircon no chem CA 180 concordant	single zircon no chem CA 180	single zircon no chem CA 180	Single zircon no chem CA 180	Single zircon no chem 14pg Pb

Sample Number	68:1A	68:1A	68:1A	55:22A	55:22A	55:22A
Unique ID	2290	2289	2288	2287	2276	2274
Fraction Code	Z-2	Z-3	Z-4	Z-1	Z-2	Z-3
chemistry code	159-15	159-17	159-18	159-19	159-20	159-21
Sample Weight (µg)	1.2	0.6	0.7	0.9	0.9	0.5
Spike Weight (g)	0.0025	0.0025	0.0025	0.0025	0.0025	0.0025
$^{206}Pb/^{208}Pb$	4.9630	5.1009	5.3681	5.8801	5.9037	4.6101
2σ % error	0.034	0.059	0.037	0.035	0.035	0.091
$^{206}Pb/^{207}Pb$	15.1088	13.6776	14.0757	13.9789	15.4580	11.9485
2σ % error	0.056	0.080	0.049	0.045	0.050	0.130
$^{206}Pb/^{205}Pb$	2.3362	1.4891	1.8412	1.5709	2.4321	1.1380
2σ % error	0.037	0.030	0.022	0.025	0.020	0.058
$^{206}Pb/^{204}Pb$	1036.0390	667.3980	756.0850	744.3300	1172.9550	450.7570
2σ % error	0.284	0.320	0.306	0.227	0.209	0.593
$^{238}U/^{235}U$	0.3973	0.2493	0.3099	0.2548	0.4012	0.1796
2σ % error	0.044	0.039	0.082	0.107	0.049	0.037
Pb Blank	0.5	1.2	1.1	1.1	0.9	0.7
U Blank	0.1	0.1	0.1	0.1	0.1	0.1
Stacey & Kramer, 1975						
model Pb age	330	325	330	340	340	340
64c	18.1917	18.1997	18.1917	18.1758	18.1758	18.1758
74c	15.6017	15.6022	15.6017	15.6007	15.6007	15.6007
84c	38.0241	38.0334	38.0241	38.0056	38.0056	38.0056
BlankUsed	0.5000	1.2000	1.1000	0.5500	0.9000	0.7000
Common Pb	0.8136	0.0588	0.5353	0.4973	0.0738	1.1058
Total Pb C	1.3136	1.2588	1.6353	1.0473	0.9738	1.8058
Pb ppm	58.4797	70.7767	76.1140	49.5883	78.6204	65.3063
U ppm	1051.4713	1316.4784	1404.0934	897.2305	1415.5691	1136.5782
Pb206U238	0.0522	0.0520	0.0522	0.0540	0.0540	0.0540
Pb206U238err	0.1747	0.2422	0.2214	0.2073	0.1847	0.2214
Pb206U238errA	9.1211	12.6033	11.5530	11.1852	9.9707	11.9498
Pb206U238age	328.1348	326.9882	327.9741	338.7279	339.0090	338.8604
Pb207U235	0.3819	0.3787	0.3814	0.3966	0.3961	0.3962
Pb207U235err	0.1961	0.2812	0.2475	0.2248	0.2032	0.3343
Pb207U235errA	7.4896	10.6502	9.4399	8.9155	8.0485	13.2423
Pb207U235age	328.4102	326.0949	328.0681	339.1704	338.7943	338.8726
Pb207Pb206	0.0530	0.0528	0.0530	0.0533	0.0532	0.0532
Pb207Pb206err	0.0891	0.1457	0.1120	0.0875	0.0858	0.2453
Pb207Pb206errA	4.7241	7.6912	5.9368	4.6632	4.5668	13.0590
Pb207Pb206age	330.3695	319.7308	328.7415	342.2104	337.3277	338.9625
Pb207Pb206ageerr	2.0204	3.3112	2.5416	1.9798	1.9448	5.5556
Pb206Pb204	5114.5044	43994.0072	6049.1175	5528.7083	58668.0660	1762.8192
Pb208Pb206	0.1705	0.1466	0.1422	0.1244	0.1413	0.1424
Rho	0.8909	0.8553	0.8917	0.9212	0.9064	0.6795
Description	Single zircon no chem 70 pg Pb	single zircon no chem 43 pg	Single zircon no chem 53pg	single zircon no chem	single zircon no chem	single zircon no chem

Sample Number	55:22A	JBSP010	JBSP010	JBSP010	JBSP010	JBSP010	
Unique ID		2273	2272	2271	2270	2269	2268
Fraction Code	Z-4	Z-1	Z-2	Z-3	Z-4	Z-5	
chemistry code	159-22	159-23	159-24	159-25	159-26	159-27	
Sample Weight (µg)		0.7	0.3	0.3	0.4	0.7	0.7
Spike Weight (g)		0.0025	0.0025	0.0025	0.0025	0.0025	0.0025
$^{206}Pb/^{208}Pb$		4.3824	4.0819	3.6360	5.1878	4.1030	3.2885
2σ % error		0.115	0.039	0.040	0.057	0.061	0.278
$^{206}Pb/^{207}Pb$		11.4513	11.8659	10.4052	15.2294	11.1337	8.7893
2σ % error		0.160	0.074	0.075	0.126	0.080	0.367
$^{206}Pb/^{205}Pb$		0.9266	0.9713	0.7201	286.8253	0.9087	0.6171
2σ % error		0.070	0.036	0.022	1.668	0.028	0.205
$^{206}Pb/^{204}Pb$		400.8970	436.4090	317.1370	944.8240	371.3620	228.9020
2σ % error		0.715	0.281	0.283	0.762	0.274	1.183
$^{238}U/^{235}U$		0.1443	0.1547	0.1109	106.5485	0.1434	0.0924
2σ % error		0.039	0.030	0.026	0.319	0.019	0.121
Pb Blank		1.2	1.5	1.0	1.5	1.5	1.5
U Blank		0.1	0.1	0.1	0.1	0.1	0.1
Stacey & Kramer, 1975							
model Pb age		340	333	332	35	332	332
64c		18.1758	18.1869	18.1885	18.6503	18.1885	18.1885
74c		15.6007	15.6014	15.6015	15.6264	15.6015	15.6015
84c		38.0056	38.0186	38.0204	38.5667	38.0204	38.0204
BlankUsed		1.2000	0.7500	1.0000	1.5000	1.5000	1.5000
Common Pb		0.2059	0.5056	0.3346	561.3845	0.1506	0.6079
Total Pb C		1.4059	1.2556	1.3346	562.8845	1.6506	2.1079
Pb ppm		36.5231	92.7863	66.4552	22746.6056	35.8485	23.7376
U ppm		651.3139	1630.4345	1165.7917	3763215.7354	647.1631	415.7745
Pb206U238		0.0539	0.0530	0.0531	0.0055	0.0530	0.0527
Pb206U238err		0.3453	0.2401	0.3623	2.1863	0.4107	0.6646
Pb206U238errA		18.6241	12.7383	19.2360	11.9529	21.7541	34.9911
Pb206U238age		338.6455	333.2112	333.5109	35.1478	332.6920	330.7816
Pb207U235		0.3973	0.3882	0.3894	0.0379	0.3880	0.3918
Pb207U235err		0.4673	0.2836	0.4204	2.2086	0.4699	1.1995
Pb207U235errA		18.5685	11.0087	16.3689	8.3634	18.2309	46.9923
Pb207U235age		339.7053	333.0345	333.9303	37.7404	332.9046	335.6686
Pb207Pb206		0.0534	0.0531	0.0532	0.0502	0.0531	0.0540
Pb207Pb206err		0.3137	0.1527	0.2207	0.3012	0.2396	0.9744
Pb207Pb206errA		16.7612	8.1036	11.7372	15.1288	12.7280	52.5830
Pb207Pb206age		346.9698	331.8067	336.8597	205.8840	334.3969	369.6726
Pb207Pb206ageerr		7.0952	3.4627	4.9997	6.9862	5.4300	21.9481
Pb206Pb204		7529.8902	3247.0965	3510.0953	954.1603	10041.5382	1604.2561
Pb208Pb206		0.1454	0.1711	0.1736	0.1556	0.1552	0.1603
Rho		0.7412	0.8427	0.8512	0.9907	0.8604	0.5840
Description	single zircon grain no column chem	Z	Z	Z?????? Weird load	Z	Z no chem Pb rerun - disregard	

Sample Number	BLANK06	BLANK06	BLANK06	Shuteen	Shuteen
Unique ID	2267	2266	2265	2303	2304
Fraction Code	B-3	B-2	B-1	Z-1	Z-2
chemistry code	159-28	159-29	159-30	163-23	163-24
Sample Weight (µg)	1.0	1.0	1.0	0.9	0.4
Spike Weight (g)	0.0025	0.0025	0.0025	0.0020	0.0020
$^{206}Pb/^{208}Pb$	0.8812	0.8882	0.9041	3.9565	3.8708
2σ % error	0.091	0.186	0.148	0.048	0.060
$^{206}Pb/^{207}Pb$	2.1751	2.1940	2.2276	12.9059	12.2700
2σ % error	0.139	0.219	0.195	0.080	0.631
$^{206}Pb/^{205}Pb$	0.0943	0.0939	0.0917	1.3466	1.2090
2σ % error	0.094	0.108	0.108	0.052	0.248
$^{206}Pb/^{204}Pb$	33.7840	34.5650	34.9050	549.7640	433.1040
2σ % error	0.244	0.589	0.509	0.449	1.010
$^{238}U/^{235}U$	0.0007	0.0008	0.0008	0.2242	0.2079
2σ % error	0.575	0.508	1.085	0.500	0.473
Pb Blank	0.0	0.0	0.0	1.1	1.1
U Blank	0.0	0.0	0.0	0.1	0.1
Stacey & Kramer, 1975 model Pb age	0	0	0	325	325
64c	18.7033	18.7033	18.7033	18.1997	18.1997
74c	15.6288	15.6288	15.6288	15.6022	15.6022
84c	38.6305	38.6305	38.6305	38.0334	38.0334
BlankUsed	0.0000	0.0000	0.0000	1.1000	1.1000
Common Pb	2.3443	2.2060	2.0368	0.2258	0.7287
Total Pb C	2.3443	2.2060	2.0368	1.3258	1.8287
Pb ppm	2.2409	2.1831	1.9725	35.4062	71.0360
U ppm	0.1410	0.2806	0.1822	631.0425	1316.5910
Pb206U238	-0.2614	-0.0268	-0.1294	0.0519	0.0495
Pb206U238err	4.9595	51.2543	13.1646	0.5743	0.6207
Pb206U238errA	-1296.5621	-1374.5586	-1703.6260	29.7781	30.7386
Pb206U238age	-1953.5094	-175.2429	-893.3683	325.8921	311.5881
Pb207U235	0.0000	1.1448	0.0000	0.3765	0.3377
Pb207U235err	11.1481	147.8566	59.1338	0.6025	1.1213
Pb207U235errA	0.0000	16927.1713	0.0000	22.6843	37.8723
Pb207U235age	0.0000	774.8017	0.0000	324.4823	295.4642
Pb207Pb206	0.4198	-0.3096	0.1985	0.0527	0.0495
Pb207Pb206err	7.2094	196.6351	47.1208	0.1843	0.9282
Pb207Pb206errA	3026.4802	-60879.4403	9353.5970	9.7056	45.9128
Pb207Pb206age	3981.5352	0.0000	2813.9250	314.3868	169.8948
Pb207Pb206ageerr	107.9087	0.0000	769.9036	4.1922	21.6744
Pb206Pb204	17.6983	18.4853	17.9632	8227.6284	2271.1412
Pb208Pb206	1.8257	2.8277	1.9537	0.1958	0.1842
Rho	0.8763	-0.9354	0.9311	0.9521	0.5611
Description	procedural blank no col chem	procedural blanks no column chem	procedural blank no column chem	CA 180	CA 180

Sample Number	BLANK?	SHUTEEN	Shuteen
Unique ID	2305	2306	2308
Fraction Code	B-1	Z-4	Z-5
chemistry code	163-25	163-26	163-27
Sample Weight (µg)	1.0	0.7	0.4
Spike Weight (g)	0.0020	0.0020	0.0020
$^{206}Pb/^{208}Pb$	0.8781	3.1241	3.3837
2σ % error	0.138	0.130	0.156
$^{206}Pb/^{207}Pb$	2.2982	10.1139	12.0381
2σ % error	0.197	0.151	0.348
$^{206}Pb/^{205}Pb$	0.0919	0.7665	1.2839
2σ % error	0.099	0.106	0.142
$^{206}Pb/^{204}Pb$	36.4050	296.3800	455.7710
2σ % error	0.316	0.500	1.385
$^{238}U/^{235}U$	0.0008	0.1207	0.2116
2σ % error	0.320	0.103	0.123
Pb Blank	0.0	1.3	1.7
U Blank	0.0	0.1	0.1
Stacey & Kramer, 1975 model Pb age	0	325	325
64c	18.7033	18.1997	18.1997
74c	15.6288	15.6022	15.6022
84c	38.6305	38.0334	38.0334
BlankUsed	0.0000	1.3000	1.7000
Common Pb	1.4752	0.2238	0.1565
Total Pb C	1.4752	1.5238	1.8565
Pb ppm	1.6208	24.9794	77.1325
U ppm	0.3666	435.3417	1340.0937
Pb206U238	0.0832	0.0519	0.0519
Pb206U238err	4.7291	0.5437	0.4477
Pb206U238errA	393.2698	28.1976	23.2361
Pb206U238age	514.9588	325.9496	326.1635
Pb207U235	2.3067	0.3769	0.3795
Pb207U235err	22.9811	0.6712	0.7941
Pb207U235errA	5300.9611	25.3013	30.1409
Pb207U235age	1214.3364	324.7826	326.6996
Pb207Pb206	0.2012	0.0527	0.0530
Pb207Pb206err	19.1533	0.4016	0.6435
Pb207Pb206errA	3853.0973	21.1675	34.1332
Pb207Pb206age	2835.7249	316.4332	330.5275
Pb207Pb206ageerr	312.3318	9.1314	14.5969
Pb206Pb204	20.0242	4463.2746	11209.2314
Pb208Pb206	4.3155	0.2163	0.2289
Rho	0.8449	0.8014	0.5864
Description	NO COLUMN CHEM	CA 180	CA 180

Appendix C

Geochemical data from various arc environments was used for comparison in Chapter 3. This data was acquired from the Georoc online geochemistry database at http://georoc.mpch-mainz.gwdg.de/georoc/. The citations for each location are listed below, and full references can be found in the bibliography (Page 169 onwards)

South Sandwich Arc; Gledhill and Baker, 1973; Frolova and Rudnik, 1974; Hawkesworth et al., 1977; Baker, 1978; Barreiro, 1983; Stern et al., 1984; Johnston, 1986; Pearce et al., 1995;

New Hebridies Arc; Gorton, 1977; Marcelot, 1981; Barsdell et al., 1982; Marcelot et al., 1983; Barsdell and Berry, 1989; Price et al., 1990; Eggins, 1993; Coltorti et al., 1994a; Coltorti et al., 1994b; Maillet e t al., 1995; Monzier et al., 1997; Peate et al., 1997; Raos and Crawford, 2004;

Lesser Antillies Arc; Shimizu and Arculus, 1975; Baker, 1984; Thirlwall and Graham, 1984; Speed and Walker, 1991; Kerr et al., 1996a; Kerr et al., 1996b; Smith et al., 1996; Thirlwall et al., 1996; Turner et al., 1996; Heath et al., 1998; Lidiak and Larue, 1998; Révillon et al., 1999; White et al., 1999; Hauff et al., 2000; Woodland et al., 2002; Lindsay et al., 2005;

Sunda; Calanchi et al., 1983; Varne and Foden, 1986; Wheller and Varne, 1986; Wheller et al., 1987; Stolz et al., 1988; Vukadinovic and Nicholls, 1989; Gill and Williams, 1990; Stolz et al., 1990; Vukadinovic and Sutamidjaja, 1995; Wensink and Van Bergen, 1995; Mandeville, 1996; Alves et al., 1999; Abdullah et al., 2000; Turner and Foden, 2001; Reubi et al., 2002; Gertisser and Keller, 2003; Reubi and Nicholls, 2004, 2005;

Honshu Arc; Kohn et al., 1989; Ujiie, 1989; Fukudome et al., 1990; Allan and Gorton, 1992; Iwamori, 1992; Jones et al., 1993; Uto et al., 1993; Miyake, 1994; Uto et al., 1994; Miyashita et al., 1995; Morris, 1995; Gust et al., 1997; Ishiwatari and Ohama, 1997; Kimura and Yoshida, 1999; Morris et al., 1999; Nakashima et al., 2000; Tamura et al., 2000; Churikova et al., 2001; Kimura et al., 2001; Kita et al., 2001; Kobayashi and Nakamura,

2001; Gasperini et al., 2002; Kimura et al., 2002; Takashima et al., 2002; Tamura et al., 2003; Tatsumi et al., 2003; Fujinawa and Kamata, 2005; Tatsumi et al., 2005; Tsuchiya et al., 2005; Shuto et al., 2006; Tatsumi et al., 2006;

Andes Central Volcanic Zone (CVZ); Thorpe et al., 1984; Buchelt M., 1986; Baker et al., 1987; Davidson et al., 1990; Tormey et al., 1991; Vatin-Perignon et al., 1992; Coira and Mahlburg, 1993; Hooker et al., 1993; Feeley and Davidson, 1994; Matthews et al., 1994; Davidson and De Silva, 1995; Stern and Skewes, 1995; Tormey et al., 1995; Ort et al., 1996; Trumbull et al., 1999; Bertotto, 2000; Richards and Villeneuve, 2002; Halter et al., 2004; Sandeman and Clark, 2004; Vergara et al., 2004; Bierlein et al., 2006; Richards et al., 2006

Geochemical data from intrusions at various locations world wide was used for comparison in Chapter 4. Again, this data was acquired from the Georoc. The citations for each location are listed below, and full references can be found in the reference list.**Andes;** Kontak et al., 1986; Brown, 1991; Parada et al., 1991; Richards et al., 2006

Australia,; Allen et al., 1997; Soesoo and Nicholls, 1999

BTVP; Pankhurst et al., 1978; Walsh et al., 1979; Meighan et al., 1984; Vogel et al., 1984; Ferry, 1985

Canadian Cordillera; Piercey et al., 2003; Miskovic and Francis Don, 2006

Honshu; Masuda et al., 1983; Luhr and Carmichael, 1985; Takagi et al., 1989; Kagami et al., 1992; Takagi, 1992; Kutsukake, 1993; Masaki, 1994; Rezanov et al., 1996; Shinjoe, 1997; Ohta et al., 1998; Shimoda et al., 1998; Verma, 2000; Ishihara and Wu, 2001; Kamei, 2002; Kutsukake, 2002

Mid African Rift; Marzoli et al., 1999

New Britain arc; Whalen, 1985

Appendix D

Mineral modal abundances

Sample number	Intrusion name	Quartz	Plagioclase	K-feldspar	Amphibole	Biotite	opaques	total
51.7A	North Mandakh Granite	40	15	207	26	4	8	300
		13.33	5.00	69.00	8.67	1.33	2.67	
51.6A	North Mandakh Granite	44	22	204	22	5	3	300
		14.67	7.33	68.00	7.33	1.67	1.00	
97.3A	Shuteen Granite	77	54	143	0	24	2	300
		25.67	18.00	47.67	0.00	8.00	0.67	
97.2A	Shuteen Granite	83	74	111	1	31	0	300
		27.67	24.67	37.00	0.33	10.33	0.00	
JBSP010	Narin Hudag Quartz Monzonite	81	126	60	13	18	2	300
		27.00	42.00	20.00	4.33	6.00	0.67	
JBSP009	Narin Hudag Quartz Monzonite	141	78	32	21	27	1	300
		47.00	26.00	10.67	7.00	9.00	0.33	
JBSP007	Narin Hudag Quartz Monzonite	74	145	44	17	16	4	300
		24.67	48.33	14.67	5.67	5.33	1.33	
JBSP006	Narin Hudag Granite	151	26	115	0	2	6	300
		50.33	8.67	38.33	0.00	0.67	2.00	
65.12A	Oyut Ulaan	65	108	95	3	20	9	300
		21.67	36.00	31.67	1.00	6.67	3.00	
88.5A	Oyut Ulaan	62	116	99	2	10	11	300
		20.67	38.67	33.00	0.67	3.33	3.67	
88.3A	Oyut Ulaan	67	135	84	0	13	1	300
		22.33	45.00	28.00	0.00	4.33	0.33	

Bibliography

Abdullah, C. I., Rampnoux, J.-P., Bellon, H., Maury, R. C., Soeria-Atmadja, R., 2000. The Evolution of Sumba Island (Indonesia) revisited in the light of new data on the geochronology and geochemistry of the magmatic rocks. *Journal of Asian Earth Sciences*, 18 533-546.

Allen, C. M., Wooden, J. L., Chappell, B. W., 1997. Late Palaeozoic crustal history of central coastal Queensland interpreted from geochemistry of Mesozoic plutons: the effects of continental rifting. *Lithos*, 42, 67-88.

Allan, J. F., Gorton, M. P., 1992. Geochemistry of igneous rocks from legs 127 and 128, Sea of Japan. *Proceedings of the Ocean Drilling Program, Scientific Results*, 127/128, 905-929.

Alves, S., Schiano, P., Allègre, C. J., 1999. Rhenium-osmium isotopic investigation of Java subduction zone lavas. *Earth and Planetary Science Letters*, 168, 65-77.

Badarch, G., Cunningham, W. D., Windley, B. F., 2002. A new terrane subdivision for Mongolia: Implications for the Phanerozoic crustal growth of Central Asia. *Journal of Asian Earth Sciences*, 21, 87 - 110.

Barry, T. L., Kent, R. W., 1998. Cenozoic magmatism in Mongolia and the origin of Central and East Asian basalts. *In*: Flower, M. F. J., Chung, S.-L., Lo, C.-H., and Lee, T.-Y., eds., *Mantle dynamics an plate interactions in East Asia.* American Geophysical Union, Washington, DC, p. 347-364.

Baker, P. E., 1978. The South Sandwich Islands: I ii. petrology of the volcanic rocks. *British Antarctic Survey Scientific Report*, 93, 1-34.

Baker, P. E., 1984. Geochemical evolution of St. Kitts and Montserrat, Lesser Antilles. *Journal of the Geological Society of London*, 141, 401-411.

Baker, P. E., Gonzáles Ferrán, O., Rex, D. C., 1987. Geology and Geochemistry of the Ojos Del Salado volcanic region. *Journal of the Geological Society of London*, 144, 85-96.

Barreiro, B. A., 1983. Lead isotopic compositions of South Sandwich Island volcanic rocks and their bearing on magmagenesis in intra-oceanic island arcs. Geochimica *et Cosmochimica Acta*, 47, 817-822.

Barsdell, M., Berry, R. F., 1989. Origin and evolution of primitive island arc ankaramites from western Epi, Vanuatu. *Journal of Petrology*, 31, 747-777.

Barsdell, M., Smith, I. E. M., Spoerli, K. B., 1982. The origin of reversed geochemical zoning in the northern New Hebrides volcanic arc. *Contributions to Mineralogy and Petrology*, 81, 148-155.

Batkhishig, B., Bignall, G., Kimura, J., Tsuchiya, N., 2003. Geochemical relationships between andesite and granodiorite in the Shuteen area, South Gobi, Mongolia. *Mongolian Geoscientist*, 21, 15-20.

Batkhishig, B., Iizumi, S., 2001. Petrographical, petrochemical and geochronological study of the Carboniferous Shuteen complex in Southern Mongolia. *Mongolian Geology*, 2, 135-145.

Bertotto, G. W., 2000. Cerro Agua Poca, a basaltic Quaternary cone bearing ultramafic xenoliths, western province of La Pampa, Argentina. *Revista de la Asociación Geológica Argentina*, 55, 59-71.

Bignall, G., Batkhishig, B., Tsuchiya, N., Delgertsogt, B., 2005. The Shuteen Cu-Au porphyry deposit. In: Seltmann, R., Gerel, O., and Kirwin, D., eds., *Geodynamics and Metallogeny of Mongolia with a special emphasis on copper and gold deposits*, CERCAMS, London, pp. 193-201.

Bierlein, F. B., Stein, H. J., Coira, B., Reynolds, P. H., 2006. Timing of gold and crustal evolution of the Palaeozoic South Central Andes, NW Argentina - implications for the endowment of orogenic belts. *Earth and Planetary Science Letters*, 245, 702-721.

Brown, M., 1991. Comparative geochemical interpretation of permian-triassic plutonic complexes of the Coastal Range and Altiplano (25°30' To 26°30'S), Northern Chile. *Special Paper for the Geological Society of America*, 265, 157-177.

Buchan, C., Cunningham, D., Windley, B. F., Tomurhuu, D., 2001. Structural and lithological characteristics of the Bayankhongor Ophiolite Zone, Central Mongolia. *Journal of the Geological Society of London*, 158, 445-460.

Buchelt M., Z. W., 1986. Petrographical and geochemical investigations on volcanites of the Jurassic porphyrite formation in the coast range of the Cordilleres from Northern Chile Berliner. *Geowiss*, 66, 191-204.

Buslov, M., Safonova, I., 2006. Accretionary-collision orogens and crustal growth of Eurasia in Vendian-Paleozoic time. *Geophysical Research Abstracts*, 8.

Calanchi, N., Lucchini, F., Rossi, P. L., 1983. Considerations on the high-K volcanic rocks of the volcanoes Muriah and Lasem (Java). *Mineralogica et Petrologica Acta*, 27, 15-34.

Carroll, A. R., Yunhai, L., Graham, S. A., Xuchang, X., Hendrix, M. S., Jinchi, C., McKnight, C. L., 1990. Junggar basin, northwest China: trapped Late Paleozoic ocean. *Tectonophysics*, 181, 1-14.

Chappell, B. W., White, A. J. R., 1974. Two contrasting granite types. *Pacific Geology*, 8, 173–174.

Chappell, B. W., White, A. J. R., 2001. Two contrasting granite types: 25 years later. *Australian Journal of Earth Sciences*, 48, 489-499.

Churikova, T., Dorendorf, F., Barman, T. R., 2001. Sources and fluids in the mantle wedge below Kamchatka, evidence from across-arc geochemical variation. *Journal of Petrology*, 42, 1567-1593.

Coira, B., Mahlburg, K. S., 1993. Implications of Quaternary volcanism at Cerro Tuzgle for crustal and mantle evolution of the Puna plateau, Central Andes, Argentina. *Contributions to Mineralogy and Petrology*, 113, 40-58.

Coltorti, M., Baker, P. E., Briqueu, L., Hasenaka, T., Galassi, B., 1994a. Petrology and geochemistry of volcanic rocks from the New Hebrides forearc region, sites 827, 829, and 830. *Proceedings of the Ocean Drilling Program, Scientific Results*, 134, 337-352.

Coltorti, M., Hasenaka, T., Briqueu, L., Baker, P. E., Siena, F., 1994b. Petrology and magmatic affinity of the North D'Entrecasteaux ridge, Central New Hebrides trench, site 828. *Proceedings of the Ocean Drilling Program, Scientific Results*, 134, 353-362.

Cunningham, D., 2005. Active intracontinental transpressional mountain building in the Mongolian Altai: Defining a new class of orogen. *Earth and Planetary Science Letters*, 240, 436-444.

Cunningham, W. D., 1998. Lithospheric controls on late Cenozoic construction of the Mongolian Altai. *Tectonics*, 17, 891-902.

Cunningham, W. D., Dijkstra, A., Howard, J., Quarles, A., Badarch, G., 2001. Active Intraplate Strike-slip Faulting and Transpressional Uplift in the Mongolian Altai. *In*, Storti, F., Holdsworth, R.E. & Salvini, F. (eds), *Intraplate Strike-slip Deformation Belts*, Geological Society, London, Special Publications, 210, 65-87.

Davidson, J. P., De Silva, S. L., 1995. Late Cenozoic magmatism of the Bolivian Altiplano. *Contributions to Mineralogy and Petrology*, 119, 387-408.

Davidson, J. P., Mcmillan, N. J., Moorbath, S., Wörner, G., Harmon, R. S., López-Escobar, L., 1990. The Nevados De Payachata volcanic region (18°S/69°W, N. Chile) Ii. Evidence for widespread crustal involvement in Andean magmatism. *Contributions to Mineralogy and Petrology*, 105, 412-432.

Dejidmaa, G., 2005. Mineral Resources and Metallogenic Belts in Southern Mongolia. In: Seltmann, R., Gerel, O., and Kirwin, D., eds., *Geodynamics and metallogeny of Mongolia, with a special emphasis on copper and gold deposits*, CERCAMS, London.

Dobretsov, N. L., Buslov, M., 2005. Central Asian accretion-collisional belts with HP and UHP rocks. In: Sklyarov, E. V., ed., Structural and tectonic correlation across the Central asia orogenic collage: north-eastern segment. *Guidebook and abstract volume of the Siberian Workshop IGCP-480.*: Irkutsk, IEC SB RAS, pp. 183-187.

Druitt, T. H., Mellors, R. A., Pyle, D., Sparks, R. S. J., 1989. Explosive volcanism on Santorini, Greece. *Geological Magazine*, 126, 95-126.

Eby, G. N., 1990. The A-type granitoids: a review of their occurrance and chemical characteristics. *Lithos*, 26, 115-134.

Eby, G. N., 1992. Chemical subdivision of the A-type granitoids: petrogenetic and tectonic implications. *Geology*, 20, 189-200.

Eggins, S. M., 1993. Origin and differentiation of picritic arc magmas, Ambae (Aoba), Vanuatu. *Contributions to Mineralogy and Petrology*, 114, 79-100.

Feeley, T. C., Davidson, J. P., 1994. Petrology of Calc-Alkaline lavas of Volcan Ollagüe and the origin of compositional diversity at Central Andean stratovolcanoes. *Journal of Petrology*, 35 1295-1340.

Ferry, J. M., 1985. Hydrothermal alteration of tertiary igneous rocks from the Isle of Skye, northwest Scotland: 2. Granites. *Contributions to Mineralogy and Petrology*, 91, 283-304.

Fisher, R. V., Schmincke, H.-U., 1994. Volcaniclastic sediment transport and deposition. *In:* Pye, K., ed., *Sediment transport and depositional processes*, Blackwell Scientific Publications, pp. 351-388.

Frolova, T. I., Rudnik, G. B., 1974. The anorthosite tendency of differentiation in volcanic rocks of the early stages of island arc development: Example of South Sandwich island arc. *Vestnik Moskov. Univ. Ser. 4, Geol.* Moscow 4, 20-36.

Fujinawa, A., Kamata, M., 2005. Development history and changes of magma plumbing systems of Adatara Volcano during recent 250000 years. *Japanese Magazine of Mineralogical and Petrological Sciences*, 34, 35-58.

Fukudome, T., Yoshida, T., Nagao, K., Itaya, T., Tanoue, S., 1990. Pliocene alkali basalts from Kyuroku-Shima Island, northeast of Japan sea. *Journal of the Japanese Association of Mineralogists, Petrologists and Economic Geologists*, 85, 10-18.

Gasperini, D., Blichert-Toft, J., Bosch, D., Del Moro, A., Macera, P., Albarède, F., 2002. Upwelling of deep mantle material through a plate window: Evidence from the geochemistry of Italian basaltic volcanics. *Journal of Geophysical research*, B107, Ecv 7-1-Ecv 7-19.

Gerel, O., Oyungerel, S., Minjin, C., 2005. Intrusive magmatism of South Mongolia. In: Seltmann, R., Gerel, O., and Kirwin, D., eds., *Geodynamics and metallogeny of Mongolia with special emphasis on copper and gold deposits*, CERCAMS, London

Gertisser, R., Keller, J., 2003. Trace element and Sr, Nd, Pb and O isotope variations in medium-K and high-K volcanic rocks from Merapi Volcano, Central Java, Indonesia: Evidence for the involvement of subducted sediments in Sunda arc magma genesis. *Journal of Petrology*, 44, 457-489.

Gill, J. B., 1981. Orogenic Andesites and Plate Tectonics. Springer-Verlag, New York.

Gill, J. B., Williams, R. W., 1990. Th isotope and U-series studies of subduction related volcanic rocks. *Geochimica et Cosmochimica Acta*, 54, 1427-1442.

Gledhill, A. R., Baker, P. E., 1973. Strontium isotope ratios in volcanic rocks from the South Sandwich islands. *Earth and Planetary Science Letters* 19 369-372.

Gorton, M. P., 1977. The geochemistry and origin of Quaternary volcanism in the New Hebrides. *Geochimica et Cosmochimica Acta*, 41, 1257-1270.

Graham, S. A., Hendrix, M. S., Johnson, C. L., Badamgarav, D., Badarch, G., Amory, J., Porter, M., Barsbold, R., Webb, L. E., Hacker, B. R., 2001. Sedimentary Record and Tectonic Implications of Mesozoic Rifting in Southeast Mongolia. *GSA Bulletin*, 113, 1560-1579.

Grant, J. A., 1986. The Isocon Diagram: A Simple Solution to Gresens' Equation for Metasomatic Alteration. *Economic Geology*, 81, 1976-1982.

Grocott, J and Taylor, G. 2002. Magmatic arc fault systems, deformation partitioning and emplacement of granitic complexes in the Coastal Cordillera, north Chilean Andes. *Journal of the Geological Society of London*, 159, 425-442

Gust, D. A., Arculus, R. J., Kersting, A. B., 1997. Aspects of magma sources and processes in the Honshu arc. *Canadian Mineralogist* 35, 347-365.

Halter, W. E., Bain, N., Becker, K., Heinrich, C. A., Landtwing, M., Von Quadt, A., Clark, A. H., Sasso, A. M., Bissig, T., Tosdal, R. M., 2004. From andesitic volcanism to the formation of a porphyry Cu-Au mineralizing magma chamber: The Farallon Negro volcanic complex, Northwestern Argentina. *Journal of Volcanology and Geothemal Research*, 136, 1-30.

Harris, N. B. W., Pearce, J. A., Tindle, A. G., 1986. Geochemical characteristics of collision zone magmatism. In: Coward, M. P., and Ries, A. C., eds., *Collision Tectonics* - Geological Society Special Publication No.19, Blackwell Scientific Publications, pp. 67-81.

Hauff, F., Hoernle, K. A., Tilton, G. R., Graham, D. W., Kerr, A. C., 2000. Large volume recycling of oceanic lithosphere over short time scales: Geochemical constraints from the Caribbean large igneous province. *Earth and Planetary Science Letters*, 174 247-263.

Hawkesworth, C. J., O'Nions, R. K., Pankhurst, R. J., Hamilton, P. J., Evensen, N. M., 1977. A geochemical study of island-arc and back-arc tholeiites from the Scotia sea. *Earth Planetary Science Letters*, 36, 253-262.

Heath, E., Macdonald, R., Belkin, H., Hawkesworth, C. J., Sigurdsson, H., 1998. Magmagenesis at Soufriere volcano, St Vincent, Lesser Antilles arc. *Journal of Petrology*, 39, 1721-1764.

Helo, C., Hegner, E., Kroner, A., Badarch, G., Tomurtogoo, O., Windley, B. F., Dulski, P., 2006. Geochemical signature of palaeozoic accretionary complexes of the Central Asian Orogenic Belt in southern Mongolia, constraints on arc environments and crustal growt. *Chemical Geology*, 227, 236-257.

Hildreth, W., Grunder, A. L., Drake, R. E., 1984. The Loma Seca tuff and the Calabozos caldera: a major ash flow and caldera complex in the southern Andes of Chile. *Geological Society of America Bulletin*, 95, 45-54.

Hooker, P. J., Davidson, J. P., Croudace, I. W., Escobar, A., 1993. Volcanological and petrological evolution of Volcan Tata Sabaya, SW Bolivia. *Journal of Volcanology and Geothemal Research*, 55, 305-355.

International Commission on Stratigraphy, 2004. International Stratigraphic Chart.

Ishihara, S., Wu, C., 2001. Genesis of Late Cretaceous-Paleogene granitoids with contrasting chemical trends in the Chubu District, Central Japan. *Bulletin of the Geological Society of Japan*, 52, 471-491.

Ishiwatari, A., Ohama, H., 1997. Clinopyroxene basalt dikes in the Miocene Iwaine formation, Hokuriku province, Japan : Various continental arc magmas including shoshonite series and origin of the clinopyroxene phenocrysts. Journal *of the Geological Society of Japan*, 103, 565-578.

Iwamori, H., 1992. Degree of melting and source composition of Cenozoic basalts in Southwest Japan: Evidence for mantle upwelling by flux melting. *Journal of Geophysical Research*, B97 10983-10995.

Janoušek, V., Farrow, C. M., Erban, V., 2006. Interpretation of whole-rock geochemical data in igneous geochemistry: introducing GCD kit. *Journal of Petrology*, 47, 1255-1259.

Johnston, A. D., 1986. Anhydrous P-T phase relations of near-primary high-alumina basalt from the South Sandwich islands: Implications for the origin of island arcs and tonalite-trondhjemite series rocks. *Contributions to Mineralogy and Petrology*, 92, 368-382.

Jones, G., Valsami-Jones, E., Sano, H., 1993. Nature and tectonic setting of accreted basalts from the Mino Terrane, Central Japan. *Journal of the Geological Society of London*, 150, 1167-1181.

Kagami, H., Iizumi, S., Tainosho, Y., Owada, M., 1992. Spatial variations of Sr and Nd isotope ratios of Cretaceous-Paleogene granitoid rocks, Southwest Japan arc. *Contributions to Mineralogy and Petrology*, 112, 165-177.

Kamei, A., 2002. Petrogenesis of Cretaceous peraluminous granite suites with low initial Sr isotopic ratios, Kyushu Island, Southwest Japan Arc. *Gondwana Research*, 5, 813-822.

Kerr, A. C., Tarney, J., Marriner, G. F., Klaver, G. T., Saunders, A. D., Thirlwall, M. F., 1996a. The geochemistry and petrogenesis of the Late-Cretaceous picrites and basalts of Curacao, Netherlands Antilles: A remnant of an oceanic plateau. *Contributions to Mineralogy and Petrology*, 124, 29-43.

Kerr, A. C., Tarney, J., Marriner, G. F., Nivia, A., Klaver, G. T., Saunders, A. D., 1996b. The geochemistry and tectonic setting of Late Cretaceous Caribbean and Colombian volcanism. *Journal of South American Earth Sciences*, 9, 111-120.

Korim, M., Delgertsogt, B., Chovan, M., Fiesh. I., 1984. The Geologic–structural features and ore potential of the Shuteen covano-plutonic magmatic activity. *The Geology and Economic Minerals of Mongolia*. 159-164 (in Russian), Monograph

King, P. L., White, A. J. R., Chappell, B. W., Allen, C. M., 1997. Characterisation and origin of aluminous A-type granites from the Lachlan Fold Belt, Southeastern Australia. *Journal of Petrology*, 38, 371-391.

Kimura, J.-I., Tanji, T., Yoshida, T., Iizumi, S., 2001. Geology and geochemistry of lavas at Nekoma volcano: Implications for origin of Quaternary low-K andesite in the North-Eastern Honshu arc, Japan. *The Island Arc*, 10, 116-134.

Kimura, J.-I., Yoshida, T., 1999. Magma plumbing system beneath Ontake volcano, Central Japan. *The Island Arc*, 8, 1-29.

Kimura, J.-I., Yoshida, T., Iizumi, S., 2002. Origin of low-K intermediate lavas at Nekoma volcano, Ne Honshu arc, Japan: Geochemical constraints for lower-crustal melts. *Journal of Petrology*, 43, 631-661.

Kirwin, D., Wilson, C. C., Turmagnai, D., Wolfe, R., 2005. Exploration history, geology, and mineralisation of the Kharmagtai gold-copper porphyry district South Gobi region, Mongolia. In: Seltmann, R., Gerel, O., and Kirwin, D., eds., *Geodynamics and metallogeny of Mongolia with special emphasis on copper and gold deposits*, CERCAMS, London.

Kita, I., Yamamoto, M., Asakawa, Y., Nakagawa, M., Taguchi, S., Hasegawa, H., 2001. Contemporaneous ascent of within-plate type and island-arc type magmas in the Beppu-Shimabara graben system, Kyushu island, Japan. *Journal of Volcanology and Geothemal Research*, 111, 99-109.

Kobayashi, K., Nakamura, E., 2001. Geochemical evolution of Akagai volcano, Ne Japan: Implications for interaction between island-arc magma and lower crust, and generation of isotopically various magmas. *Journal of Petrology*, 42, 2303-2331.

Kohn, S. C., Henderson, C. M. B., Mason, R. A., 1989. Element zoning trends in olivine phenocrysts from a supposed primary high-magnesian andesite: An electron- and ion-microbrobe study. *Contributions to Mineralogy and Petrology*, 103, 242-252.

Kontak, D. J., Clark, A. H., Farrar, E., Pearce, T. H., Strong, D. F., Baadsgaard, H., 1986. Petrogenesis of a neogene shoshonite suite, Cerro Moromoroni, Puno, Southeastern Peru. *Canadian Mineralogist*, 24, 117-135.

Krogh, T. E., 1982. Improved accuracy of U-Pb ages by the creation of more concordant systems using an air abrasion technique. *Geochimica et Cosmochimica acta*, 46, 637-649.

Kutsukake, T., 1993. An initial continental margin plutonism - Cretaceous older Ryoke Granitoids, Southwest Japan. *Geological Magazine*, 130 15-28.

Kutsukake, T., 2002. Geochemical characteristics and variations of the Ryoke Granitoids, southwest Japan: Petrogenetic implications for the plutonic rocks of a magmatic arc. *Gondwana Research*, 5, 355-372.

Lamb, M. A., Badarch, G., 1997. Paleozoic sedimentary basins and volcanic-arc systems of southern Mongolia; new stratigraphic and sedimentologic constraints. *Intenational Geology Review*, 39, 542-576.

Lamb, M. A., Badarch, G., 2001. Paleozoic sedimentary basins and volcanic arc systems of southern Mongolia; new geochemical and petrographic constraints. In: Hendrix, M. S., and Davis, G. A., eds., *Paleozoic and Mesozoic Tectonic Evolution of Central and Eastern Asia: From Continental Assembly to Intracontinental Deformation.* Geological Society of America (GSA), Boulder, CO, p. 117-149.

Lamb, M. A., Cox, D., 1998. New $^{40}Ar/^{39}Ar$ age data and implications for porphyry copper deposits of Mongolia. *Economic Geology*, 93, 524-529.

Lamb, M. A., Hanson, A. D., Graham, S. A., Badarch, G., Webb, L. E., 1999. Left-lateral sense offset of upper Proterozoic to Paleozoic features across the Gobi Onon, Tost, and Zuunbayan faults in southern Mongolia and implications for other Central Asian faults. *Earth and Planetary Science Letters*, 173, 183-194.

Laurent-Charvet, S., Charvet, J., Shu, L., Ma, R., Lu, H., 2002. Palaeozoic late collisional strike-slip deformations in Tianshan and Altay, Eastern Xinjiang, NW China. *Terra Nova*, 14, 249-256.

Le Bas, M. J., Le Maitre, R. W., Streckeisen, A., Zanettin, B., 1986. A chemical classification of volcanic rocks based on the total alkali-silica diagram. *Journal of Petrology*, 27, 745-750.

Li, J. Y., 2006. Permian geodynamic setting of Northeast China and adjacent regions: closure of the Paleo-Asian Ocean and subduction of the Paleo-Pacific Plate. *Journal of Asian Earth Sciences*, 26, 207-224.

Lidiak, E. G., Larue, D. K., 1998. Geochemistry of intrusive igneous rocks, St. Croix, U.S. Virgin Islands. *Special Paper for the Geological Society of America*, 322, 133-153.

Lindsay, J. M., Trumbull, R. B., Siebel, W., 2005. Geochemistry and petrogenesis of late Pleistocene to recent volcanism in Southern Dominica, Lesser Antilles. *Journal of Volcanology and Geothemal Research*, 148, 253-294.

Loiselle, M. C., Wones, D. R., 1979. Characteristics and origin of anorogenic granites. *Geological Society of America Abstract Programs*, 11, 468.

Ludwig, K. R., 1980. Calculation of uncertainities of U-Pb isotope data. *Earth and Planetary Science Letters*, 46, 212-220.

Ludwig, K. R., 1993. Pbdat: a computer program for processing Pb-U-Th isotope data. *United States Geological Survey, Open file reports.*, 88-542, 1-34.

Ludwig, K. R., 2003. Isoplot 3.00: A geochronological toolkit for Microsoft Excel. *Berkeley Geochronology Centre Special Publication*, 4, 0-71.

Ludwig, K. R., 1980. Calculation of uncertainities of U-Pb isotope data. *Earth and Planetary Science Letters*, 46, 212-220.

Ludwig, K. R., 1993. Pbdat: a computer program for processing Pb-U-Th isotope data. *United States Geological Survey, Open file reports.*, 88-542, 1-34.

Luhr, J. F., Carmichael, I. S. E., 1985. Jorullo Volcano, Michoacan, Mexico (1759-1774): The earliest stages of fractionation in calc-alkaline magmas. *Contributions to Mineralogy and Petrology*, 90, 142-161.

Maillet, P., Ruellan, E., Gerard, M., Person, A., Bellon, H., Cotten, J., Joron, J.-L., Nakada, S., Price, R. C., 1995. Tectonics, magmatism, and evolution of the New Hebrides backarc troughs (Southwest Pacific) *In*: Taylor, B., ed., *Backarc Basins: Tectonics And Magmatism*, Plenum Press, London, pp. 177-235.

Mandeville, C. W., 1996. Magma mixing, fractional crystallization and volatile degassing during the 1883 eruption of Krakatau Volcano, Indonesia. *Journal of Volcanology and Geothemal Research*, 74, 243-274.

Marcelot, G., 1981. Geochemistry of the lavas of Erromango island (New Hebrides): Petrogenetic implications. *Bulletin de la Societie Geologique de France*, 23, 367-376.

Marcelot, G., Maury, R. C., Lefevre, C., 1983. Mineralogy of Erromango lavas (New Hebrides): Evidence of an early stage of fractionation in island arc basalts. *Lithos*, 16, 135-151.

Marsaglia, K. M., Ingersoll, R. V., 1992. Compositional trends in arc-related, deep-marine sand and sandstone; a reassessment of magmatic-arc provenance. *Geological Society of America Bulletin*, 104, 1637-1649.

Marzoli, A., Renne, P. R., Piccirillo, E. M., Francesca, C., Bellieni, G., Melfi, A. J., Nyobe, J. B., N^Ni, J., 1999. Silicic magmas from the continental Cameroon volcanic line (Oku, Bambouto And Ngaoundere): 40Ar-39Ar Dates, petrology, Sr-Nd-O isotopes and their petrogenetic significance. *Contributions to Mineralogy and Petrology*, 135, 133-150.

Masaki, Y., 1994. Timing of intrusion of the Otagiri granite with respect to the deformation and metamorphism in Ryoke Belt in the Ina district, Central Japan: Examination by Rb-Sr whole rock isochron ages. *Journal of the Japanese Association of Mineralogists, Petrologists and Economic Geologists*, 89 269-284.

Masuda, Y., Yagi, S., Mitsuji, T., Nishimura, S., 1983. Trace element contents in the granitic rocks from southwestern Japan (1) Chugoku district. *Journal of the Japanese Association of Mineralogists, Petrologists and Econonomic Geologists*, 78, 41-50.

Matthews, S. J., Jones, A. P., Gardeweg, M. C., 1994. Lascar volcano, Northern Chile: Evidence for steady-state disequilibrium. *Journal of Petrology*, 35, 401-432.

Mattinson, J. M., 2005. Zircon U-Pb chemical abrasion ("CA-TIMS") method: Combined annealing and multi-step partial dissolution analysis for improved precision and accuracy of zircon ages. *Chemical Geology*, 220, 47-66.

Maughan, D. T., Keith, J. D., Christiansen, E. H., Pulsipher, T., Hattori, K., Evans, N. J., 2002. Contributions from mafic alkaline magmas to the Bingham porphyry Cu-Au-Mo deposit, Utah, USA. *Mineralium Deposita*, 37, 14-37.

McConnell, B. J., Menuge, J. F., Hertogen, J., 2002. Andesite petrogenesis in the Ordovician Borrowdale Volcanic Group of the English Lake District by fractionation, assimilation and mixing. *Journal of the Geological Society of London*, 159, 417-424

McIntyre, G. A., Brooks, A. C. Compston, W and Turek, A. (1966). The statistical assessment of Rb)Sr isochrons. J. Geophys. Res. **71**, 5459-68.

McMillan, W. J., Pantaleyev, A., 1988. Porphyry Copper Deposits. *In*, Roberts, R.G., Sheahan, P.A. eds., *Ore Deposit Models*. Geoscience Canada, Ontario, p. 45-58

Meng, Q., Hu, J., Jin, J., Y., Z., Xu, D., 2003. Tectonics of the late Mesozoic wide extensional basin system in the ChinaMongolia border region. *Basin Research*, 15, 397-415.

Meighan, I. G., Gibson, D., Hood, D. N., 1984. Some aspects of Tertiary acid magmatism in NE Ireland. *Mineralogical Magazine*, 351-363.

Middlemost, E. A. K., 1985. Magmas and Magmatic Rocks: An Introduction to Igneous Petrology. Longman, London, 266 pp.

Miskovic, A., Francis Don, M., 2006. Interaction between mantle-derived and crustal calc-alkaline magmas in the petrogenesis of the Paleocene Sifton Range volcanic complex, Yukon, Canada. *Lithos* 87, 104-134.

Miyake, Y., 1994. Geochemistry of igneous rocks of Shimane Peninsula, formed within a Miocene back-arc rifting zone at the Japan sea margin. *Geochemical Journal*, 28, 451-472.

Miyashita, S., Tsuchiya, N., Ikeda, Y., Sakamoto, I., 1995. Petrology of the Okushiri ridge basalts in the Japan sea basin : Arc- and plume-type magma series. *Memoir of the Geological Society of Japan*, 44, 1-21.

Monzier, M., Robin, C., Eissen, J.-P., Cotten, J., 1997. Geochemistry Vs. seismo-tectonics along the volcanic New Hebrides central chain (Southwest Pacific). *Journal of Volcanology and Geothermal Research*, 78, 1-29.

Morris, P. A., 1995. Slab melting as an explanation of Quaternary volcanism and aseismicity in Southwest Japan. *Geology*, 23, 395-398.

Morris, P. A., Miyake, Y., Furuyama, K., Puelles, P., 1999. Chronology and petrology of the Daikonjima basalt, Nakaumi lagoon, eastern Shimane prefecture, Japan. Journal of the Japanese Association of Mineralogists, *Petrologists and Economic Geologists*, 94, 442-452.

Mossakovsky, A. A., Dergunov, A. B., 1985. The Caledonides of Kazakhstan, Siberia, and Mongolia: a review of structure, development history, and palaeotectonic environments. . In: Gee, D. G., and Sturt, B. A., eds., *The Caledonide Orogen - Scandinavia and related areas*. London, Wiley, pp. 1201-1215.

Mossakovsky, A. A., Ruzhentsev, S. V., Samygin, S. G., Keheraskova, T. N., 1994. Central Asia fold-belt: geodynamic evolution and formation history. *Geotectonics*, 27, 445-474.

Mundil, R., Ludwig, K. R., Metcalfe, I., Renne, P. R., 2004. Age and timing of the End Permian mass extinctions: U/Pb geochronology on closed-system zircons. *Science*, 305, 1760-1763.

Nairn, I. A., Kobayashi, T., Nakagawa, M., 1998. The ~10 ka multiple vent pyroclastic eruption sequence at Tongariro Volcanic Centre, Taupo Volcanic Zone, New Zealand: Part 2. Petrological insights into magma storage and transport during regional extension. *Journal of Volcanology and Geothermal Research*, 86, 45-65.

Nakashima, T., Shimoda, G., Tatsumi, Y., 2000. Porphyritic magnesian andesites in the Setouchi volcanic belt, S.W. *Japan Bulletin of the Volcanological Society of Japan*, 45, 259-269.

Noble, S. R., Tucker, R. D., Pharoah, T. C., 1993. Lower Palaeozoic and precambrian igneous rocks from eastern England and their bearing on late Ordovician closure of the Tornquist sea: constraints from U-Pb and Nd isotopes. *Geological Magazine*, 130, 835-846.

Ohta, E., Kawano, Y., Nakagawa, M., Kagami, H., 1998. Petrochemistry of late Miocene to Quaternary igneous rocks and metallogenesis in Southwest Hokkaido, *Japan Resource Geology (Tokyo)*, 48 183-195.

Oliver, M. A., Webster, R., 1990 Kriging: A method of interpolation for geographical information systems. *International Journal of Geographical Information Systems*, 4, 313-332.

Ort, M. H., Coira, B., Mazzoni, M. M., 1996. Generation of a crust-mantle mixture: Magma sources and contamination at Cerro Panizos, Central Andes. *Contributions to Mineralogy and Petrology*, 123, 308-322.

Pankhurst, R. J., Walsh, J. N., Beckinsale, R. D., Skelhorn, R. R., 1978. Isotopic and other geochemical evidence for the origin of the Loch Uisg Granophyre, Isle of Mull, Scotland. *Earth and Planetary Science Letters*, 38, 355-363.

Parada, M. A., Levi, B., Nyström, J. O., 1991. Geochemistry of the Triassic to Jurassic plutonism of Central Chile (30 To 33°S): Petrogenetic implications and a tectonic discussion. *Special Paper for the Geological Society of America*, 265, 99-112.

Pearce, J. A., 1983. Role of the subcontinental lithosphere in magma genesis at active continental margins. In: Hawkesworth, C. J., and Norry, M. J., eds., *Continental basalts and mantle xenoliths*. Shiva Publishing, Nantwich, pp. 210-230.

Pearce, J. A., Baker, P. E., Harvey, P. K., Luff, I. W., 1995. Geochemical evidence for subduction fluxes, mantle melting and fractional crystallization beneath the South Sandwich island arc. *Journal of Petrology*, 36, 1073-1109.

Peate, D. W., Pearce, J. A., Hawkesworth, C. J., Edwards, C. M. H., Hirose, K., 1997. Geochemical variations in Vanuatu arc lavas: The role of subducted material and a variable mantle wedge composition. *Journal of Petrology*, 38, 1331-1358.

Perello, J., Cox, D., Garamjav, D., Sanjdorj, S., Diakov, S., Schissel, D., Munkhbat, T.-O., Oyun, G., 2001. Oyu Tolgoi, Mongolia; Siluro-Devonian porphyry Cu-Au-(Mo) and high-sulfidation Cu mineralization with a Cretaceous chalcocite blanket. *Economic Geology*, 96, 1407-1428.

Petterson, M. G., Beddoe-stephens, B., Millward, D., Johnson, E. W., 1992. A pre-caldera plateau-andesite field in the Borrowdale Volcanic Group of the English Lake District. *Journal of the Geological Society of London*, 149, 889-906.

Piercey, S. J., Mortensen, J. K., Creaser, R. A., 2003. Neodymium isotope geochemistry of felsic volcanic and intrusive rocks from the yukon-tanana terrane in the Finlayson Lake Region, Yukon, Canada. *Canadian Jornal of Earth Sciences*, 40, 77-97.

Price, R. C., Johnson, L. E., Crawford, A. J., 1990. Basalts of the North Fiji basin: the generation of back arc basin magmas by mixing of depleted and enriched mantle sources *Contributions to Mineralogy and Petrology*, 105, 106-121.

Raos, A. M., Crawford, A. J., 2004. Basalts from the Efate island group, central section of the Vanuatu arc, SW Pacific: Geochemistry and petrogenesis. *Journal of Volcanology and Geothermal Research*, 134, 35-56.

Reubi, O., Nicholls, I. A., 2004. Magmatic evolution at Batur volcanic field, Bali, Indonesia: Petrological evidence for polybaric fractional crystallization and implications for caldera-forming Eruptions. *Journal of Volcanology and Geothemal Research*, 138, 345-369.

Reubi, O., Nicholls, I. A., 2005. Structure and dynamics of a silicic magmatic system associated with caldera-forming eruptions at Batur volcanic field, Bali, Indonesia. *Journal of Petrology*, 46, 1367-1391.

Reubi, O., Nicholls, I. A., Kamenetsky, V. S., 2002. Early mixing and mingling in the evolution of basaltic magmas: Evidence from phenocryst assemblages, Slamet volcano, Java, Indonesia. *Journal of Volcanology and Geothemal Research*, 119, 255-274.

Révillon, S., Arndt, N. T., Kerr, A. C., Tarney, J., 1999. Petrogenesis of picrites from the Caribbean plateau and the North Atlantic magmatic province. *Lithos*, 49, 1-21.

Rezanov, A. I., Kenji, S., Iizumi, S., 1996. A Rb-Sr whole rock isochron age of the Gozu granite, Niigata Prefecture, *Central Japan. Journal of the Geological Society of Japan*, 102, 828-831.

Richards, J. P., Ullrich, T., Kerrich, R., 2006. The late Miocene-Quaternary Antofalla volcanic complex, Southern Puna, NW Argentina: Protracted history, diverse petrology, and economic potential. *Journal of Volcanology and Geothemal Research*, 152, 197-239.

Richards, J. P., Villeneuve, M. E., 2002. Characteristics of late Cenozoic volcanism along the Archibarca lineament from Cerro Llullaillaco to Corrida De Cori, Northwest Argentina. *Journal of Volcanology and Geothemal Research*, 116, 161-200.

Rollinson, H., 1993. Using geochemical data: evaluation, presentation, interpretation. Longman, 352 pp.

Rundle C.C., 1981. Discussion on the age of mineralisation at Parys Mountain, Anglesey. *Journal of the Geological Society of London*. 138, 755-756.

Ruzhentsev, S. V., Pospelov, I. I., 1992. The south Mongolian Variscan fold system. *Geotectonics*, 26, 383-395.

Sandeman, H. A., Clark, A. H., 2004. Commingling and mixing of S-type peraluminous, ultrapotassic and basaltic magmas in the Cayconi volcanic field, Cordillera De Carabaya, S.E. Peru. *Lithos*, 73, 187-213.

Saunders, A. D., Tarney, J., Weaver, S. D., 1980. Transverse geochemical variations across the Antarctic Peninsula: implications for the genesis of calc-alkaline magmas. *Earth and Planetary Science Letters*, 46, 344-360.

Selby, D., Creaser, R. A., Hart, C.J.R., Rombach, C.S., Thompson, J.F.H., Smith, M.T., Bakke, A.A., and Goldfarb, R.J., 2002. Absolute timing of sulfide and gold mineralization: A comparison of Re-Os molybdenite and Ar-Ar mica methods from the Tintina Gold Belt, Alaska. *Geology*, 9, 791-794

Şengör, A. M. C., Natal'in, B. A., Burtman, V. S., 1993. Evolution of the Altaid tectonic collage and Palaeozoic crustal growth in Eurasia. *Nature*, 364, 299-307.

Şengör, A. M. C., Natal'in, B. A., 1996. Palaeotectonics of Asia: fragments of a synthesis. *In*: Yin, A., and Harrison, M., eds., *The Tectonic Evolution of Asia*, Cambridge University Press, Cambridge, pp. 486-640.

Shand, S. J., 1943. The Eruptive Rocks. John Wiley and Sons, New York, New York.

Shimizu, N., Arculus, R. J., 1975. Rare Earth Element concentrations in a suite of basanitoids and alkali olivine basalts from Grenada, Lesser Antilles. *Contributions to Mineralogy and Petrology*, 50, 231-240.

Shimoda, G., Tatsumi, Y., Nohda, S., Ishizaka, K., Jahn, B.-M., 1998. Setouchi high-Mg andesites revisited: geochemical evidence for melting of subducting sediments. *Earth and Planetary Science Letters*, 160, 479-492.

Shinjoe, H., 1997. Origin of the granodiorite in the forearc region of southwest Japan: Melting of the Shimanto accretionary prism. *Chemical Geology*, 134, 237-255.

Shuto, K., Ishimoto, H., Hirahara, Y., Sato, M., Matsui, K., Fujibayashi, N., Takazawa, E., Yabuki, K., Sekine, M., Kato, M., Rezanov, A. I., 2006. Geochemical secular variation of magma source during early to middle Miocene time in the Niigata area, NE Japan: Asthenospheric mantle upwelling during back-arc basin opening. *Lithos*, 86, 1-33.

Sillitoe, R. H., 1997. Characteristics and controls of the largest porphyry copper-gold and epithermal gold deposits in the circum-Pacific region. *Australian Journal of Earth Sciences*, 44, 373-388.

Smith, T. E., Thirlwall, M. F., Macpherson, C. G., 1996. Trace element and isotope geochemistry of the volcanic rocks of Bequia, Grenadine Islands, Lesser Antilles arc: A study of subduction enrichment and intra-crustal contamination. *Journal of Petrology*, 37, 117-143.

Soesoo, A., Nicholls, I. A., 1999. Mafic rocks spatially associated with Devonian felsic intrusions of the Southern Lachlan Fold Belt: A possible mantle contribution to crustal evolution processes. *Australian Journal of Earth Sciences*, 46, 725-734.

Speed, R. C., Walker, J. A., 1991. Oceanic crust of the Grenada Basin in the Southern Lesser Antilles arc platform. *Journal of Geophysical Research*, B96, 3835-3851.

Stacey, J. S., Kramers, J. D., 1975. Approximation of terrestrial lead isotope evolution by a two stage model. *Earth and Planetary Science Letters*, 26, 207-201.

Stein, H.J., Markey, R.J. and Morgan, J.W., 2000. Robust Re-Os Molybdenite Ages for the Hemlo Au Deposit, Superior Province, Canada. *Goldschmidt Journal of Conference Abstracts*, 5, 995

Stern, C. R., Futa, K., Mühlenbachs, K., 1984. Isotope and trace element data for orogenic andesites from the Austral Andes. *In*: Harmon, R. S., and Barreiro, B. A., eds., Andean Magmatism; *Chemical And Isotopic Constraints*, Shiva, pp. 31-46.

Stern, C. R., Skewes, M. A., 1995. Miocene to present magmatic evolution at the northern end of the Andean Southern volcanic zone, Central Chile. *Revista geológica de Chile*, 22, 261-272.

Stolz, A. J., Varne, R., Davies, G. R., Wheller, G. E., Foden, J. D., 1990. Magma source components in an arc-continent collision zone: The Flores-Lembata sector, Sunda arc, Indonesia. *Contributions to Mineralogy and Petrology*, 105, 585-601.

Stolz, A. J., Varne, R., Wheller, G. E., Foden, J. D., J., A. M., 1988. The geochemistry and petrogenesis of K-rich alklaine volcanics from the Batu Tara volcano, eastern Sunda arc. *Contributions to Mineralogy and Petrology*, 98, 374-389.

Sun, S. S., McDonough, W. F., 1989. Chemical and isotopic systematics of ocean basalts: Implications for mantle composition and processes In: Saunders, A. D., and Norry, M. J., eds., Magmatism in Ocean Basins, 42, *Geology Society Special Publications*, pp. 313-345.

Takagi, T., 1992. Mineral equilibria and crystallization conditions of Ukan Granodiorite (Ilmenite-Series) and Kayo Granite (Magnetite-Series), San'yo Belt, Southwest Japan. *Journal of the Geological Society of Japan*, 98, 101-124.

Takagi, T., Kagami, H., Iizumi, S., 1989. Petrography And Geochemistry Of Two Contrasting I-Type Granites, The Mitsumori And Ikuridani Granites, San'In Belt, Southwest Japan. *Journal of the Geological Society of Japan*, 95, 905-918.

Takashima, R., Nishi, H., Yoshida, T., 2002. Geology, petrology and tectonic setting of the late Jurassic ophiolite in Hokkaido, Japan. *Journal of Asian Earth Sciences*, 21, 197-215.

Tamura, Y., Yuhara, M., Ishii, T., 2000. Primary arc basalts from Daisen volcano, Japan: Equilibrium crystal fractionation versus disequilibrium fractionation during supercooling. *Journal of Petrology*, 41, 431-448.

Tamura, Y., Yuhara, M., Ishii, T., Irino, N., Shukuno, H., 2003. Andesites and dacites from Daisen volcano, Japan: Partial-to-total remelting of an andesite magma body. *Journal of Petrology*, 44, 2243-2260.

Tatsumi, Y., Shukuno, H., Sato, K., Shibata, T., Yoshikawa, M., 2003. The petrology and geochemistry of high-magnesium andesites at the western tip of the Setouchi volcanic belt, S.W. Japan. *Journal of Petrology*, 44, 1561-1578.

Tatsumi, Y., Shukuno, H., Yoshikawa, M., Chang, Q., Sato, K., Lee, M. W., 2005. The petrology and geochemistry of volcanic rocks on Jeju island: Plume magmatism along the Asian continental margin. *Journal of Petrology*, 46, 523-553.

Tatsumi, Y., Suzuki, T., Kawabata, H., Sato, K., Miyazaki, T., Chang, Q., Takahashi, T., Tani, K., Shibata, T., Yoshikawa, M., 2006. The petrology and geochemistry of Oto-Zan composite lava flow on Shodo-Shima island, SW Japan: Remelting of a solidified high-Mg andesite magma. *Journal of Petrology*, 47, 595-629.

Taylor, S. R., McLennan, S. M., 1985. The Cotinental Crust: its Composition and Evolution. Blackwell Scientific Publications.

Thirlwall, M. F., Graham, A. M., 1984. Evolution of high-Ca, high-Sr C-series basalts from Grenada, Lesser Antilles: Contamination in the arc crust. *Journal of the Geological Society of London*, 141, 427-445.

Thirlwall, M. F., Graham, A. M., Arculus, R. J., Harmon, R. S., Macpherson, C. G., 1996. Resolution of the effect of crustal assimilation, sediment subduction, and fluid transport in island arc magmas: Pb-Sr-Nd-O isotope geochemistry of Grenada, Lesser Antilles. *Geochimica et Cosmochimica Acta*, 60, 4785-4810.

Thorpe, R. S., Francis, P. W., O'Callaghan, L. J., 1984. Relative roles of source composition, fractional crystallization and crustal contamination in the petrogenesis of Andean volcanic rocks. *Philosophical Transations of the the Royal Society of London*, A310, 675-692.

Ujiie, M., 1989. Zonal structure of the Orikabe plutonic complex, Kitakami mountains. *Journal of the Japanese Association of Mineralogists, Petrologists and Economic Geologists*, 84, 226-242.

Uto, K., Hirai, H., Arai, S., 1993. K-Ar Ages for Quaternary alkali basalts from Kurose, Fukuoka prefecture and Kifune Yamaguchi prefecture, *Southwest Japan Bulletin of the Geological Survey of Jap*an, 44, 693-698.

Uto, K., Takahashi, E., Nakamura, E., Kaneoka, I., 1994. Geochronology of alkali volcanism in Oki-Dogo island, Southwest Japan: *Geochemical evolution of basalts related to the opening of the Japan sea. Geochemical Journal*, 28, 431-449.

Varne, R., Foden, J. D., 1986. Geochemical and isotopic systematics of eastern Sunda arc volcanics: Implications for mantle sources and mantle mixing processes. In: Wezel, F. C., ed., *The Origin Of Arcs*. Amsterdam, Elsevier, pp. 159-189.

Vatin-Perignon, N., Oliver, R. A., Goemans, P., Keller, F., Briqueu, L., Salas, A. G., 1992. Geodynamic interpretations of plate subduction in the northernmost part of the central volcanic zone from the geochemical evolution and quantification of the crustal contamination of the Nevado Solimana volcano, southern Peru. *Tectonophysics*, 205, 329-355.

Vergara, M. M., López-Escobar, L., Palma, J. L., Hickey-Vargas, R., Roeschmann, C., 2004. Late tertiary volcanic episodes in the area of the city of Santiago De Chile: New geochronological and geochemical data. *Journal of South American Earth Sciences*, 17 227-238.

Verma, S. P., 2000. Geochemical evidence for a lithospheric source for magmas from Los Humeros Caldera, Puebla, Mexico. *Chemical Geology*, 164, 35-60.

Vogel, T. A., Younker, L. W., Williams, S. N., Kampmueller, E., 1984. Magma mixing: The Marsco Suite, Isle Of Skye, Scotland. *Contributions to Mineralogy and Petrology*, 87, 231-241.

Tomurtogoo, O., 1999. Geological map of Mongolia, Mineral Resources Authority of Mongolia.

Tormey, D. R., Frey, F. A., López-Escobar, L., 1995. Geochemistry of the active Azufre-Planchon-Peteroa volcanic complex, Chile (35°15'S): Evidence for multiple sources and processes in a cordilleran arc magmatic system. *Journal of Petrology*, 36, 265-298.

Tormey, D. R., Hickey-Vargas, R., Frey, F. A., López-Escobar, L., 1991. Recent lavas from the Andean volcanic front (33 To 42°S); Interpretations of along-arc compositional variations. *Special Paper for the Geological Society of America*, 265, 57-77.

Trumbull, R. B., Wittenbrink, R., Hahne, K., Emmermann, R., Büsch, W., Gerstenberger, H., Siebel, W., 1999. Evidence for late Miocene to recent contamination of arc andesites by crustal melts in the Chilean Andes (25° - 26°) and its geodynamic implications. *Journal of South American Earth Sciences*, 12, 135-155.

Tsuchiya, N., Suzuki, S., Kimura, J.-I., Kagami, H., 2005. Evidence for slab melt/mantle reaction: Petrogenesis of early Cretaceous and Eocene high-Mg andesites from the Kitakami mountains, Japan. *Lithos*, 79, 179-206.

Tucker, M. E., 1991. Sedimentary Petrology: an introduction to the origin of sedimentary rocks. Blackwell Science, Oxford, 260 pp.

Turner, S. P., Foden, J. D., 2001. U, Th and Ra disequilibria, Sr, Nd and Pb isotope and trace element variations in Sunda arc lavas: Predominance of a subducted sediment component. *Contributions to Mineralogy and Petrology*, 142, 43-57.

Turner, S. P., Hawkesworth, C. J., Van Calsteren, P. W., Heath, E., Macdonald, R., Black, S., 1996. U-series isotopes and destructive plate margin magma genesis in the Lesser Antilles. *Earth and Planetary Science Letters*, 142, 191-207.

Vukadinovic, D., Nicholls, I. A., 1989. The petrogenesis of island arc basalts from Gunung Slamet volcano, Indonesia: Trace element and Sr87/Sr86 constraints. *Geochimica et Cosmochimica Acta*, 53, 2349-2363.

Vukadinovic, D., Sutamidjaja, I., 1995. Geology, mineralogy and magma evolution of Gunung Slamet volcano, Java, Indonesia. *Journal of Southeast Asian Earth Sciences*, 11, 135-164.

Walsh, J. N., Beckinsale, R. D., Skelhorn, R. R., Thorpe, R. S., 1979. Geochemistry and petrogenesis of Tertiary granitic rocks from the island of Mull, Northwest Scotland. *Contributions to Mineralogy and Petrology*, 71, 99-116.

Wang, Q., Liu, X., 1986. Paleoplate tectonics between Cathaysia and Angaraland in Inner Mongolia, China. *Tectonics*, 5, 1073-1088.

Watanabe, Y., Stein, H. J., 2000. Re-Os ages for the Erdenet and Tsagaan Suvarga porphyry Cu-Mo deposits, Mongolia, and tectonic implications. *Economic Geology*, 95, 1537-1542.

Webb, L. E., Johnson, C. L., 2006. Tertiary strike slip faulting in southeastern Mongolia and implications for Asian tectonics. *Earth and Planetary Science Letters*, 241, 323-335.

Wensink, H., Van Bergen, M. J., 1995. The tectonic emplacement of sumba in the Sunda-Banda arc: Paleomagnetic and geochemical evidence from the early Miocene Jawila volcanics. *Tectonophysics*, 250, 15-30.

Wheller, G. E., Varne, R., 1986. Genesis of dacitic magmatism at Batur volcano, Bali, Indonesia: Implications for the origins of stratovolcano calderas. *Journal of Volcanology and Geothemal Research*, 28, 363-378.

Wheller, G. E., Varne, R., Foden, J. D., Abbott, M. J., 1987. Geochemistry of Quaternary volcanism in the Sunda-Banda arc, Indonesia, and three-component genesis of Island-arc basaltic magmas. *Journal of Volcanology and Geothemal Research*, 32, 137-160.

White, R. V., Tarney, J., Kerr, A. C., Saunders, A. D., Kempton, P. D., Pringle, M. S., Klaver, G. T., 1999. Modification of an oceanic plateau, Aruba, Dutch Caribbean: Implications for the generation of continental crust. *Lithos*, 46, 43-68.

Wilson, M., 1989. Igneous petrogenesis; a global tectonic approach. Unwin Hyman, London, 466 pp.

Woodland, S. J., Pearson, D. G., Thirlwall, M. F., 2002. A platinum group element and Re-Os isotope investigation of siderophile element recycling in subduction zones: Comparison of Grenada, Lesser Antilles arc, and the Izu-Bonin arc. *Journal of Petrology*, 43, 171-198.

Whalen, J. B., 1985. Geochemistry of an island-arc plutonic suite: The Uasilau-Yau Yau intrusive complex, New Britain, P.N.G. *Journal of Petrology*, 26, 603-632.

Wilson, M., 1989. Igneous petrogenesis; a global tectonic approach. Unwin Hyman, London, 466 pp.

Wu, F.-y., Sun, D.-y., Li, H., Jahn, B.-m., Wilde, S., 2002. A-type granites in northeastern China: age and geochemical constraints on their petrogenesis. *Chemical Geology*, 187, 143-173.

Wu, F., Jahn, B., Wilde, S., Sun, D., 2000. Phanerozoic crustal growth: U-Pb and Sr-Nd isotopic evidence from the granites in northeastern China. *Tectonophysics*, 328, 89-113.

Xiao, W., Windley, B. F., Hao, J., Zhai, M., 2003. Accretion leading to collision and the Permian Solonker suture, Inner Mongolia, China: Termination of the central Asian orogenic belt. Tectonics, 22, 1069, doi:10.1029/2002TC001484.

Xiao, W., Windley, B. F., Sun, S., Li, J., Qin, K., Wang, Q., 2004. Palaeozoic accretionary and convergent tectonics of the southern Altaids: implications for growth of Central Asia. *Journal of the Geological Society of London*, 161, 339-342.

Zheng, Y., Zhang, Q., Wang, Y., Liu, R., Wang, S. G., Zuo, G., Wang, S. Z., Lkaasuren, B., Badarch, G., Badamgarav, Z., 1996. Great Jurassic thrust sheets in Beishan (North Mountains); Gobi areas of China and southern Mongolia. *Journal of Structural Geology*, 18, 1111-1126.

Zhu, Y., Sun, S., Gu, L., Ogasawara, Y., Jiang, N., Honma, H., 2001. Permian volcanism in the Mongolian orogenic zone, northeast China: geochemistry, magma sources and petrogenesis. *Geological Magazine*, 138, 101-115.

Zoback, M.L., Anderson, R.E., Thompson, G.A., 1981. Cainozoic Evolution of the State of Stress and Style of Tectonism of the Basin and Range Province of the Western United States. *Philosophical Transactions of the Royal Society of London. Series A, Mathematical and Physical Sciences,* Volume 300, Issue 1454, p. 407-434

Zorin, Y. A., 1999. Geodynamics of the western part of the Mongolia-Okhotsk collisional belt, Trans-Baikal region (Russia) and Mongolia. *Tectonophysics*, 33-56.

Zorin, Y. A., Belichenko, V. G., Turutanov, E. K., Kozhevnikov, V. M., Ruzhentsev, S. V., Dergunov, A. B., Filippova, I. B., Tomurtogoo, O., Arvisbaatar, N., Bayasgalan, T., Biambaa, C., Khosbayar, P., 1993. The South Siberia-central Mongolia transect. *Tectonophysics*, 225, 361-378.